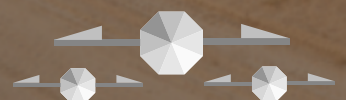
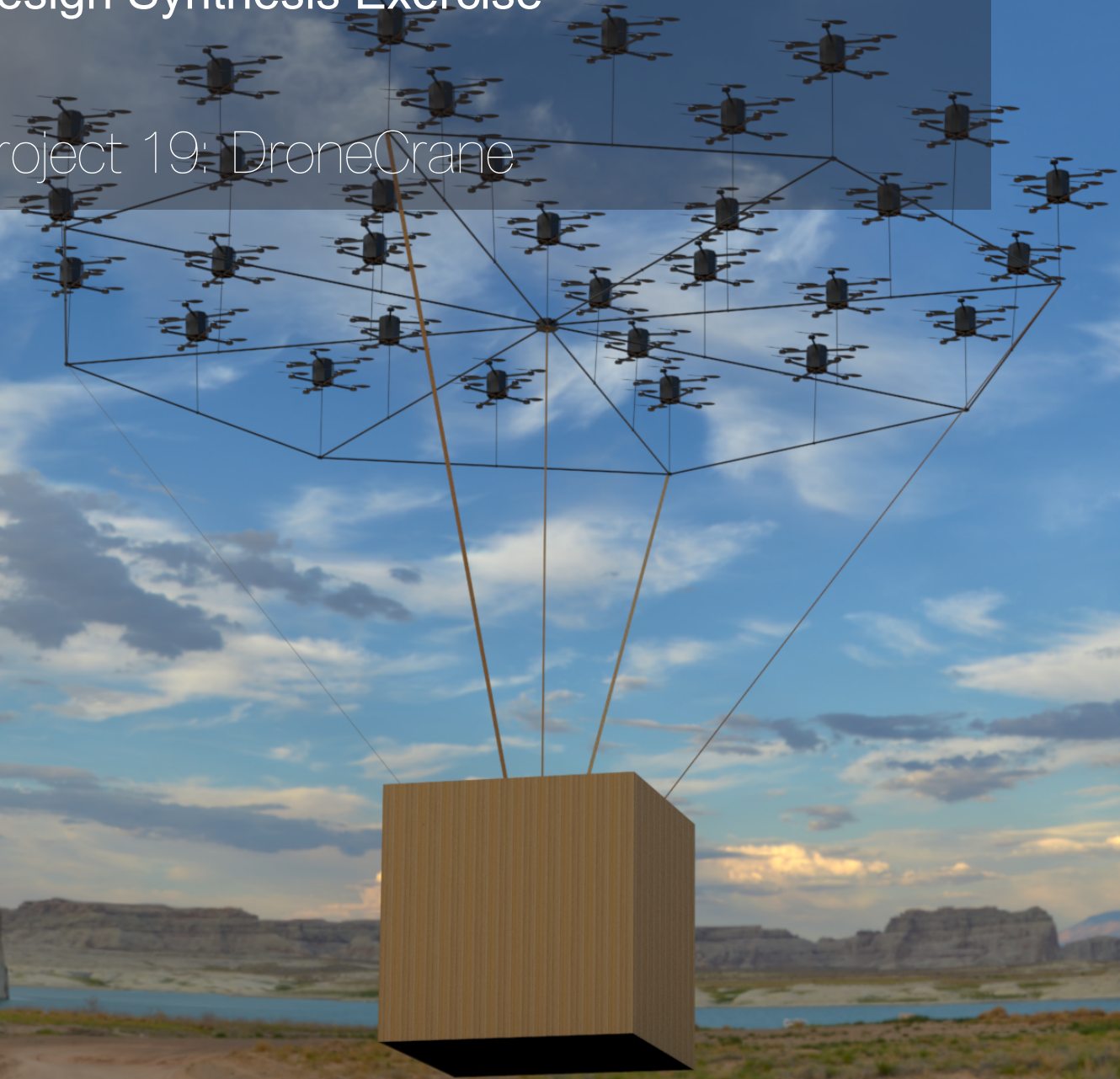


Final Report

Design Synthesis Exercise

Project 19: DroneCrane

Delft University of Technology



This page is intentionally left blank.

Final Report

Design Synthesis Exercise

by

Members of Project 19: DroneCrane

Aaron Bracke	4992679
Tyme Chatupanyachotikul	5011485
Maxim Džubinský	5056144
Giovanni Ghisalberti	5017688
Thomas Groothoff	4647750
Robin Kos	4843568
Ojas Mandlekar	5034876
Dequan Ou	5095441
Bryan Quadras	5040698
Giacomo Sofi	5049261

Date of submission: June 21, 2022

Course code: AE3200

Course name: Design Synthesis Exercise

Academic year: 2021 - 2022

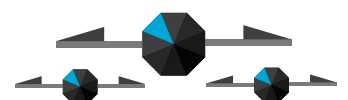
Project name: DroneCrane

Tutor: Dr. Ewoud Smeur

Coaches: Dr. Nick Eleftheroglou
Ir. Jurriaan van 't Hoff

Status of report: Final

Cover Image: (own work)



List of Abbreviations

Abbreviations	Full name
AGL	Above Ground Level
AHP	Analytical Hierachal Process
AMSL	Above Mean Sea Level
B2B	Business-to-business
CAD	Computer aided design
CAGR	Compound Annual Growth Rate
CFD	Computational Fluid Dynamics
CFRTP	Carbon Fibre Reinforced Thermoplastic
CoG	Centre of Gravity
FBD	Functional Breakdown Diagram
FEM	Finite Element Method
FFD	Functional Flow Diagram
I2C	Inter-Integrated Circuit Bus
ICA	Internal Collision Avoidance
LFRS	Lateral Force Relief System
MANET	Mobile Ad-Hoc Network
MNS	Mission Need Statement
PES	Polysulfane
RAMS	Reliability Availability Manufacturability Safety
RPM	Revolution per Minute
SOC	State of charge
SPI	Serial Peripheral Interface
SWOT	Strength Weakness Oppoturnity Threat
TRL	Technlogy Readiness Level
UART	Universal Asynchronous Receiver-Transmitter
USB	Universal Serial Bus
WBD	Work Breakdown Diagram

List of Symbols

Symbols	Full name
A	Area
B	Body reference frame
c	Clearance
C	Battery capacity
C_d	Drag coefficient
c_Q	Torque coefficient
C_t	Safety factor for operating temperature
c_T	Thrust coefficient
D	Diameter
\hat{D}	Drag vector
d	Length of a side of a square
dl	Long moment arm
ds	Short moment arm
E	Energy
E	Fixed-Earth reference frame
F	Force
g	Mean gravitational acceleration at sea level
h	Height
I	Current
I	Moment of inertia
i_0	No-load current
K	Column effective length factor
K_v	RPM per volt
L	Length
L_A	Equivalent radial load
L_S	Basic dynamic load
M	Mass
M	Bending moment
m	Mass
n_{drone}	Number of drones
n_{rotor}	Number of rotors
p	Likelihood
P	Power
P	Failure rate
P_{cr}	Maximum allowable force in a section for buckling
P_e	Electrical power
P_m	Mechanical power

Q	Required torque
R	Motor internal resistance
T	Thrust
T_x	Thrust in x-direction
T_y	Thrust in y-direction
T_z	Thrust in z-direction
t	Thickness
T_m	Time taken for a motor to reach 80% of speed
W	Weight
y	Distance to neutral axis
ω	Angular speed
$\hat{\omega}$	Angular speed vector
η	Efficiency
ϕ	Roll angle
ψ	Yaw angle
λ	Failure rate
ρ	Density
σ	Stress
θ	Pitch angle

Preface

To finish the Bachelor's degree in Aerospace Engineering at TU Delft, 10 students came together to design a complex system in 10 weeks. We, as Group 19, had the chance to explore innovative payload lifting mechanisms that employ a swarm of drones to deliver payload to great heights. After several iterations, hours spent around a table and many update meetings, we are glad to present in this paper the final design selected for DroneCrane. The overall design process gave to the group members insights on the new opportunities that swarms of drones can provide, and gave knowledge on how to implement system engineering into the design of a complex system.

After the project we want to thank our principal tutor Ewoud Smeur and our coaches Jurriaan van't Hoff and Nick Eleftheroglou for their guidance and feedback throughout all the main phases of the design, from the start until the very end. Furthermore, special thanks to Wieger Moen, Sales and Tendering Manager of the innovation department at Mammoet, who provided us with relevant information on the world of heavy payload lifting mechanisms. We also want to express our gratitude towards all other staff members, friends and families who gave us support during the past weeks.

DSE Group 19

Delft, June 2022

Executive Overview

This chapter was written by: Robin.

Drones have been an emerging trend in the last few years. They are used in multiple industries already, from photography and videography to racing. More use cases are now being conceived, such as using drones to deliver packages and food to people at home, using drones for inspections, or even using them as rescue searching vehicles in hostile environments. Even more possibilities open up once the drones bundle their forces to create swarms. The lifting capabilities of drones are still somewhat limited, but in a swarm they might be able to lift heavy payloads. This report covers the design of a concept of a payload carrying swarm, intended to lift cargo up to 500 kg to even the top of a tall building.

In order to start the design process, the project objectives and goals were laid out first. On the top most level, this means that the project objective statement and the mission statement were created.

The project objective statement of DroneCrane is: "To design an industry-ready drone swarm capable of lifting payloads up to 500 kg to heights of at least 200 m." The mission need statement is: "To provide a flexible payload lifting system that is competitive with the current market."

The first week of DSE was thus mostly used to plan out the remainder of the design phases. In this early stage, the work breakdown structure was made to create an overview of all of the expected work, as well as the workflow diagram that indicates which tasks have to be performed sequentially and which ones could be completed in parallel. Lastly, a detailed Gantt chart was made in order to plan the time of all team members effectively. These diagrams would be updated throughout the weeks as more detail became known. The last true effort in the planning phase of the design of DroneCrane was the risk assessment. This covers, in detail, the risks that DroneCrane could encounter during design and operation. The risk assessment was performed two-fold, one with a view on organisational risks, and another with view on the technical risks of the design. These risks were then analysed, and judged on their likelihood and severity of consequence. The total risk is then determined by product of these two variables. If the risk was too high, a mitigation strategy was put in place. This in organisational view could for example be to properly back-up any documentation to prevent a catastrophic loss of data. In technical risks, this could for example lead to increased safety factors, or redundant systems to prevent total failures.

A solution can only be found, if a problem exists. Thus, before the design of DroneCrane was started, a market analysis was performed in order to determine the appropriate problems that this idea could actually fix. It soon became apparent that DroneCrane would have to fill a niche market, with a maximum payload capacity of 500 kg. Looking at the market of lifting mechanism, conventional cranes are quickly identified as main competitor, especially larger ones that can carry tons in payloads. They are however very costly and thus do not fall under the same market as DroneCrane. Instead, competition can be found in mobile cranes, helicopters, and other drone-based aerial cranes. The main competitive niches that have been found involve 5G antenna installation, rooftop units installation and replacement, and mountainous area delivery such as a ski resort.

Now that the problems have been identified in which DroneCrane can be competitive, the design requirements had to be finalised. A full list of requirements was drafted and some of the key requirements are given to illustrate this: REQ-USR-01, DroneCrane shall have a payload-lifting capacity of 500 kg. REQ-USR-04, DroneCrane shall have a probability of safety-critical malfunction lower than 1×10^{-5} per system flight hours. REQ-USR-10, DroneCrane shall have 80% of its weight recyclable or reusable. These requirements were analysed for their feasibility and frozen early in the conceptual design phase.

A challenging requirement of DroneCrane is to make at least 80% of the mass recyclable. As the

batteries are a large part of its mass, it is required for these to be sustainable. This means that the selected batteries should be either recyclable, or re-usable. The priority lies with re-using batteries. At the end of life, the state of charge (SOC) should be monitored. If this is above 80%, the battery can be re-used. If however the performance is not sufficient anymore, recycling must be considered. Though the process is expensive and not always environmentally friendly, it has seen heavy investments due to the increase of battery usage. Thus recycling is becoming more accessible and economical. The design of propulsion has mainly been focused on becoming as efficient as possible to ensure that a minimum amount of batteries would be required. The efficiency of the propulsion subsystem is one of the main deciders in total energy usage of the swarm, and this is why this was of main concern. The structures have also been designed to be as light as possible, while still managing to use a recyclable material. Both novel materials and manufacturing methods are planned to be used to keep this project as sustainable as possible, such as carbon fibre reinforced thermoplastics (CFRTP) and additive manufacturing. In the second part of the DSE, the preliminary design phase started. In this phase, multiple concepts were created and analysed, in order to be able to trade off the different concepts based on their performance in many categories such as energy efficiency, sustainability and reliability.

The concepts that were created for DroneCrane were diverse, as the team attempted to keep an open mind to different technologies. The design was kept modular throughout the departments. Many different considerations came up. For the drone structure, a conventional octocopter, coaxial octocopter, and a multicopter design were considered. For the swarm, three options were presented as well. These included a centralised swarm, with one larger drone that would carry the majority of the batteries and computing power, another option with clusters including some larger drones that again take up the task of carrying the batteries and computing power, and lastly a decentralised swarm in which each drone is the same and carries their own necessary resources. To counteract the angles in the connection cables that are induced by the change in area from a small connection point on the payload to the large area that the drones cover, either a lateral force relief system (LFRS) can be created, or the efficiency penalty can be taken to save weight. In the propulsion group, a consideration of using ducted propellers was made. Lastly, a trade-off would be made considering an in-air energy storage, versus a cable that could provide power from the ground.

During the trade-off, scores were given to the four concepts created with combinations of different options for each subsystem. The winner of this analysis was however not the best option, this is due to the fact that there was no concept made with the best solutions for each subsystem. Consequently, thanks to the modularity of the system, a final design was created combining the best solutions. This resulted in a decentralised drone swarm with an in-air energy storage, an LFRS, non-ducted rotors, and drones with a conventional octocopter shape. An extensive sensitivity analysis was performed, which indicated that the design parameters were very stable. The current design choice would win the trade-off approximately 99.2% of the time, in a process of randomising the weight assigned to the criteria used to judge the designs.

The concept was now known, but the amount of detail was still lacking. Therefore, a piece of software was conceptualised to keep track of the changing specifications of each department. In a broad overview, this software consists of an overarching iteration method that calls all of the functions created by each department in a specific order. The software is initialised with a certain amount of drones, which is a variable that can be experimented with. The iterations are then called, until the mass of a loop changes less than one percent leading to converged solutions. From all of the information in the program, plots are generated which in turn show the specifications. These specifications can also be exported into an external json file for precise readings.

To create this software, each department has to interface properly with all others. Thus, it is important to be aware of all the dependencies between them. Thus, an N2 chart was created showing all of the important dependencies. Lastly, certain constraints had to be put upon the design. Among them were the maximum allowed weight per drone of 25 kg, the maximum system cost of €100 000, and finally a limit to the amount of drones put at 36 due to the operational constraints in a setup of maximum an

hour.

The propulsion sizing is based on databases containing information about off-the-shelf propellers and electric motors. The iteration starts with an initial input of a thrust to weight ratio, with this the required thrust of the swarm is calculated. The databases are then searched to find an optimal propeller type, setting the dimensions of the propellers, the RPM and torque, and the required mechanical power to reach the performances. With this information, an optimal electric motor is selected based on the lowest energy required, the cost and the maximum operating voltage.

After the first iterations, it became apparent that the conventional octocopter drone would require an area too large for normal operations, but a solution was found. An optimally distributed three-dimensional design was found, which has the same controllability characteristics of a conventional octocopter but can implement a larger propeller for a smaller diameter of the drone. Therefore, this configuration was used to allow for a smaller diameter for the swarm while avoiding major efficiency losses due to the interference between the upper and lower layers of propellers.

The electronics iteration takes in the specified power of the propulsion system. A database of different existing batteries was created so it could be iterated through. As it was already known that the batteries would be a major mass addition, the software iterations optimise the battery choice with respect to a minimal mass. The battery masses and volumes are then calculated based on the total power required. This power required consists of the previously calculated propulsion power, and the power required by the sensors added by the control department.

Lastly, the mass of the structures is calculated to complete the estimations. This is done for both the individual drones, as well as the LFRS. In order to determine an estimation of the total mass, simplified structures were analysed. From this, formulas were generated that can determine the total mass based on the specified minimum diameter of the drones and of the swarm. Combined with the loads caused by the weight of the swarm, these lead to the required mass of the structures.

After these approximations were done, the full details of the design could be identified. Starting with the propulsion group, the propellers were decided to be bought off-the-shelf. Though this simplifies the design, it does have certain complications. In order to find the optimal size and pitch, a trade-off was made between the sizing, which negatively influences other subsystems such as the structures, and the energy efficiency of the propellers. A final consideration is an estimated noise, which resulted in a maximum 101 dB at very close range, which is below the sound levels of a helicopter. However, operators working close to the system should wear earplugs to avoid any physical issues. The final motor selection followed the choice of propeller, mostly paying attention to the compatibility and maximum efficiency of all motors and thus selecting the optimal one. A sensitivity analysis was performed to gain confidence in these decisions. Finally, the reliability due to the propulsion was estimated to be approximately $3.24 \cdot 10^{-8}$ failures per hour for an individual drone.

The design of controls is a complex matter in the DroneCrane project. As a swarm needs to be coordinated, a large amount of information needs to be communicated between the drones. With a high number of drones, this becomes harder as the required computing power increases. To limit the size of communication, only the necessary information should be sent and received by any given drone.

The control system is divided into the controls of a single drone, and the controls of the swarm. The drones themselves have to be able to stabilise while heading to locations that the swarm controller indicates. To do so, an off-the-shelf flight controller is used for the individual drones, as developing one could take a serious amount of time, thus creating a large potential risk. Even though off-the-shelf components are used, a software simulation has still been made to look at the controls of an individual drone. The swarm control has to be implemented differently from the controls of an individual drone. The communication is the first obstacle, as it has to be robust, while being kept at a minimum. The actual communication will be done across a wifi-network, to which each drone is connected via a Wi-Fi card built into the Raspberry Pi Zero 2 W's that will be used in the swarm design. Even though in the preliminary design phase it was already determined that a decentralised swarm would be used,

this does not mean that there are no differences in behaviour of the drones in the swarm. Four of the drones, for example, will attempt to keep a specific virtual centre at all times to function as a reference point for the remaining drones. Lastly, to make sure the drones do not crash into each other, an internal collision avoidance system is used. The distance between drones is measured in order to determine the risk of a collision. This is then communicated back to the swarm controller, which will give new positions to save the swarm.

The design of the batteries is focused on providing redundancy and keeping down cost. Therefore, it has been decided to split the battery packs into two isolated systems. This means that if one were to fail, the other battery system could still supply power, albeit for a reduced amount of time. Aside from this, a battery was selected based on the applicable voltage, the cost, and the energy density. For controls, it is convenient to have a radial symmetry, so the battery is divided into four blocks that can be placed symmetrically around the core of the drone structure.

The final structural design of the drones is primarily influenced by the loading that the drones experience. The bending forces between the propellers and the attachment point in the centre of the drones should be optimised for. Initially, it was imagined that an arched design could perform this task the best, but after a FEM-analysis, it turned out that a straight beam is the more mass-efficient design, so this was selected for the structural design of the drone. To minimise the weight of the structure, the design was sized for bending, while keeping torsional stiffness in mind. The square shape gives enough torsional stiffness, while the bending loads are taken up by the large amounts of areas at the top and bottom of these designs. The material initially chosen was an aerospace grade 7075-Aluminium. However, the mass was not light enough to create a working system. Thus, a new material was found. This is Carbon Fibre Reinforced Thermo Plastic, or CFRTP in short. This is an easier to recycle variant on CFRP, or carbon fibre reinforced polymer, while keeping much of the same properties that make CFRP so preferable in design.

The LFRS had three proposed design ideas. One is a circular design with beam-like spokes attached in the centre. The next, an octagonal one with the same beam-like spokes. The last, a square design with connected corners and centres. The octagonal shape has been selected, as the performance on the main load, buckling, is much better than the square section due to its shorter beams, while the octagonal shape is easier to manufacture than the circular one. The material used is the same as the one of the drones, using the recyclable properties of thermoplastics, while having the performance of a carbon fibre reinforced matrix.

With a full design, the specifications are now known. The drones are made out of CFRTP as mentioned earlier, where the structure of each drones has a diameter of approximately 0.96 m. The mass per drone of the structures is 2.19 kg, the mass for propulsion is 1.46 kg, and that of the electronics is 20.8 kg. This totals to around 24.45 kg per drone. Approximately 5292 Wh is stored in the batteries of a drone, and a peak power of almost 9 kW can be achieved. The LFRS weighs in at only 24.53 kg.

When DroneCrane arrives on location, the drones and the LFRS, which are stored in boxes, are assembled in their required 12x12 meter area. All ropes will have to be attached by the operators. Finally, the cameras are turned on and the controller is connected to the swarm. The LFRS will be broken down in smaller pieces to ensure the transportability. In flight, DroneCrane can be set to a maximum vertical speed of 1.5 m/s. Safety has been considered as well. The general rules that will have to be implemented in DroneCrane operations are as follows: no human is allowed to be present directly underneath the payload at any time, the flight conditions are limited to clear weather and a wind speed lower than 10 m/s, a safety check has to be performed between each operation, and finally a flight has to be reported and approved by the local government and air control departments.

The reliability of the swarm of drones is critical. In order to meet the requirements, many redundancies have been implemented. The batteries have for example been divided into two groups in each drone, and the flight controllers have been doubled. Due to all these measures, the reliability meets the strict requirements set early in design.

The goal of the design of DroneCrane was to be able to present a system cost of less than €100

000 in total, and operational costs of less than €5 000 in a typical day. The total normal cost of the DroneCrane system is approximately €108 000 without taking into account the bulk discounts that can be achieved in buying many components at once. Including these discounts can bring the total cost down to €95 906.24. The operational costs are approximately €4 000 for a typical operational day, including the operators, electricity uses and maintenance.

The production of DroneCrane involves many off-the-shelf components. The electronics and propulsion units are all bought and just need to be assembled on the drone frames. The structures on the other hand have to be manufactured by DroneCrane, or by a third party company on commission. To save costs and increase production speeds, a combination of an additive manufacturing technique, thermoforming, and hot pressing are used in order to create these structures. Then, the sub-components have to be assembled into individual drones, which can be arranged into swarms at any location to prepare for operations.

The design of DroneCrane has been a challenge with many obstacles. The resulting design will be able to fill some of the niches identified in the earlier discussed market analysis, but the size of the swarm may limit the places in which it can be used. Transportation remains a challenge. With an outlook on the future, DroneCrane has the potential to become a lot more viable as battery technology progresses. DroneCrane may not yet be fully ready for the current market, but it possibly has a bright future.

Contents

List of Abbreviations	i
Executive Overview	v
I Approach & Concepts (Background)	1
1 Introduction	2
2 Functional breakdown and budgets	4
2.1 Functional Flow and Breakdown Diagrams	4
2.2 Technical Risk Assessment and Risk Map	7
3 Market Analysis	13
3.1 Current Market	13
3.2 Target Market and Applications	13
3.3 Competitors	15
3.4 SWOT Analysis	16
4 Design Requirements	17
4.1 User Requirements	17
4.2 Technical Requirements	18
4.3 Operational Requirements	19
II Design Setup	21
5 Preliminary Design	22
5.1 Summary of Designs	22
5.2 Trade-off Method	23
5.3 Trade-off Summary	24
5.4 Trade-off Sensitivity Analysis	25
6 Sustainability	26
6.1 Electrics	26
6.2 Propulsion	29
6.3 Structures	29
7 Design Iterations	31
7.1 Overall	31
7.2 Propulsion	33
7.3 Electrics	38
7.4 Structures	39
7.5 Verification of Software	43
7.6 Results	44
7.7 Sensitivity Analysis	45
III Detailed Design Specifications	47
8 Propulsion	48
8.1 Propeller Design	48
8.2 Motor Design	49
8.3 Requirement Compliance	49
8.4 Sensitivity Analysis	52
8.5 Reliability	55
9 Control	57
9.1 Hardware Structure	57
9.2 Software Characterisation	60
9.3 Communication	62

9.4 Individual Drone Simulation	67
9.5 Swarm Control	81
9.6 Reliability	87
10 Electrics	89
10.1 Design Decisions	89
10.2 Design Characteristics	90
10.3 Electrical Block Diagram	91
10.4 Sensitivity Analysis	93
10.5 Production Plan	93
10.6 Reliability	94
11 Structures	95
11.1 Drone Structural Design	95
11.2 LFRS Structural Design	98
11.3 Virtual Reality for Swarm Visualisation	101
12 Detailed Design and Analysis of Properties	102
12.1 Summary of the Design	102
12.2 Performance	103
12.3 Operations and Logistics Description	104
12.4 Final Design Resource Allocation	106
12.5 RAMS	107
12.6 Financial Evaluation	110
12.7 Compliance Matrix	113
12.8 Production Plan	117
IV Outlook of the Future	119
13 Future Endeavours	120
13.1 Project Design & Development Logic	120
13.2 Gantt Chart	120
13.3 Recommendations	122
14 Conclusion	124
Bibliography	125
A Technical Drawings	130



Approach & Concepts (Background)

1. Introduction

This chapter was written by: *Giovanni*

Payload lifting mechanisms have historically been ground based cranes [1]. Since the development of helicopters, they have been the go-to method for those business interested in reaching high or inaccessible places. However, the development of drone technologies in the last couple of decades [2] proved their helpfulness in fields such as surveillance [3], agriculture [4], delivery [5] and military [6]. Their involvement in the payload moving market opens a third way to take goods off the ground, especially as they have the potential to be less expensive, faster to operate, more versatile, and safer [7]. As drones can also be designed as fully electric vehicle, they represent a simpler to make sustainable system.

Single drones have already been exploited to lift and deliver payloads up to 225 kg¹ and their extensive employment in as flagship autonomous systems of modern industries [8] limits the market potential of a new product [9]. "Collections of drones, on the other hand, have mostly been studied with a theoretical mindset, and researchers have concentrated their efforts on finding suitable ways to control and coordinate them [10]. The lack of companies that produce swarm of drones for direct use in the payload-moving industry [11] is an indicator of a potential business opportunity and novel knowledge development. To address the gap, DroneCrane has been conceptualised as a payload-moving swarm of drones that can be deployed as a competition for conventional cranes and helicopters [12]" [9].

Thus, the working group set out to develop the payload-lifting swarm of drones DroneCrane from a blank sheet [13], starting with the identification of customer requirements and the technical ones that followed. The project was set up and planned to include an initial concept phase where an options brainstorm was performed eliminating all those technologies which could not be implemented for reasons such as their readiness level or adequacy with requirements and use cases[11]. The concept phase was terminated having identified in DroneCrane an appreciable level of modularity: it has been possible to consider the five major subsystems as separate and almost independent units until integration. They are the propulsion, control, and electrical systems, the drone configuration, and the payload support structure. These five elements were assessed and preliminary designed in a few varied forms that were brought forward to the trade-off process[9]. Options such as a tethered power system were analysed against a battery-based one, and hexacopter configurations were weighed against coaxial and conventional octocopter ones. The trade-off procedure yielded a winner design that could integrate all the five subsystems: conventional octocopters make up the swarm, mechanically powered by ducted propellers and electrically by battery packs; an intermediate structure is placed between the drones and the payload to minimise the later workload on the drones, that are controlled from the ground by an operator but autonomously implement the commands they receive.

Having this base, the final phase of the design is initiated. This report has the goal of illustrating all the steps taken to advance the design to a feasible ensemble of preliminary sized elements: at the end of the work presented here, the DroneCrane project will be able to be detailed to the level of production instructions, holding for the future a clear path, since all major design choices will have been taken and justified. The detailed design presented in this report was approached by dividing the work packages according to the following subsystems: structure, power, propulsion, and control. In relation to the five elements distinguished before in the trade-off, the structure department has been concerned with the single drone structure and the drone-payload intermediate one. The remaining four elements match the rest of the departments naturally.

The report is structured as follows: in Part I, the necessary background information concerning the functionalities that DroneCrane is expected to fulfil is presented in Chapter 2, together with the schematics drawn representing the full functional breakdown and flow. In the same chapter, the

¹<https://www.hwlibre.com/en/griff-300-multirotor-capable-of-loading-225-kg/> [Accessed in May 2022]

assessment of the technical risks with risk maps are presented to give the reader the same perspective that the working group had on the challenges that the design had to be designed for and against. Chapter 3 address the market analysis performed to pinpoint the business opportunities for DroneCrane, as well as the calibre of the competition on DroneCrane's horizons. The analysis is followed by Chapter 4, where the requirements are presented starting from user requirements, going on to technical requirements, and finally operational requirements. To complete the background information, Chapter 6 describes the sustainable approach taken by each technical department in the design of DroneCrane.

Part II illustrates the trade-off procedure as a summary of the work carried out previously[9] with Chapter 5. It is followed by a description of the system engineering approach taken in the integration of all subsystems in Chapter 7: the software used to iterate the design and converge to a final one. The technical work done by each department is thoroughly presented in Part III, with one chapter for each department: propulsion in Chapter 8 and controls in Chapter 9, so that Chapter 10 can illustrate the work done on the electrics with all the necessary information already outlined. The structures content follows in Chapter 11, and the part is concluded with the overall design analysis of Chapter 12. The final part of the report, Part IV, presents the reader with the plans for the future of DroneCrane: Chapter 13 presents the Project Design & Development Logic together with a Gantt chart for the future, followed by recommendations. The report ends with the conclusive Chapter 14.

2. Functional breakdown and budgets

The work carried out in the earlier stages of the design [9, 11] built up the knowledge required to the detailed phase undertaken with this report. Part of the background includes the identification of the functionalities that DroneCrane must fulfil to address its customer requirements. This chapter presents to the reader the functional breakdown and the functional flow of a DroneCrane mission in Section 2.1. Moreover, the chapter is completed with Section 2.2, where the risk assessment performed at the beginning of DroneCrane development is detailed.

2.1. Functional Flow and Breakdown Diagrams

This section was written by: *Ojas and Tyme*

In this section the construction of the Functional Flow and Functional Breakdown Diagrams will be further explained. The functional analysis will provide a better overview of the different required tasks and steps that the product needs to do. Firstly the Functional Flow Diagram will be constructed based on the mission need statement (MNS) to ensure that the product fulfils its purpose, and it will show in chronological order the different functions performed. Once this is done the Functional Breakdown Diagram will be constructed, where similarly repeated tasks are grouped together. This diagram will aid with discovering the different possible hardware required to perform different tasks, and the discovery of requirements for the different functions that need to be fulfilled.

The Functional Flow Diagram of the DroneCrane system can be found in Figure 2.1. This is very similar to the diagram implemented in the baseline report [11], however a major change on the controls was done. A semi-manual control method was implemented, where an operator controls the swarm as a whole instead of having an autonomous system. There are four main parts to DroneCrane operations: Preparation, Deployment, Undeployment and Maintenance. These functions are then further divided into more detailed ones, which can be seen in both the Functional Flow and Functional Breakdown diagrams. There are four levels of functions, each providing a deeper level of detail.

The first stage of DroneCrane's operation begins with the preparation phase. As safety is an integral aspect of DroneCrane, prior to any operations the compatibility of the payload with the system will be checked then all the hardware required will be inspected. After the system is transported to the lifting site, the entire system will be assembled and properly initialised.

The second stage of the operation is the deployment of the system, where the swarm of drones and the payload will take off, whilst monitoring the different degrees of freedom of the swarm as a whole and the individual drone. The swarm will then manually follow a route to the designated location. During this phase, the system will continuously monitor itself and the commands sent by the operator. Once the operator sends a drop-off command, the system will safely detach the payload at the desired location. After the payload has been removed, the swarm will follow a similar procedure on the way back. Once the operator confirms that the swarm has arrived at its destination, the swarm will safely land where required. Finally, if a new payload has to be delivered, the swarm will once again be set up, and the mission can commence anew.

If no additional payload is to be delivered, the third stage is initiated, to conclude the deployment of the system through a set of ordered steps: all systems are turned off and the LFRS with the connections are disassembled. Once all is ready, the equipment is loaded onto the transportation system.

The fourth, final stage of operations is making sure all systems and equipment are in order through a set of maintenance protocols. The maintenance kicks off with a testing of all subsystems. Once the tests are concluded, the results are evaluated and based on them, either nothing is done, or a repair is started, or, in the worst case scenario, a disposal is initiated. Once the maintenance is completed, the system is ready for a new cycle of operations.

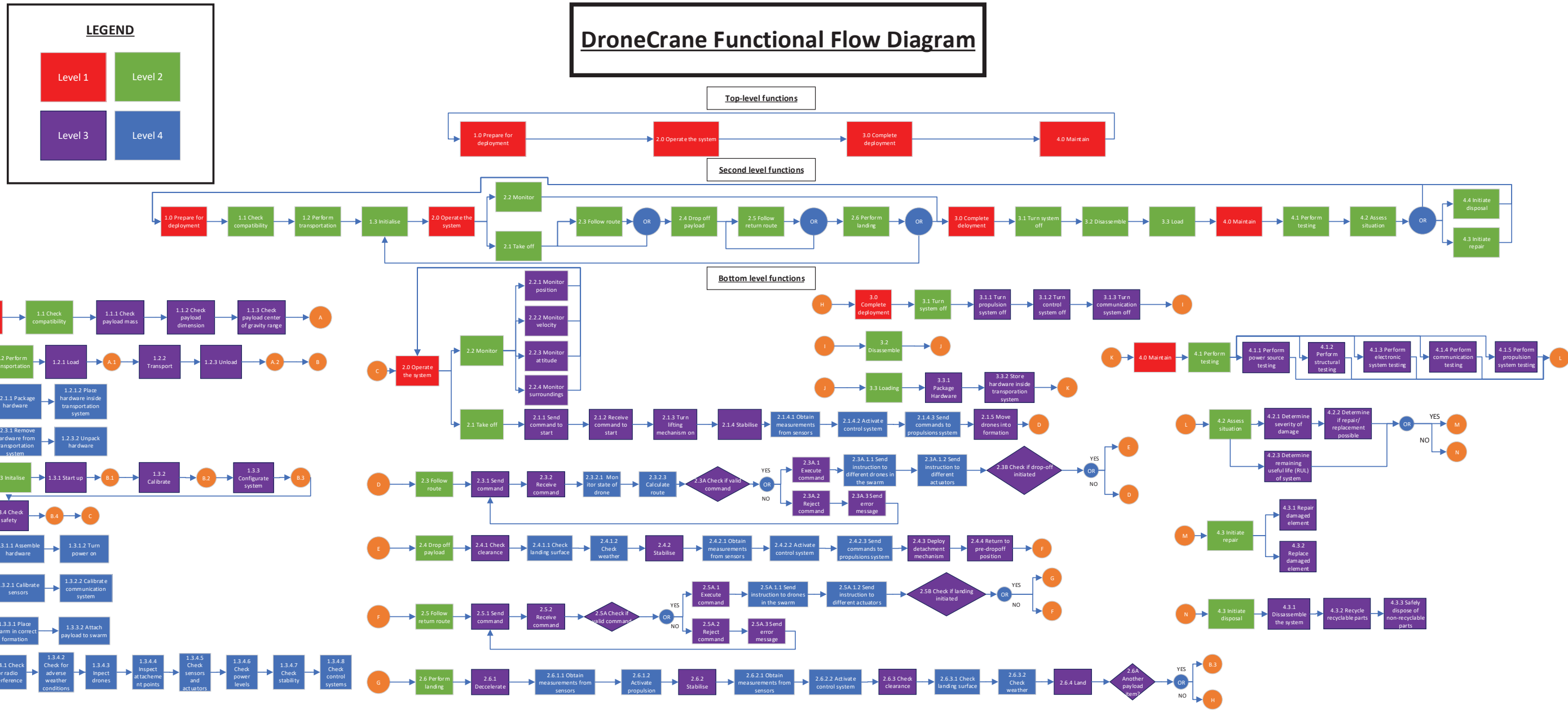


Figure 2.1: Functional Flow Diagram (own work).



Figure 2.2: Work Breakdown Structure (own work).

2.2. Technical Risk Assessment and Risk Map

This section was written by: *Maxim*

During a design process, one must take into account all relevant technical risks which can affect the final product. In order to minimise or account for these risks, a mitigation strategy needs to be set up. This section describes the risks and their probability, impact and consequence as well as the mitigation plan that was created in order to reduce the likelihood of the risk and/or the severity of its consequences.

Subsection 2.2.1 describes the scales used to quantify the impact and the likelihood of the identified risks. The risk assessment is performed in Subsection 2.2.2, while in Subsection 2.2.3 the mitigation strategy is defined.

2.2.1. Impact and Likelihood

In this subsection, the impact and likelihood terms are defined. The impact of the risks depends on the nature of the risk, whether they are performance risks or cost risks [14]. The definition of a performance risk or of a cost risk will be explained in Subsection 2.2.2. The performance impacts are explained in Table 2.1, while the likelihood per mission p of the risks is evaluated as shown in Table 2.2.

Table 2.1: Performance and cost impacts categorised by their potential damage level on DroneCrane.

Impact level	Effect on performance	Effect on cost
Catastrophic	failure of the mission and to collateral damage	unprofitable product
Critical	impact on the success of the mission by decreasing performance or even lead to mission failure	impact on the competitiveness and financial viability of the product
Marginal	little impact on the mission	little impact on the product
Negligible	no impact on the mission	no impact on the product

Table 2.2: Quantification of the likelihood scale used to assess the risks potentially affecting DroneCrane.

Very likely	Likely	Somewhat likely	Unlikely	Very unlikely
$p > 70\%$	$70\% \geq p > 50\%$	$50\% \geq p > 30\%$	$30\% \geq p > 1\%$	$1\% > p$

2.2.2. Risk Assessment

Risks can be categorised into two overarching groups: performance risks and cost risks. Performance risks are related to the system's performance, i.e. anything that has to do with operating the system. Cost risks are related to the events that can negatively impact the budgetary facets of the design process. This chapter only focuses on so-called external risks, i.e. risks which are not directly affected by the design. Internal risks are assumed to be taken care of during the design, as they are closely tied to the requirements. The identified risks, their categories as well as their probability and impact are shown in Table 2.3. More detailed information on what these risks entail is given directly after the table. A risk map is displayed in Figure 2.3.

Table 2.3: *Technical risks.*

Identifier	Risk	Likelihood	Impact
TR-PRF-1	Incorrect assessment of the payload weight by the operators	Somewhat likely	Critical
TR-PRF-2	Weather conditions do not permit the operation of DroneCrane	Somewhat likely	Critical
TR-PRF-3	Failing drone interferes with swarm and causes total failure	Unlikely	Catastrophic
TR-PRF-4	Loss of controls	Unlikely	Catastrophic
TR-PRF-5	Loss of communication with ground due to interference	Somewhat likely	Critical
TR-PRF-6	Loss of communication with ground due to technical failure	Unlikely	Critical
TR-PRF-7	Personal drones in the airspace	Somewhat likely	Critical
TR-PRF-8	Payload is not properly secured	Unlikely	Catastrophic
TR-PRF-9	System gets hijacked	Unlikely	Catastrophic
TR-PRF-10	Loss of thrust due to technical failure	Unlikely	Catastrophic
TR-PRF-11	Loss of power	Unlikely	Catastrophic
TR-PRF-12	Attachment system interferes with the swarm during failure of drone	Unlikely	Catastrophic
TR-CST-1	Market demand is lower than expected	Unlikely	Critical
TR-CST-2	Unexpected competitors enter the market	Somewhat likely	Marginal
TR-CST-3	Shortage of raw materials	Unlikely	Marginal
TR-CST-4	Unavailable off-the-shelf parts	Somewhat likely	Critical

TR-PRF-1: Incorrect assessment of the payload weight by the operators

There exists a possibility that the users of the system incorrectly assessed the weight of the payload, surpassing the 500 kg limit. This could eliminate the safety of single drone failure not causing a total mission failure, or even hinder the lifting of the payload.

TR-PRF-2: Weather conditions do not permit the operation of DroneCrane

DroneCrane needs to be able to operate in an outside environment. Therefore, if the weather happens to get in the way of operations, it could stop the mission for extended periods of time, either due to posing a risk to the system or to the surroundings.

TR-PRF-3: Failing drone interferes with swarm and causes total failure

In the case that a technical failure leads to a total failure of a drone, there exists a possibility that the failing drone will interfere with the whole system. This could, in the worst case, lead to a total failure of the system, either by destroying more drones or by damaging/loosening the payload.

TR-PRF-4: Loss of controls

In the event of interference between the drones or a technical failure, a loss of controls could occur. This could cause a loss of formation, collisions, and total failure of the system, as the individual drones are no longer receiving commands.

TR-PRF-5: Loss of communication with ground due to interference

Another possible risk is the loss of communication with ground, due to external interference. In this case, the ground station would no longer get updates from the swarm, thus losing all information about the circumstances of the system, and the system would no longer be able to operate.

TR-PRF-6: Loss of communication with ground due to technical failure

Communication can also be lost due to a technical failure. Once again, if not properly accounted for, it can lead to a mission ending failure.

TR-PRF-7: Personal drones in the airspace

While it may be possible to restrict the airspace for some operational cases, for many it is not possible, and the airspace can thus contain other civilian or possibly military flying vehicles. If not properly accounted for, these could cause a collision leading to possible failures.

TR-PRF-8: Payload is not properly secured

The system is made to be almost entirely autonomous, however some tasks still need to be performed by operators, including loading and securing the cargo. If this action is performed improperly, it could cause a loss of cargo, potentially damaging the payload or anything below it.

TR-PRF-9: System gets hijacked

One possible problem during the operation of the system is a third party hijacking the control system. This could lead to a loss of system and payload or a purposeful incapacitation of the system.

TR-PRF-10: Loss of thrust due to technical failure

Another risk concerning the drones would be the possible loss of thrust due to technical failure of the propulsion system. This could lead to a loss of redundancy for the swarm, loss of control or incapacity to perform the mission altogether.

TR-PRF-11: Loss of power

A further performance risk would be a loss of power for the drones. This would result in a failure of all the onboard systems, leading straight to a mission failure.

TR-PRF-12: Attachment system interferes with the swarm during failure of drone

The last performance risk present is an entanglement of the attachment system with the rest of the swarm, when one of the drones fails. This could lead to a loss of stability and potentially cause a chain reaction of drone failures.

TR-CST-1: Market demand is lower than expected

The basis of the whole design process was that the final product should be appealing, competitive and useful on the identified market. However, a possibility exists that the demand for the product will be substantially lower than expected, leading to a poor performance of the product on the market.

TR-CST-2: Unexpected competitors enter the market

In a similar direction as the previous risk, the final product could also end up competing with a different new product. This new product could outperform DroneCrane (in certain aspects or altogether), leading to a lower market share and lower revenue.

TR-CST-3: Shortage of raw materials

When designing the system, it is assumed that the materials necessary for the manufacturing will be available at the same or similar price as during design. However, a shortage of material could lead to an unexpected increase in manufacturing cost, causing the company to operate at a loss or simply being unable to manufacture the product.

TR-CST-4: Unavailable off-the-shelf parts

During the manufacturing of the system, it could occur that the necessary parts are not available on the market, either due to a depletion of stock or the discontinuation of the product by the supplier. Were this to happen, the manufacturing of the system would be unable to proceed.

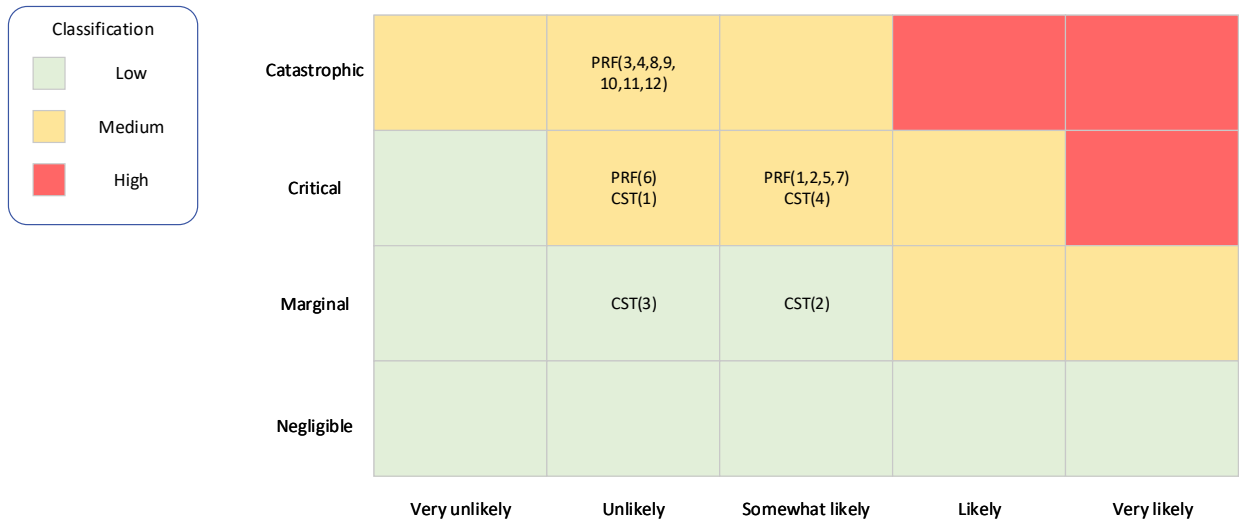


Figure 2.3: Risk map for technical risks (own work).

2.2.3. Risk Mitigation

Once the risks have been defined, a mitigation strategy must be set up. The goal of this strategy is to minimise the likelihood or the impact of all risks deemed too dangerous. In this case, it would be all risks outside of the "green" section of the risk map in Figure 2.3. For this reason, not all risks will be present in the mitigation, as the added cost/weight/other factor needed to mitigate it outweighs the reliability gain. The individual mitigation plans are described in Table 2.4 and the post-mitigation risk map is shown in Figure 2.4.

Table 2.4: *Mitigation for technical risks and the post-mitigation likelihood and impact*

Identifier	Mitigation	Likelihood	Impact
TR-PRF-1	Properly document and communicate the system limitations, while also implementing a maximum thrust setting for all drones while in hover mode, which if surpassed sends warning to the user or does not allow the system to take-off at all	Very unlikely	Critical
TR-PRF-2	Water-proof the electronics and outline the acceptable weather conditions for operations, and incorporate a dangerous weather detection protocol during startup	Somewhat likely	Marginal
TR-PRF-3	Incorporate evasive manoeuvres for the swarm	Unlikely	Critical
TR-PRF-4	Have a pruning protocol set up	Unlikely	Critical
TR-PRF-5	Have a protocol to go into standby mode until communication is reestablished, if not reestablished within a timeframe, execute emergency landing	Somewhat likely	Marginal
TR-PRF-6	Have a backup communication system	Very unlikely	Critical
TR-PRF-7	Restrict airspace and make pre-flight checks for any intruders	Unlikely	Critical
TR-PRF-8	Properly document and instruct operators on the usage protocols and implement a payload loading system (net, belts) which does not allow for improper cargo loading	Very unlikely	Catastrophic
TR-PRF-9	Use End-to-End encryption and have the backup transceiver use a different frequency	Very unlikely	Catastrophic
TR-PRF-10	Have a safety factor on the minimum number of drones	Unlikely	Critical
TR-PRF-11	Have separate sets of batteries and a power distribution system to ensure redundancy	Very unlikely	Catastrophic
TR-PRF-12	Have the detachment mechanism activate if drone deemed out of operation	Very unlikely	Catastrophic
TR-CST-4	Verify the availability of the product and, if deemed necessary, find an alternative	Unlikely	Critical

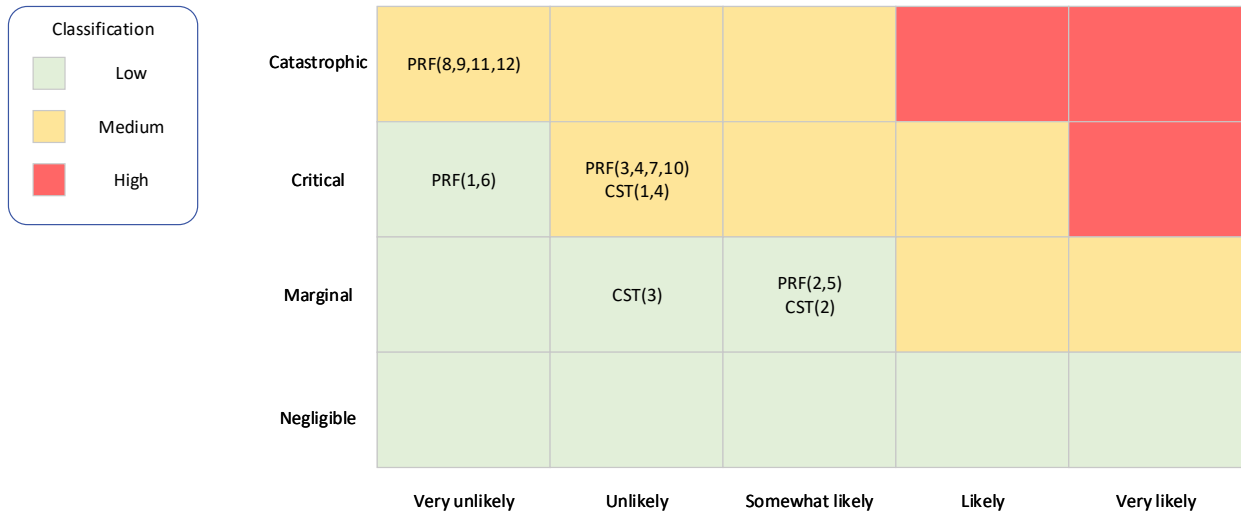


Figure 2.4: Risk map post-mitigation (own work).

2.2.4. Implementation of Mitigation

The goal of the mitigation strategy was to outline what had to be done in order to reduce the consequence of risks. However, it does not describe how this mitigation will be implemented. This section discusses the methods used and decisions made during the design to incorporate the laid-out mitigation.

Depending on the risk, the mitigation implementation can be more or less clear. Mitigations for **TR-PRF-2**, **TR-PRF-6**, **TR-PRF-9**, **TR-PRF-10** and **TR-PRF-11** could be directly implemented during the iterative design of the system (e.g. size the system with 1 additional drone, create the topology of the drones in a way that allows for separate sets of batteries to be implemented). These were the easiest to implement, as they simply became a quantifiable or quasi-quantifiable requirement, and could thus be directly applied to the design.

Next to these, mitigations for **TR-PRF-1**, **TR-PRF-2**, **TR-PRF-3**, **TR-PRF-4**, **TR-PRF-5**, **TR-PRF-8**, **TR-PRF-12** and **TR-CST-4** were slightly more tricky - the goal was clear, but the path to it not so much. Many of these mitigations consisted of setting up an algorithm within the control system of the drones (e.g. adding a maximum thrust setting, create a stand-by loop for the system), which would then perform the required actions. As such, these required more creativity from the team, as they were not equivalent to simply adding a safety factor to a number.

Finally, mitigations for **TR-PRF-1**, **TR-PRF-2**, **TR-PRF-7** and **TR-PRF-8** are to be implemented after the design is complete. These mitigations did not directly impact the design, however they still had to be kept in mind to some degree (e.g. make the system easy to use for the operators), as they remain key for the safety and reliability of the system.

3. Market Analysis

This chapter was written by: *Dequan*

In this chapter, a market analysis will be performed to locate the positioning of DroneCrane in the market. An understanding of the competitors products and their characteristics will also provide some inspiration to the design process. The current market will also be described in Section 3.1. Then a target market will follow to find out the applications of DroneCrane in Section 3.2. After, the competitors who performs similar mission as DroneCrane will be investigated and used as inspiration in Section 3.3. Finally, a SWOT analysis in Section 3.4 will be done to understand the strength, weakness, opportunities, and threats in the market.

3.1. Current Market

With the growth in demand of the cranes, the cranes market has been growing rapidly in the recent years. In 2020, the size of the global crane market was valued at \$34.5 billion. Fortune Business Insights projects that this market size will grow from \$36.36 billion in 2021 to \$49.64 billion in 2028 with a compound annual growth rate (CAGR) of 4.5%. The main players in the crane market worldwide are international equipment manufacturers such as Liebherr and Zoomlion [1]. In Netherlands, Mammoet is one of the biggest crane manufacturers.

The types of cranes can be further categorised into mobile cranes, tower cranes, floating cranes, aerial cranes and so on. Given the concepts of DroneCrane, the tower cranes and big mobile cranes have way more payload capacity. And some of the big aerial cranes such as big helicopter cranes are very expensive and have limiting accessibility in urban environment. Thus, the comparable types of cranes in the market are small mobile cranes and other drone cranes. Mobile cranes can be moved between locations on a truck carrier. The set-up time of this type of cranes can be as low as 30 minutes. Aerial cranes is a new type of lifting mechanism that uses helicopters or drones designed for special missions, such as lifting and transporting payloads to places that are difficult to reach. The aerial crane market size in 2019 was valued at \$2.81 billion and projected to reach \$3.22 billion in 2027 with a CAGR of 3.86% [15].

3.2. Target Market and Applications

Given DroneCrane's characteristics, it will mainly focus on short-duration, short-term and vertical transporting missions. Therefore, the following three applications are introduced:

- 5G antenna installation
- Rooftop units installation and replacement
- Mountain area delivery such as ski resort

5G antenna installation

5G provides fast speed, great capacity, ultra-low latency, support for Internet of Things (IoT) devices. Due to the rising needs, the 5G antenna towers need to be expended or upgraded in different areas. The 5G antennas with a weight of over 100 kg are typically placed at a height of 20 m to 60 m. A projection shows that the number of 5G antennas will increase by 10 000 units in 2022 ². An example of a typical 5G tower can be found in Figure 3.1.

²<https://dutchreview.com/culture/innovation/tens-of-thousands-of-5g-masts-to-be-installed-in-public-spaces/> [Accessed in June 2022]



Figure 3.1: 5G tower antenna.³

Rooftop units installation and replacement

The outdoor units of Heating, Ventilation and Air Conditioning (HVAC) is one of the examples of rooftop units. Figure 3.2 shows a typical configuration of a HVAC. These types of outdoor units are usually placed on the rooftop of the high-rise building with a height up to hundreds metres.



Figure 3.2: HVAC rooftop unit.⁴

Mountain area delivering

As DroneCrane has the capability to operate at an altitude of 1000 m above sea level, some mountainous region delivery such as supplies for ski resort or refuge can be considered. These restaurants or hotels are usually built in the altitudes of thousands metres and hard to be reached by wheeled vehicle. Figure 3.3 shows an example of refuges in Ochsenkopf at an altitude of around 1000 m. DroneCrane can take the responsibility of delivery payloads such as mattresses and bathtubs for the hotels or weekly supplies for the resorts and restaurants.

³<https://dutchreview.com/culture/innovation/tens-of-thousands-of-5g-masts-to-be-installed-in-public-spaces/> [Accessed in June 2022]

⁴<https://www.maxwellroofing.com/blog/how-rooftop-hvac-systems-can-affect-your-roof/> [Accessed in June 2022]

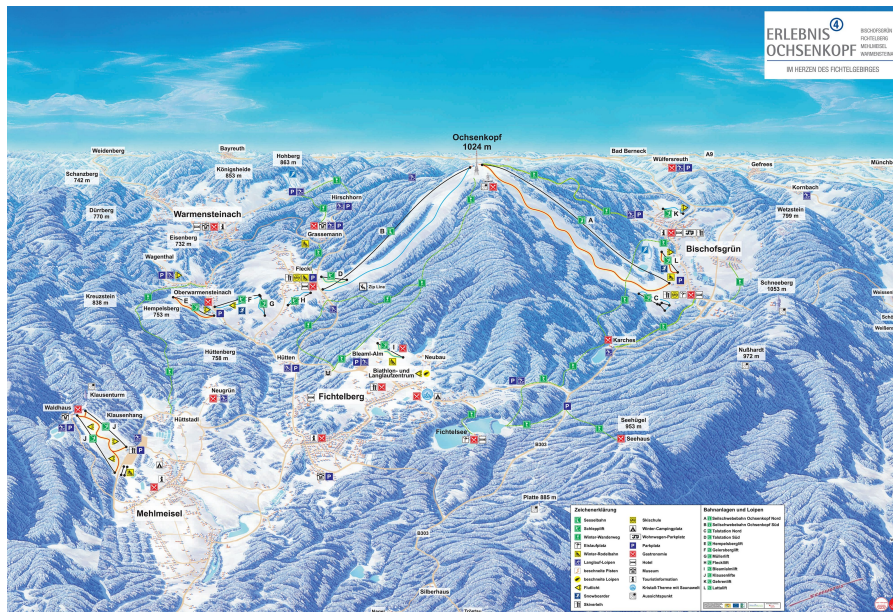


Figure 3.3: Ochsenkopf with a height of around 1000 m in Germany.⁵

3.3. Competitors

After DroneCrane's target market and applications are defined, its competitors can be identified and further analysed. These competitors include the Bocker AK52 which is a crane that is designed for 5G antenna installation, the other vertical payload lifting solution using single drones which are the Volodrone and the Griff Aviation 300, and the utility helicopter crane Kaman K-MAX.

Boker AK52

This crane is unique because it can provide relative high transport capabilities for low capacity transport. It can lift a maximum payload of 12 tons to a height of 52 m. In addition to that, its compact footprint and space-saving design allows the mission to be carried out on the roadside while traffic is still going. Its unique and variable outriggers also ensure great flexibility and safety during setting-up. The set-up process before lifting takes about 30 minutes. However, the equipment cost ranges between €100 000 and €500 000, which is larger than the cost of DroneCrane with a lower operational ceiling limit.⁶

VoloDrone

Another existing and tested payload-carry mechanism is the VoloDrone. It is an autonomous, fully electric utility drone designed by the German company Volocopter. VoloDrone has a payload capacity of 200 kg and a flight time of 30 minutes. At the ITS World Congress in October 2021, VoloDrone performed a 3-minute test flight and reached a maximum altitude of 22 m. The drone itself has a diameter of 9.15 m and a height of 2.15 m. Its development trend is fully electric with an autonomous beyond visual line of sight (BVLOS) capacities.⁷

Griff Aviation 300

A competitor to be mentioned here is Griff Aviation 300, designed by a company based in Norway. They are designing a drone crane that carries loads up to 250 kg to a height of at least 300 m and can stay in the air for 45 min. Their drone's major use is transporting building equipment and materials across challenging terrains. One of the goals they are trying to achieve is to make the Griff Aviation 300 easy to transport, assemble and operate. Griff Aviation 300 aims to provide the most optimal

⁵<https://nl.bergfex.com/ochsenkopf/panorama/> [Accessed in June 2022]

⁶<https://www.internationalcranes.media/news/truck-crane-in-demand-for-5g-work/8009709.article> [Accessed in June 2022]

⁷<https://www.volocopter.com/newsroom/successful-public-flight-volodrone/> [Accessed in May 2022]

interaction between the operator and the controlling system. If needed, equipment such as cockpits, a full view of the map, and a video feed could be designed and manufactured. Their next model aims to deliver a payload as heavy as 800 kg.⁸

Kaman K-MAX Aerial Crane

Some helicopters can be used as a crane by connecting the payloads with long cables or slings. Several helicopters were designed specifically for payload lifting, such as Sikorsky S-64 and Kaman K-MAX. The Kaman K-MAX is discussed in this subsection as it has more comparable characteristics to the DroneCrane.

The payload performance of the helicopter crane depends on the transporting height. Generally, the Kaman K-MAX is capable of lifting 2500 kg payload and reaching a maximum height of 1500 m.⁹ The price of this helicopter is as high as \$8 million.¹⁰

Finally, the table in Table 3.1 summarises the related specifications of the competitors.

Table 3.1: Summary of the related specs of the competitors.

Product	Payload capacity [kg]	Vertical range [m]	Price [€]	Endurance [min]
Boker AK52	12 000	52	500 000	N.A.
Kaman K-MAX	2 500	>1500	8 000 000	720
VoloDrone	200	N.A.	N.A.	30
Griff Aviation 300	250	300	N.A.	45
DroneCrane (aim)	500	200	100 000	30

3.4. SWOT Analysis

Finally, a SWOT analysis is performed to understand the competitiveness of DroneCrane in the market. The strengths and weaknesses are decided by comparing to the existing products in the market, especially the competitors mentioned in Section 3.3. The opportunities and threats are recognised by looking at the different aspects of trends in the world such as regulatory environment and technology development.

STRENGTHS	WEAKNESSES
<ul style="list-style-type: none"> High flexibility in operation Capability of moving horizontally Good Transportability Competitive price Pioneer in payload lifting using drone swarm 	<ul style="list-style-type: none"> Constraint by weather conditions during operation Complexity in set-up Constraint in mission area required Limiting flight/mission time Low market needs
OPPORTUNITIES	THREATS
<ul style="list-style-type: none"> Environmentally friendly needs Future development in the drone industry 	<ul style="list-style-type: none"> Improvement in the performance of single drone Environmental regulations in industrial drone flight Difficulties in obtaining certification

Figure 3.4: DroneCrane SWOT market analysis in the market (own work).

⁸<https://dronelife.com/2016/12/20/griff-aviation-launches-griff-300-one-big-drone/> [Accessed in May 2022]

⁹<https://www.flyingmag.com/aircraft-helicopters-kaman-restarting-k-max-k-1200-production/> [Accessed in May 2022]

¹⁰<https://www.flyingmag.com/aircraft-helicopters-kaman-restarting-k-max-k-1200-production/> [Accessed in May 2022]

4. Design Requirements

This chapter was written by: *Giacomo*

In this chapter the requirements that DroneCrane has to meet are discussed. The requirements are made to limit the design space and reach the goal of producing a competitive design for the current market. The values defined in this section are inputs for the design phase.

In Section 4.1 the user requirements are displayed, while in Section 4.2 the technical requirements for the subsystem are set. Finally, Section 4.3 describes the characteristics that DroneCrane need to have in order to be operable and succeed in the mission.

4.1. User Requirements

User requirements are defined in this section. The requirements are created such that they are verifiable, achievable, logical, integral, definite (VALID) and represent the top-level drivers for future design decisions. They have been taken from the tutor's instruction [12] and follow from the stakeholder needs. The user requirements identified by the group are presented in Table 4.1. In addition, the requirements which are key to the design and has a larger influence on the state of the final design are indicated by a key symbol, , near the identifier. The rationale driving these requirements is to make DroneCrane competitive in the market while meeting the user's requirements and ensuring safe operations. Furthermore, sustainability is key and requirements have been formulated to make it possible for DroneCrane to still use power from the grid through a green energy plan.

Table 4.1: User requirements

ID	Requirement
REQ-USR-01 	DroneCrane shall have a payload-lifting capacity of 500 kg.
REQ-USR-02	DroneCrane shall have a minimum altitude ceiling of 1000 m AMSL.
REQ-USR-03	DroneCrane shall be able to deliver payloads to an altitude of least 200 m AGL.
REQ-USR-04 	DroneCrane shall have a probability of safety-critical malfunction lower than 1×10^{-5} per system flight hour.
REQ-USR-05	Failure of one drone of the DroneCrane system shall not lead to dropping of the payload.
REQ-USR-06	Failure of one drone of the DroneCrane system shall not lead to failure of the other drones.
REQ-USR-07	The failure of any communication link between drones shall not lead to safety-critical malfunction of the system.
REQ-USR-08	The loss of GPS signal for the system shall not lead to safety-critical malfunction of the system.
REQ-USR-09 	DroneCrane shall be fully operated on green energy.
REQ-USR-10 	DroneCrane shall be 80% recyclable or reusable by weight.
REQ-USR-11 	A single drone of DroneCrane shall not weigh more than 25 kg.
REQ-USR-12	A single DroneCrane system shall not cost more than €100 000.

REQ-USR-13	Operation of a DroneCrane system shall not cost more than €5 000 per day.
REQ-USR-14	DroneCrane shall be deployable by six operators in an hour.
REQ-USR-15	DroneCrane shall be operable by two operators.

4.2. Technical Requirements

From the user requirements, technical requirements that limit the design space are created. The system requirements with the respective subsystem requirements are given in Table 4.2, Table 4.3, Table 4.4, Table 4.5.

Table 4.2: Requirements deriving from non-technical regulatory mission constraints.

ID	Requirement
REQ-REG-ENV-1	DroneCrane shall comply with environmental regulations as stipulated by the authorities of the Dutch market.
REQ-REG-ENV-2	DroneCrane shall not produce noise greater than 100 dB at a distance of 10 m AGL.
REQ-REG-AIR-1	DroneCrane shall comply with the Dutch airspace regulations corresponding to its product category.

Table 4.3: Requirements generated from operational mission blocks, power, and propulsion.

ID	Requirements
REQ-OPR-WEA-1	DroneCrane shall be operable with wind speeds up to level 5 on the Beaufort scale [16].
REQ-OPR-WEA-2	The drone shall have an IP rating of at least 4 for protection against water.
REQ-OPR-PER-1 🔑	DroneCrane shall have a flight time of 30 min with a payload of 500 kg.
REQ-OPR-PER-2	DroneCrane shall have a flight time of 60 min with a payload of 100 kg.

Table 4.4: Requirements generated for the communication system, the swarm, and the structural subsystems.

ID	Requirements
REQ-SCC-STB-1	The swarm configuration shall be able to be stabilised with the control system under all specified conditions.
REQ-SCC-MAN-1	The swarm configuration shall be able to travel at 1.5 m s^{-1} vertically.
REQ-SCC-PER-1	The swarm configuration shall be capable of hovering for 15 min.
REQ-STR-INT-1	Vibrations induced by the drones on the payload attachment structure shall not match its natural frequency.

Table 4.5: Requirements generated for communication.

ID	Requirements
REQ-COM-S&R-1	Any digital wireless communication link of DroneCrane shall be encrypted.

The rationale behind some of the requirements will now be discussed. The ones that are not discussed are deemed trivial.

- **REQ-OPR-WEA-1**: The Beaufort wind resistance level is a measure of the range of wind speed in which the drones are still operable. A Beaufort wind resistance level of 5 shows that the system shall be operable under wind speeds up to 10.73 m s^{-1} . This was determined from analysing different drones in the current market and ensuring that operations are possible under a variety of wind speed conditions [16].
- **REQ-OPR-WEA-2**: An IP rating for protection against water is obtained from a standardised test, and this will determine the extent of waterproofness of the drone and its readiness for operation under rainy conditions. An IP rating of 4 will certify that the drones are operable under drizzle conditions.
- **REQ-OPR-PER-1** and **REQ-OPR-PER-2**: These requirements are based on the market analysis. Considering the performance of the competitors of DroneCrane, it was determined that for a payload mass of 500 kg a flight time of 30 min would be adequate. Similarly, for a payload mass of 100 kg, a flight time of 60 min was decided upon.
- **REQ-SCC-MAN-1**: The vertical speed was chosen such that DroneCrane is competitive within the market identified in Chapter 3.
- **REQ-SCC-PER-1**: The hovering time was chosen such that DroneCrane will be able to fulfil its purpose within the targeted market such as wind turbine maintenance and the installation of 5G antennas.

4.3. Operational Requirements

The logistics and operations of DroneCrane have a critical role for the usage of the design. For this reason, several requirements are created to assure the completion of the mission. In order to simplify the operations, the mission has been divided into 5 parts: transportation, set-up, usage, end, and maintenance. The requirements for each of the part are displayed in Table 4.6, Table 4.7, Table 4.8, Table 4.9, and Table 4.10 respectively.

Table 4.6: *Transportation requirements*

ID	Requirement
REQ-OPR-TSP-01	The length of any element shall be under 4 m.
REQ-OPR-TSP-02	The width of any element shall be under 2 m.
REQ-OPR-TSP-03	The weight of each LFRS segment shall be under 25 kg.
REQ-OPR-TSP-04	The frame of the drone shall be retractable.
REQ-OPR-TSP-05	The landing gear of the drone shall be retractable.

Table 4.7: *Set-up requirements*

ID	Requirement
REQ-OPR-SET-01	The time needed to take out all the drones and connect them shall be lower than 30 min.
REQ-OPR-SET-02	The time needed to assemble the LFRS shall be under 10 min.
REQ-OPR-SET-03	The boot time of each drone shall be under 30 s.
REQ-OPR-SET-04	The boot and set-up time of all the controllers shall be under 5 min.
REQ-OPR-SET-05	The in-air swarm formation shall be initialised under 3 min.
REQ-OPR-SET-06	The drones shall have labels.

REQ-OPR-SET-07 | The rope connecting device shall be able to attached under 5 seconds.

Table 4.8: Usage requirements

ID	Requirement
REQ-OPR-USG-01	DroneCrane shall have a continuous rate of operability of at least 2 hours/day.
REQ-OPR-USG-02	The range of transmission device in the drone shall be greater than 500 m.
REQ-OPR-USG-03	The range of transmission device in the ground controller shall be greater than 500 m.

Table 4.9: End of mission requirements

ID	Requirement
REQ-OPR-END-01	Different components of the system shall be available for inspection after a mission is completed.

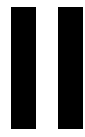
Table 4.10: Maintenance requirements

ID	Requirement
REQ-OPR-MTC-01	The battery pack change of each drone shall take less than 1 min.
REQ-OPR-MTC-02	The charging time for the battery shall be less than 1 h.

The rationale behind some of the requirements will now be discussed. The ones that are not discussed are deemed trivial.

- **REQ-OPR-TSP-01 & REQ-OPR-TSP-02** : The length of an element is limited by the dimensions of the transportation system. As a reference the Mercedes-Benz Sprinter Luton was chosen, where the maximum cargo length is 4080 mm and the maximum cargo width is 2025 mm ¹¹.
- **REQ-OPR-TSP-03** : For the feasibility of the operation, each segment of the LFRS shall not weigh too heavy otherwise the operators may have difficulties setting up the LFRS and may take too much time.
- **REQ-OPR-SET** : The requirements in this category specifies a set up time for each stage of the preparation to ensure that the overall set up time stays within 1 hour.
- **REQ-OPR-USG-01** : The continuous rate of operability ensures that a certain number of operations can be completed per day and the down time between each operation is not too large. This will increase the possible income per day.
- **REQ-OPR-USG-02 & REQ-OPR-USG-03** : This requirement ensures that that the ground controller and the drone can communicate throughout the entire operation without failure. The range of transmission is greater than 200 m, which is our maximum operating height AGL, to compensate for horizontal movement of the system.

¹¹<https://www.mercedes-benz.co.uk/vans/en/sprinter-luton> [Accessed in June]



Design Setup

5. Preliminary Design

In this chapter, a summary of the trade-off of DroneCrane’s design performed in the midterm report is given [9]. The trade-off was performed with the Analytic Hierarchical Process (AHP). In this chapter, an overall description of all aspects tied to this trade-off is presented. Section 5.1 gives a summary of the design options available for each subsystem. Consequently, Section 5.2 discusses the trade-off method used and the outputs are summarised in Section 5.3. Finally, a sensitivity analysis was performed and the results are described in Section 5.4.

5.1. Summary of Designs

This section was written by: *Ojas*

The trade-off started with 4 primary design options, as seen in Table 5.1. These designs were created after a thorough analysis of all possible configurations and options for all subsystems.

Table 5.1: Description of all 4 design options.

	Design 1	Design 2	Design 3	Design 4
Drone	Star-shaped octocopter	Co-axial octocopter	Co-axial octocopter	N-copter
Swarm	Centralised	Decentralised	Clustered	Decentralised
Attachment	Without LFRS	With LFRS	Without LFRS	With LFRS
Propulsion	Unducted	Ducted	Unducted	Ducted
Power	Ground-based	Individual	Dedicated carrier	Individual

An explanation for each of the possible options is listed below:

- **Star-shaped octocopter:** Octocopter with all propellers in the same plane.
- **Co-axial octocopter:** Octocopter with pairs of propellers in the same vertical plane.
- **N-copter:** Drones with more than eight propellers, in a conventional one-plane configuration
- **Centralised swarm:** All calculations are performed by a single computer on a single drone, while all other drones simply follow the commands.
- **Decentralised swarm:** All drones have a flight computer and perform their own calculations, while communicating with the other drones.
- **Clustered swarm:** Similar to the centralised, except that there are multiple groups of follower drones, all with one brain drone, which communicates with the other brain drones.
- **LFRS:** Lateral force relief structure, which is placed between the payload and the drones. Its goal is to remove any need of an angled flight during vertical climb.
- **Ducted propellers:** Propellers, which are surrounded by a duct. The effect of the duct is a higher efficiency of the propellers by reducing tip losses, with the disadvantage of additional weight and complexity during manufacturing.
- **Ground-based power:** Power is provided to the system through a wire from a ground station.
- **Dedicated power carrier:** One or multiple drones carry the bulk of the batteries.
- **Individual power:** Each drone carries its own batteries.

5.2. Trade-off Method

This section was written by: Ojas

The Analytic Hierarchical Process (AHP) is a decision making process that aims to simplify group decision making. It relies on pair-by-pair comparisons for deciding criteria weights, as well as scoring options on those weights [17]. The process contains three parts: the problem that is aimed to be solved; the possible solutions, known as alternatives; and the different criteria that the alternatives will be judged on. The objective of AHP is to provide a methodology to fairly and rationally select an option in a structured way in contrast to other methods.

To implement AHP for our trade-off process, several criteria were carefully defined for each of the subsystems. Once these were formulated, they were further categorised into five overarching sets. These criteria then would become the basis of the trade-off. Structuring the criteria in this way gives the team a good idea on which subsystems are connected to which category, which allows for an overall easier analysis.

Once the criteria were categorised, a pair-by-pair comparison was made, first for the categories and next for the criteria themselves. This was done by all group members, in order to eliminate any outliers that could surface in one member’s grading and to increase the robustness of the trade-off. Additionally, once the comparisons were completed, a group consensus of 78.8% was found, leading to the conclusion that the team agreed, for the most part, on what the most important factors were. A breakdown of all the category and subcriteria weights can be seen in Figure 5.1

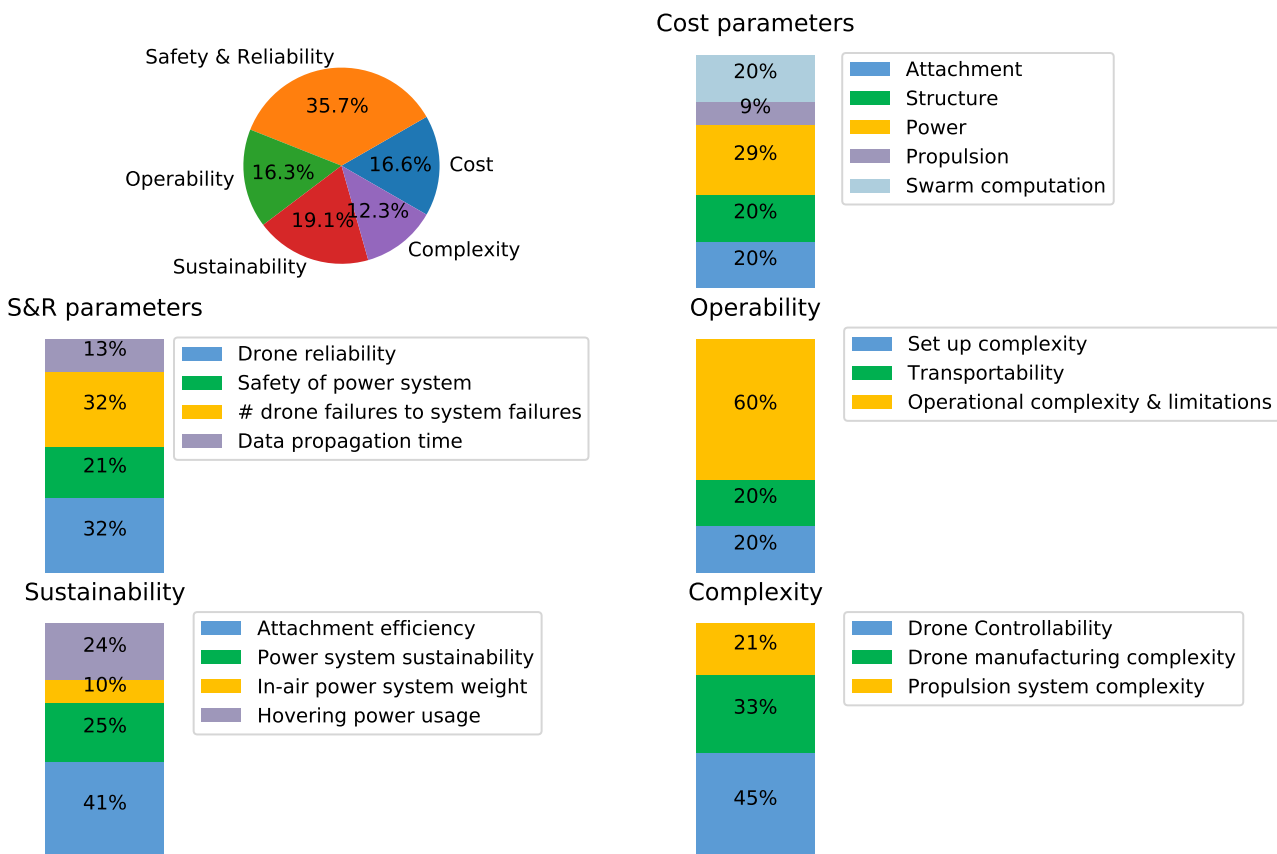


Figure 5.1: Distribution of weights in terms of categories and subcategories (own work).

dAs for the scores themselves, AHP is also used in this regard. The scoring consisted of, once again, pair-by-pair comparisons for all of the subsystems. These were mostly done with the input of the heads of departments, as they had the highest amount of information and could provide quantitative assessments. The pair-by-pair comparisons resulted in ratings for each of the subsystems, which allowed the group to choose the best design. The use of AHP assures that the scores for all subsystems

stay consistent and provide a reliable trade-off result. These ratings, as well as their implications, will be discussed in the following section.

5.3. Trade-off Summary

This section was written by: *Maxim, Ojas*

As mentioned previously, the trade-off was done through a pair-by-pair comparison, similarly to the weights. The results of the trade-off are shown in Table 5.2. The scores in each category sum up to 100, in order for the weighting to be applied consistently. Next to it, Table 5.3 shows the rating of the individual subsystems for all of the concepts.

Table 5.2: Trade-off scoring of the four designs.

Category	Cost	Safety & Reliability	Operability	Sustainability	Complexity	Total score
Weight	0.166	0.357	0.163	0.191	0.123	1
Design 1	25.1 Yellow	19.9 Red	21.5 Red	22.8 Red	32.4 Green	23.1
Design 2	23.0 Red	36.4 Green	25.8 Yellow	32.5 Green	15.4 Red	29.1
Design 3	29.7 Green	17.9 Red	26.9 Green	12.0 Red	21.5 Red	20.7
Design 4	22.3 Red	25.8 Yellow	25.8 Yellow	32.7 Green	30.7 Yellow	27.2

Table 5.3: Subsystem Scores

	Design 1	Design 2	Design 3	Design 4	Design 5	Winner
TOTAL	23.11	29.11	20.65	27.15	34.53	
Power	4.48	10.25	4.33	10.25	10.25	Individual batteries
Attachment	4.36	4.47	4.36	4.47	4.47	With attachment
Propulsion	2.46	1.98	2.49	2.02	2.49	Unducted
Swarm	2.91	8.43	5.50	2.91	8.43	Decentralised, identical
Drone	8.89	3.97	3.97	7.50	8.89	Conventional octocopter

From the preliminary results, it can be seen that the four designs are very close to each other in terms of the score. However, the scores for the individual categories vary depending on which subsystems were selected for each option. Therefore, in order to have the best possible outcome, a fifth concept was created. This concept was based on the subsystems that scored the highest during the trade-off. This resulted in a decentralised swarm of conventional octocopters, with a support structure present between the drones and the payload. The power is provided from individual batteries and the propellers are unducted. The final score of the new design is shown in Table 5.4. As can be seen, the new design wins or ties in cost, safety & reliability and complexity, barely loses out in operability, while staying very competitive in sustainability. Therefore, it comes out as the winner of the trade-off.

Table 5.4: Trade-off scoring of the new fifth design.

Category	Cost	Safety & Reliability	Operability	Sustainability	Complexity	Total score
Weight	0.166	0.357	0.163	0.191	0.123	1
Design 5	29.9 Green	44.3 Green	25.8 Yellow	29.1 Yellow	32.4 Green	34.5

5.4. Trade-off Sensitivity Analysis

This section was written by: *Ojas*

As seen in Section 5.3, the final scores of the initial 4 designs were very close. This could mean that by slightly changing the weights of individual criteria, the design ranking would swap around. Design 5 combines the best aspects of each of the concepts, and as such, is expected to score better than all of them. This is, however, not guaranteed, and to confirm that the chosen design is indeed the best option, a sensitivity analysis must be performed.

To investigate the sensitivity of the choice of the final design option to changes in weights, the weights of the 5 primary categories were changed. Every category was allowed to take on a weight between 2% and 50%, with steps of 2%. Furthermore, given that the purpose of this analysis was to explore the sensitivity of the result, if a result only changes with extreme modifications to the weights, it was neglected in the final result. This resulted in over 148 000 different options, with the chosen design, Option 5, winning 99.2% of the time. Designs 2 and 4 won 0.06% and 0.74% of the time, respectively. This in itself gives great certainty that Design 5 is the best option, and should be taken into the detailed design phase.

However, this assumes that the scores for the categories are fixed; yet these depend on the weights of the subcategories themselves. For the most part, the group consensus on these was high, and minor changes did not result in any meaningful changes on the final results. However, the category of cost represents an exception to this. Here, the group only had an AHP group consensus of 52%. It was therefore decided to also explore the sensitivity of the chosen design option to weights within this category. All the different inputs for the weights within this category were investigated, and the most critical chosen, so that the previously chosen sensitivity analysis could be performed again, yet this time with differing points for the cost category due to the changed weighting within the criteria itself. This resulted in slightly different winning frequencies for the different design options, yet this was not significant enough to change the winning concept, as seen in Figure 5.2

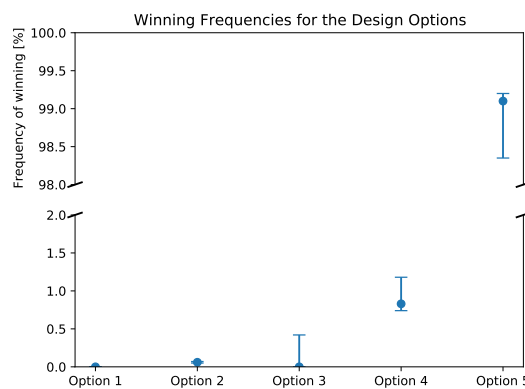


Figure 5.2: *Winning Frequencies for the different designs (own work).*

It can be seen that Design 5 is by far the strongest option. It wins about 99 times more than the next closest option. The only scenario when Design 5 does not win occurs when Safety & Reliability is undervalued. The highest weight this criteria gets in this case is 14%, so even less than if the criteria were equally distributed. In addition, the Sustainability criteria is overvalued when Option 5 does not win. If it is weighted below 26%, Design Option 5 always wins. This indicates that Option 5 is in fact the desired option. Safety & Reliability is an important criteria for this project, and must be weighted accordingly. This in itself is a reason to discard the cases, where Option 5 is not the winner. Although Sustainability is an important aspect, this should not come at the expense of Safety & Reliability.

With this explored, it was stated with confidence that Design Option 5 is the definitive winner of the trade-off and the team can move on to the detailed design.

6. Sustainability

Designing for the future means more than just creating a design that performs well. Nowadays it is also important that a design is sustainable. It should be made out of recyclable materials, make use of renewable energy sources and has a high durability. DroneCrane has been designed with sustainability in mind from the start, using recyclable materials whilst minimising weight to save energy.

This chapter gives an overview of the sustainability approach used in the power, propulsion and structure subsystems in Section 6.1, Section 6.2, and Section 6.3 respectively. Finally, the chapter is concluded with Subsection 6.3.1 where the characteristics of materials that could be used for the batteries and for the structures are listed.

6.1. Electrics

This section was written by: *Tyme*

The main aspects of sustainability in electric systems involve energy storage system and the source of power. In this section both of these aspects will be analysed and a solution to reduce the impact of the electrics subsystem on the environment will be proposed.

6.1.1. Re-usability

For the energy storage, it is important to select a system that is re-usable or recyclable, as disposing energy storage systems may pose hazardous threats at waste sites, particularly with batteries due to the reactivity of the chemicals contained within the cathodes [18]. Furthermore, the waste in the batteries contain critical materials, that are subjected to supply risks, such as Cobalt, Nickel, Lithium etc. [19]. Therefore it is important for DroneCrane to come up with a strategy to prolong the life of the batteries by refurbishing and finding a feasible second use for these batteries, and extracting the materials found in the batteries for recycling purposes.

The use of Lithium-Ion batteries had been increasing substantially in the past years, due to the rise of demand of electric vehicles and a growth in the electrical vehicle market. The Lithium-Ion battery market is expected to expand at a CAGR of 15.3 % from 2022 to 2030 [20]. The production of these batteries and the extraction of the materials cause negative social and environmental impacts, such as depleting local source of water supply and polluting nearby regions [21]. Furthermore, with the current growth rate a global supply shortage of certain materials contained in the battery can be expected, therefore a push towards a circular economy for batteries is of utmost importance [22].

With increasing demand of the batteries, more investments are being supplied to the end of life dismantling of batteries providing better alternative solutions to recycling and reusing batteries. As considerable value is embedded in Lithium Ion batteries, it had been suggested that their use should be cascaded through the waste-management hierarchy to optimise material use and life cycle impact [23]. The waste management system hierarchy is a concept which ranks the waste management options from most to least environmentally friendly as seen in Figure 6.1.

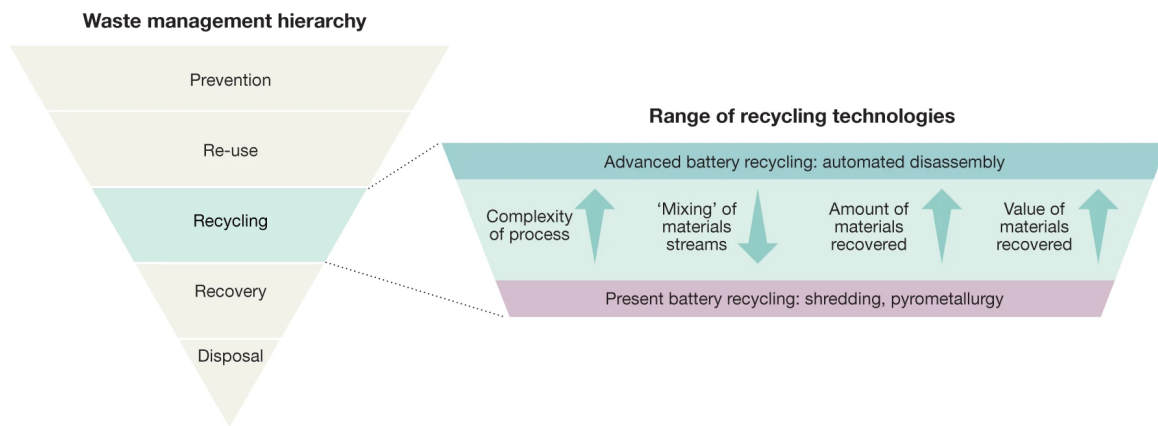


Figure 6.1: Waste Management Hierarchy [23].

According to the waste management hierarchy, re-use is preferable over recycling as it extracts maximum economic value and minimises environmental impact, therefore once the batteries used in DroneCrane have reached its end-of-life the priority will be focused on finding a second-use for the batteries. Second-use battery projects have started to develop in locations with regulations and market alignments, particularly for stationary energy storage application where lower current density is required. However, the supply of second use battery is larger than the demand, which means that re-using the batteries is not always an option and recycling must also be considered.

Stationary energy storage application includes utility-scale grid, buildings and telecommunication tower storage [24]. In order to re-use the batteries, the State of Health (SOH) of the batteries must have a value of 80 %, then batteries with similar power and life are sorted and re-assembled into new battery packs [24]. The SOH is the ratio of the maximum battery charge to the rated capacity. DroneCrane will not perform this procedure itself, but will provide the batteries to an external third party source to re-purpose and distribute the batteries. To ensure that the batteries provided possess the desired adequate properties, the SOH of the batteries will be monitored throughout its lifetime to ensure that it does not drop below 80 %. In order to determine the SOH of the battery, the Coulomb Counting method will be implemented, where a charging/discharging current will be measured and integrated over time to calculate the remaining energy within the battery [24]. The end-of-life usage of batteries will be reached after 500 cycles of charging/discharging, where the SOH is expected to be greater than 80 %, which assuming that two operations per day takes place, will take approximately 250 days to reach its end of life stage.

To ensure that the batteries are adequately monitored a strategy is implemented, where at the end of each operational day, the SOH of one sample battery from each drone will be measured and stored in a database, to view the trend of the SOH and to ensure that the value remains above 80 % . Once the batteries have reached this limit, the operational use of the batteries will be terminated, stored and then distributed to external third parties which re-purposes the batteries. However, if the demand of the second-use battery is low or the SOH of batteries falls below the 80 % mark, then recycling is considered. This process will both benefit the feasibility of the batteries for recycling and the performance of the batteries itself.

6.1.2. Recycling

Recycling batteries has been a difficult task to achieve, due to the limited technology available for recycling. It is typically an expensive, energy intensive and environmentally unfriendly task. However, with the increase in consumption of Lithium-Ion batteries over the previous years more investments have been flowing into this field and different companies are finding alternative solution for a more efficient method of recycling batteries. The main materials extracted during the recycling process are found in the cathode. Typically, recycling processes refurbishes the cathode in order to manufacture a new one for a new battery. A study formed by X. Ma et al. discovered that recycled LiNi/Mn/Co/O batteries has a superior rate and cycle performance than a new battery [25]. This offers great potential

for the adoption of recycled batteries in commercial industries.

Due to the high complexity and high cost associated with recycling batteries, DroneCrane will not facilitate the process of recycling itself, but will supply an external third party with the batteries. There are several companies which have a highly sophisticated method for recycling batteries, which allow up to 91 % extraction of materials and does not emit any hazardous gas ¹². To give an insight on the process, the recycling method applied by Duesenfeld, a battery recycling company based in Germany, will be further examined.

The recycling method consists of a combination of mechanical, thermodynamic and hydrometallurgical processes. The whole process can be seen in Figure 6.2.

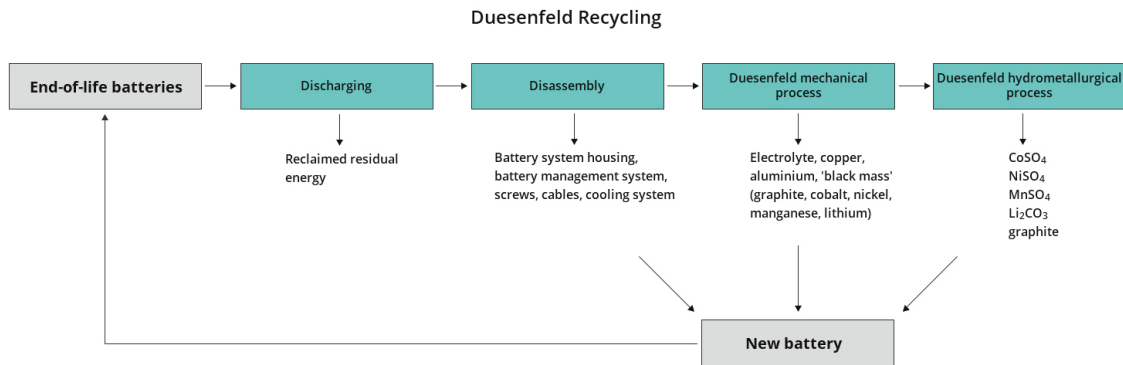


Figure 6.2: Recycling process of Lithium Ion battery. ¹²

After discharging and disassembling, the remaining battery goes through a mechanical process, where the batteries are shredded under an inert gas and the electrolytes are extracted through a process of vacuum distillation. The remaining shredded material are separated based on physical properties then further processed metallurgically. The iron, copper and aluminium extracted are then sent for further recycling. To process the electrode active materials such as Cobalt, Lithium and Nickel a hydrometallurgical process is performed. The distribution of the collected materials compared to the entire composition of the battery is shown in Figure 6.3. The culmination of all the materials allow for manufacturing of a new battery.

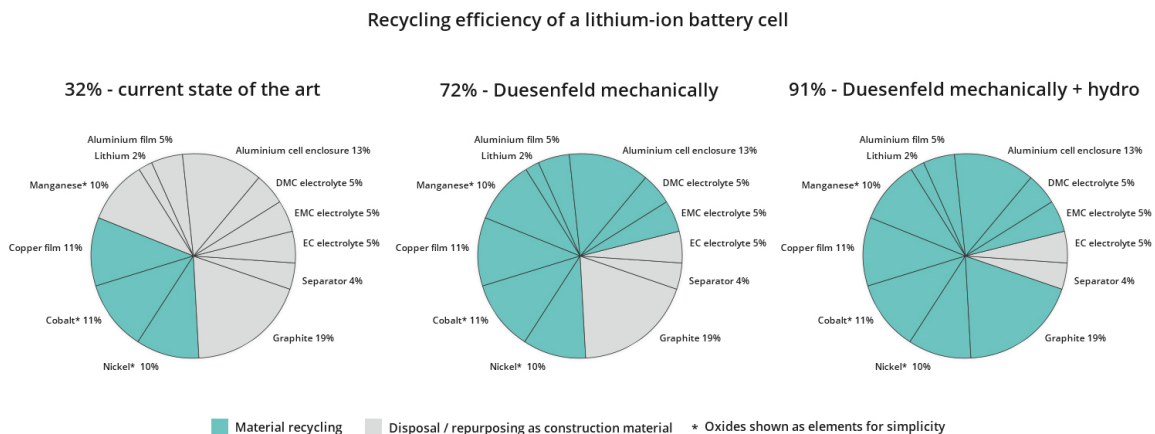


Figure 6.3: Recovered material from Lithium-Ion battery. ¹²

This process compared to conventional method allows for more than twice the material recovery rate,

¹²https://www.duesenfeld.com/recycling_en.html [Accessed in June 2022]

through mechanical processing where electrolytes are recovered, and the CO_2 produced is 8.1 tons less per one ton of battery produced compared to primary extraction methods of raw materials ¹².

6.2. Propulsion

This section was written by: *Maxim*

For propulsion, the sustainability revolved mainly around the energy consumption. This is due to the fact that a lower energy requirement leads to a lower amount of batteries. Despite the explanations given in the previous section, batteries are inherently difficult to recycle and have a relatively clear and unavoidable degradation. Thus, having as few of them as possible makes the overall design much more sustainable. On top of that, batteries turned out to be the largest mass contributor. Therefore, lowering the number of batteries will have an even larger snowball effect on the final product.

Another important factor is the efficiency of the motors. Following the same logic, the higher the efficiency, the lower the amount of batteries. Therefore, a good match between propeller and motor needs to be found, in order to maximise the transformation of electrical power to mechanical power.

When it comes to the propellers and motors themselves, not much can be done about their sustainability, since they are not designed but simply chosen off-the-shelf. Of course, aspects such as the materials used for the motor and propeller play a role, but may end up being ignored due to the parts being the only plausible choice. One way to circumvent this would be to actually design and manufacture the parts. While this is outside of the scope of this project, it is something that could be considered further in the future, and is discussed in more detail in Chapter 13.

6.3. Structures

This section was written by: *Robin and Dequan*

In the structures department there were two main considerations. The first is to create a structure that is as light as possible, which not only reduces usage of material, but can impact the weights and sizes of the drones due to a decrease in the total weight that needs to be carried. Apart from optimising a structure, the material choice is incredibly important and influenced greatly by the sustainability of a material. Novel materials were sought in order to meet all requirements within the structures and the limits imposed by requirement on recyclability.

When it comes to the manufacturing of the structures, there is also a great influence on sustainability. As will be explained in 12.8 the decision was made to select a variant of CFRTP, or Carbon Fibre Reinforced Thermo Plastics. This material has not been used much in industry, but is gaining traction and is much easier to recycle than the more commonly used CFRP, or Carbon Fibre Reinforced Polymers. Furthermore, the manufacturing methods have also been influenced. Methods that create more waste material, such as sheet lamination, a process within the additive manufacturing, was discarded. Instead, the preference was given to another process that could reduce weight, perhaps at the cost of complexity. More about manufacturing can be read in Section 12.8. Next the potential choice of materials used will be considered.

6.3.1. Material Characteristics

For further analysis and calculations in the later design phase, the characteristics of materials potentially used for several parts of DroneCrane are defined.

The two most important properties of structural materials are weight and strength [26]. Therefore, the parameters such as density, yield stress, E-modulus are interesting here and are listed in Table 6.1. This data is gathered from material databases such as MatWeb¹³ and MatMatch¹⁴. In addition, properties such as corrosion resistance need to be taken into consideration while choosing material, due to the special outdoor environment that DroneCrane might be operating in.

The commonly used materials for drone frames are aluminium alloys, magnesium alloys, titanium alloys, carbon fibre and thermoplastics, including polystyrene, polyester, and nylon [26, 27]. Aluminium

¹³<https://www.matweb.com/> [Accessed in May 2022]

¹⁴<https://www.matmatch.com/> [Accessed in May 2022]

alloys are one of the most frequently used and successful materials in the aerospace industry due to their light weight and strength [28]. Titanium alloys are also regularly used in aircraft and spacecraft for their high performance in strength [29]. Thermoplastic polymers are inexpensive and could be made into complex parts using injection moulding [26]. Carbon fibre has a very low weight but has a chance to block radio signals. Magnesium alloys such as AZ91D have been proven by being applied to the mature product DJI Mavic Air. They have advantages such as high strength, high resistance to corrosion and ease of manufacture [27]. For each material above, several specific materials that were used or could be used in drones are found shown in Table 6.1.

Table 6.1: Structural material characteristic.

Material	Density [g/cm ³]	E-Modulus [GPa]	Yield Stress [MPa]	Ultimate Stress [MPa]	Poisson's Ratio [-]	Elongation [-]	Fatigue Strength [MPa]
MG-AZ91D-F¹⁵	1.81	44.8	150	230	0.35	0.03	N.A.
Compound WF006XXP¹⁶	1.53	9.3	N.A.	125	N.A.	0.02	N.A.
Elix ABS M205FC¹⁷	1.005	2.5	50.5	36.5	N.A.	0.15	N.A.
Nylon PA12 3D¹⁸	1.02	1.4	N.A.	51	N.A.	0.5	N.A.
Al-2024-T8510¹⁸	2.78	72.4	448	483	0.33	0.07	117
Al-6061-T6¹⁹	2.7	68.9	276	310	0.33	0.17	96.5
Al-7075-T6²⁰	2.81	71.7	572	503	0.33	0.11	159
Ti-6Al-4V²¹	4.43	114	1100	1170	N.A.	0.1	N.A.
Ti-6Al-2Sn-4Zr-2Mo²²	4.54	118	1050	1110	0.325	0.13	N.A.
Carbon Fibre T300²³	1.6	240	N.A.	3400	0.25	0.017	N.A.
Carbon Fibre T700²³	1.6	250	N.A.	4900	0.25	0.017	N.A.
CFRTP (Nylon Matrix) [30]	1.8	137	N.A.	1400	0.25	0.017	N.A.

¹⁵<https://www.matweb.com/search/DataSheet.aspx?MatGUID=07baafbb9c364fb18fd413bceced867f> [Accessed in May 2022]

¹⁶<https://matmatch.com/materials/sabi007740-lnp-thermocomp-compound-wf006xxp-> [Accessed in May 2022]

¹⁷<https://matmatch.com/materials/elpo0019-elix-abs-m205fc> [Accessed in May 2022]

¹⁸<https://www.matweb.com/search/datasheet.aspx?matguid=bb241e7d15fd46eca8b1ff8c171a1ea9> [Accessed in May 2022]

¹⁹<https://www.matweb.com/search/DataSheet.aspx?MatGUID=b8d536e0b9b54bd7b69e4124d8f1d20a&ckck=1> [Accessed in May 2022]

²⁰<https://www.matweb.com/search/DataSheet.aspx?MatGUID=4f19a42be94546b686bbf43f79c51b7d&ckck=1> [Accessed in May 2022]

²¹<https://kyocera-sgstool.co.uk/titanium-resources/titanium-information-everything-you-need-to-know/ti-6al-4v-grade-5-titanium-alloy-data-sheet/> [Accessed in May 2022]

²²<https://www.azom.com/article.aspx?ArticleID=9298> [Accessed in May 2022]

²³<https://matmatch.com/materials/jinj0001-t300-carbon-fiber-sheet> [Accessed in May 2022]

7. Design Iterations

After having selected the configuration of the final design, its sizing needs to be performed. This chapter discusses the approach used to iterate over the different subsystems sizing and the process used to select off-the-shelf components.

Section 7.1 shows the method used to run the iteration with all the subsystems combined. Consequently, the approach used in the propulsion, the power and the structure departments is explained in Section 7.2, Section 7.3, and Section 7.4 respectively. In addition, Section 7.5 gives an overview of the verification performed on the program. Finally, the chapter is concluded with Section 7.6 that shows the high level results obtained from the iteration and Section 7.7 which discusses the sensitivity analysis that was carried out to check the robustness of the final design.

7.1. Overall

This section was written by: *Ojas, Tyme*

In Section 5.3, the final design was evaluated and chosen via a trace-off method, and in this section the different properties of each subsystem are further refined via a program. Due to the dependencies between each of the subsystem, an iterative process is performed in order to converge to a final design. In this section, the structure of the code and the iterative process will be explained.

7.1.1. Code overview

An object orientated programming approach is used for the iterative process. The entire system of DroneCrane is initialised as a Design class, and the resulting structure of the initialisation process is shown in Figure 7.1.

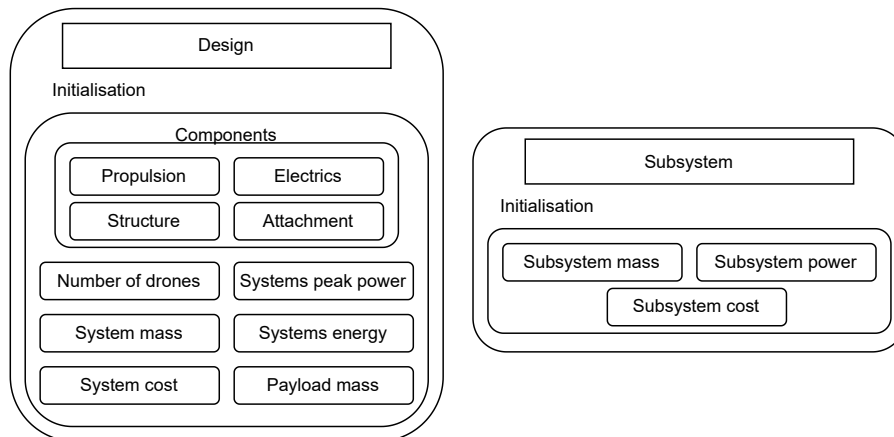


Figure 7.1: *Initialisation of classes (own work).*

As seen in Figure 7.1, the design is initialised with the number of drones, the peak power, the mass, the cost, the energy, the mass of the payload and a list called components, which includes the different subsystems. Furthermore, each subsystem itself inherits the Subsystem class, where the mass, the power and the cost of the subsystem are defined.

Furthermore, each subsystem also inherits two functions, Refresh Characteristics and Print, from the Subsystem class. The Refresh Characteristics function will update all the parameters of that particular subsystem based on the state of the Design class, and the Print function will print out the parameters.

7.1.2. Structure of the code

The Design class contains 3 functions: Iterate, Inner Iteration and Outer Iteration. The Iterate function calls the Refresh Characteristics function of each subsystem, updating their parameters. Then it sums the mass, the cost, the power and the energy of all the subsystems and stores the results. The Inner Iteration function calls the Iterate function until the mass, power and energy of the system converge. This is defined as two successive iterations having a difference of less than 1%. Finally, the Outer Iteration function calls the Inner Iteration function over a range of different number of drones and plots the mass and cost of the system. This Outer Iteration function itself was run multiple of times, over a range of different system area restrictions until the Design goal is achieved

In order to execute the code, the Outer Iteration function will be ran. Figure 7.2 shows the flow and the structure of the overall code.

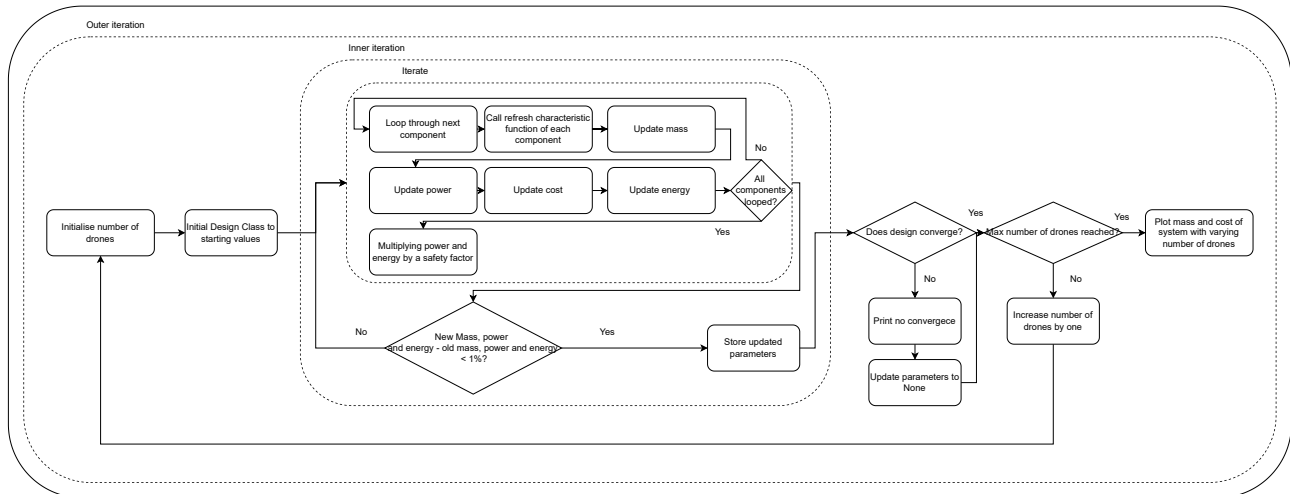


Figure 7.2: Code flow diagram of the iteration process (own work).

The output of the code consists of the mass per drone, the cost of the system and all the stored parameters for each subsystem with varying number of drones.

7.1.3. Dependency of subsystems

The dependency between each subsystem and the inputs and the outputs required are summarised in a N2 chart, shown in Figure 7.3. This gives an insight on the interaction of each subsystem and how the parameters are updated.

Design	Total mass Number of drones	Design power Design energy Number of drones	Total mass Number of drones	Total mass Number of drones
Peak prop. power Mission prop. energy Propulsion cost Propulsion mass	Propulsion		Swarm Diameter	Drone arm length Thrust per drone
EPS mass EPS cost	EPS mass	Electrics		Battery volume
Attachment mass Attachment cost			Attachment	
Drone structure mass	Drone structure mass Drone structure cost			Drone structure

Figure 7.3: N2 chart of the subsystems (own work).

7.1.4. Design space

Finally, now that all the characteristics of each subsystem and the parameters of the systems are calculated, the next step is to determine the method to choose the optimal design.

Due to a large variety of controllable variables of the design, a design space must be defined. Firstly, three requirements are set up to filter out the unfeasible options. Firstly, the mass of each drone must not exceed 25 kg, as stated in [REQ-USR-11](#). Next, the cost of the entire system must not exceed €100 000, as stated in [REQ-USR-12](#).

Next, the operational area of the system will be varied starting from a total swarm diameter of 5 m, then incrementing until a feasible design option that matches the requirement is found .

7.2. Propulsion

This section was written by: *Maxim, Tyme, Giacomo*

The design of the propulsion subsystem was implemented such that the outputs required by the other subsystems, as shown in Figure 7.3, were defined in the propulsion code upon initialisation as the propulsion sizing is the starting point of the iterations. The sizing of the propulsion subsystem was divided in several functions, that can be visualised as blocks in Figure 7.4. To start, the thrust to weight ratio and the thrust required for each drone are calculated based on the current mass of the entire swarm and the mass of a single drone. In addition, two databases are initialised for the propeller and motor selection. These databases were created from off-the shelf components. Consequently, a propeller is selected based on interpolations between thrust required and RPM, RPM and power, and torque and RPM. The propeller with the minimum energy required for the mission is selected. Finally, the motor with the lowest energy required is matched with the selected propeller. Checks on the costs and maximum voltage are performed in order to fulfil the requirements set by the user and the other subsystems. A clear overview of the propulsion sizing implementation is shown in Figure 7.4.

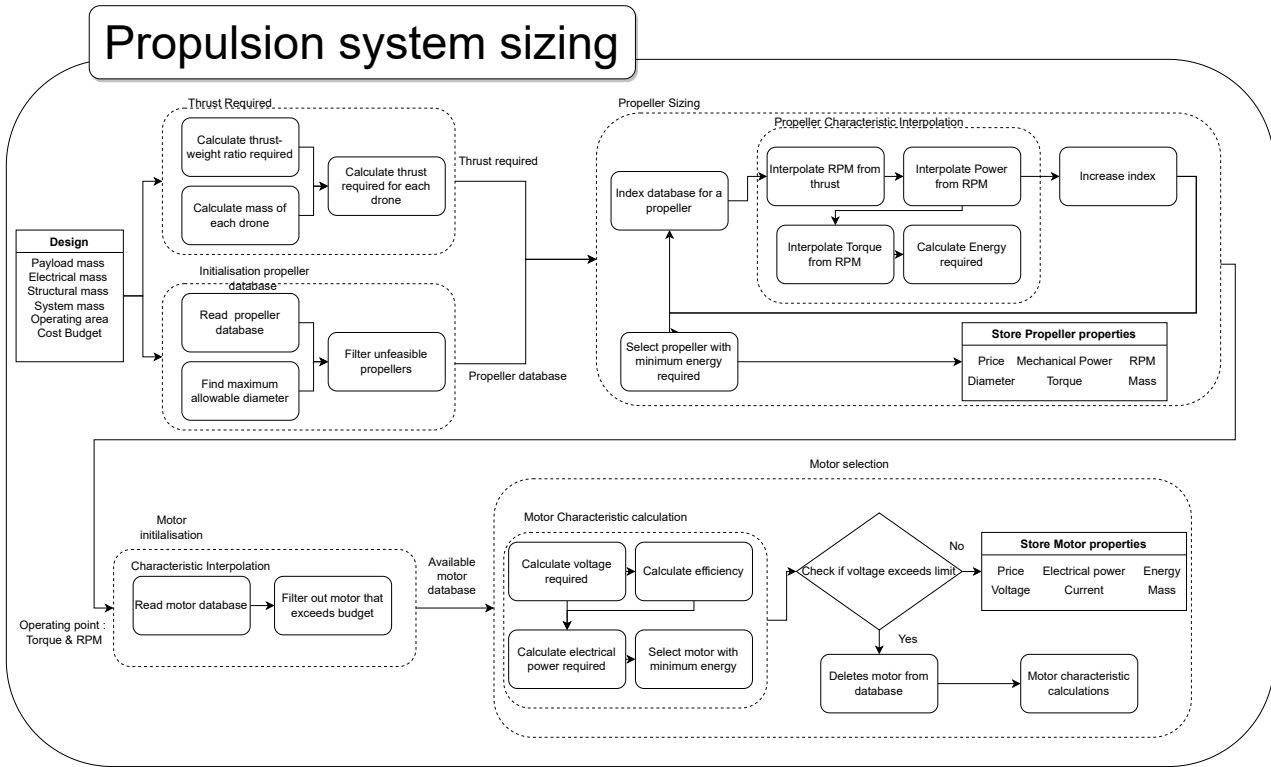


Figure 7.4: Code Flowchart of Propulsive system (own work).

7.2.1. Thrust required

To size the propulsion subsystem the thrust required per rotor is calculated based on the thrust to weight ratio of the system (T/W_{sys}). In order to retrieve the T/W_{sys} , three different phases of DroneCrane's mission are identified: ascending, hovering and descending.

For ascending, the T/W_{sys} must be selected to ensure that the requirements of the designs are met. **REQ-SCC-MAN-1** states that the DroneCrane system shall have a maximum vertical speed of 1.5 m/s [11]. It was decided that the system shall reach this speed within 5 seconds, therefore the required acceleration will be 0.3 m/s^2 .

In order to evaluate the T/W_{sys} required for this acceleration, Newton's second law was firstly used resulting in Equation 7.1.

$$T_{sys} - W_{sys} = M \cdot a_{req} \quad (7.1)$$

Where T_{sys} is the thrust of the system and W_{sys} is the weight of the system. The required acceleration is defined as a_{req} . Dividing by W_{sys} and rearranging the equation, the T/W_{sys} can be calculated as shown in Equation 7.2.

$$\frac{T}{W_{sys}} = \frac{a_{req}}{g} + 1 \quad (7.2)$$

The T/W_{sys} required for ascending was calculated to be 1.03, however an additional 2% is implemented as safety margin to take into account for air resistance. Therefore, a value of 1.05 is used for the T/W_{sys} of the ascending phase.

For the hovering phase, the system needs to reach equilibrium. As a consequence, the T/W_{sys} is considered to be 1. However, an additional margin of 3% was added to ensure that enough thrust can be produced to counteract any external interferences, hence the T/W_{sys} for hovering was chosen to be 1.03.

Finally, the design T/W_{sys} for the descending phase is assessed to be 1. This is due to the fact that for descending, the system has to carry only its own weight, and due to the detachment of the payload, less aerodynamic interference on the system can be expected compared to the two previous aforementioned mission phase.

After defining the required T/W_{sys} for the different phases of the mission, the thrust to weight ratio of the single drone, T/W_{drone} , for each phase can be calculated. Ascending and hovering can be analysed using Equation 7.3.

$$T/W_{drone} = \frac{T/W_{sys} \cdot M_{sys}}{M_{drone} \cdot (n_{drone} - 1)} \quad (7.3)$$

n_{drone} is the number of drones used in the current outer iteration where one drone is subtracted to implement redundancy as required by **REQ-USR-05** [11]. Therefore, if one drone fails the payload can still be lifted and DroneCrane can successfully complete the mission. Furthermore, M_{sys} and M_{drone} are the masses of the system and single drone. The mass of the system includes the payload, the LFRS and the drones themselves, while the mass of the single drone is calculated summing the current values for the mass of the structure, the power subsystem and the propulsion. These values are taken from the previous inner iteration if there was one, or from the initialise values as explained in Section 7.1.

For the descending T/W_{drone} , the payload mass, $M_{payload}$, needs to be removed from the system mass. This is due to the fact that DroneCrane descends when the payload is already detached and delivered to the selected location. Therefore, Equation 7.4 is used to calculate the T/W_{drone} of the descending phase.

$$T/W_{drone} = \frac{T/W_{sys} \cdot (M_{sys} - M_{payload})}{M_{drone} \cdot (n_{drone} - 1)} \quad (7.4)$$

The masses and the number of drones change for every inner/outer iteration leading to new values for the T/W_{drone} of each phase for every iteration. Finally, the thrust required per rotor can be calculated with Equation 7.5.

$$T_{rotor} = 1.1 \cdot \frac{T/W_{drone} \cdot M_{drone}}{n_{rotor}} \quad (7.5)$$

Since octocopters are used for the swarm of drones, the number of rotors, n_{rotor} is equal to 8. In addition, a margin of 10% is implemented in Equation 7.5 to take into account for the change in atmosphere properties when reaching 1000 m above sea level, as due to the decrease in atmospheric density a decrease of 10 % of thrust can be expected [31]. The thrust required per rotor is calculated for all the different phases and it is used as an input for the Propeller Sizing function.

7.2.2. Propeller initialisation

Having found the required thrust per rotor, the next step was to find a corresponding propeller. However, before doing so, different options have to be explored. This was done through importing a database of propellers, which contained the sizes of the propellers and their specifications.²⁴ An example of the database for a propeller of 16 inch can be seen in Table 7.1. Afterwards, an initial estimation of the maximum diameter of a propeller was performed, using the allowed area for operations of the system and the necessary clearances between the drones and the propellers. Equation 7.6 is used to calculate the maximum diameter of the propeller, D_{prop} , where $D_{swarm_{max}}$ is the maximum diameter of the whole swarm, D_{frac} is the fraction of the total swarm diameter that one drone can take up and c_{drone} is the clearance between drones which was set to be one third of the drone diameter to minimise the aerodynamic interference between the rotors [32].

The numbers in the denominator were found using Pythagoras theorem for the arms of the drone including the clearance between propellers, set to be one third of the propeller diameter. The estimation used data for optimal packing of circles into a larger circle, which allowed it to find the maximum diameter of one drone including the clearance.²⁵

²⁴<https://database.tytorobotics.com/propellers> [Accessed in June 2022]

²⁵<http://hydra.nat.uni-magdeburg.de/packing/ci/> [Accessed in June 2022]

$$D_{prop} = \frac{D_{swarm_{max}} \cdot D_{frac} \cdot c_{drone}}{\frac{8}{3\sqrt{2}} + 1} \quad (7.6)$$

During the design of the propulsion system, an important discovery was made. Seeing as the conventional octocopter configuration was not able to provide enough thrust within a reasonable amount of drones or swarm area, research into a different configuration was performed. Research led to the discovery of an octocopter in a two-plane configuration [33] as shown in Figure 7.5.

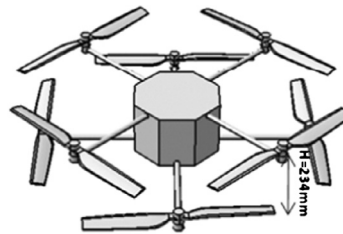


Figure 7.5: Two-plane configuration of the octocopter [33].

This new configuration would allow the team to choose 84% larger propellers, leading to higher amounts of thrust. The interference of the propellers does induce a slight decrease in efficiency of 6%, however this is largely outweighed by the additional thrust. Furthermore, the controllability of this configuration was assessed to be the same as the one of a conventional octocopter therefore not leading to any losses in reliability and robustness of the drone. As such, the decision was made to use this new configuration during the detailed design phase.

From this, the maximum diameter of the propeller can be calculated. This led to a smaller, more manageable design space. However, in order to find the final propeller, further analysis must be performed.

7.2.3. Propeller selection

Sizing the propellers is a very arduous task, there is no direct answer on which propeller should be chosen for which thrust, as multiple propellers can fulfil the same thrust requirement. After performing an initial estimation of the maximum diameter and eliminating the non-feasible options, a list of technically possible designs was left. With this list, the performance of each propeller could be estimated.

The estimation consisted in performing three linear spline interpolation (thrust vs RPM, RPM vs torque, RPM vs power) of the data for each propeller and subsequently calculating the energy required for each option by matching the RPM with the thrust required. This was done for all phases of the flight (ascending, hovering, descending) and their respective required thrusts. Out of these propellers, the one with the lowest energy required was chosen. Its diameter, pitch, mechanical power, required torque, required RPM, mass, and price were stored. Furthermore, the length of the drone arm was calculated using the diameter of the selected propeller and rearranging Equation 7.6. From which the actual diameter of the swarm can be calculated leading to a different area from the one of the input.

The reason for using a linear spline interpolation was that often, in order to acquire the data that was necessary, an extrapolation had to be performed on top of the interpolation. However, this would often lead to skewing the trend of the data, and in certain cases the extrapolation of the data points lead to negative mechanical power. Therefore, the linear spline interpolation was used.

The propeller, however, is not the only part of the propulsion subsystem. The following step is to match the selected propeller with an appropriate motor.

Table 7.1: Specifications of a 16 inch propeller.

Rotational speed [RPM]	Thrust [kgf]	Torque [N · m]	Power [W]
0	0	0	0
729	0.0286	0.0058	0.4458
1216	0.0779	0.0166	2.1208
1650	0.1441	0.0317	5.4884
2142	0.2552	0.0532	11.9328
2594	0.3973	0.0816	22.1809
3029	0.5553	0.1126	35.7245
3550	0.7662	0.1510	56.1540
3944	0.9773	0.1909	78.8432
4345	1.1578	0.2308	105.003
5106	1.6194	0.3167	169.344
5468	1.9164	0.3771	215.950
5843	2.1948	0.4184	256.037
6179	2.4195	0.4755	307.672
6511	2.7081	0.5228	356.477
6787	2.9794	0.5784	411.099

7.2.4. Motor initialisation

Having chosen a propeller, a matching engine which can deliver the required torque and RPM must be selected. However, similarly to the propeller selection, the first step is to setup a database with all possible options. Unfortunately, unlike the propeller database, the engine one had to be created manually, by searching for motors online.²⁶ The database contained the name of the motor, the mass, the price, the Kv value, the internal resistance of the motor, and the no-load current. Having all the engines, a preliminary filtering could be done based on the price of each motor and the number of drones, as the propulsion system could only cost up to €50 000, that is half of the budget. Once these unfeasible options were discarded, the actual motor selection procedure could go ahead.

7.2.5. Motor selection

After creating the database for the motors, the matching with the selected propeller was performed. Equation 7.7 was used to calculate the voltage required to provide the torque and the RPM calculated for the selected propeller based on a circuit model of the motor as seen in Figure 7.6 [34].

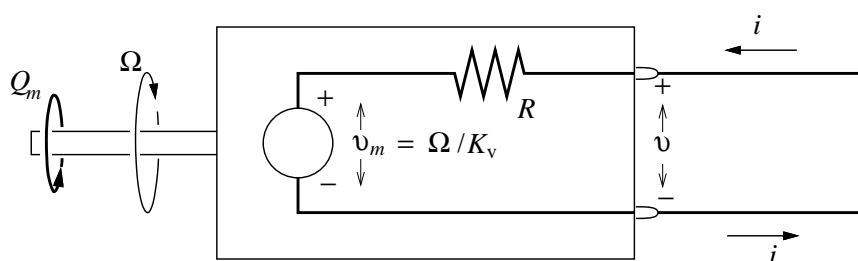


Figure 7.6: Equivalent Circuit for a DC electric motor [34].

$$V = (K_v \cdot Q + i_0) \cdot R + \frac{\Omega}{K_v} \quad (7.7)$$

²⁶<https://uav-en.tmotor.com/> [Accessed in June 2022]

Q is the required torque, R is the internal resistance, Ω is the required RPM and i_0 is the no-load current. The calculation is performed for each phase of the mission and the worst case scenario, namely the highest voltage, is used to match the motor to the propeller. With the required voltage the efficiency of the motor can be calculated using Equation 7.8 [34].

$$\eta = \left(1 - \frac{i_0 \cdot R}{V - \frac{\Omega}{K_v}}\right) \cdot \frac{\Omega}{V \cdot K_v} \quad (7.8)$$

From the efficiency of the motor and the mechanical power retrieved from the propeller selection, the electrical power needed to reach the required performance can be calculated using Equation 7.9. The mechanical power used in this equation corresponds to the sizing phase of the mission which led to the highest voltage in the previous calculation.

$$P_e = \frac{P_m}{\eta} \quad (7.9)$$

Furthermore, using the electrical power and the voltage, the current is also computed using Equation 7.10.

$$I = \frac{P_e}{V} \quad (7.10)$$

Finally, the motor which requires the lowest electrical energy is selected to be the match for the chosen propeller. However, a check on the voltage needs to be performed. This is due to the fact that certain motors, which required voltages higher than 50 V to reach the required performances, were selected. Voltages higher than 50 V were assessed to be unfeasible to reach for the power subsystem. As a consequence, a maximum of 50 V was set as a constraint. If the motor selected does not meet the constraint the motor is deleted from the database for that inner iteration and the selection of the motor is re-run. When a matching motor is found, the price, the electrical power, the voltage, the current, the energy and the mass are stored.

7.3. Electrics

This section was written by: *Aaron*

The electrics affect the design mainly through the related mass and cost, while volume was deemed to be of lower importance and was hence not considered in the iterative tool. First, the battery sizing will be discussed. Afterwards, the other electrical components, i.e. the flight controller, transceivers, and sensors, will be considered.

7.3.1. Battery Sizing

The data of some promising battery cells such as the Samsung INR21700 series and the Keppower IMR26650 series was collected and stored into a small database.^{27,28} Based on the preliminary design [9], it was determined that the batteries should be optimised for mass. The cost and volume corresponding to the choice of a battery cell could afterwards be checked to ensure the design remained feasible and within bounds set by the requirements.

For every battery cell type, the required number of battery cells is determined with respect to the peak power requirement as well as the mission energy requirement. The peak power situation has to be assessed since the battery packs should be capable of discharging at a rate that delivers that power. Next to that, the mission energy is assessed to ensure the battery packs have enough capacity to provide the energy for the entire mission.

The peak power and mission energy follow practically entirely from propulsive subsystem. The other contributor is the control system which only requires little power. The required number of battery cells for the entire swarm to provide the peak power, $n_{batt_{power}}$, is given by Equation 7.11, where P_{peak} is

²⁷https://www.nkon.nl/rechargeable/samsung-inr21700-50e.html?gclid=EAlaIqobChMI-aHDkO6u-AIVhoXVCh0SZwtWEAAYASAAEgJfTPD_BwE [Accessed in June 2022]

²⁸<https://eu.nkon.nl/samsung-inr21700-33j-3270mah-3-2a.html> [Accessed in June 2022]

the total peak power, V is the voltage of a single battery cell, the C-rating and the capacity are also corresponding to a single battery cell.

$$n_{batt_{power}} = \frac{P_{peak}}{C\text{-rating} \cdot \text{Capacity} \cdot V} \quad (7.11)$$

The required number of battery cells for the entire swarm to provide the energy, $n_{batt_{energy}}$ is given by Equation 7.12, where $E_{mission}$ is the total mission energy, capacity and voltage V are again corresponding to a single battery cell.

$$n_{batt_{energy}} = \frac{E_{mission}}{\text{Capacity} \cdot V} \quad (7.12)$$

Since both the power and energy requirements need to be fulfilled, the highest required number of battery cells is to be considered in further sizing. This number of battery cells needs to be divided across the drones in the swarm. Next to that, the battery cells have to be configured in series, called strings, in order to obtain the proper voltage for the engines. The number of battery cells that are to be put in series in a string, $n_{batt_{string}}$, is calculated with Equation 7.13, where V_{engine} is the voltage required by the engine, and V_{cell} is the voltage of a single battery cell.

$$n_{batt_{string}} = \left\lceil \frac{V_{engine}}{V_{bat}} \right\rceil \quad (7.13)$$

The number of strings per drone, n_{string} , is found by dividing the total number of battery cells, $n_{batt_{tot}}$, by the number of drones, n_{drone} as given by Equation 7.14. However, the number of strings per drone can only be an integer number, therefore it is rounded up to the next integer.

$$n_{string} = \left\lceil \frac{n_{batt_{tot}}}{n_{drone} \cdot n_{batt_{string}}} \right\rceil \quad (7.14)$$

With the number of battery cells per string, the number of strings per drone, and the number of drones in the swarm, the total number of battery cells can be calculated as in Equation 7.15.

$$n_{batt_{tot}} = n_{batt_{string}} \cdot n_{string} \cdot n_{drone} \quad (7.15)$$

From the total number of battery cells, the cost of the battery packs can be calculated. The number of battery cells per drone determines the weight of the battery per drone. The remaining electrics weight of the control system is added in order to find the complete electrics weight per drone.

7.4. Structures

This section was written by: *Robin, Thomas*

In order to estimate the mass of the structures within the swarm for any iteration, the structures were divided into the structure of a drone and the structure of the LFRS. As it is too costly with respect to time to iterate with a FEM-analysis, estimations based on simplified structures were used instead. Then, the forces in the structures are calculated based on the previous iteration. These lead to stresses, which then lead to a new sizing of the structure. Finally, these sizes relate to the new mass of the structure.

Drone structure estimation

The drone structure can be identified as built up out of three different parts. The top arms, the core, and the bottom arms. Both the top and bottom arms can be estimated in the same way, as they are the same in shape and size. To estimate the mass of the arm structures, the following methodology was used: first, it is assumed that bending is the primary loading, due to the way that the forces are applied to a single arm. This can be seen in figure Figure 7.7

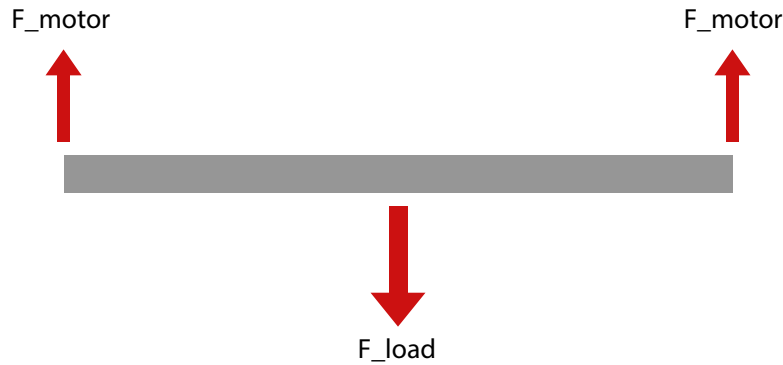


Figure 7.7: Idealised beam loading for the drone arm stress analysis (own work).

Then, a square cross section with an increased thickness at the top and bottom was selected as the optimal choice against this bending loading. Ideally an I-beam would be used against bending, but the structure should be quite resistant against torsion to make sure that the drones could not become uncontrollable due to rotation of the beams causing rotation of the propellers. Finally, the length of the beam is given by earlier calculations in the iteration loop. The assumption was made, that the moment of inertia with this shape is primarily determined by the thick walls with a large distance to the neutral axis with respect to the bending load.

The calculations are explained with the following equations: Firstly, the stress in the beam can be calculated via Equation 7.16, where M is the bending moment, y the distance to the neutral axis, σ is the maximum allowable stress and I the second moment of inertia.

$$\sigma = \frac{M \cdot y}{I} \quad (7.16)$$

The moment induced on the structure can be calculated via Equation 7.17, where F is the load force put on the centre of the beam and, L is the length of the beam.

$$M = \frac{F \cdot L}{4} \quad (7.17)$$

Next, the moment of inertia of the beam can be calculated via Equation 7.18, where A_1 is the area of the thick walls, and d is the length of a side of the square cross-section.

$$I = A_1 \cdot \left(\frac{1}{2}d\right)^2 \quad (7.18)$$

Finally, the area of the thick walls can be calculated via Equation 7.19, where t_1 is the thickness of the thick walls.

$$A_1 = d \cdot t_1 \quad (7.19)$$

Using Equation 7.16, Equation 7.17, Equation 7.18, and Equation 7.19 it can be derived that:

$$d = \left(\frac{F \cdot L}{4 \cdot \sigma \cdot t_1} \right)^{\frac{1}{2}} \quad (7.20)$$

Then it is possible to calculate the total area of the cross section.

$$A_{total} = d \cdot 2 \cdot (t_1 + t_2) \quad (7.21)$$

Where t_2 is the chosen thickness for the thin wall. Then finally the mass is calculated.

$$m_{arms} = A_{total} \cdot L \cdot \rho \quad (7.22)$$

where m_{arms} is the mass of an arm, and ρ is the density of the selected material.

This calculation is ran in every iteration, resulting in the new weight for the structure of the arms of the drone. The force introduced in this section is based on the amount of weight that is carried by each arm. It can be calculated by dividing the total weight of the system by eight and then dividing this force by the number of drones. As an arm is connected to two propellers this number should then be multiplied by two again to finally obtain the force used in this calculation loop.

Next, a mass estimation for the core of the structure is performed. The core of the drones is mostly loaded in either tension or compression depending on the phase in operation. Some extreme cases were analysed in order to find a critical one. Cases such as all four lower engines failing and having the drone as well as the weight of the payload pull on the core, creating a relatively large tension. This however proved to be achievable with the minimal required dimensions and thicknesses with respect to bending loads. Another case which turned out to be much more critical, was one that can be foreseen in operation. An average sized human might for example lean on, or attempt to sit on a drone of large size such as those used in design here. It should not break in this situation, so the case was considered and was critical due to the large relative forces. The mass of the core was then calculated in the following way:

$$\sigma = \frac{F}{A_{core}} \quad (7.23)$$

where σ is the maximum allowable stress, F is the maximum force that is required to be resisted and A_{core} is the cross-sectional area of the core. As the force and maximum allowable stress are both known at the beginning of an iteration, the area can be calculated using Equation 7.23.

Then the total mass is calculated using:

$$m_{core} = A_{core} \cdot h \cdot \rho \quad (7.24)$$

where m_{core} is the total mass of the core of a drone, h the specified height of the core and ρ the density of the selected material.

LFRS structure estimation

In order to estimate a mass of the LFRS purely based on the diameter of the swarm, some simplifications were made to the design to ease the calculations in each iteration. The structure is now assumed to be an octagonal truss structure, in which all corners are connected to the centre by a single beam. This simplified shape can be seen in figure Figure 7.8

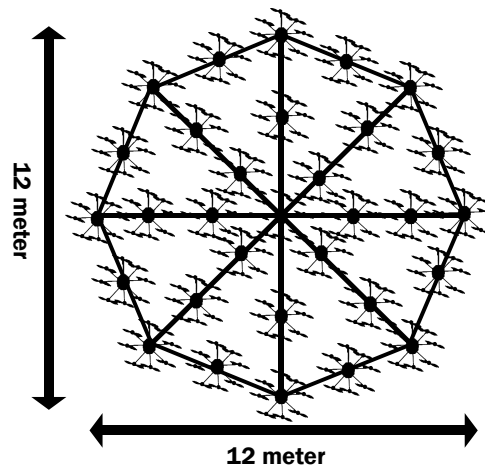


Figure 7.8: Idealised shape of the octagonal LFRS (own work).

First, the forces on this structure stem from the lateral component induced by the angles in the cables hanging under the LFRS. A visualisation of this is given in figure Figure 7.9. In order to keep a consistent behaviour for the LFRS with respect to stability, the angles in the cables are kept consistent and thus the force that compresses the LFRS stays consistent.

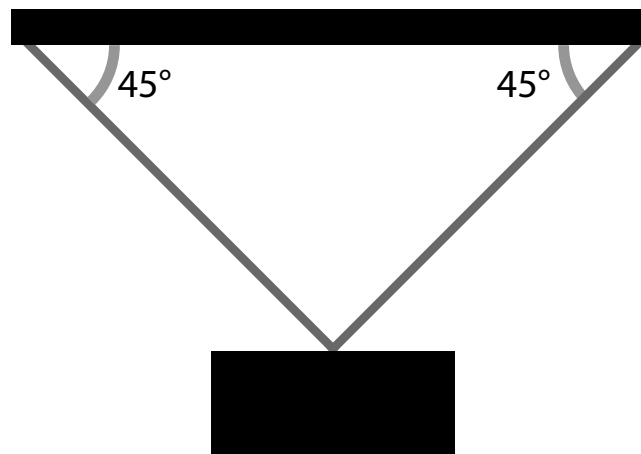


Figure 7.9: The angles in cables created by use of LFRS (own work).

Next, the maximum stress was attempted to be found by using the assumptions of a truss structure. The structure is assumed to be symmetric and a method of sections was used. This entails that a part of the structure is cut and a free body diagram is set up in an analysis in order to determine the internal forces.

Resulting from the analysis, which will not be included due to its length, the forces in the beams that run to the centre are half of the force put on a single point, while the force in one of the beams connecting the outsides will go as high as approximately 0.65 times the force put onto a single point.

In the code, the failures for tension, compression and buckling are all calculated. Then the maximum stress in each section is compared and a design is chosen in accordance to the highest stress in the structure. The tension case is calculated in accordance with Equation 7.23, where A_{core} is replaced with the area of the beams of the LFRS. Compression is calculated similarly, but a different maximum allowable stress is used due to the differences in material properties with respect to tension and compression. Buckling was calculated with Euler buckling, represented by

$$P_{cr} = \frac{\pi^2 \cdot E \cdot I}{K \cdot L^2} \quad (7.25)$$

where P_{cr} is the maximum allowable force in a certain section, E is the Young's modulus, I is the moment of inertia, K is the column effective length factor, and L is the length of the beam. The factor K relates to the constraints on the beam. In this structure the beams are clamped at both ends which relates to a K factor of 0.5 [35].

Rewriting Equation 7.25 results in a required moment of inertia stemming from applied forces. The remaining variables are known material properties or variables calculated by different parts of the program.

For the LFRS the section has beams optimised for buckling. For this, a round section will be used as the most area can be concentrated as far away from the neutral axis as possible. With a circular cross-section, it is possible to calculate the required outer diameter if a thickness is chosen. The thickness is a parameter that can be adjusted in order to make the design work while attempting to stay within realistic manufacturable sizes. Then the dimensions of the beams are known. Then, similarly to Equation 7.22 the mass of the LFRS can then be calculated by multiplying the areas, lengths and densities of a beam and adding all of the beam masses.

Now to calculate the total weight of the drone structures, the mass of a single drone can be multiplied by the amount of drones in the current iteration. Then the weight of the LFRS will be added on top of this to complete the estimation of the structural weight for a single iteration.

7.5. Verification of Software

This section was written by: *Maxim*

Before the developed code can actually be used for the design, the team must be certain it functions as intended. This is the goal of the verification procedure, to be performed on all software.

During the code implementation, each department set up unit tests, aimed at verifying the individual functions. These unit tests were performed by calling functions from the code and assessing whether the outputs matched the expected values from hand calculations, through the use of the *pytest* package. Afterwards, a HTML report was generated for the coverage of the tests in order to check whether all functions were tested accordingly. An example of a test functions is shown in Listing 7.1 .

Listing 7.1: Example of a propulsion unit test (own owrk).

```
def test_interp_char():
    sys = Design(16, 12)
    sys.prop.T_req_list = [5, 3, 1]

    prop_size, prop_database = sys.prop.csv_to_pandas(prop=True)
    prop_size = prop_size[-1]
    prop_database = prop_database[-1]
    energy, torque, rpm, power = sys.prop.interp_char(prop_database)

    torque_expected = [5, 3, 1]
    rpm_expected = [5, 3, 1]
    power_expected = [3.808996939, 1.971238898, 0.5523598776]
    energy_expected = 1.020526034

    assert torque_expected == torque
    assert rpm_expected == rpm
    assert power_expected[1] - power[1] < abs(1e-6)
    assert energy_expected - energy < abs(1e-6)
```

The report looks as shown in Figure 7.10. The coverage percentages are slightly misleading, as the Print function is not tested, however all functions used for calculations are. The number of missing tested lines are different for each modules as the number of printed elements differ from module to module.

<i>Module</i>	<i>statements</i>	<i>missing</i>	<i>excluded</i>	<i>coverage</i>
Attachment.py	75	13	0	83%
Design.py	105	61	0	42%
Drone.py	44	14	0	68%
Electrics.py	59	13	0	78%
Propulsion.py	277	22	0	92%

Figure 7.10: Coverage report from the unit testing (own work).

7.6. Results

This section was written by: *Giacomo*

The iteration program was created to converge to a solution for the design which can successfully complete the mission. The two iterations performed: the inner and the outer iteration, go through the mass of the drone and the number of drones respectively. Furthermore, the main input that makes the design converge or diverge is the diameter assigned to the area of the entire system. Finally, for the solutions that converge, the mass of the single drone is checked to be below 25 kg as constrained by [REQ-USR-11](#) and the cost of DroneCrane is checked to be below €100 000 to meet [REQ-USR-12](#). The code was run for diameters from 5 m with 1 m steps until a converging design was found. The first diameter which gave a converging solution was at 14 m. Figure 7.11 shows a plot of the number of drones against the mass of each drone for a diameter of the entire swarm of 14 m. Several points do not converge, this is due to the fact that a snowball effect is induced in the mass of the subsystems making the mass of a single drone diverge with increasing number of iterations. Furthermore, a line is traced at the 25 kg mark to see which solutions meet the requirement.

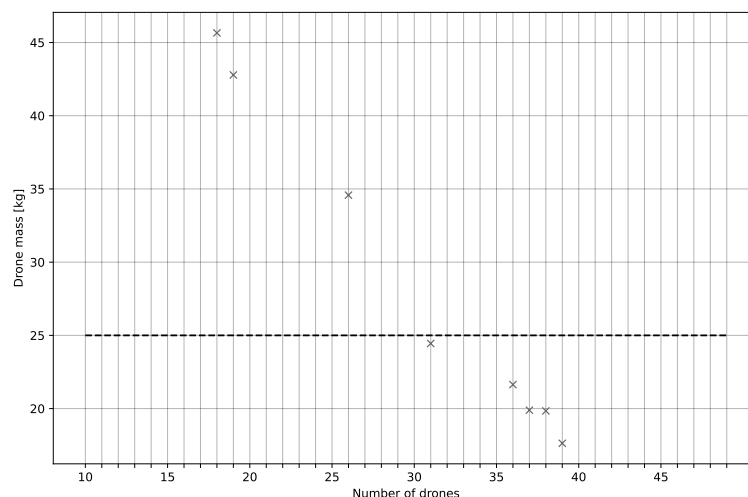


Figure 7.11: Plot of the mass of the single drone against the number of drones with a 25 kg mark and a diameter of the entire system of 14 m (own work).

As can be seen from Figure 7.11, the first solution that meets the requirement for the mass of the single drone is using 31 drones with a diameter of 14 m and a mass per drone of 24.45 kg. However, as explained in Subsection 7.2.3 the actual diameter of the system is different from the one of the input.

In this case, the actual diameter is equal to 12.29 m leading to an area of 118.63 m². Furthermore, Figure 7.12 shows the cost of the entire system using the same inputs as the figure above.

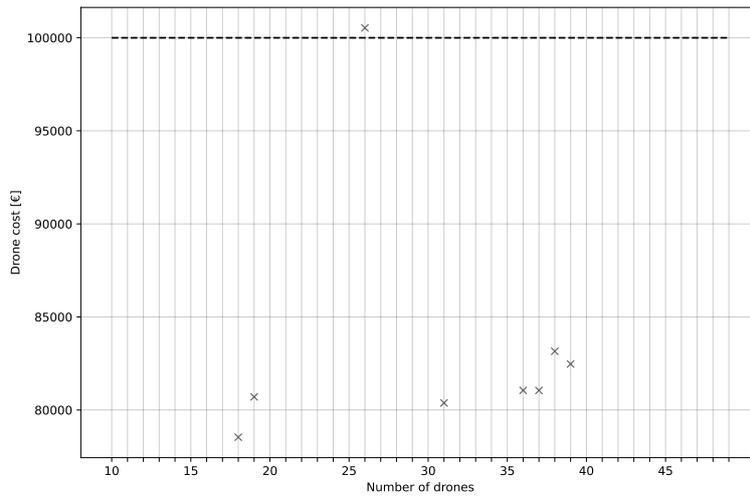


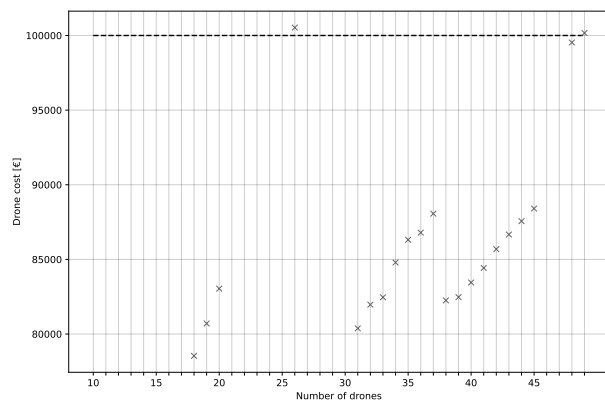
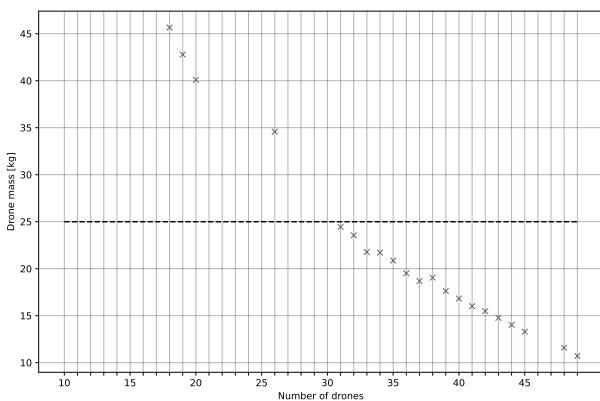
Figure 7.12: Plot of the cost of the entire system against the number of drones with a €100 000 mark and a diameter of the entire system of 14 m (own work).

Figure 7.12 shows that the requirement on cost is also fulfilled by the aforementioned combination, with the 31 drone option raking in at €80 379.25. Since, for operational and market reasons, the lowest the diameter the more competitive the final design is, the converged solution obtain for the 31 drones and an actual diameter of 12.29 m is selected as final design for DroneCrane. Finally, in order to converge to this overall design each subsystem had to be sized. The results for each subsystem can be found in the following chapters.

7.7. Sensitivity Analysis

This section was written by: *Giacomo*

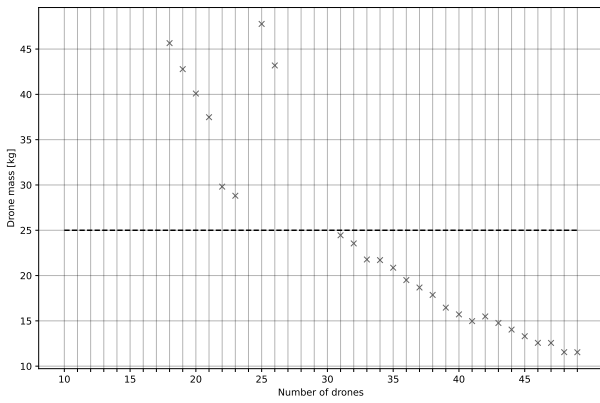
A sensitivity analysis of the overall code is performed in this section. This is done to define how sensitive the final design is to change in the inputs. The main input that is outside the inner and outer iteration is the diameter of the system. As explained in Section 7.6, the combination of smallest diameter and lowest number of drones which met the requirements on mass and cost was selected. However, increasing the diameter of the system gives more solutions that could be used. The plots of the mass of the single drone and of the cost of DroneCrane against the number of drones for diameters from 15 m up to 17 m are shown in Figure 7.13, Figure 7.14, and Figure 7.15.



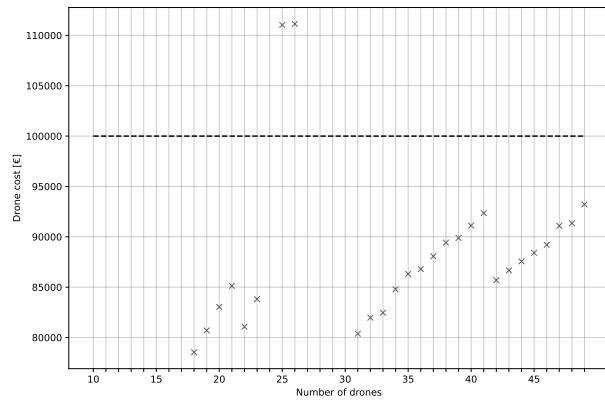
(a) Plot of the mass of the single drone against the number of drones with a 25 kg mark (own work).

(b) Plot of the cost of the entire system against the number of drones with a €100 000 mark (own work).

Figure 7.13: Plots for a diameter of the system of 15 m.

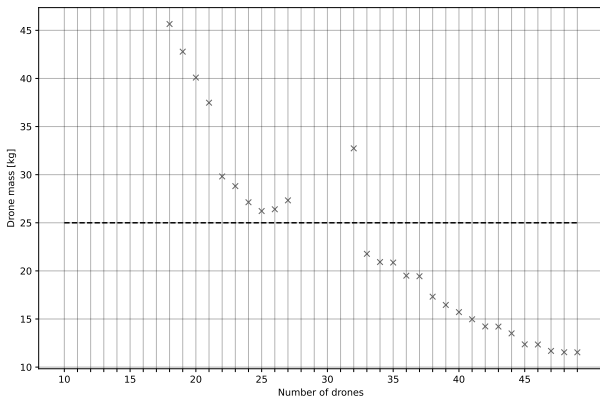


(a) Plot of the mass of the single drone against the number of drones with a 25 kg mark (own work).

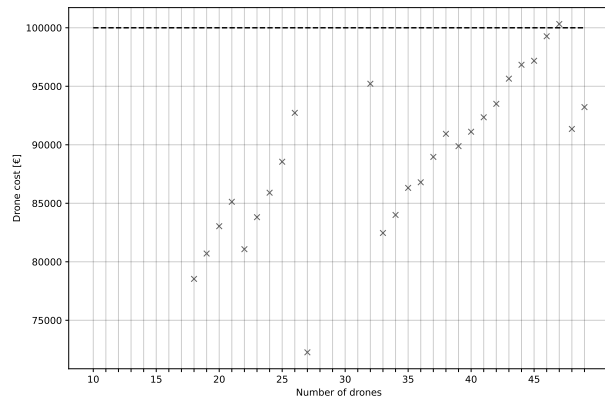


(b) Plot of the cost of the entire system against the number of drones with a €100 000 mark (own work).

Figure 7.14: Plots for a diameter of the system of 16 m.



(a) Plot of the mass of the single drone against the number of drones with a 25 kg mark (own work).



(b) Plot of the cost of the entire system against the number of drones with a €100 000 mark (own work).

Figure 7.15: Plots for a diameter of the system of 17 m (own work).

From Figure 7.13 and Figure 7.14 it can be seen that the solutions that use the lowest number of drones and that converge and meet the requirements are found at 31 drones both for 15 m and 16 m diameter. The number of drones is the same as the final designed discussed in Section 7.6, this is due to the fact that the increase in area was not enough to select a bigger propeller. Both designs use a 50.8 cm propeller and the final mass of the drone is the same.

Looking at Figure 7.15, the best solution for a diameter of 17 m is found at 33 drones which is a larger amount of drones than the number of drones used for the final design, thus creating a heavier system. Therefore, the selected design is still the most suitable solution for DroneCrane. After the sensitivity analysis, it can be stated the overall design is not sensitive to variation in the diameter of the system.



Detailed Design Specifications

8. Propulsion

Designing the propulsion system was a complex task, on one hand, all relevant parts were chosen off-the-shelf and thus did not have to be designed from scratch. On the other hand, choosing off-the-shelf parts meant that the team had less freedom with the design and had to make some compromises. This all led to certain decisions being made during the process, which ended up influencing the final choice. In this chapter, these choices will be discussed along with the characteristics and properties of the final design.

Section 8.1 and Section 8.2 discuss the design choices for the propeller and for the motor respectively. Consequently, in Section 8.3, noise and crosswind analysis are performed to make sure the requirements set on propulsion are met. Finally, the chapter ends with a sensitivity analysis in Section 8.4 and a reliability study in Section 8.5.

8.1. Propeller Design

This section was written by: *Maxim*

The design of the propeller consisted in choosing the appropriate one for all the possible combinations of the system's area and number of drones. This led to some constraints on what the final product would look like and how it would perform. On top of that, the decision did not simply come down to which propeller can output the necessary performance, as multiple different ones could attain the required threshold. Thus, a choice on what would be the deciding factor had to be made.

8.1.1. Design Decisions

For the propeller design, two main factors influenced the final decision: the mechanical energy necessary for the fulfilment of the mission and the size of the propeller. The first factor stemmed from the reasoning that a higher energy requirement would lead to a larger amount of batteries, which would lead to more weight and thus to a higher thrust requirement. This could create a snowball effect that would eventually push the total mass of each drone far above the maximum set by **REQ-USR-11** of 25 kg. Therefore, the decision was made to choose the propeller with the lowest energy requirement.

However, choosing a propeller purely based on its energy requirement proved to not be the correct approach. This is due to the fact that in general, a larger propeller will require a lower RPM to produce the same amount of lift as a smaller propeller, and consequently will always require less energy. But choosing a giant propeller will lead to other issues, namely the size of the drones and of the system as a whole. This could lead to the inability of the system to function in urban environments due to its size, which would cause a loss of a significant part of the market. For that reason, a limit on the total area that the entire system of drones could take up was set. This limit was not a hard stop, as that could lead to an impossible design, but rather a reminder that a lower area of the system leads to a broader applicability and easier setup. Nevertheless, in general the team considered a circular area with a diameter between 5 m and 15 m.

8.1.2. Characterisation of Propeller

After performing the design iterations, a final decision was made. The chosen propeller is the T-Motor NS20x62²⁹, with a diameter of 20 inch and a pitch of 6.2 inch. The material used is T800 carbon fibre, leading to a weight for each propeller of 23 g and a weight for the entire system of 5.7 kg. Each propeller costs €57.37, which leads to a total propeller cost of €14 227.76, without taking into account bulk business-to-business, B2B, discounts. As for the performance characteristics, each propeller is expected to provide a peak thrust of 60.59 N. To provide this thrust, it requires a mechanical power of 945.61 W, a torque of 1.37 N m and a rotational speed of 6304 RPM.

²⁹<https://store.tmotor.com/goods.php?id=965>[Accessed in June 2022]

8.2. Motor Design

This section was written by: *Maxim*

Similarly to the propeller design, the motor had to be chosen from a list of existing motors. This was due to the fact that designing a motor from scratch was beyond the scope of this project. As such, criteria for the selection of the motor had to be set up.

8.2.1. Design Decisions

The motor selection consisted of mostly checking the compatibility of the motor with the chosen propeller, and whether it could provide the necessary torque and rotational speed to the system. Nevertheless, as in the case with the propeller, additional criteria had to be set up in order to find the best option. These criteria were the electrical energy requirement of the motor, the price of the motor and the maximum necessary voltage of the motor.

The energy criterion is quite self-explanatory and similar to the propellers case; the lower the energy required, the better the motor. The argumentation is also the same: more energy requires more batteries, which implies more weight, which implies more thrust, which implies more energy. As such, the motor that requires the least energy was chosen.

Price-wise, the motors have a wide range of costs, with some engines costing in the thousands. Therefore, in order to not go over-budget, a limit on the total price of the propulsion system was set to €50 000. This should assure that the motors do not end up leading the project to exceed the cost requirement.

Finally, a limit had to be set on the required voltage for the motor. This stemmed from two considerations. Firstly, the motors themselves have a maximum acceptable voltage that they can operate on. Therefore, if the calculated voltage ends up above this threshold, the motors will not be able to function correctly. Secondly, the PDBs necessary for high voltages ended up being very hard to find and those that were found ended up having compatibility issues. Thus, based on these two observations, the maximum voltage of the motors was limited to 50 V.

8.2.2. Characterisation of Motor

With the analysis complete, the motor of choice ended up being the T-Motor Antigravity MN6007II KV160³⁰. It can provide a maximum power of 1120 W at a peak current of 23.7 A and an efficiency of 0.84. It weights 159 g and costs just under €124.31 a piece, leading to a total pre-discount price of €30 828.88.

Having chosen both the propeller and the motor, a validation of the choice needs to be performed. This is done through a check for the requirement compliance and a sensitivity analysis.

8.3. Requirement Compliance

While the chosen elements may be the best in terms of performance, there exist other, non-performance requirements which need to be met. In this section, the compliance of the system with these requirements will be discussed.

8.3.1. Noise

An important aspect to consider was the noise the propellers created. As the system would operate in urban conditions, it would have to adhere to the noise regulations set by the local authority. However, performing a full noise analysis would require a finite-element method to be employed, which is unfeasible due to a lack of geometrical and aerodynamical data available of the propeller. Therefore, a more statistical approach was taken. Reference data was taken from a coaxial octocopter, the Gryphon Dynamics GD28X, which is a heavy lifter drone with a similar weight and propeller size as the drones of DroneCrane. This drone was found to produce 62 dB of noise at a distance of 122 m [36]. This can be adjusted by converting the value into W and using the inverse-square law to find the

³⁰<https://store.tmotor.com/goods.php?id=1113>[Accessed in June 2022]

noise at different distances. After scaling it to 31 drones, the noise ends up being 76.9 dB and when reducing the distance to 10 m, the noise becomes 98.6 dB. This, while being relatively high, is still within an acceptable range, and more importantly it is below the noise level of a helicopter, which at a distance of 152 m generates 87 dB and at a distance of 10 m generates 110.6 dB. Therefore, as long as the final drone design ends up being similar to the example, it can be assumed that it is, in fact, feasible in terms of noise, with the operators being advised to use hearing protection at startup.

8.3.2. Crosswind

In this section a crosswind analysis is performed, to confirm the correct functioning of the propulsive subsystem and that it complies with **REQ-OPR-WEA-1**. The DroneCrane system shall have a Beaufort wind resistance level of 5, and to ensure that the propulsive subsystem can withstand the additional moments induced, an analysis on crosswind is performed.

Since the cross-sectional shape of the blade and its aerodynamic properties along the radial position could not be found for the T-Motor NS20x62 propeller, an accurate finite element modelling of the blade and a simulation of the flow acting on it could not be performed. Instead, a method proposed by L. Ding and Y. Li was used based on the momentum theory [37].

Firstly, the thrust produced by each propeller was modelled by momentum theory, which states that the thrust produced equals the change in momentum, as shown in Equation 8.1.

$$T = \rho \cdot A_{prop} \cdot V_p \cdot (V_e - V_0) \quad (8.1)$$

In the equation above, V_p is the induced velocity by the propeller, V_e is the exhaust velocity and V_0 is the incoming velocity. V_p is found to be the average of V_e and V_0 . Substituting this in Equation 8.1, V_p is found via Equation 8.2.

$$V_p = \frac{1}{2} \left(V_0 + \sqrt{\frac{2T}{A} + V_0^2} \right) \quad (8.2)$$

V_p was found to be 11.82 m s^{-1} for the most critical phase, which is ascending at a vertical speed of 1.5 m s^{-1} . Now that the induced velocity by the propeller is found under nominal conditions, the effects of crosswind can be superposed. With the exhaust velocity of the nominal condition, the total thrust can be found and then the additional induced forces can be examined with the effect of crosswind [37]. The equations used to calculate these parameters are shown in Equation 8.3 and Equation 8.4[37].

$$T = f_{m_i} + f_{w_i} = 2\rho \cdot A_{disk} \cdot V_l \cdot V_p \quad (8.3)$$

$$V_l = \sqrt{(V_{w_i} \cdot \cos(\alpha) + V_p)^2 + (V_{w_i}) \cdot \sin(\alpha)^2} \quad (8.4)$$

The α is the angle between the direction of the thrust produced and the incoming flow as shown in Figure 8.1.

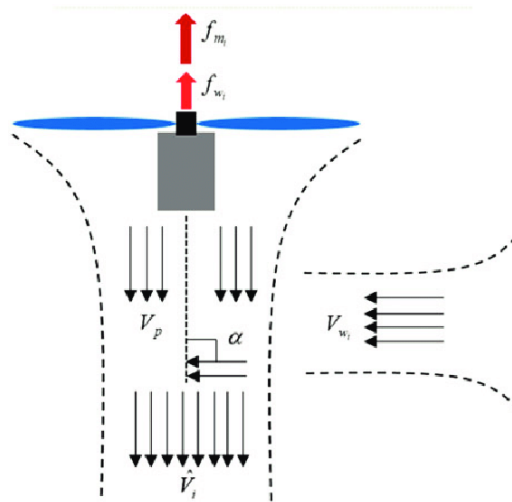


Figure 8.1: Modelling of crosswind [37].

Since the speed of the crosswind is known, and the thrust operated during ascending is known, the thrust induced by the crosswind can be calculated. Once the induced thrust is known for each propeller, the total moment induced can be calculated via Equation 8.5.

$$M_x = f_{w_1} \cdot l + f_{w_2} \cdot l \cdot \sin(45) + f_{w_3} \cdot l \cdot \sin(45) - f_{w_6} \cdot l \cdot \sin(45) - f_{w_7} \cdot l \cdot \sin(45) - f_{w_8} \cdot l \quad (8.5)$$

Each subscript refers to each propeller within the drone as shown in Figure 8.2.

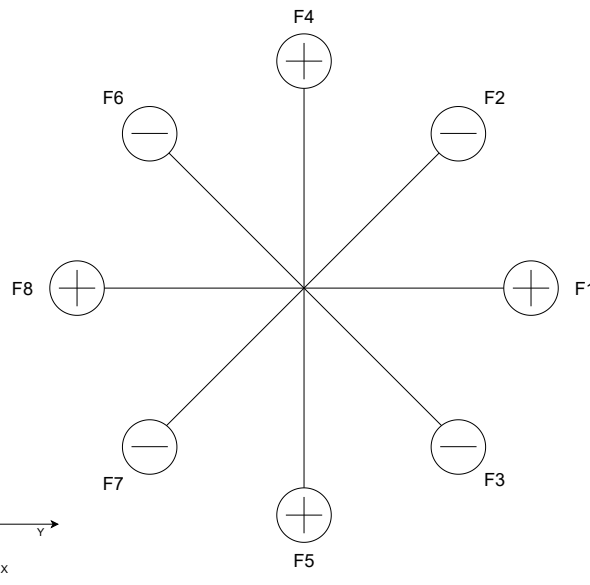


Figure 8.2: Configuration of drone (own work).

The moments around the x-axis and the y-axis are not coupled if the x and y-axis are perpendicular and parallel to the direction of the wind. Hence, the maximum moment induced due to crosswind can be evaluated from either the x or the y-axis. The moment will be simulated at the critical case, which is ascending since the exhaust velocity and the thrust produced by the propeller are the greatest, and the margin for additional thrust is the lowest. Furthermore, the induced cross wind velocity will be

modelled as followed : at propeller position 1, 2 and 3 it will be equal to w ; at position 4 and 5 it will be $0.9 \cdot w_i$; and at position 6, 7 and 8 it will be $0.8 \cdot w_i$. This is due to the fact that the interference between the propellers and the wind will reduce the velocity at the wake of the rotors. Since an accurate estimate is not obtainable without the accurate geometry of the propellers, an estimate of 10% and 20% velocity reduction is applied. The moment calculation was done over a range of α and the result is shown in Figure 8.3.

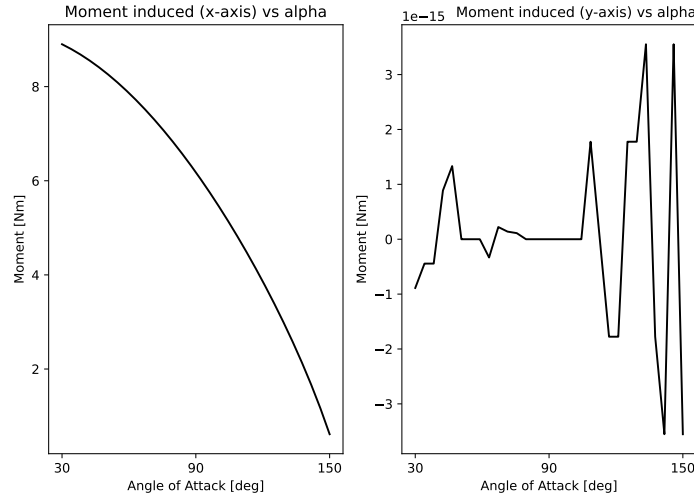


Figure 8.3: Moments induced due to cross wind with variation of angle of attack (own work).

As can be seen in Figure 8.3, the maximum moment induced on the drone is 9.1 N m at 30° . The results are not simulated below 30° , as below this value it is expected that the wind speed distribution along the drone will be similar, and no asymmetrical induced loading is expected. To further verify on the fact that the moment around the x and y-axis are decoupled, the simulated rolling moment induced (on the y-axis) is calculated and its magnitude is found to be $1 \times 10^{-14} \text{ N m}$. The value produced is not 0 due to rounding errors. In order to ensure equilibrium, the propeller at position 6, 7 and 8 must provide a force of 6.4 N each. The thrust margin for each propeller between a thrust to weight ratio of 1 for the system and the maximum thrust to weight ratio achievable is 9.76 N . Therefore, it can be concluded that the propulsion system is capable to produce enough thrust to ensure equilibrium at this crosswind speed with a margin of 34.3%.

Next, the yawing moment induced on the drones will be examined. The induced yaw moment is a result of the change in motor torque as a result of aerodynamic drag [37]. The torque for each motor is calculated via Equation 8.6 [37].

$$m_{drag} = \rho \cdot A \cdot V_{w_i}^2 \quad (8.6)$$

Using the same induced wind distribution as before and taking into consideration that each adjacent motor spins in the opposite direction, it was found that the yaw moment induced is 4.8 N m . Since the rotation of the propellers is fixed, only 4 motors are allowed to change the torque level to counteract the yawing moment of the drone in the same direction. This means that each motor is required to increase/decrease the torque by 1.2 N m , which falls within the maximum torque that a motor can produce of 1.33 N m .

8.4. Sensitivity Analysis

This section was written by: *Tyme*

In this section a sensitivity analysis will be performed on the propulsive subsystem in order to evaluate the effects of different parameters on the final design choice, and how the uncertainty of each

parameter could affect the final design choice. Firstly, the sensitivity of the selection of the propeller will be analysed then the one of the motor is analysed.

8.4.1. Sensitivity of propeller selection

Firstly, the variation of mechanical power with the number of drones is examined to analyse any trends and the parameters that affects it. The variation is shown in Figure 8.4. The gaps in the figures shown below are a consequence of the inability for the design to converge.

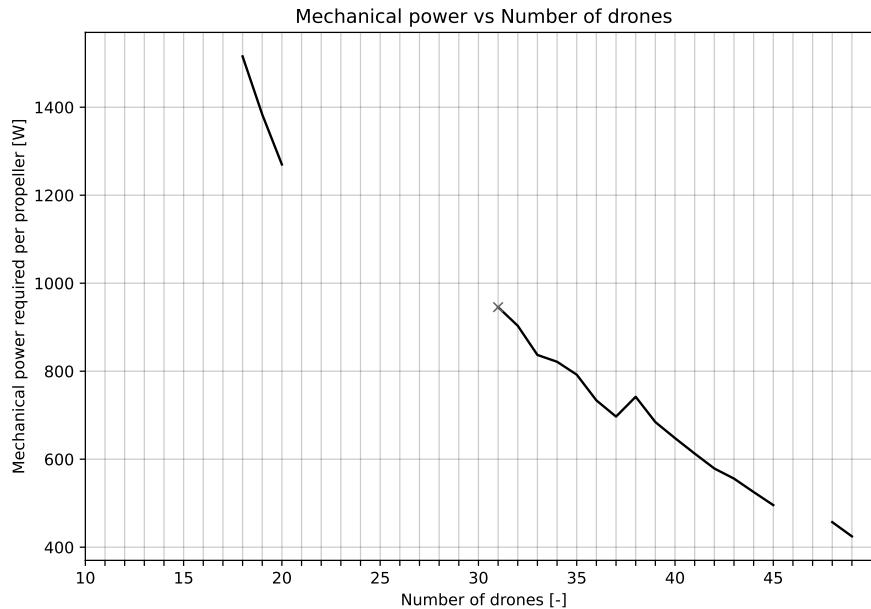


Figure 8.4: Variation of mechanical power required per propeller with number of drones (own work).

As seen in Figure 8.4, the trend of the mechanical power required for each propeller is that it decreases with increasing number of drones, however at 38 drones the mechanical power required increased compared to the last converged value, then continues decreasing. The decrease of mechanical power required with an increase of number of drones can be explained by the fact that with increasing number of drones, the thrust required for each propeller decreases due to the increased distribution of required weight carrying capacity of each drone. To corroborate this, the variation in thrust and torque required of each propeller with increasing number of drones is shown in Figure 8.5.

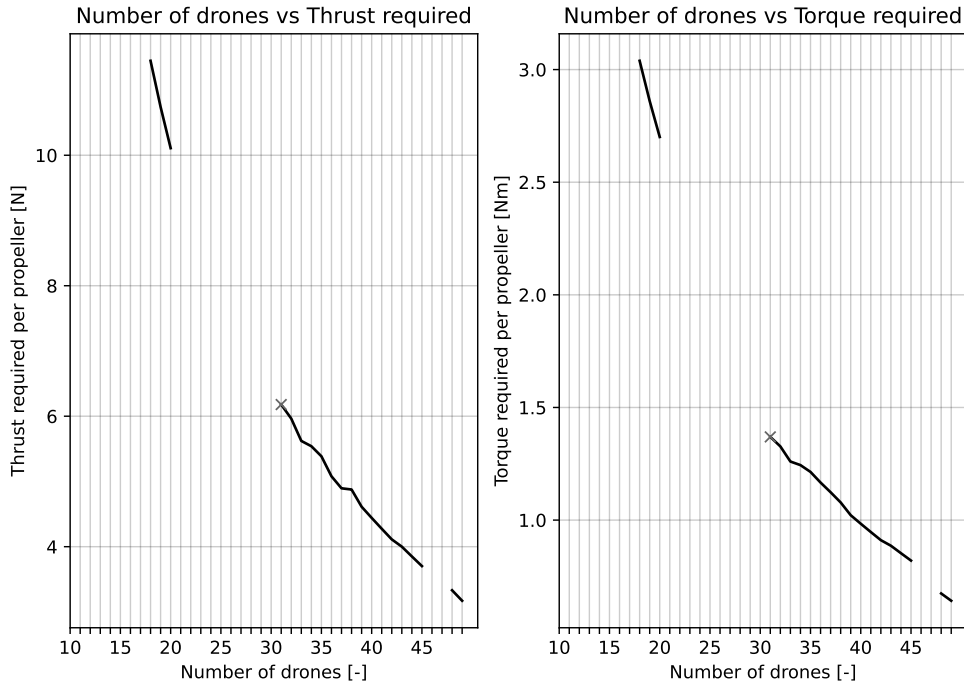


Figure 8.5: Variation of torque required and thrust required with increasing number of drones (own work).

To explain the increase in mechanical power required despite the decrease in thrust, the selection of the propellers and the RPM required for each propeller is further examined and shown in Figure 8.6.

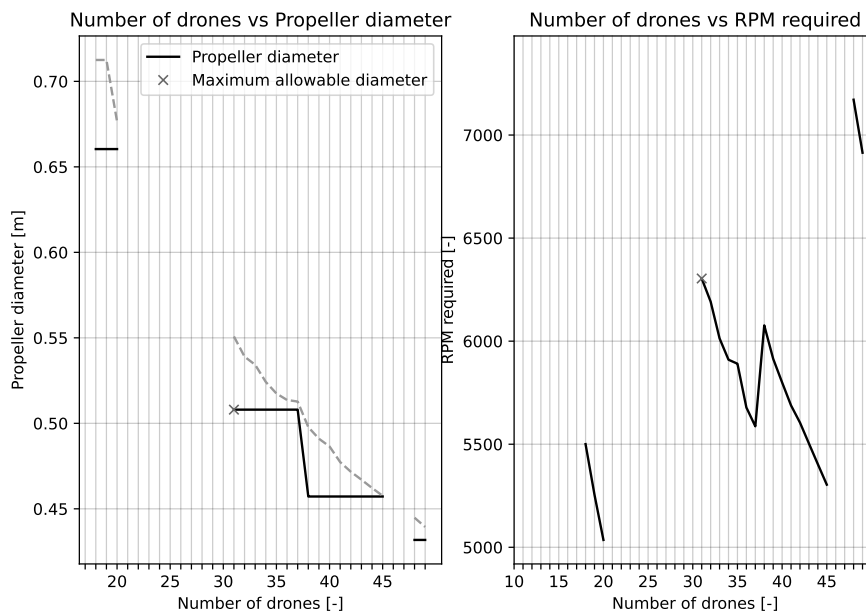


Figure 8.6: Variation of torque required and thrust required with increasing number of drones (own work).

As seen in Figure 8.6, the number of drones required which results in an increase in mechanical power is also associated with a smaller propeller selection due to the limitations of the available area, causing the RPM to increase. The trend of the RPM required is similar to the mechanical power required, where a decrease in diameter of the selected propeller leads to a higher RPM required. Furthermore, it is seen that the propeller chosen is always the largest available propeller, as a lower

RPM required leads to lower mechanical power. The maximum allowable diameter of the propeller is derived from the maximum allowable diameter of the swarm, which does not come from constraints but a parameter that needs to be minimised. Therefore, in order to determine whether the final selected diameter of the propeller will change, a range of the diameter of the swarm will be evaluated and examined to see whether this will lead to a change in selected propeller.

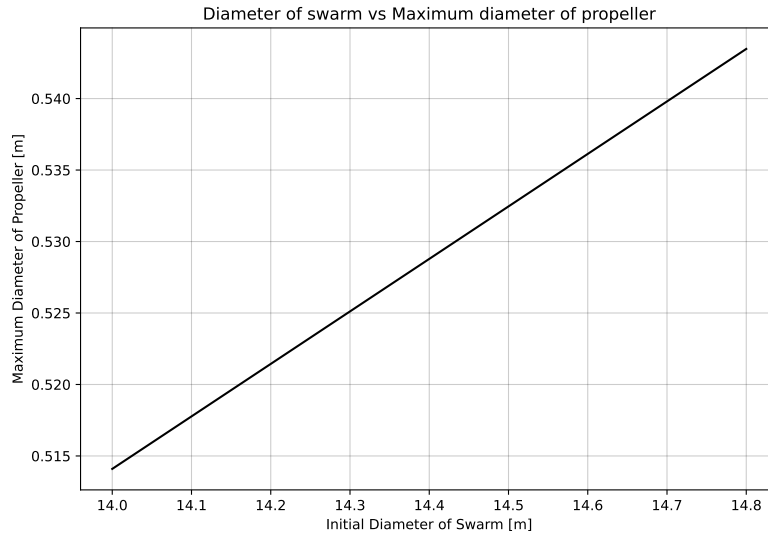


Figure 8.7: Swarm diameter vs Maximum propeller diameter (own work).

As seen in Figure 8.7, with an increase of 0.8 m of the diameter of the entire swarm, the maximum diameter of the propeller is 0.54 m. The next largest propeller which could be selected has a diameter of 0.56 m, which exceeds the limit shown in the graph. Increasing the diameter of the swarm larger than this will limit the space where DroneCrane will be operable, particularly in urban environment, hence it can be concluded with high confidence that the selected propeller is the optimal one.

8.4.2. Sensitivity of motor selection

The selection of motor will be analysed by changing the number of drones in the design. After running the iteration process, the motor selected for 31 drones and greater is always T-Motor Antigravity MN6007II KV160.

The selection of the motor is based on the operating point of the motor, which includes the torque and the RPM. As seen in Figure 8.5 and Figure 8.6, the RPM and the torque required for 31 drones onward lie in the same region, hence it is expected that the same motor was chosen.

The motor selected for lower number of drones was found to be U10 PLUS KV170, however for these drones the selected propeller has a diameter of 0.71 m, which operates with a significantly different operating point, as the RPM required is lower and the torque required is higher. Since it was concluded in Subsection 8.4.1 that there is a high confidence that the selected propeller is the optimal one, and the selection of motor is highly dependent on the propeller used, then it can be concluded that the final selected motor is the optimal one.

8.5. Reliability

This section was written by: *Maxim*

The propulsion system is a rather integral part of the drones and its failure would lead to catastrophic consequences. Therefore, a reliability analysis must be performed, to assess whether the propulsion's failure rate exceeds acceptable margins.

The failure rate of the motor per hour is defined in Equation 8.7 [38], with $\lambda_{bearing}$ being the failure rate of the bearing and $\lambda_{winding}$ the failure rate of the winding.

$$\lambda = \lambda_{bearing} + \lambda_{winding} \quad (8.7)$$

The bearing failure rate can be calculated according to Equation 8.8 [38], with Ω being the RPM, C_t being a safety factor for the operating temperature and L_S and L_A being the basic dynamic load, given in the specifications of the bearing, and the equivalent radial load, calculated by dividing the torque with the radius of the bearing.

$$\lambda_{bearing} = \frac{1}{60 \cdot \Omega} \cdot \left(\frac{L_S}{L_A}\right)^3 \cdot C_t = \frac{1}{60 \cdot 6244} \cdot \left(\frac{1700}{223}\right)^3 \cdot 1.3 \quad (8.8)$$

For the failure rate of the winding, a life of 20 000 hours is assumed, which is typical value for winding [38].

$$\lambda_{winding} = \frac{1}{20000} \quad (8.9)$$

Adding these two failure rates provides the total failure rate of the motor, as shown in Equation 8.10.

$$\lambda = 5 \cdot 10^{-5} + 1.54 \cdot 10^{-3} = 1.59 \cdot 10^{-3} \quad (8.10)$$

Having the failure rate of one motor, the reliability of the total drone with regards to its propulsion system can be calculated. For a drone to fail, a minimum of 3 propellers need to go out of operation, as that is the controllability threshold of the octocopter [39]. The definition of a drone failure is when it is unable to provide enough thrust to carry its own weight, or when it is unable to control its attitude. Thus, to find the failure rate of the drone, all possible combinations of 3-motor failure are calculated, multiplied by the probability of three motors failing and finally multiplied by the proportion of uncontrollable 3-motor failures. The proportion of uncontrollable combinations is calculated as shown in Equation 8.11, with p being the uncontrollable proportion, u being the number of uncontrollable configurations (for three motor failures, there are 8 possibilities, under the assumption that control of yaw is not required, as pitch and roll already gives full control of the drone) and n number of motors required to fail:

$$p = 1 - \frac{C_{8-u}^n}{C_8^n} \quad (8.11)$$

This is also done for 4 and 5 failures. Any amount of failures beyond that is deemed too improbable, and would not impact the total failure rate. The total failure rate of the drone due to the propulsion is shown in Equation 8.12.

$$\lambda_{drone} = \lambda_3 + \lambda_4 + \lambda_5 = 3.24 \cdot 10^{-8} \quad (8.12)$$

9. Control

The control subsystem is one of the most important and critical parts of the DroneCrane system. Throughout the control subsystem development, the fundamental idea is to design with efficiency and responsiveness in mind. In this project, it was done by ensuring that all components only receive the data they really need. This is important not only for good component design, but it also ensures that the design presented here really solves the problem that was introduced in preliminary design phase.

The main aim is to setup and manage the control of the individual drones and, on a inherent level, the well-coordinated control of the swarm as one unit. By focusing on these two different aspects separately and defining the interface between the two, it makes it possible to use well-tested and reliable individual drone control systems for the former, and a custom swarm algorithm that works well with the other subsystems, for the latter.

The physical components necessary for the control of the swarm and their integration are detailed in Section 9.1. Then, a general structure of the software of the control system is outlined in Section 9.2. Next, the requirements for communication; the systems used and details on how they are connected are discussed in Section 9.3. Following that, the individual drone control simulation framework; its approach and results and the research done to better understand individual control are discussed in Section 9.4. Furthermore, the swarm control system and the different aspects of its design are explored in Section 9.5. Finally, reliability of the control subsystem is presented in Section 9.6.

9.1. Hardware Structure

This section was written by: *Bryan*

The hardware required for this project is quite novel and therefore complex, especially when it comes to the swarm aspects. As such, it was decided that for the individual drone control, an off-the-shelf open flight controller would be the final choice of component which covered the requirements set for individual control. The main reason for this decision was that any controller custom developed, without the proper testing, verification and validation required, would pose a large risk to the DroneCrane system as it would not sufficiently cover, and react to, all the different situations and stimuli during flight. In addition, using an off-the-shelf flight controller would be more safe and reliable as it has gone through rigorous testing and is used in multiple industries, outside of the drone industry [40]. Lastly, using an open flight controller rather than one with a closed source, was important to consider, as it is important for the possibility to tweak the controller physically or change other parameters should there be a need in the future to do this.

Even though ultimately a flight controller will be used for the individual drone control system, it was deemed necessary to cover the different control loops and procedures that occur in the individual control system in order to better understand the interfaces needed for interaction from the swarm controller and to understand how the input from the swarm controller can affect the functioning of the individual drone controller. This is done by creating a simulation framework to model the different forces and dynamics of the individual drone. It can be found in Section 9.4.

In Figure 9.1, the Hardware Block Diagram is shown. This diagram provides a glance at the complete overview of the hardware used in the DroneCrane system. There are two main groups of hardware: hardware that is used in the drone, and hardware that is used at the ground station. In the diagram, lines in between components represent a physical wiring and it is also indicated the purpose of the wiring between two pairs of components. The rationale and requirements behind the hardware chosen will be discussed in Section 9.3.

In the Drone hardware group, for controls: the flight controller used is the Pixhawk 4; the swarm con-

troller used is the Raspberry Pi Zero 2 W (with the Red Bear IoT pHAT³¹); the two RTK GPS modules used are the u-blox NEO-M8P³²; the ultra-wide band transceiver used is the Qorvo WM1000³³; the radio control transceiver used is the Adafruit RFM95W³⁴; the camera (independent) system used is the Caddx Nebula Pro.³⁵

In the Ground hardware group, for controls: the RTK GPS module, radio control module, and camera module remains the same as in the Drone hardware group. The only other hardware is the ground controller which will be a portable workstation and the joystick which is the RadioMaster TX12.³⁶

³¹<https://www.adafruit.com/product/3283> [Accessed in June 2022]

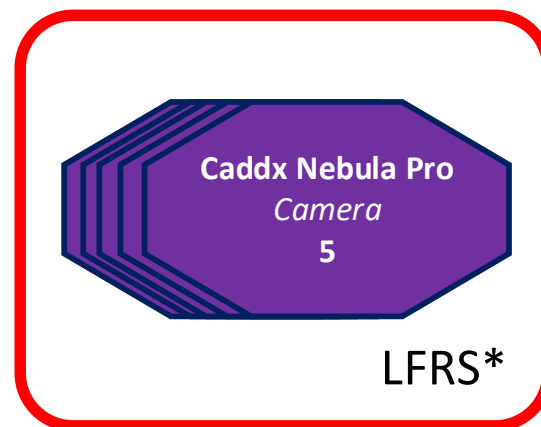
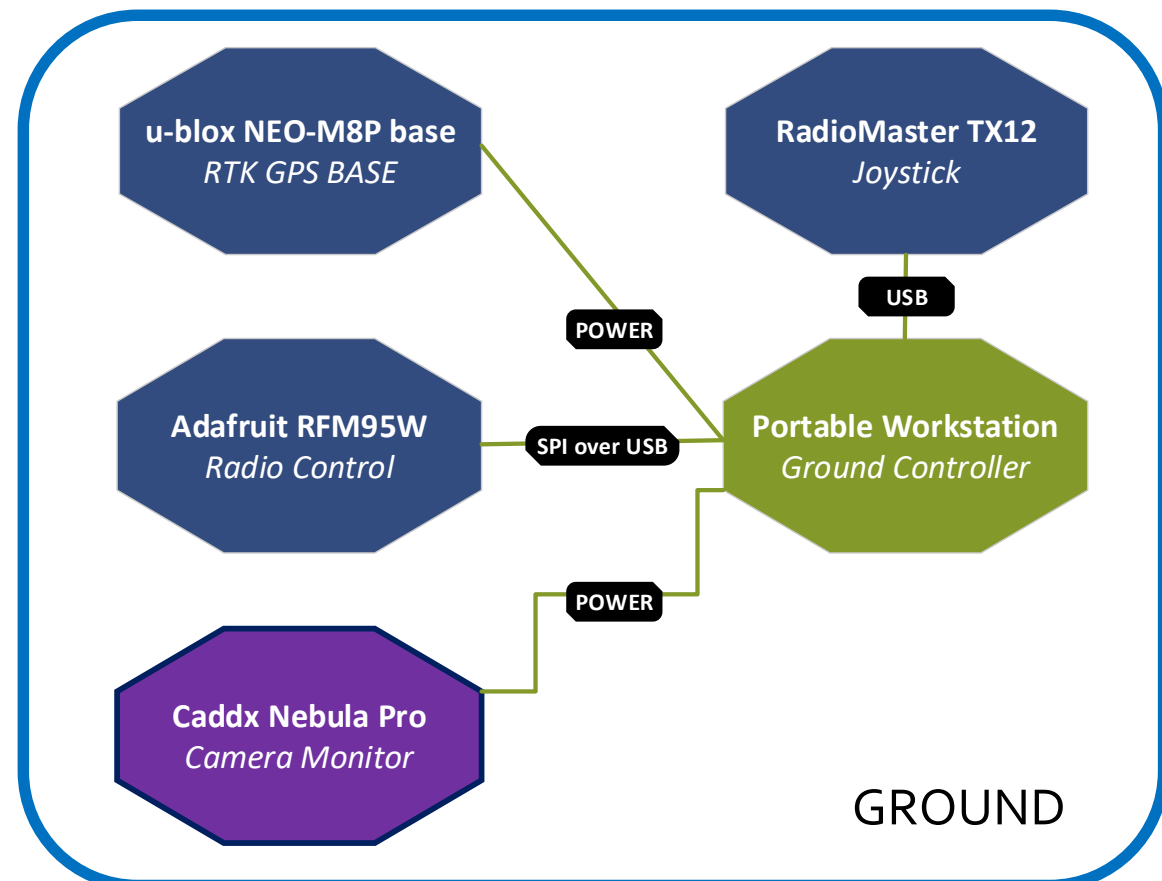
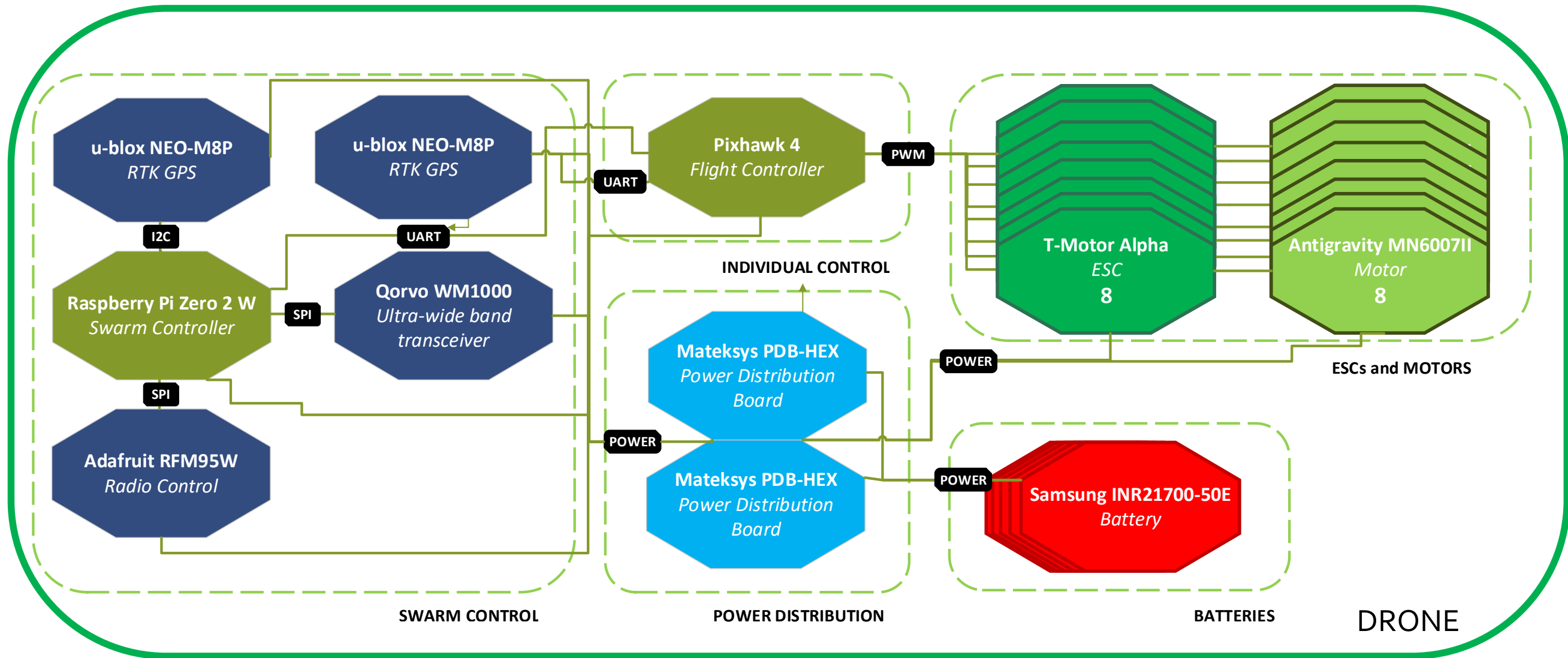
³²<https://www.u-blox.com/en/product/neo-m8p-series> [Accessed in June 2022]

³³<https://nl.mouser.com/ProductDetail/Qorvo/DWM1000> [Accessed in June 2022]

³⁴<https://www.adafruit.com/product/4074> [Accessed in June 2022]

³⁵<https://www.unmannedtechshop.co.uk/product/caddx-nebula-pro-camera/> [Accessed in June 2022]

³⁶<https://droneshop.nl/radiomaster-tx12> [Accessed in June 2022]



* Only on specific drones

Figure 9.1: Hardware Block Diagram (own work).

9.2. Software Characterisation

This section was written by: *Giovanni, Bryan*

The control system is ideated to be decentralised in nature as a result of the trade-off performed at the end of the preliminary design phase [9], as summarised in Section 5.3. As such, each drone is given the same software and hardware with which to perform the mission in coordination with the other ones. With the flight controller choice presented in Section 9.1, it is important to highlight the necessity for the development of an in-house control system framework. This happens because of the novelty of DroneCrane, an application that has not yet seen the light and is thus to be explored. At the same time, there is the need for a simulation framework that can validate the early claims on power, redundancy, and reliability of DroneCrane. It guarantees that the analysis performed by the propulsion department of the working team is robust.

The development of the control system is approached in a modular manner, diving the controls that stabilise the system from those that organise the swarm. The former take care of controlling the actuators on the drone, i.e. the propellers; the latter leads the drone and formally produces commands for the first. By means of this subdivision, it is possible to tune the low level (individual drone) controls independently of the high level (swarm) controls.

To avoid incurring in discrepancies in the control system design as the development progresses, interfaces were designed and settled early on, and mostly refer to the fact that the inner loop receives as input the desired position from the swarm-controlling decentralised algorithm. Additionally, all the states concerning the drone conditions in the fixed-Earth frame are fed from the inner loop to the outer one too. The interfaces that the control system as a whole has with the system external to the swarm include the communication link between the ground operator and each of the drones. A summary of this interface is given in Table 9.1, where the row indicate outputs and the columns indicate inputs, so that an element in any of the internal cells of the table comes from the part of the system in its row, and is fed to that giving its column a name.

Table 9.1: *Interfaces between the low level controls (inner loop), high level drone controls (outer loop), and the ground station.*

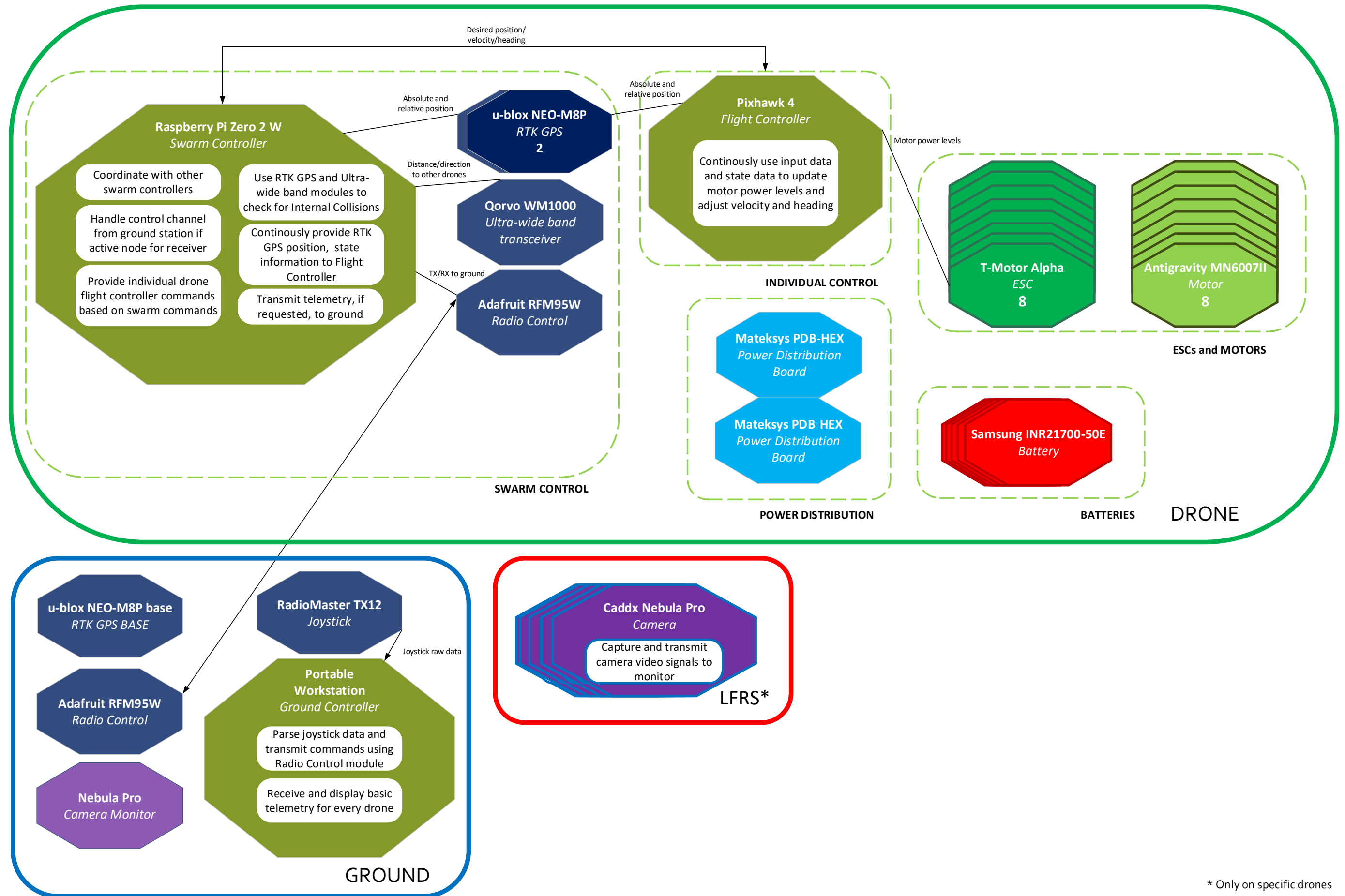
	Inner loop	Outer loop	Ground station
Inner loop	-	States: position and its derivatives, rope tension	-
Outer loop	Position of centre of gravity (COG)	-	Centroid location
Ground station	-	Centroid location	-

A very high level overview of the software of the DroneCrane system is shown in Figure 9.2. A lower level overview is not drawn, in part because of the intricacies of lower-level concepts with respect to the operating system and inner routines which are not relevant to the focus of this chapter, and because most of the finer details of software will be discussed in the later sections of this chapter.

Under the flight controller, swarm controller and ground controller, the different functions of the software are detailed. In addition, lines are drawn between components when software will take advantage of this link and the data being transferred between the components.

The Flight Controller (Pixhawk 4) will use the open-source PX4 Autopilot³⁷ software.

³⁷<https://github.com/PX4/PX4-Autopilot> [Accessed in June 2022]



* Only on specific drones

Figure 9.2: Software Block Diagram (own work).

9.3. Communication

This section was written by: *Bryan*

Communication systems can make or break an otherwise well defined and developed control system. It is important to establish that communication must be as reliable as possible and also use available techniques which mitigate any issues arising from information arriving late or information being lost.

In this section, the requirements of the communication system are first derived, then the different communication channels that are set up in the system will be discussed and a motivation given on why the particular communication channel is sufficient for the purpose it has been set up for. Finally, an telecommunications analysis will be done to determine whether the communication links are sufficient and meet the requirements.

9.3.1. Requirements

It is important to look at the requirements for communication as it forms the basis of the architecture for the communication of data.

Looking at the DroneCrane system with a higher level overview, we have the following uses for communication links for which it is yet to be determined the requirement in terms of data rate:

1. Swarm to Ground
2. Drone to Drone (in Swarm)

For communication between swarm and ground, there must be enough data rate per second in order to control the swarm from ground controller equipment i.e. a joystick. This necessitates first looking at the maximum messages that will be transmitted per second, and then exploring the right type of communication link which has enough data rate to sustain the requirement for messages per second while still keeping sufficient range. It is important to keep in mind that processing on the swarm side also needs to take place, therefore a value of about five Hertz, with respect to number of messages being sent, is the requirement set for communication between swarm and ground.

With a message size of 280 bytes (Mavlink), for five messages per second, that is 1400 bytes per second or 11.2 Kbps. In addition, from operations it is obtained a required range of 500 m.

For communication between drone to drone, there is an higher requirement on data rate per second because of the higher volume of messages that will be sent between the drones in order to coordinate the swarm and maintain formation. However, range is not much of an issue here in comparison with swarm to ground communication; covering the swarm sufficiently is important.

With a maximum of ten messages per second per drone, using a message size of 508 bytes (UDP), it is obtained that a data rate of 1.26 Mbps is required.

With the key requirements stated here, the following subsections will delve into the chosen communication links and their specifications.

9.3.2. Communication Methods

Swarm (Drone-to-Drone) Network

For the swarm network, a communication link is set up such that it is possible for one drone to contact any other drone in the swarm, either by direct link (single hop) or by relay (multiple hops). It is important to emphasise that even if connections are possible between drones, either directly, or through means of a relay, that communication sent should be kept to the minimum required for full functionality. This principle will be addressed further in the coming sections of the chapter.

To that effect, the communication system will use an Mobile Ad-Hoc Network (MANET), which uses Wi-Fi 4 (IEEE 802.11n³⁸), for the network connection between the drones. Wi-Fi was chosen here because of the relatively inexpensive cost and because it has a link speed of 72 Mbps at 20 Mhz channel width, at a range of up to 90 meters [41]. In addition, Ad-Hoc mode is used in contrast to

³⁸<https://standards.ieee.org/ieee/802.11n/3952/> [Accessed in June 2022]

Infrastructure mode because there is then no longer a need to rely on one specific drone for connection to the swarm, hence being more responsive and reliable as a result [42].

Each drone has a builtin Wi-Fi card as part of the Raspberry Pi Zero 2 W swarm controller and an additional Wi-Fi card as part of the Red Bear IoT pHAT. The former will be used to connect to the nearest transmitting MANET relay (another drone) and the latter will be used for repeating and relaying the Wi-Fi network if the signal for the former is relatively weak, and in coordination with neighbouring drones. This will be checked dynamically by measuring the RSSI value for the Wi-Fi radio signal strength.

Now that the link has been established between drones for a collective swarm Wi-Fi network, for communication to be able to take place between any pair of drones, IP addressing needs to be established. Since there are 31 drones in the swarm, the shortest IPv4 subnet that can contain these number of nodes is a /26 (CIDR) subnet. This allows for 62 usable hosts, which is enough for the needs of the swarm network. The numbering scheme can directly follow from the label given to the drone, a number from 1 to 31. Therefore, drone number 27 would have an IP address of 10.0.0.27/26 if the network used was 10.0.0.0/26. Using a numbering scheme like this has the added bonus of improving readability when debugging the system or manually monitoring different drones.

The links have been setup and the drones can now communicate to each other directly. In Subsection 9.5.2, the different types of data traffic that are sent and the protocols that are used for communication are discussed.

Ground-to-Swarm

For the Ground-to-Swarm communication, the 868 MHz radio frequency is used through the facilitation of the Adafruit RFM95W Long Range (LoRa) transceiver.³⁹ This transceiver is used in both the ground station workstation and the swarm controller. In addition, a second transceiver of the same type is used in the flight controller for increased safety and reliability in case of failure.

At the start of the operation of the DroneCrane system, one of the drones is set as the active drone with respect to the transceiver and thus acts as the entry point for commands into the swarm and data out of the swarm. The transceivers on the other drones are set to a dormant state and are set up so that they can replace the active transceiver should there be an issue with it, either because of the detachment of one of the drones, or otherwise.

The transceivers on the swarm are configured to directly communicate to the transceiver in the ground station in a star topology, with the exception that the swarm transceivers cannot communicate directly with each other. The advantage of this configuration is that there is very less configuration needed on the software side in order to facilitate communication, making it more reliable for quick recovery in the event of an error.

9.3.3. Telecommunications Analysis

When communication is involved, there will always be limits to the data rate, transmission time and other factors based on the type of communication used, and the size of the messages being sent and received. Therefore, it is important to evaluate whether the swarm can function with these limits by exploring them for each type of communication in the Controls subsystem.

The Data Handling Block Diagram, which shows the maximum data bit rate for each interface, is shown in Figure 9.3. The Communication Flow Diagram, which shows the types of information exchanged between interfaces, is also shown in Figure 9.4

Drone Hardware

For the analysis of the hardware on an individual, it is important to consider that everything is connected physically, but over different interfaces and protocols.

As can be seen, for the interface between the swarm controller and RTK GPS module, an Inter-Integrated Circuit (I2C) bus is used with a maximum data rate of 3.4 Mbps. RTK GPS messages sent

³⁹<https://www.adafruit.com/product/4075> [Accessed in June 2022]

to the swarm controller from the RTK GPS module are of the size of 4 bytes⁴⁰. Therefore, with an data frequency of 60 Hz, this link is more than sufficient for this transmission.

Next, for the interface between the flight controller and the swarm controller, Universal Asynchronous Receiver/Transmitter (UART) is used with a maximum data rate of 1.5 Mbps. For messages exchanged between the controllers, the Mavlink protocol is used. The maximum size of a Mavlink message is 280 bytes. With a data rate of 1.5 Mbps, this allows for around 660 Mavlink messages per second, when the maximum size is used per message.

Furthermore, for the interface between the swarm controller and ultra-wide band transceiver, Serial Peripheral Interface (SPI) is used with a maximum data rate of 3.0 Mbps. Messages sent by the transceiver to the swarm controller are 127 bytes per message⁴¹. With a data rate of 3.0 Mbps, this allows for around 2950 messages per second, although in practice 50 Hz is sufficient.

For the interface between the swarm controller and the radio transceiver, SPI is used. The maximum data rate used is 20.9 Kbps. This value is limited in comparison to previous interfaces, since the data rate here depends on the wireless radio communication link. Messages sent between the transceiver and swarm controller use the Mavlink protocol, and therefore are 280 bytes per message. With a data rate of 20.9 Kbps, this allows for around 9 messages per second, when sending the maximum payload per message. While this is considerably lower than previous links, the requirements are still met, as commands being sent will be no more than two bytes, for a total of 16 bytes per message with an overhead of 14 bytes, as is discussed further in Subsection 9.5.3. With 16 bytes per message, the number of messages per second achieved increases to around 160 messages per second, which is more than sufficient to meet the requirement. The different parameters used for the wireless radio communication will be discussed in detail in the next subsection.

Ground-to-Swarm

For the link between the ground and the swarm, the radio transceivers are used; these transceivers use the 868 MHz frequency in operation. They were chosen over other radio transceivers operating at other frequencies because of the LoRa modulation scheme that is used. This scheme allows for lower power transmission, longer range transmission and chirp spread spectrum modulation which spreads signals sent over a wider bandwidth than is required. This is done to improve reliability and reduce the chance of signals not being received. Because of this spread, it is also very resistant to interference in a single channel.

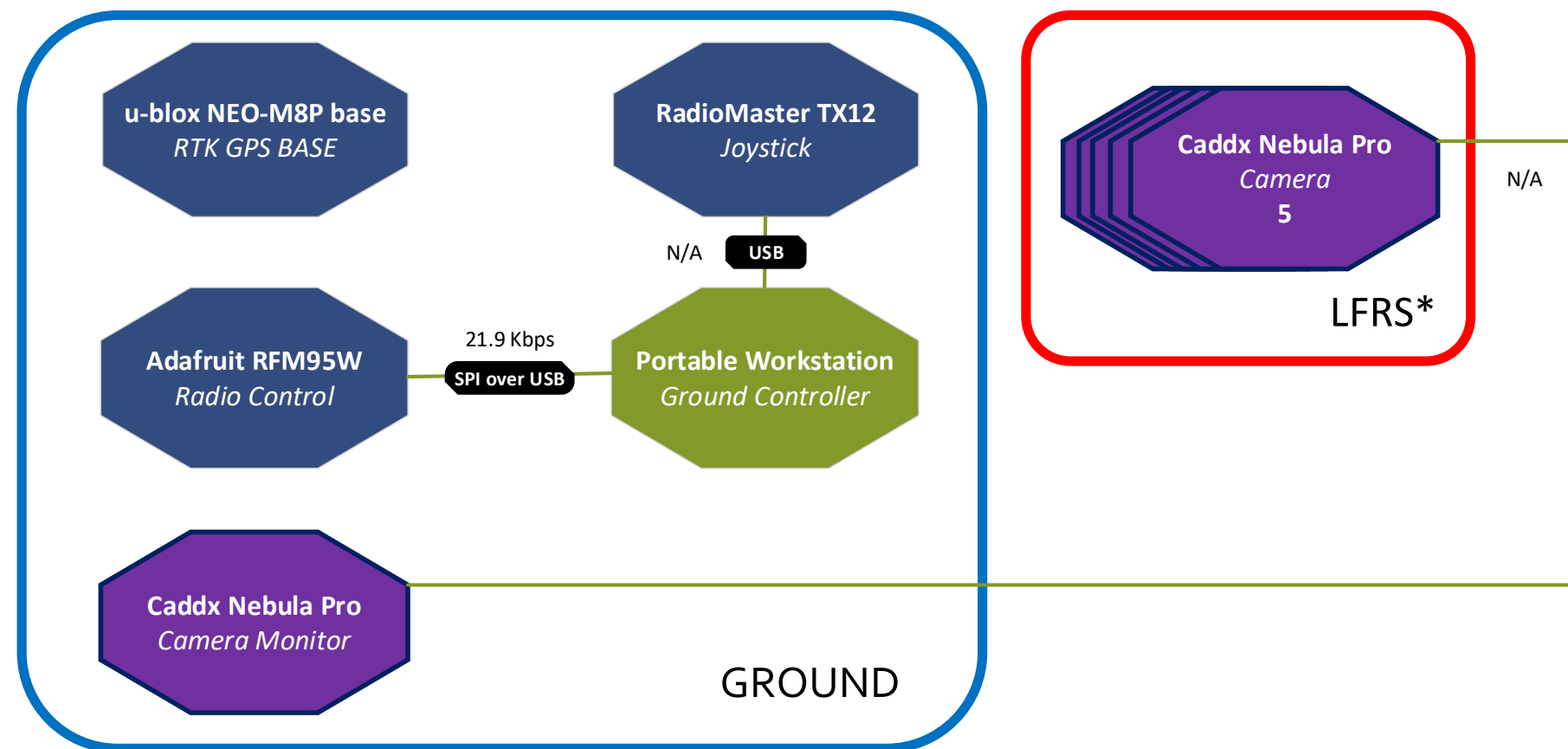
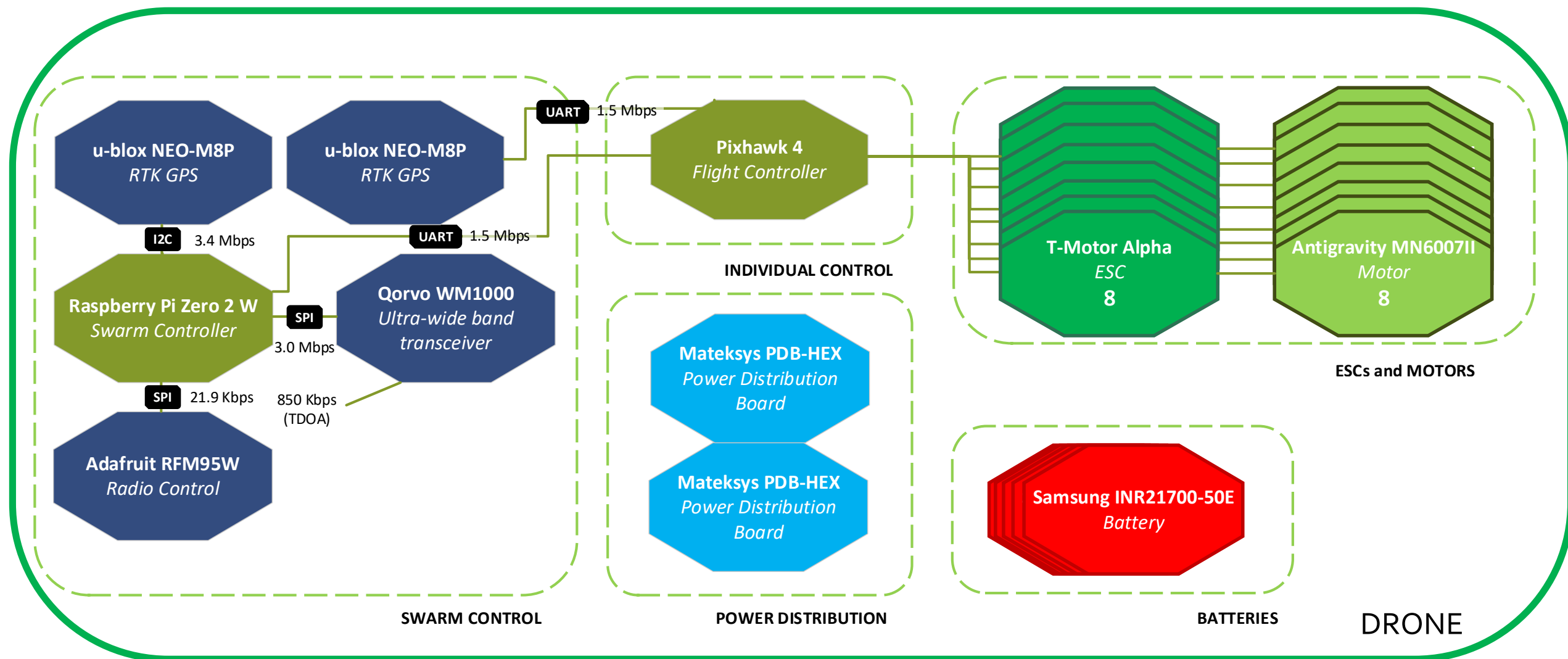
Using this module, a choice must also be made for the different LoRa parameters used, as this influences the max data rate per second. The parameters used include bandwidth, spreading factor and coding rate. Using a bit rate calculator⁴² with bandwidth set to 500 kHz, spreading factor 7 and coding rate set to 4:5, yields a bit rate of 20.9 kbps. This is sufficient for our requirements, as was discussed previously.

Independent from the drone electronics, the camera system will operate at 5.8 Ghz, a frequency not used by any other component on the drone. Operating on a high frequency will allow for lower latency and at sufficient range, much higher data rate for video feeds, at the cost of increased power usage. Batteries specifically designed for the camera system will be used on five drones and will be mounted on the LFRS at different angles.

⁴⁰<https://www.u-blox.com/docs/UBX-13003221> [Accessed in June 2022]

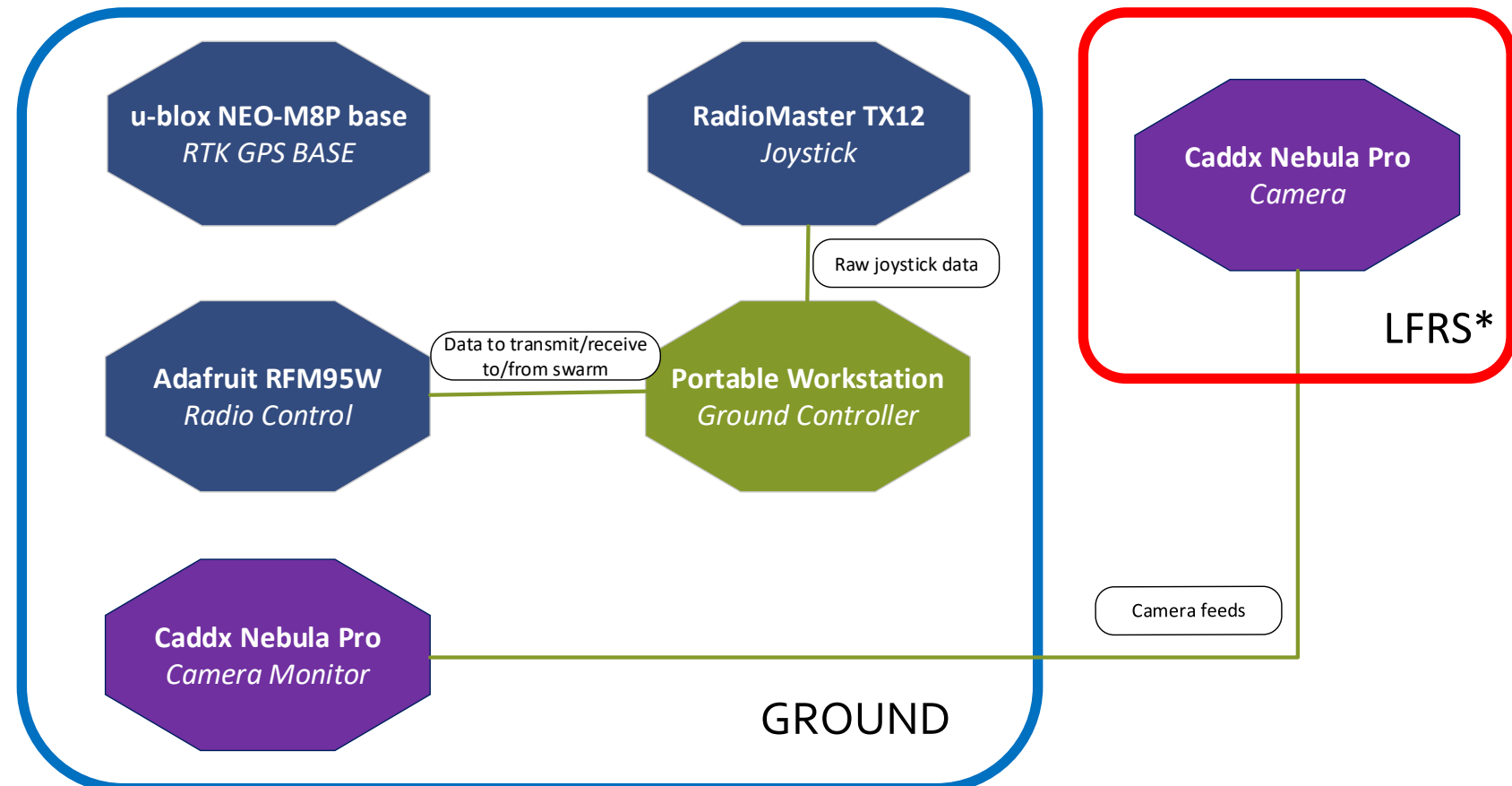
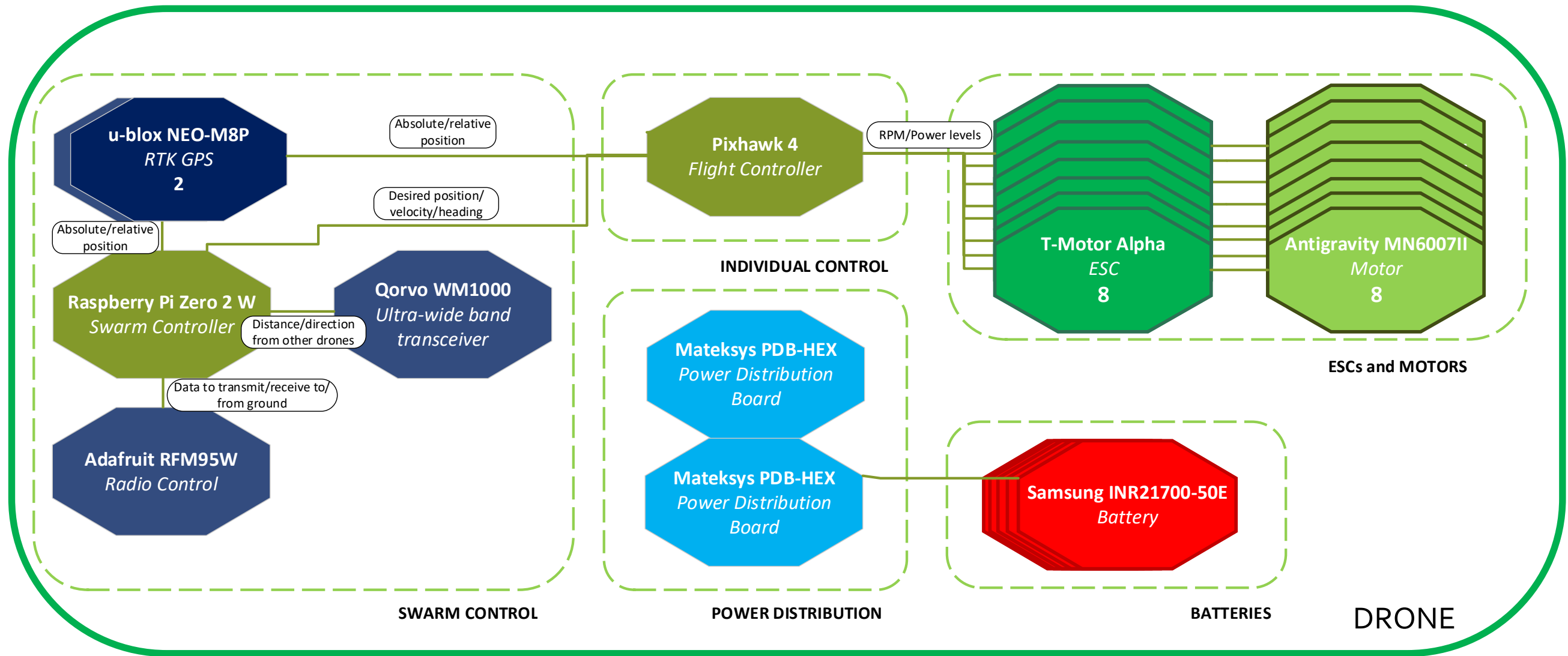
⁴¹<https://www.decawave.com/sites/default/files/resources/dw1000-datasheet-v2.09.pdf> [Accessed in June 2022]

⁴²<https://unsigned.io/understanding-lora-parameters/> [Accessed in June 2022]



* Only on specific drones

Figure 9.3: Data Handling Block Diagram (own work).



* Only on specific drones

Figure 9.4: Communication Flow Diagram (own work).

9.4. Individual Drone Simulation

This section was written by: *Giovanni*

Responding to the needs of a simulation framework, a control algorithm valid for each individual drone was developed and presented in this section. This "inner loop" in the control system of the swarm is dedicated to studying the octocopter and physically simulating it to provide verification methods for the design process. Despite this simulation not being the actual control algorithm that DroneCrane's drones are expected to use, it was built to compensate for the absence of a fast and simple method to emulate the Pixhawk controller in the time span available to the working group. The interfaces between these two loops have been defined in Section 9.2, and are the inputs that the individual drone control is expected to receive, i.e. the position required. Outputs of the inner loop are the updated position and reference states of the drone.

This section develops into a description of the drone model that was developed in Matlab SIMULINK⁴³ as a tool to predict and validate the power requirements, controllability, and redundancy claims made in previous stages of the design process [9, 11]. The model presented in this section serves as basis for future development of a simulation framework in which it would be possible to implement and approximate more of the factors that in reality would affect the drone in the swarm.

The mathematical formality of this chapter has been intentionally kept to a minimum to facilitate the reading: not containing novel research, the content nonetheless provides the reader with all the necessary information to replicate the modelling work in a structured manner. SIMULINK blocks are referenced when necessary to reduce the amount of details that are presented in this report.

9.4.1. Drone Physical Model

The drone model is constructed in a three-dimensional Cartesian space, with a right-handed inertial fixed-Earth reference frame used as reference, and a right-handed body-axis system located at the centre of mass of the drone, that is idealised to be fully rigid. The centre of mass of the octocopter is located in its geometric centre. Both axis systems have by default their z-axis oriented downwards, towards the ground, on the same line along which gravity (9.81 m s^{-2}) acts. The symmetrical nature of the octocopter, as seen from above, makes it so that a convention is introduced to reference its propellers: they are numbered as shown in Figure 9.5, where propellers with an odd index spin counterclockwise and those with an even index spin clockwise as seen from above.

The different vertical coordinates of each drone are not relevant to the current analysis as the thrust generated by each propeller is assumed to be fully parallel to the vertical axis, and the disturbances that the propeller exert on each other are neglected to reduce the complexity of the development, without compromising excessively on the quality of the results [33]. The reader shall note that no linearising assumptions were made and that any external loads, such as drag and payload weight, are assumed to act through the centre of gravity of the drone.

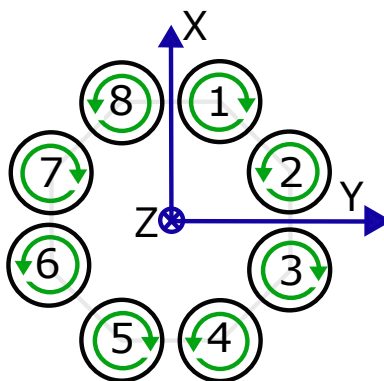


Figure 9.5: Propellers indexing system as adopted for the DroneCrane octocopter, with their direction of rotation indicated with respect to the body reference frame (own work).

⁴³https://nl.mathworks.com/help/simulink/index.html?s_tid=srchtitle_simulink_1 [Accessed in June 2022]

The rotation matrix from the fixed-Earth E to the body axis system B is defined as the Euler-angles rotation matrix of Equation 9.1 [43], in the conventional aerospace definition of rotation $Z - Y - X$ (where matrices are written in the reverse order $X - Y - Z$). These angles are the roll ϕ , the pitch θ , and the yaw ψ . In SIMULINK, the rotation is taken care of by the 6DOF block⁴⁴.

$$\mathbb{T}_{EB} = \mathbb{T}_X(\phi)\mathbb{T}_Y(\theta)\mathbb{T}_Z(\psi) \quad (9.1)$$

The dynamics of the point mass with which the drone is approximated are those presented in multiple works [43–50], which are vector equations that take into account the rotational movement of the body-axis system in the fixed-Earth one. Around the three axis the eight propellers can generate moments, whereas they can generate a force only parallel to the z-axis. This force is the thrust T and it is assumed to be positive upwards, in the negative z-direction. The formal objective of the control system is to determine the rotational speeds ω_i of each these eight actuators in order to keep the drone in stable flight. The physical dynamics are well modelled by the standard aforementioned SIMULINK block, which requires as input the drone mass m and the inertia tensor I_O .

Physical constraints

To provide the model with some necessary limitations that derive from the parts chosen to create a DroneCrane drone, the following physical constraints are imposed on the model:

- propellers can only spin in their intended direction to avoid inefficiencies and incongruities in the simulation framework;
- propellers can only spin as fast as 6300 RPM to account for the maximum rotational speed of the motors;
- the response time of a motor to a steady-state input is not instantaneous, but related to it by the transfer function in Laplace space presented in Equation 9.3;
- the lateral force that the drone is allowed to generated by rolling or pitching is limited in either of the horizontal directions to avoid excessive rolling or pitching.

No limitations on the maximum achievable linear or angular speed and acceleration of the drone are set to allow for a control-tuning process that is not slowed down by additional constraints. Drag forces are modelled according to Equation 9.2[51], where Cd values have been chosen to be unitary as if the drone were almost as draggy as a flat plate.⁴⁵ Density drag is assumed to be constant at sea level conditions of 1.225 kg m^{-3} for the whole simulation, as a 10% reduction in drag is found not to noticeably affect the results, and the loss in thrust due to altitude is simulated by increasing the downward pulling force on the drone.

The response function of the motor is formulated in Equation 9.3 [43]: this response considers the motor to be lagging in its response due to the inertia of the propeller and the internal mechanisms of the rotor itself, with the time constant T_m representing the time taken for the motor to reach 62.3% of the intended rotational speed [43, 44]. Because the thrust and torque of a propeller are linearly proportional to the square of the rotational speed [43], it is more convenient to find the transfer function that models the squared response of the motor's angular speed. By employing Equation 9.4, the model can become tidier and avoid the numerical issues that potential square root calculation would involve. Figure 9.6 shows the slightly difference shape of the output of the two transfer functions reacting to a step input. The force and torque generated by a motor are given by Equation 9.5 and Equation 9.6 [43], where c_T and c_Q are respectively the thrust and torque coefficients, whose specification for the current DroneCrane designs are given in Table 9.2 together with the time constant used for the motor response function. The latter value is chosen to be that of a well responsive motor [44], while the former two follow from the specification of the motor-propeller combination designed in Chapter 8.

⁴⁴<https://nl.mathworks.com/help/aeroblks/6dofeulerangles.html> [Accessed in June 2022]

⁴⁵<https://www.grc.nasa.gov/www/k-12/airplane/shaped.html> [Accessed in June 2022]

$$\hat{D} = -\frac{1}{2}\rho\hat{V} \cdot (C_d \cdot A) \quad (9.2)$$

$$\Omega(s) = \frac{1}{T_m \cdot s + 1} \quad (9.3)$$

$$\Omega^2(s) = \frac{1}{\frac{1}{2}T_m^2 \cdot s^2 + \frac{3}{2}T_m \cdot s + 1} \quad (9.4)$$

$$T = c_T \cdot \omega^2 \quad (9.5)$$

$$Q = c_Q \cdot \omega^2 \quad (9.6)$$

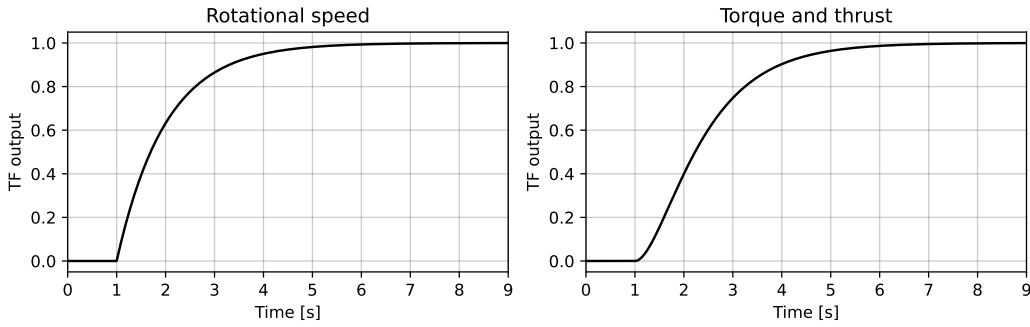


Figure 9.6: Response shape of Equation 9.3 (left) and Equation 9.4 (right) to a unit step input applied at 1 s, simulated with a unit time constant parameter (own work).

Table 9.2: Thrust, weight coefficient and motor time constant specifications.

Variable	Magnitude and units
c_T	$1.39 \times 10^{-4} \text{ N s}^2$
c_Q	$2.98 \times 10^{-6} \text{ N m s}^2$
T_m	0.1

The drone model is completed by modelling the forces, generated by the rotation of each propeller, along the z-axis and the moments generated around its three axis, as seen in Equation 9.7. This system is described through relations commonly accepted in literature [43, 44, 47–50]. In Equation 9.7, τ_ϕ , τ_θ , and τ_ψ represent the rolling, pitching, yawing moments. The term ds is the short moment arm, as long as half of the drone's octagonal contour's half-side, whose exact length given by Equation 9.8. The term dl is the long moment arm, described by Equation 9.9. In both equations, l represents the distance between the projections of the COG of the drone and any of the motor's rotational axis on the XY plane.

$$\begin{bmatrix} \tau_\phi \\ c_T \\ \tau_\theta \\ c_T \\ \tau_\psi \\ c_Q \\ T \\ c_T \end{bmatrix} = \begin{bmatrix} -ds & -dl & -dl & -ds & ds & dl & dl & ds \\ dl & ds & -ds & -dl & -dl & -ds & ds & dl \\ 1 & -1 & 1 & -1 & 1 & -1 & 1 & -1 \\ 1 & 1 & 1 & 1 & 1 & 1 & 1 & 1 \end{bmatrix} \begin{bmatrix} \omega_1^2 \\ \omega_2^2 \\ \omega_3^2 \\ \omega_4^2 \\ \omega_5^2 \\ \omega_6^2 \\ \omega_7^2 \\ \omega_8^2 \end{bmatrix} \quad (9.7)$$

$$ds = \frac{\sqrt{2 - \sqrt{2}}}{2} \cdot l \tag{9.8}$$

$$dl = \frac{\sqrt{2 + \sqrt{2}}}{2} \cdot l \tag{9.9}$$

The drone model as formulated above is useful to determine how any control input changes the force and the moments acting on it, while at the same time providing a paradigm to determine what control inputs to give the system in order to achieve the desired movement. The exact formulation of the problem that, when solved, yields an acceptable solution for $\hat{\omega}$ in Equation 9.7 is presented below in Subsection 9.4.2. In Table 9.3, the reader can find the physical parameters used for the drone: the moments of inertia were taken from early CAD designs of DroneCrane’s octocopter, and non-diagonal entries of the inertia tensor are considered to be null due to the unavailability of greater detail from the CAD models at the current stage of detail.

Table 9.3: Physical parameters used for the model of the drone.

Mass	Moment arm length	I_{xx}	I_{yy}	I_{zz}
24.4 kg	0.479 m	2 kg m ²	2 kg m ²	3 kg m ²

9.4.2. Control Model

The individual drone control simulation algorithm is composed of four main blocks that are configured to be modular, and whose interfaces clearly mark the information flowing between them: as shown in Figure 9.7, the control is initiated by a reference input vector containing the 3D coordinates of the desired location for the drone. This information is fed to the controller block where it is filtered with cascaded P or PI controllers to compute the required moments and forces desired to minimise the position error. Indeed, this second block received the information about the states of the vector as feedback information. The third block accepts the required force and moments and determines the steady-state commands to be fed to each of the eight propellers. The final block physically simulates the response to such request: the dynamics of each rotors are individually simulated and their output (the actual rotational speed of each motor) is used to compute the thrust and moments acting on and around the drone. Finally, the states of the drone are updated and the information sent to the start of the loop.

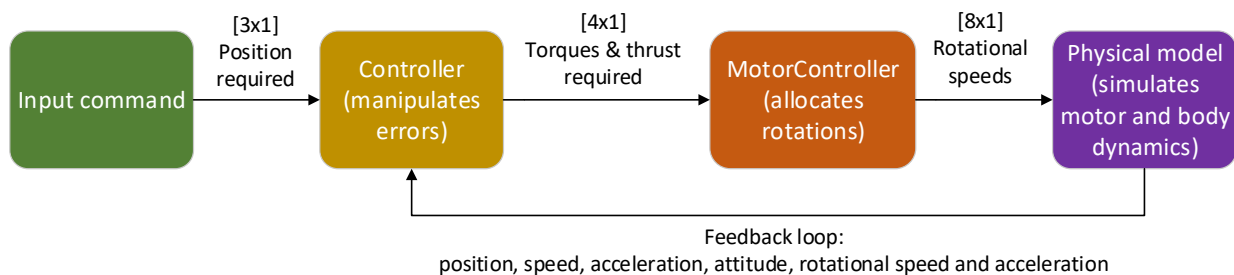


Figure 9.7: Control system macro-blocks for the individual drone control in the inner loop of the control system (own work).

Input Command

The input command is rather simply the position which the swarm control algorithm requires the drone itself to achieve. It is defined in the 3D space and the only requirement it has to satisfy is that it outputs a single-dimensional vector of size three.

Controller

The controller is the block that receives both inputs and outputs of the system, uses them to calculate the associated errors, and delivers a request to the motorcontroller block. This block is structured as a set of P and PI controllers in cascade that process the errors in parallel to distinguish between vertical and horizontal movements: due to the different nature of the two types of translation, different gains facilitate the tuning process, as described in Subsection 9.4.6 below.

The vertical movement controller processes the vertical position error, which is converted to velocity to compute the first derivative error, and then again processed to apply the same process in order to receive a required vertical thrust after the PI controller on the acceleration error has acted on the information stream. The horizontal movement controller repeats in a similar fashion the same steps taken by the vertical controller, and once the required acceleration is known, the lateral forces to achieve such accelerations are computed. Note that in order for the lateral force to be limited an upper bound on its magnitude is set at 30 N, which limits the maximum roll or pitch angles to at most 7° in hovering conditions. This keeps the drone in the set of possible states that could also be modelled linearly, so to in any case avoid incurring in undesired unexpected, counter-intuitive non-linear behaviour. Additionally, two feedforward controllers are used to limit the thrust as well: one D controller on the position error whose output is fed directly into the computation of the required horizontal thrust (before the limiter), and a PI controller on the absolute velocity of the drone. The latter acts to limit the horizontal velocity of the drone, while the former requires an inversion of thrust when approaching the desired target location to avoid excessive overshoot. Then, in order, respectively with Equation 9.10, Equation 9.11, and Equation 9.12, the total thrust, roll and pitch angle required are computed [50]. These equations involving inverse trigonometric relations are guaranteed to provide results, under the assumptions made, at least when the vertical thrust required is bigger in magnitude than any of the horizontal ones (in the x and y-direction). This situation is extremely unlikely to be out of scope for the cases simulated in this chapter.

To achieve the necessary angles, a cascade of P, P, and PI controllers is applied again to both roll and pitch angles, their first and second derivatives to yield the moment required around the X and the Y body axes. Throughout this process, yaw is neglected and assumed to be zero, yielding a system with one less degree of freedom, hence simpler. This is done for a series of reasons:

- the ropes connecting the drone to the LFRS should not be torsioned;
- the symmetry of the octocopter configuration employed allows yaw to be required to be constant and null;
- the drone's yaw attitude is not relevant to the correct functioning of the swarm (see Section 9.5

The output of the block in the end is a required total thrust and an attitude, ready to be distributed in form of squared rotational speeds by the motorcontroller module.

$$T = \sqrt{T_x^2 + T_y^2 + T_z^2} \quad (9.10)$$

$$\phi = \arcsin \frac{T_x \sin \psi - T_y \cos \psi}{T} \quad (9.11)$$

$$\theta = \arctan \frac{T_x \cos \psi + T_y \sin \psi}{T_z} \quad (9.12)$$

Motor Controller

The MC block represents the computation that the onboard flight computer performs to assign each rotor a rotational speed command to achieve the thrust and moments that the controller would expect the drone to generate. As mentioned earlier, the system to solve in this case is the one presented in Equation 9.7, where the solution $\hat{\omega}$ is given implicitly. However, due to the different dimensions of

the force vector and $\hat{\omega}$, the matrix pre-multiplying the latter is not invertible.⁴⁶ The issue can be seen as a direct consequence of the fact that the drone has eight actuators and only four outputs, thus characterising itself as an over-actuated system [52].

A common method found in literature to find a solution to the system nonetheless is the employment of a Moore-Penrose pseudoinverse matrix [52], which conveniently allows to assign a squared rotational speed to each rotor while at the same time minimising the overall power required by the system [53]. This solution can be seen as a least-squares solution to the problem posed, and may very well offer a quick and computationally affordable way to design the motorcontroller. Unfortunately, this method does not allow for constraints to be put on the solution: it is not possible to account for saturation before solving the system, and an iterative algorithm has to be run to find a solution within the prescribed bounds [44].

Alternative ways of solving the system for $\hat{\omega}$ are to optimise the system through more computationally expensive methods designed specifically to automatically determine the squared rotational speed expected from each rotor while satisfying the imposed constraints [52, 54]. The implementation of this method allows for a better representation of reality, but the faster pseudoinverse matrix can be used to go faster through simulation rounds when tuning is happening and physically unachievable inputs can be intentionally avoided by employing the saturation checking methods described in the implementation description.

Physical model

In the final block of the forward section of the control model, the dynamics of the drone are simulated from the steady-state rotations that the motorcontroller commands the motors to achieve. Hence, the motor dynamics are simulated with eight parallel blocks representing Equation 9.4, whose outputs are the thrust and torque as acting on the drone, following the principle of action-reacting. This means the counter-clockwise rotating propellers generate a clockwise torque on the drone and vice versa, explaining the signs of the third row of the matrix in Equation 9.7. The forces on the body are an input to the block that simulates the dynamics of the point mass with axis system, and its outputs are all the states of the drone: position, speed, and acceleration in the fixed-Earth frame; attitude, angular rates and acceleration of the body frame with respect to the fixed-Earth frame and the associated rotation matrix. These outputs can be looped back to the first block of the system to compute the errors of the states with respect to the input.

9.4.3. Observability

What is fed back from the physical simulation to the controller block can only be used if it is possible to estimate it on the drone, so it depends on how observable the system is. Common literature performs a thorough mathematical analysis of the matter to demonstrate the observability of the system[43, 44, 55]. In this context, Table 9.4 is used to justify each of the loops that are used, where each state that is used in the loop is accompanied by the sensors contributing to its observability properties. The accuracy of the measurements methods is treated in Section 9.1 and Section 9.5.

Table 9.4: States of the individual drone and their observability, justified by the presence of sensors and estimators.

State	Frame	Sensors
Position	E	RTK
Velocity	B	RTK and IMU estimation
Acceleration	B	IMU
Attitude	B	IMU, Gyroscope, Magnetometer
Angular rates	B	IMU, Gyroscope
Angular accelerations	B	IMU, Gyroscope

⁴⁶<https://mathworld.wolfram.com/InvertibleMatrixTheorem.html> [Accessed in June 2022]

9.4.4. Limitations of the Simulation Model

The model described above nears reality for conditions that are close to hovering and where movement is restricted, as all the disturbances that appear as the flow around the drone speeds up are neglected [56]. Similarly, the errors that observations carry with themselves are also not simulated as advanced literature does [50, 57, 58]. Together with the simplifications and assumptions illustrated above, the simulation is characterised by a series of limitations that are made explicit in the list below. All of the simplifications are accepted since their effect is negligible at the current stage of the design process, nevertheless allowing for a critical interpretation of the simulation results.

- **Limitation:** the drone's inertia tensor is assumed to be a diagonal matrix;
 - **Cause:** lack of accurate data from early CAD design;
 - **Effect:** roll and pitch rotations are marginally faster [47].
- **Limitation:** the motor time constant is equal whether it is speeding up or down;
 - **Cause:** lack of data from the motor manufacturer;
 - **Effect:** minimally faster or slower motor response [44, 59].
- **Limitation:** the motor thrust and torque scale linearly with ω^2 ;
 - **Cause:** lack of data from the motor manufacturer;
 - **Effect:** Minimum and maximum thrust and torque delivered are inaccurate [59].
- **Limitation:** the effect of the two-layer octocopter configuration is neglected;
 - **Cause:** lack of specific CFD or testing data;
 - **Effect:** thrust efficiency is overestimated by a factor of approximately 5% [33].
- **Limitation:** motor electrical efficiency is not accounted for;
 - **Cause:** lack of data from the motor manufacturer;
 - **Effect:** electrical power cannot be accurately estimated.
- **Limitation:** altitude effects are accounted for with a thrust safety factor of 1.1;
 - **Cause:** otherwise increased computational complexity;
 - **Effect:** estimation of mid-altitude power requirements not possible.
- **Limitation:** drone-to-drone aerodynamic interference is neglected;
 - **Cause:** lack of CFD or testing data;
 - **Effect:** drone performance is likely overestimated.
- **Limitation:** rope force is assumed acting at the drone's COG;
 - **Cause:** otherwise increased computational complexity;
 - **Effect:** the drone's lateral movement power requirements are underestimated.
- **Limitation:** rope force is assumed active vertically at all times;
 - **Cause:** lack of Drone-LFRS-Payload vibrational model;
 - **Effect:** the drone's overall power requirements are underestimated.
- **Limitation:** rope force is constant;
 - **Cause:** lack of Drone-LFRS-Payload vibrational model;
 - **Effect:** the drone's vertical excitation are less noisy than in reality.

- **Limitation:** observation of the drone's states is not noisy nor erroneous;
 - **Cause:** otherwise increased modelling complexity;
 - **Effect:** the simulation does not represents effective working conditions [56].
- **Limitation:** drag coefficient and frontal area values are approximative;
 - **Cause:** lack of CFD or testing data;
 - **Effect:** lateral speed potential is potentially overestimated [46].
- **Limitation:** maximum speed values are not set;
 - **Cause:** lack of more accurate simulation runs;
 - **Effect:** drone reactivity to input is potentially overestimated.
- **Limitation:** propeller pressure distribution is assumed independent of local airspeed;
 - **Cause:** otherwise increased modelling complexity;
 - **Effect:** lateral movement stability and control are non-realistic.
- **Limitation:** wind gusts are neglected;
 - **Cause:** otherwise increased modelling complexity;
 - **Effect:** the simulation does not represents effective working conditions.

9.4.5. SIMULINK Implementation

As mentioned earlier, the drone model is implemented in Matlab SIMULINK and evaluated in that environment. The blocks as described in Subsection 9.4.2 are correspondingly created in the simulation environment with particular care with respect to unit consistency and modularity, so that they can be changed while having a solid awareness of the flow of information. The four blocks are created individually and imported in a larger model file. To speed up the full simulation, function blocks are employed to keep the simulation as fast as possible, as SIMULINK takes more time to compile the model created by means of the graphic interface⁴⁷. The schematics of the simulation is presented in Figure 9.8.

9.4.6. Tuning

Tuning the gains of the nine controllers present in the model is a highly complex procedure that from scratch has given the working group a serious challenge. In order to facilitate the process, it was decided to tune the gains as independently as possible from the complete model, in an effort to reduce the time taken to find them and ensure stability to the system. To do so, a second, simpler model was created in SIMULINK. The simplifications applied to the model included the exclusion of eight-motor models from the beginning, and the simulation of the drone dynamics through the use of integrators rather than the 6DOF block.⁴⁸ The dynamics of the rotational and translational system are still analysed with the same assumptions holding for the full model.

The first step of the simpler model is created for vertical gains tuning: an input is used as position reference, from which the error is found thanks to the feedback in the loop. To this first error a P gain is applied, followed from a summation with the negative velocity, yielding the speed error. To this error, a P controller is applied. Finally, the same happens for the acceleration and its error. The resulting value is treated as the required vertical thrust. It is then scaled by the thrust coefficient c_T and by the number of propellers on the octocopter, i.e. 8, to yield the squared rotational speed required from each of the motors. This value is saturated with bounds 0 and 6300 RPM (or 660 rad/s) and it is passed through the motor response function of Equation 9.4. It is then squared and converted back

⁴⁷<https://nl.mathworks.com/company/newsletters/articles/improving-simulation-performance-in-simulink.html> [Accessed in June 2022]

⁴⁸<https://nl.mathworks.com/help/simulink/sref/integrator.html> [Accessed in June 2022]

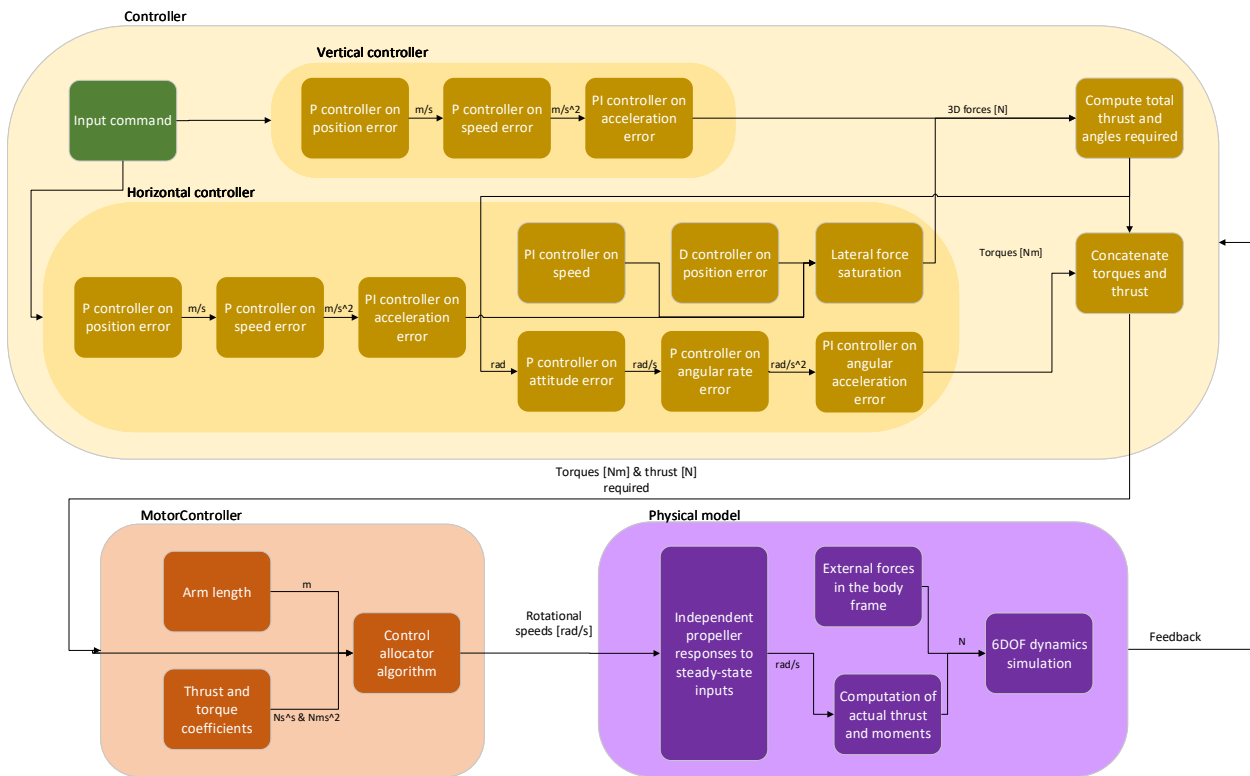


Figure 9.8: Schematics detailing the structure of the SIMULINK implementation of the individual drone control simulation (own work).

to thrust, which is in turn scaled by the mass of the drone. The information is thus converted to an acceleration, which can be fed back in the loop and integrated to find the speed and the position of the drone along the vertical axis.

The tuning process is run by considering first the most inner loop and then expanding outwards. Starting from the innermost loop, the PI controller is tuned, followed by the speed controller and subsequently the position controller. As the vertical response was stabilised, the simpler model was expanded to model the horizontal response in a single direction, with the direct implication of the assumption that stabilising in roll meant stabilising in pitch as well. The coupled dynamics of vertical and horizontal movement, as well as pitch and roll movements is not considered to be detrimental to the exercise: this is proven to be the case at a later stage.

Once the system’s response is tuned in the simplified model, it is integrated in the larger simulation framework. Finally, gains are tuned, again by hand, to check that the overall system works well as a unity. The process is conducted to stabilise the system and provide it with an appreciable response speed, small to negligible oscillations, and little overshoot for inputs whose order of magnitude does not exceed 10 to 20 m. This is an acceptable compromise on the quality of the results considering the time and resources allocated to the development of the simulation. Once the larger model was running, it was found that by adding downwards vertical forces the overshoot of the system was greater. In order to dampen the consequent response, decreasing the P controller on the vertical position error revealed to be sufficient. The results of the tuning process are given in Table 9.5, Table 9.6, Table 9.7.

Table 9.5: Gains of the cascaded controllers as applied to the vertical controller of the drone system. The gains are applied to the errors in position and its first and second time-derivative.

Gain type	Acting on	Magnitude	Output
P	Position error	0.5	Required speed
P	Speed error	1.6	Required acceleration
P	Acceleration error	300	Required vertical force
I	Acceleration error	150	

Table 9.6: Gains of the cascaded controllers as applied to the horizontal position controller of the drone system. The gains are applied to the errors in position and its first and second time-derivative.

Gain type	Acting on	Magnitude	Output
P	Position error	2.2	Required speed
P	Speed error	4	Required acceleration
P	Acceleration error	10	Required horizontal force
I	Acceleration error	0.5	
P	Speed	-70	
I	Speed	-9	
D	Position error	10	

Table 9.7: Gains of the cascaded controllers as applied to the roll and pitch controller of the drone system. The gains are applied to the errors in attitude and its first and second time-derivative.

Gain type	Acting on	Magnitude	Output
P	Angle error	3	Required speed
P	Angular rate error	33	Required acceleration
P	Angular acceleration error	2	Required moment

9.4.7. Stability Results

The system as tuned in the previous section is simulated with horizontal and vertical inputs and the behaviour shown in this section, whose goal is to make the reader aware of the basic systems' behaviour. Relevant states are plotted for different inputs, as well as the motor response in rotations per minute, and more considerations on the results presented here are given in later sections.

Vertical negative unit step input response

From an hovering, resting condition, the system is told to move 1 m in the negative z-direction. The response for a drone-only system (unloaded) and that of a drone carrying an additional 100% of its unloaded mass are shown in Figure 9.9. The percentage figure comes from the results of the sizing process of Chapter 8, as for hovering it was considered that each propeller would generate approximately 6 kg of thrust, and the octocopter weighs a little more than 24 kg.

The differences between the two simulation instances are the slight but noticeable overshoot of the loaded response and the saturation of the motors when close to 6300 RPM. The extreme case for a thrust-to-weight ratio of the system accounts for atmospheric conditions at 1000 m altitude, where the system is pushed to its limits. It is clear that saturating the propellers is not a safe operating condition, and limits the amount of manoeuvrability of each drone.

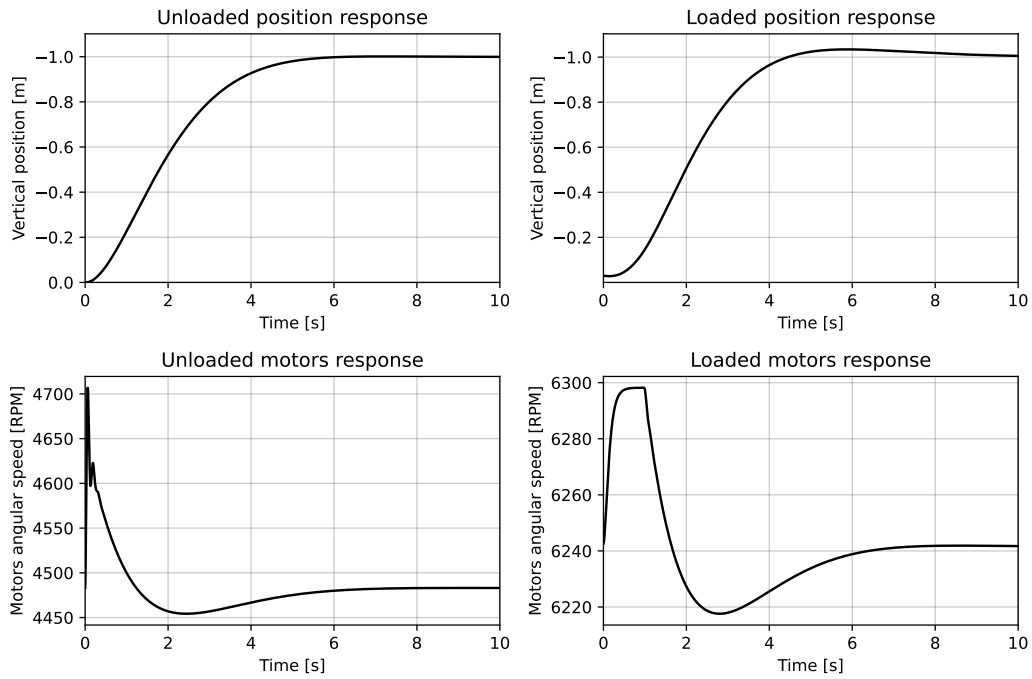


Figure 9.9: Response of the tuned system to an upwards displacement input from hovering conditions, both in unloaded and loaded mode (own work).

Horizontal unit step input response

From an hovering, loaded, resting condition, the system is commanded to move 1 m in the positive x-direction. The response of the system is shown in Figure 9.10, where the plots show respectively the horizontal position response, the vertical one, the pitch angle, and the motors response. In the latter plot, four lines are present, as the eight motors have a symmetrical lift distribution with respect to the y-axis.

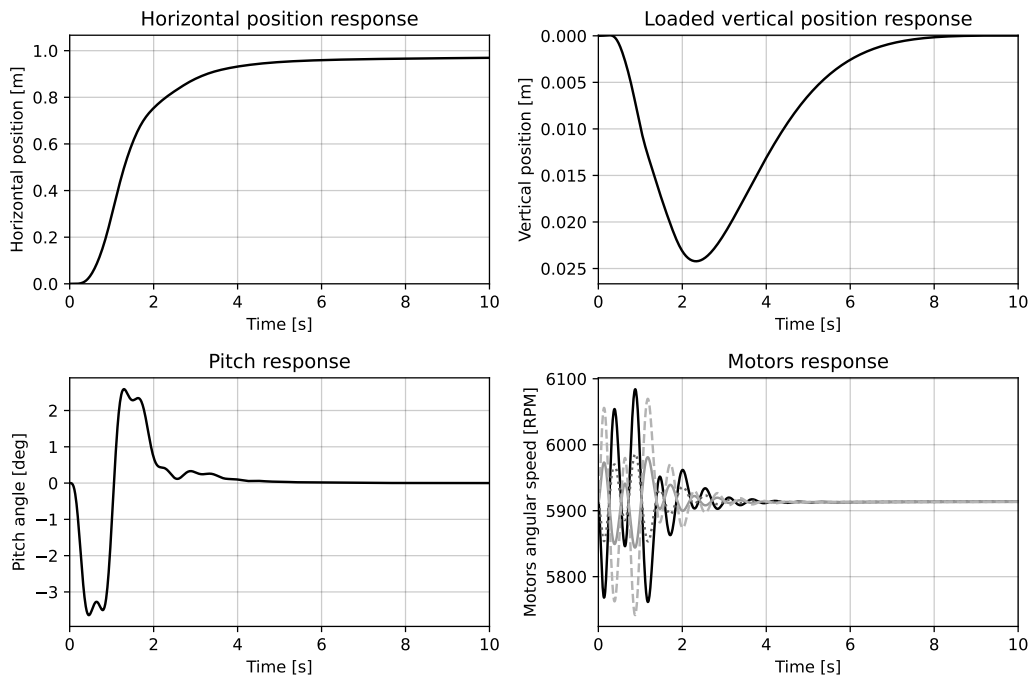


Figure 9.10: Response of the tuned system to a horizontal displacement input from hovering conditions (own work).

9.4.8. Verification of Power Requirements

The simulation allows to test the power used by the system by means of a simple manipulation procedure on the rotational speed of the propellers at any instant: by using Equation 9.13, it is possible to compute the total power needed by the drone. The formula is derived from Equation 9.5 and the classical definition of rotational power as the time derivative of the rotation work done by a torque over an angular displacement. An integration of power yields the total energy that the system uses. In order to provide the engineering team with useful results from this simulation, three research questions are defined for the procedure, they are analysed and the conclusions drawn are summarised at the end of this report.

The target questions are the following:

- the determination of the greatest accelerations the drone's control system can expect to be able to perform;
- the analysis of manoeuvrability and the attitude changes that can be performed when loaded;
- the exploration of design limits or involuntary potential in the design of DroneCrane's drones.

$$P = c_Q \cdot \omega^3 \quad (9.13)$$

Vertical acceleration

It has been noted already in Subsection 9.4.7 that when highly loaded the single drone saturates if trying to imitate the same position response curve of an unloaded peer. The overshoot that appears in Figure 9.9 is due to the gains of the system being fine tuned for a system that was loaded at 1.74 of thrust-to-weight ratio. The lower loading appears when at sea level conditions and with all drones in the swarm operative.

Therefore, the first insight revealed by the simulation is that for the system to be safely operable in the extreme cases, the vertical acceleration should be limited, so that at low altitude conditions the system has good margins of manoeuvrability, and at limit conditions it is still safe to operate. When at 1000 m altitude, nominal thrust conditions are diminished by a factor of 1.1, as presented in Chapter 8. They imply a potential maximum acceleration of 0.21 m s^{-2} that would allow reaching the desired cruising vertical speed of 1.5 m s^{-1} in 3 s. Because this is regarded as a very reasonable figure by the designing team, acceleration is allowed to be at most half of such value: 0.1 m s^{-2} .

The new saturation block⁴⁹ added in the simulation changes the behaviour of the system, so that the P gain on the position error of the vertical controller has to be decreased once more to 0.3 to avoid overshoot in the system. Following this manual modification, the motorcontroller requests to the motor hits a ceiling at a lower rotational speed, going from 6300 RPM to 6260 RPM. The marginal change in the speed can be directly compared to the speed change shown in Figure 9.10, which was in the range of 2 to 3 RPM. A higher limit on the vertical acceleration would then make DroneCrane much slower in response, and nevertheless not as responsive in lateral movement either. Indeed, by sacrificing all of the vertical push for horizontal movement margins would bring the rotations of each propeller just over 120 RPM away from its maximum rotational speed.

Horizontal movement

The key requirements of DroneCrane concern vertical displacement only, as the system is targeted to a market that is mostly concern with vertical range. However, in previous work[9, 11], the possibility of moving horizontally was considered. The initial considerations made on horizontal speed were that it would have been able to be higher than for vertical speed as the work required to move against gravity was higher. With the simulation tool at the team's disposal, it is possible to validate the earlier claims.

⁴⁹<https://nl.mathworks.com/help/simulink/slref/saturation.html> [Accessed in June 2022]

The analysis consists in analysing the energy used by the system to perform a lateral manoeuvre of 10 m from hovering, resting conditions. Due to the large movement, the system overshoots by more than 3 m to then oscillate to the forced position. To keep the simulation realistic, the P gain value of the controller on horizontal position is lowered to 1.15. The response to a step input in the lateral direction is presented in Figure 9.11, where horizontal position, horizontal speed, pitch angle, motor response, mechanical power, and energy are given.

Let the reader recall that the presence of the payload on the drone is now simulated by increase the effective mass of the drone by the same factor used to increased the vertical pull on it, i.e. the aforementioned 200%. Now it is possible to notice from the plots of Figure 9.11 the response of the system to a step command in the x-direction. The speed increases linearly up to almost 2.5 m s^{-1} because of the limitations imposed on the maximum pitch angle mentioned in Subsection 9.4.2. The motors can be seen reacting when changes in the acceleration are required, and power being higher for all the time span of the simulation. However, the total energy used is almost constant, so much that the two lines plotted overlap completely. The difference in the two simulations runs is so small that it is deemed negligible for the purpose of the analysis, and surely dependent on the step size of the simulation, which in both cases never goes above 0.01 s.

Since it is found that horizontal movement does not significantly increase the energy consumption, it is possible to deem DroneCrane able of flying horizontally greater distances than those it can reach vertically, verifying claims made in previous stages of the design process[9, 11].

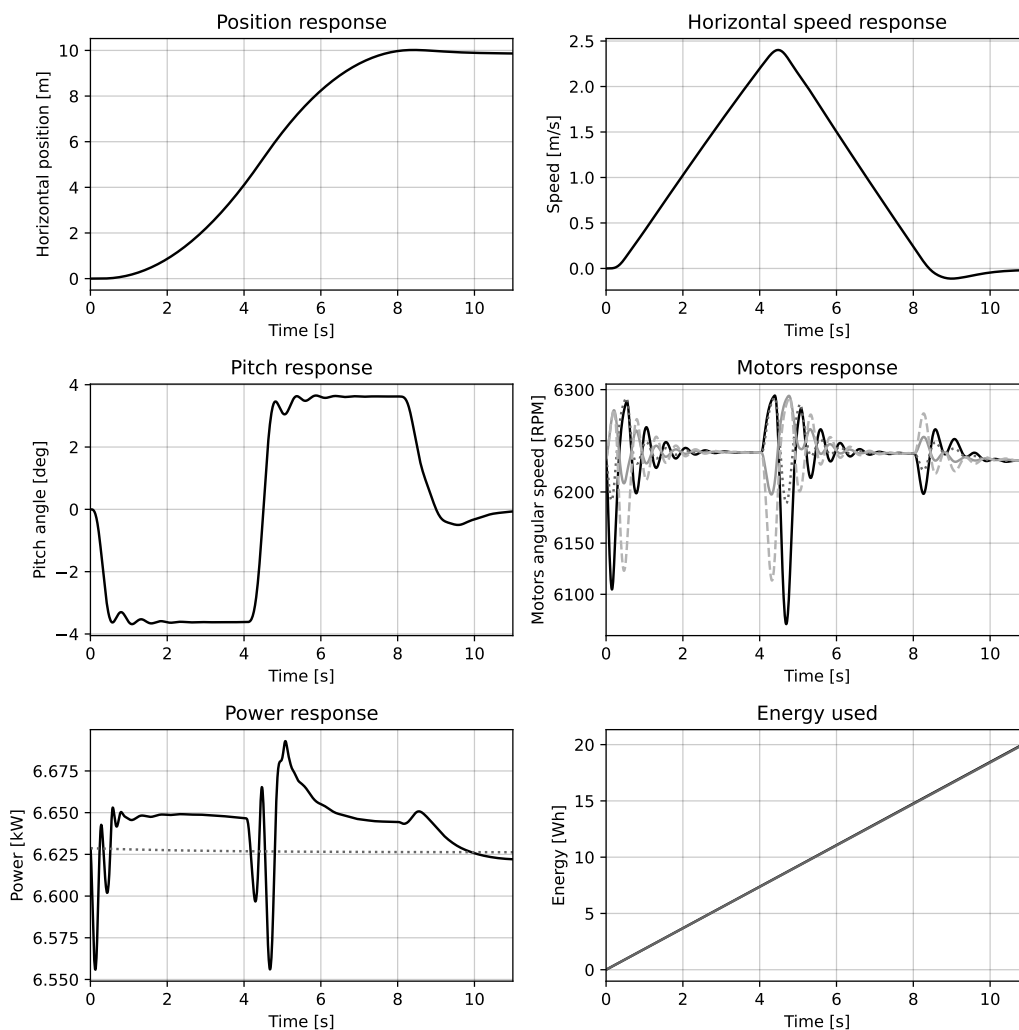


Figure 9.11: Response of the tuned loaded system to a 10 m horizontal displacement input from hovering conditions (own work).

Controllability

The reason why DroneCrane is a swarm of octocopters instead of drones with any other number of propellers stands in the fact that drones with a smaller number of rotors lack redundancy or enough symmetry to survive past the case of one of the rotors failing[9, 11]. The design choice was justified for not choosing a smaller number of propellers; indeed, the reason for not going higher was dictated by the lack of literature concerning the control of what the team called N-copters, those with an arbitrarily high number of propellers. This raised concerns concerning the technology readiness level (TRL) of the potential design, hence why the option was disregarded. This section deals with the consequences of such choice, and investigates whether indeed the loss of one or two propellers for DroneCrane's octocopter can be considered a minor failure that does not lead to the loss of one drone's utility.

To simulate the loss of any propellers in the model implementation, two situations could be considered: that in which the motorcontroller is unaware of the unresponsiveness of the motor, and the opposite case. Because it is reasonable to expect fault detection in professional drones, only the latter case is considered. Because of the symmetric properties of the octocopter, a one rotor failure can be modelled disregarding its own index, as defined in Figure 9.5.

Literature has shown that it is possible to redistribute the thrust among the remaining propellers without losing control of the drone provided the motors are far enough from saturation [60–62]. However, in a simpler way, hand-written analysis can on its own yield insightful results applicable to the current design problem: losing one propeller would reduce the available thrust by 12.5%, thus nullifying the margin factor accounted for the possibility of flying at 1000 m altitude. Still, DroneCrane would be operable at sea level conditions, where the thrust-to-weight ratio needed for operations is closer to 1.7. It is concluded that in any operating condition, the loss of another propeller would deny any octocopter the possibility of continuing and concluding the mission safely.

9.4.9. Simulation's Contribution to the Design Process

The results of the simulations presented above are undeniably a point of concern for the designer of DroneCrane, and despite the limitations of the simulation and the limited number of cases analysed, the potential of the simulation is extremely high and had the working group been able to have it at their disposal from the beginning of the design process it would have certainly affected many of the designing software illustrated in Part II, as well as the decisions presented in Part III. For future development, DroneCrane will have to rely on simulation methods to verify the design before manufacturing may be started.

Points of Improvement

The aforementioned limitations of the simulation presented in Subsection 9.4.4 can be seen as a starting document for the software developers that may in the future expand the simulation. Specifically, for the benefit of DroneCrane, a more realistic simulation will benefit from the short term implementation of the following:

- drone-to-drone aerodynamic interference, to be modelled through CFD runs of the model, potentially simplified by considering symmetry conditions around the circles inscribing the drones in the swarm configuration depicted in Section 9.5. The control model can be set up to predict for the change in performance that drones in the swarm experience;
- rope force influences, to be modelled through inertial and vibrational models for the swarm-LFRS-payload system. The control model can also model the rope through sensing of its tension or indirectly by sampling the state's measurement to estimate rope tension and direction. The latter option may however require the integration of sensor that are currently not budgeted for;
- Pixhawk behaviour and response time, which can help by enabling a more realistic simulation of the system;
- swarm control algorithm, so that the control system may be tuned according to the magnitude and frequency of the inputs that the "outer loop" control feeds to the Pixhawk itself.

9.5. Swarm Control

This section was written by: *Bryan, Dequan*

Now that the control of an individual drone has been covered extensively and the communication principles explored, it is imperative to look at the other half of the control system of DroneCrane. The Swarm Control aspect of this project is what makes it unique to other projects that carry payloads with just one drone; the payload must be carried by 31 drones, each one carrying a small share of the weight while propelling, in coordination, towards a new direction.

At the same time, operating in the swarm is no easy task as it requires instant-time coordination and a system that is designed from the ground up to correct for errors over time. In addition, operating in a decentralised manner, which was chosen from the trade off in [9], further signifies the constraint that communication time and computational time have on the time-coordination of the swarm of drones.

The aim of this section is to walk through the different design ideas and their motivations for the swarm control, and to paint a broader picture of how the swarm inter operates with the individual control part to form a complete control system that operates the swarm, in unison, as one.

9.5.1. Swarm Architecture

As was decided in the preliminary design phase [9], the architecture of the swarm will be decentralised. The parts of the swarm control that will be decentralised will be the coordination of the swarm of drones when a command is received. However, it is important to reiterate that commands that are sent to the swarm are sent from an operator. Hence, the swarm architecture only refers to the drones working together in order to fulfill a command sent from the ground, and to maintain their formation.

Abstraction is used here so that the swarm appears to be one. As such, the operator uses one joystick input and this input is accepted by the active transceiver of the swarm.

With the decision to make the swarm decentralised, one would assume this simply means that every drone performs the same tasks at all times, often working on tasks for the individual control. However, this is not the case here. There are specific drones that have some specialised tasks: these are four inner drones that have the task and responsibility to maintain a virtual center for the swarm frame reference, and to broadcast this reference point, in real-time, to the other drones.

In every other case, however, the drones perform the same tasks with the philosophy that each drone shares data and information with the swarm when it is necessary and information that is received from the swarm is used is curated for the individual drone control system such that it applies the correct actions on the specific drone.

One instance why this would be required is when turning the swarm. In this case, outer drones would need to apply a higher change in yaw in comparison to inner drones. Hence, it is important that a swarm command has been adapted for the specific drone before it is sent to the individual drone control system.

9.5.2. Swarm Configuration

The swarm configuration is shown in Figure 9.12. A static configuration is chosen from the start rather than dynamically assigning numbers to the drones, since this is more predictable and does not then require complex algorithms and techniques in order to figure out which drone has which label, which could be an issue in a race condition when starting up.

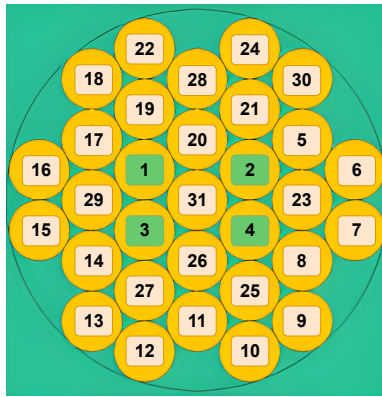


Figure 9.12: Swarm Configuration (own work).

The position of drones 1-4, also highlighted in green in Figure 9.12, will be used to calculate the virtual center as has already been described earlier. To minimise computational work required and minimise communication link time, the virtual center will be computed by the drones (1-4) in a round robin manner and the virtual center will be updated, in realtime, on these drones such that the other drones in the swarm can probe these drones for this.

9.5.3. Swarm Data Protocol

Underlying Protocol

For efficient communication, the higher level protocol that will be used for messages sent between the drones in the swarm, is defined. It is important to state here that this subsection is not defining a new protocol on its own, but it is rather describing the different types of messages that will be sent between the drones. This subsection also serves as a means to keep a higher level overview on the data being transmitted and received in the network.

As for the underlying protocol being used, this will be using Mavlink over User Datagram Protocol (UDP). UDP is one of the most established communication protocols in networking alongside Transmission Control Protocol (TCP) in the transport layer, and in this case is used instead of TCP as there is no error checking processing done, which significantly reduces computational power needed to verify and check correct transmission of messages [63]. This is acceptable in the scenario of DroneCrane because any data packets that arrive late are most likely already out of date in a realtime environment, therefore it makes sense to instead include a timestamp as part of the datagram so that the drone can check whether the data is up to date with respect to current time.

Mavlink is a protocol operating in the application layer and is often used extensively with drones. The reason it is chosen over other protocols in its space is because it is very widely accepted and has good support for concurrent systems, in contrast to other protocols such as UranusLink and UAVCan [64]. In addition, it provides methods to detect dropped packets and corruption during travel, while having only 14 bytes of overhead and no additional framing⁵⁰.

Types of Messages

In the following paragraphs, any descriptions of the types of messages are those sent from one drone, in the swarm, to another drone. Unicast messages are messages sent directly to one drone; multicast to specific drones and broadcast to all drones.

The first category of messages that will be sent are presence messages. These are ping packets that will be sent at an interval of 15 seconds as a multicast message to specific drones assigned as probe drones. This is done in contrast to broadcasting the message, in order to prevent unintentional Distributed Denial-of-Service (DDOS). This forms as a swarm health check as it allows drones to ensure that the other drones are working correctly. In case a ping message sent by one drone is not received correctly by another drone. The second drone will wait an additional 15 seconds, and in

⁵⁰<https://mavlink.io/en/> [Accessed in June 2022]

the off-chance that after this interval the ping is still not received, the second drone will directly probe the first drone to check their health. If after a period of one minute there is no response from the first drone, then the first drone is considered inactive to the second drone and this information is then shared as a broadcast to the swarm.

The next category of messages that will be sent are commands received from ground and updates back to the ground. These messages are simple packets, encoded via the radio transceiver, that are received by the drone with the active transceiver. These packets contain instructions for the update of the swarm position, velocity, altitude, and heading. Once they are received, they are then broadcast to the other drones. In addition, if a response back for the status of the command is requested, this is sent by the other drones to the drone with the active transceiver and then this is sent back to the ground controller.

Another category of messages that will be sent are virtual centre update messages. In contrast to the previous category, this is only sent to a drone (from drone 1-4) if this has been requested by that particular drone. Drones 1-4 all act as delegates for themselves and respond to the sender with the latest virtual centre that has been stored. The virtual centre position is an absolute GPS coordinate with which the RTK corrections have been already applied.

One other category of messages that will be sent and received are those to do with the maintenance of the Wi-Fi network used, that was previously described in Subsection 9.3.2. These messages will be unicast and will be sent by a drone with a lower signal strength to one with a higher signal strength, in order to activate the repeater on the latter.

The last category of messages are emergency messages. These are messages broadcast out to all drones in the situation that one drone is experiencing any issues and needs to detach from the LFRS structure. This message will be broadcast three times in a burst in a span of three seconds in order to ensure that all drones receive the message.

9.5.4. Swarm Formation Maintenance

As previously mentioned, the drone swarm formation will be controlled manually like one single drone. This approach is called virtual structure [65]. The basic principle of virtual structure is that each drone will maintain its relative position inside the formation with respect to a reference point. And each drone will move to its desired position when a input of velocity, heading, or altitude is given by the controller [66].

The effect of round Earth can be neglected because DroneCrane will not be travelling in long distances horizontally. Therefore, the swarm formation maintenance will mainly be focused on the horizontal plane. In the vertical direction, which is z axis, only an altitude command will be giving to make sure all the drones to stay in the same plane in a certain altitude.

Reference Frame

Two reference frames are introduced here for swarm formation: the inertial reference frame O and the swarm formation reference frame F. The former has a original point at the the ground station and remains fixed. The latter has an original point inside the swarm and will move and rotate with the swarm. The swarm is designed to do yawing only. Roll and pitch are not a functionality for the swarm. The horizontal plane of the swarm reference frame will only be rotating around z axis. Therefore, as shown in Figure 9.13, with the current heading ψ measured by the sensor, and the input heading ψ_r given by the joystick command, the transform matrix between the two frames can be defined:

$$C_{OF} = \begin{bmatrix} \cos(\psi + \psi_r) & -\sin(\psi + \psi_r) & 0 \\ \sin(\psi + \psi_r) & \cos(\psi + \psi_r) & 0 \\ 0 & 0 & 1 \end{bmatrix} \quad (9.14)$$

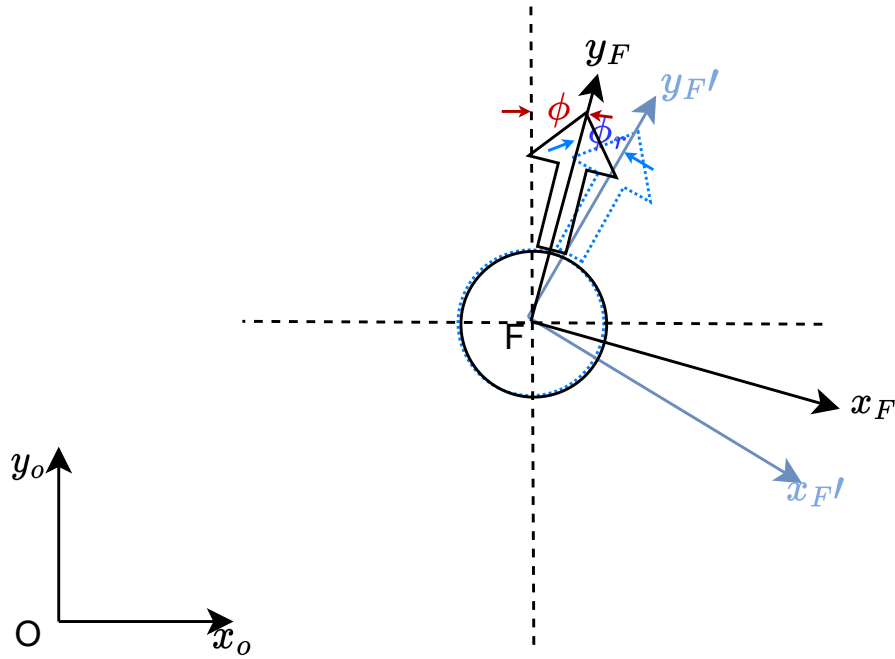


Figure 9.13: Top view of inertial reference frame and formation reference frame transformation (own work).

Reference Point

Next, the reference point of the swarm formation is defined. To avoid a single point of failure, this point will be defined as the geometric centre of four of the drones around the swarm centre. This is because four drones provide enough redundancy, as well as limiting number of communication need to be transmitted to the other drones. Therefore, the reference point P_{RO} in the inertial frame can be defined using the other four reference drones $P_{r_1O}, P_{r_2O}, P_{r_3O}, P_{r_4O}$ with their x,y,z position in the inertial frame:

$$P_{xRO} = \frac{\sum_{i=1}^4 P_{xr_iO}}{4} \quad (9.15)$$

$$P_{yRO} = \frac{\sum_{i=1}^4 P_{yr_iO}}{4} \quad (9.16)$$

$$P_{zRO} = \frac{\sum_{i=1}^4 P_{zr_iO}}{4} \quad (9.17)$$

Desired Position When a command signal $T_r = [V_r, \psi_r, H_r]$ is given by the operator using joystick, the reference point P_{RO}^{new} will be updated during the timestep δt :

$$P_{xRO}^{new} = P_{xRO} + V_r \delta t \sin(\psi + \psi_r) \quad (9.18)$$

$$P_{yRO}^{new} = P_{yRO} + V_r \delta t \cos(\psi + \psi_r) \quad (9.19)$$

$$P_{zRO}^{new} = P_{zRO} + H_r \quad (9.20)$$

As the swarm configuration has been previously introduced in Subsection 9.5.2, the desired position P_{iF}^d of each drone in the swarm formation frame is also defined. When the swarm formation is moving, this desired position in the the inertia frame P_{iO}^d can be transferred from formation reference frame using:

$$P_{iO}^d = P_{RO}^{new} + C_{OF} P_{iF}^d \quad (9.21)$$

Data Output and Implementation in Single Drone

Finally, this desired position for each drone will be sent to the flight controller as single drone command during every small timestep. The single drone is expected to move the desired position with a certain velocity, or try to reach the desired position with a maximum drone velocity.

9.5.5. Internal Collision Avoidance (ICA)

The virtual structure approach maintains the swarm in a formation during moving and turning. However, when any external force acting on part of the drones that causes potential collision between them, the internal collision avoidance (ICA) is required. To implement ICA, ultra wide band that measures the distance with its neighbour drones will be used to have faster refresh rate without communication delay. The principle of the ICA is that each drone will measure the distances between itself and the other two neighbour drones. These distance measuring protocol will be predefined. When the UWB sensor detects that it is within a certain threshold distance $d_t h$, its new desired altitude will be 0.4 m lower than the current position.

In this case, the collision can be avoided as they are not in the same plane. In the next timestep, their new desired position will be updated by the formation maintenance algorithm. All the drones will move back to their desired positions again in the formation.

The swarm control flow diagram with formation maintenance and internal collision avoidance is shown in Figure 9.14.

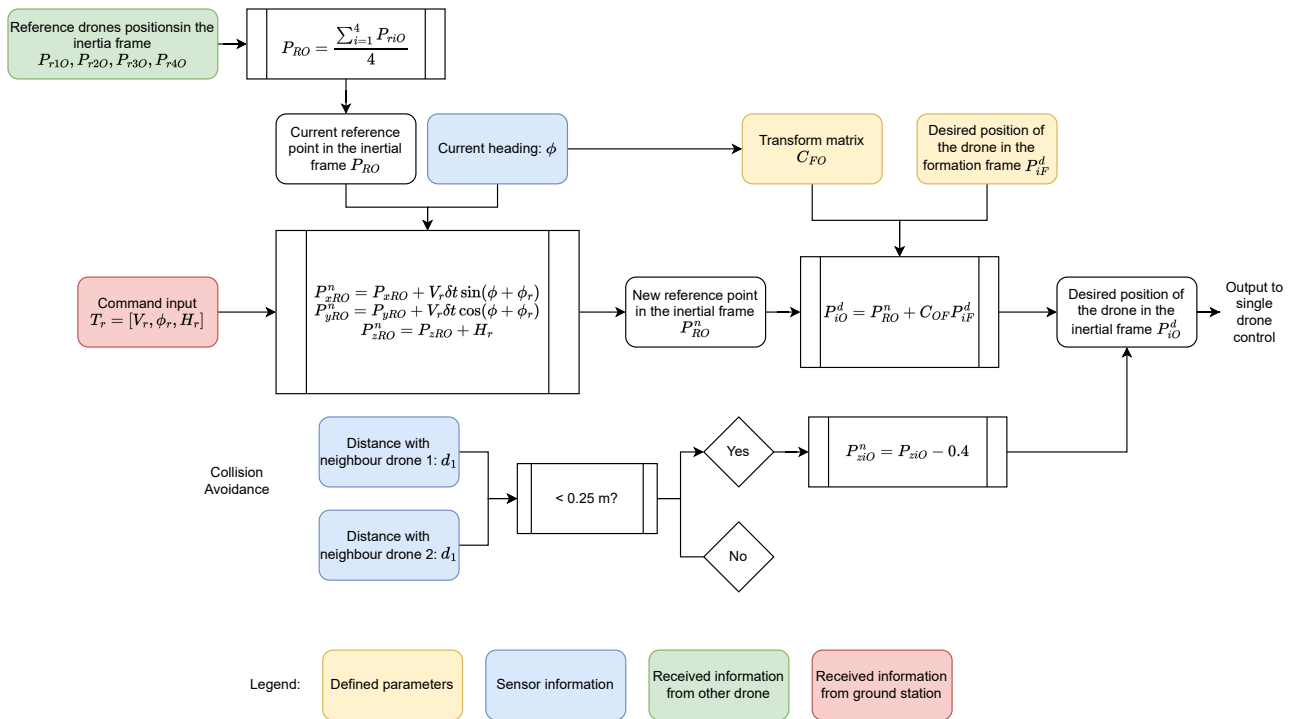


Figure 9.14: Swarm control flow diagram (own work).

9.5.6. Simulation Plan

A simulation will be performed to test the swarm formation algorithm when they are encountering situation such as a wind gust pushes certain drones away from the swarm formation, doing basic maneuvering, and potential collision when two drones are getting close to each other.

Simulation Model

For the swarm configuration, a simulation model is built with 16 drones in a symmetrical layout is shown in Figure 9.15. Each drone has a diameter of 2 m and starts at their desired positions in the swarm formation reference frame. The four referencing drones are marked as red in the figure. The timestamp for each movement update is assumed to be 0.2 s. The the drone swarm starts at a initial speed of 1 m/s with zero heading.

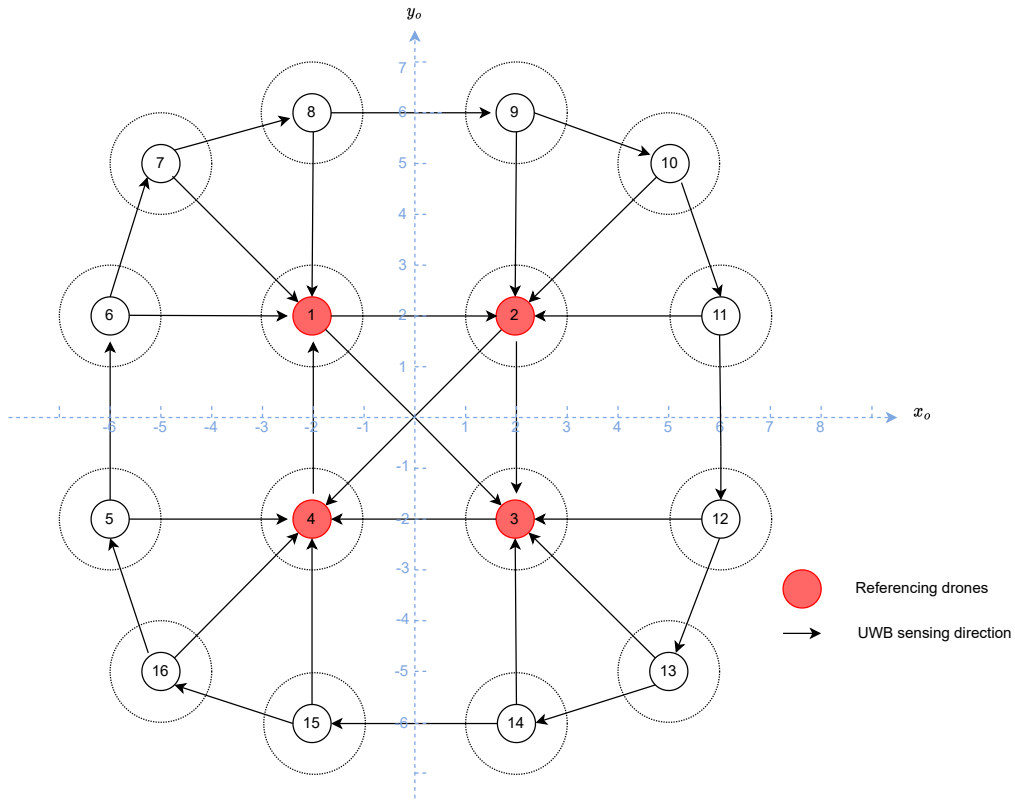


Figure 9.15: The simulation model of swarm formation (own work).

In addition to that, the characteristic each single drone has to be defined. Each drone is assumed to have a horizontal acceleration of 6.2 m/s^2 with a maximum horizontal speed of 5 m/s . This assumption is made based on the speed limit of the whole swarm formation and the acceleration of DJI Phantom 4[67]. In vertical direction, each drone is assumed to have an acceleration of 5 m/s^2 with a maximum vertical speed of 3 m/s .

Basic Manoeuvring

The drone swarm starts at a constant speed of 1 m/s toward zero heading. It first accelerates to 1.5 m/s , then make a turn of 90° with a constant heading rate of $2^\circ/\text{s}$. All paths of each drone will be plotted to visualise how the drone swarm formation will be maintained.

Wind Gust

To simulate a wind gust moves certain drones away, the last row of drones (drones 13-16) are shifted 1 m in both the negative x-axis and negative y-axis in the swarm formation frame as shown in Figure 9.16, while the formation is moving towards zero heading with a speed of 1 m/s . These drones are expected to go back to their desired position in the reference frame.

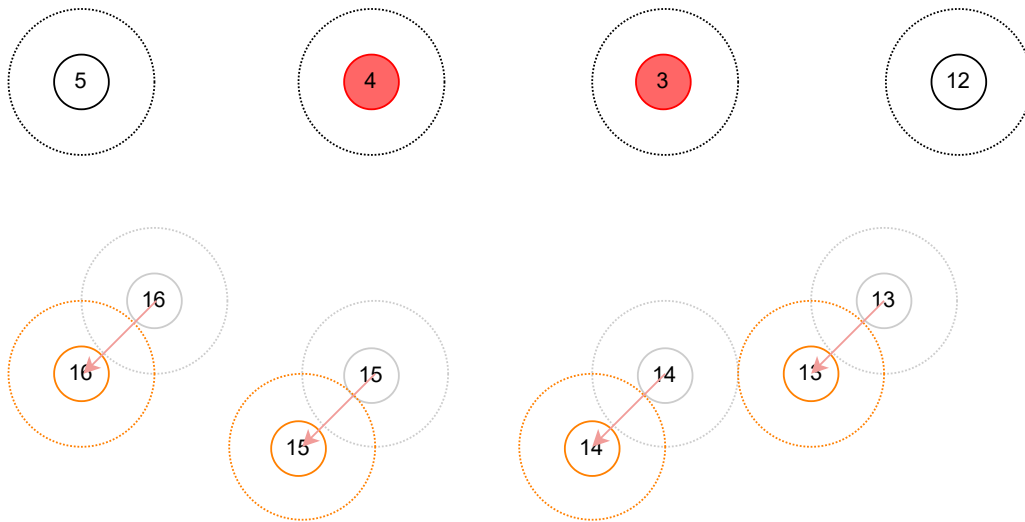


Figure 9.16: Simulation of wind gust while drone 13-16 are relocated (own work).

Potential Internal Collision

The third scenario to simulate here is when the swarm formation is moving toward a certain direction and one of the drones is getting close to the others. The threshold distance mentioned in Subsection 9.5.5 has been set to 2.4 m. It is assumed the swarm is still moving towards head of zero. Drone 10 is moving towards heading of 180° with a velocity of 2 m/s. And its coordination in the swarm formation reference is relocated to (6, 4.25) in the x-y plane as shown in Figure 9.17.

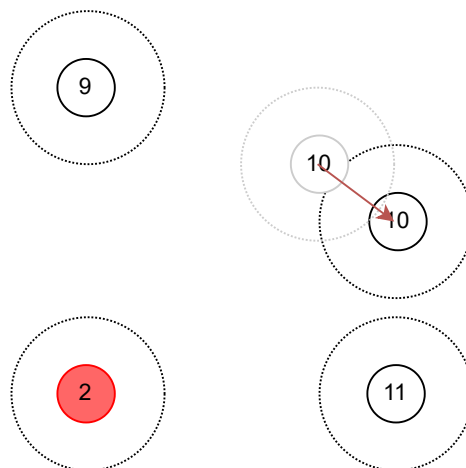


Figure 9.17: Simulation of potential internal collision while drone 10 is relocated (own work).

9.6. Reliability

This section was written by: *Bryan*

When evaluating the reliability of a complex system, all avenues of possible errors must be explored. For Controls, the hardware and software used will be evaluated for their reliability both qualitatively and quantitatively, when possible.

9.6.1. Hardware

The hardware that will be used in the DroneCrane system for control has been detailed previously in Section 9.1. The hardware includes sensors, controllers and other equipment. Quantifying the reliability for these components can be quite tricky as in most cases, no figures on reliability are present directly from the manufacturers. Therefore, this section will instead provide a plan to test and measure the reliability of the different components to identify the mean time between failures of

each of the components and also to explore how the interaction between the hardware can affect the reliability.

The plan to test for reliability will be to first stress test a minimal system of two drones with only necessary sensors needed for control, namely the u-blox NEO-M8P and Adafruit RFM95W. Both the controllers will be used here as normal. A testing procedure will be prepared with multiple manoeuvres to test all possible modes of operation and check whether individual control works. This alone will not be enough to test the swarm control, therefore later in the test, more drones will be added to the flying swarm and their formation adaptability tested. This means live changes in formation and one drone failure situations will be tested.

All observations and data recorded during these tests are later used to determine a proven figure for reliability. These results could also contribute towards possible certification testing for market readiness.

9.6.2. Software

Specifying the reliability for software is much more straightforward than it was for hardware. Testing reliability here comes down to the different frameworks used for the control software and testing done during software development.

For the software used in the Pixhawk 4, the PX4 Autopilot is used as was mentioned in Section 9.2. The software is open-source and is licensed under BSD 3-clause license⁵¹, which allows for extensive testing and contribution from the open-source and drone community. As such, validation and software testing is done very periodically with every software release⁵². It is possible that in future development, the in-house control model will want to be used instead of the pre-built control model present in PX4. In this case, extensive testing including verification and validation, will need to be applied to any custom software developed.

In any case, there can be errors from calibration or sensor values that are extreme or nonsensical. The best practice for reliability is to ensure that the software will behave as expected even when sensors misbehave and provide rogue values. If the control software is tested and has protection against rogue inputs, there can be certainty that the system will be very reliable.

For the software used in the Raspberry Pi Zero 2 W: this is developed by the team, in contrast to the Pixhawk 4. Therefore, from the start, unit testing, system testing and interface testing must be used as part of the software development cycle. Tools such as Gantt charts and PERT charts also help to structure this software development and will help to develop safe and well-tested software from day one.

9.6.3. Quantification

As for quantifying reliability, in order to get the probability of failure for instance, this is much harder to do when it comes to hardware and software. Hardware devices themselves contain printed circuit boards (PCBs) which contain components such as transistors and switches. Many of these components are used hundreds of times in a single PCB, therefore calculating the reliability directly is difficult. Looking at software, even though reliability could be calculated from regular testing done, tests are very likely not to include all the different cases that could occur in errors.

Fortunately, methods to better estimate hardware and software reliability exist. These include methods outlined in "Estimating software reliability from test data" by Eldred Nelson and "Methods for assessing the reliability of software and hardware systems" by Ekatarina Lavrischeva [68, 69].

A further analysis on the quantification of reliability for the control system will not be carried out, because this requires the swarm software to be in development and this project is still in a detailed design phase.

⁵¹<https://opensource.org/licenses/BSD-3-Clause> [Accessed in June 2022]

⁵²<https://docs.px4.io/master/> [Accessed in June 2022]

10. Electrics

The electric subsystem is of fundamental importance to the system as a whole since without power there is no flight. In this chapter, first the design decisions for the electric subsystem and the reasoning behind them will be presented in Section 10.1. It is followed up by Section 10.2, where the design characteristics of the resulting subsystem are specified. In Section 10.3, the electrical block diagram is presented and briefly discussed. A sensitivity analysis is performed in Section 10.4. Finally, the production plan and the reliability of the electric subsystem are discussed in Section 10.5 and Section 10.6 respectively.

10.1. Design Decisions

This section was written by: *Aaron*

Batteries can be configured in many different ways. The characteristics of the electric subsystem design which will be presented later in this chapter, are to an extent the result of the properties of the other subsystems. Decisions in the design of this subsystem were made in order to improve the characteristics of not only the electric but also the other subsystems. Those design decisions will be discussed in this section. In Subsection 10.1.1, the design decisions for the battery pack are treated. Those for the power distribution board and the electronic speed controllers are discussed in Subsection 10.1.2 and Subsection 10.1.3 respectively.

10.1.1. Battery Pack Design

From the preliminary design [9], it was clear that no battery packs would be available off-the-shelf that could satisfy the parameters of the design. The combination of these design parameters, i.e. the engine voltage, the peak power, and the mission energy, shape very specific constraints. Hence, the conclusion was reached that a battery pack had to be assembled from battery cells to achieve the required properties. For the control system, a radially symmetric weight distribution is desired since in that case pitch and roll properties are the same and no distinction in properties needs to be made between the two. To achieve this radial symmetry in battery weight distribution and to create some space for air to cool the system, the battery is divided into four blocks, each of which is positioned in a quadrant of the core. When those blocks are connected in pairs of two, but the two pairs are decoupled from each other, a redundant power system can be created. Each pair of battery blocks is in fact a battery pack in itself and is connected to a power distribution board (PDB). In case one of the two battery pairs or their PDB completely fails, the drone will effectively lose half of its nominal power. The remaining power is not enough to significantly help the swarm in carrying of the payload. However, with half of its power and proper distribution of the engines across the two PDBs, the drone has enough power to fly individually using four out of eight engines. The drone would detach from the swarm and would be able to safely land itself. This will avoid the safety hazard of a drone crashing when a single failure occurs in the power supply circuit.

10.1.2. Power Distribution Board

PDBs that can provide power and signal to eight ESCs and are rated for relatively high voltage and current are not easily found. Hence, the decision was made to instead implement two PDBs that are rated for high power. These PDBs are then no longer required to be able to individually provide power and signal to eight engines. A PDB designed to have four or six engines attached is much easier to find off-the-shelf. Another advantage is the added redundancy as discussed in Subsection 10.1.1. Each PDB has its own battery pack, decoupled from the battery pack of the other PDB, and provides power and signal to four engines. In order to be able to control the drone in case it loses half of its engines, the engines that are attached to the same PDB need to be opposite pairs. Hence, looking at Figure 9.5, engines 1, 4, 5, and 8 are decided to be wired up to a single PDB. Engines 2, 3, 6, and 7 are wired up to the other PDB. In case one PDB or its power source is lost, the drone still has full

controllability. Both PDBs will power the flight controller in a circuit where if one of the power providers fails, the other provider is not influenced. This power supply redundancy for the flight controller will be addressed in Section 10.3. The pads on the PDBs that provide power to the ESCs also need to be able to withstand the required current corresponding to the chosen engine under peak power.

10.1.3. Electronic Speed Controller

The electronic speed controllers (ESCs) need to be rated for the voltage of the engines and must be capable of enduring the high current. Hence, the final choice of which ESCs are implemented can only be made after an engine has been selected. The current that the engines require for peak power needs to be below the ESCs maximal continuous current rating.

10.2. Design Characteristics

This section was written by: *Aaron*

The results of the iterative tool with respect to the electric subsystem will be discussed in this section. First, the specifications of the battery packs are given in Subsection 10.2.1. It is followed up by Subsection 10.2.2 where the choice for the power distribution boards is presented. The selected electronic speed controllers are briefly mentioned in Subsection 10.2.3. Finally, an overview on the costs and weight of the components that have to do with the power supply are summarised in Table 10.1.

10.2.1. Battery Packs

The final design consists of 9 300 battery cells for the entire swarm of the type Samsung INR21700-50E.⁵³ The 9 300 battery cells are spread out equally across the 31 drones, resulting in 300 battery cells per drone. This results in a mass of 20.7 kg and a volume of 9.4 L for the batteries on a drone. The battery packs are configured in strings of 12 battery cells in series resulting in a voltage of 12S, where each Samsung INR21700-50E battery cell has an average voltage of 3.6 V, a capacity of 4900 mA h and a discharge rate of 2C. Hence, 25 of these strings are present on every drone. The 25 strings each provide 9.8 A, resulting in a total current of 245 A. This means that a current of 30.625 A is available to each engine which satisfies their 24.1 A peak current need. Since the number of strings is not divisible by four, three out of the four battery blocks on the drone will contain six strings while one block will contain seven. This results in that block having a slightly higher mass, which would cause a moment around the geometric centre of the drone. To prevent this unbalance, the slightly heavier battery block is moved inward compared to the other three such that the geometric centre and the centre of gravity coincide. Considering the placement of the batteries within the CAD model which will be presented in Section 11.1, where the distance between the centre of the drone and the centre of a battery block is 9.3 cm, it is concluded by balancing the moments that the battery block which contains seven strings needs to be 1.33 cm closer to the centre of the drone than the other battery blocks.

10.2.2. Power Distribution Board

The PDBs were chosen to be the Mateksys PDB-HEX 12S.⁵⁴ This PDB is compatible with the 12S engine and battery voltage. A single board is capable of enduring 140 A. The four engines connected to that PDB require $24.1 \cdot 8 = 96.4$ A peak current which is well below 140 A. Each ESC pad on the PDB can withstand 60 A of current, which is sufficient compared to the 24.1 A peak current from the engines. The PDB also allows ESC telemetry on the engine RPM to be sent to the flight controller.

10.2.3. Electronic Speed Controller

The ESCs are the ALPHA 60A 12S V1.2.⁵⁵ With their 60 A current rating, they can easily withstand the required peak engine current of 24.1 A. They have a signal cable that is used to relay information about the engine RPM to the flight controller.

⁵³https://www.nkon.nl/rechargeable/li-ion/21700-20700-size/samsung-inr21700-50e.html?gclid=EAlaIqobChMI1-Tk3uGv-AIVgc13Ch3yIQ9dEAAAYASAAEgLywvD_BwE [Accessed in June 2022]

⁵⁴<http://www.mateksys.com/?portfolio=pdb-hex> [Accessed in June 2022]

⁵⁵<https://store.tmotor.com/goods.php?id=582> [Accessed in June 2022]

Table 10.1: An overview of the electrical power components for a single drone (bulk discounts not incorporated).

Component	Amount	Total Cost	Total Weight
Samsung INR21700-50E ⁵³	12x25	€1 095	69 g
Mateksys PDB-HEX 12S ⁵⁴	2	€44.06	24 g
ALPHA 60A 12S V1.2 ⁵⁵	8	€841.44	584 g

10.3. Electrical Block Diagram

This section was written by: *Aaron*

The electrical block diagram is presented in this section. It gives an overview of the different components of the control system and the power supply system and how they are connected to each other electrically. The electrical block diagram is shown in Figure 10.1. ^{54, 55,56,57,58,59,60,61}

The two PDBs are seen, both connected to a separate power input. The two power inputs on the Pixhawk 4 are there for the power supply redundancy that was discussed previously. Telemetry on the engine RPM is sent back from every ESC along the PDB to the flight controller. The PDB also sends current and the battery voltage telemetry to the flight controller. The RTK module and the ultra-wideband module are connected to the swarm controller such that it can effectively coordinate the swarms within the drone. The swarm controller is connected to the flight controller and converts the commands from swarm controls into commands for the individual drone. One long range transceiver is connected to the swarm controller and is the one that is actually being used. Another one is connected to the flight controller for redundancy in case the main transceiver fails.

⁵⁶<https://store.tmotor.com/goods.php?id=1113> [Accessed in June 2022]

⁵⁷https://shop.holybro.com/pixhawk-4beta-launch_p1089.html [Accessed in June 2022]

⁵⁸<https://www.raspberrypi.com/products/raspberry-pi-zero-2-w/> [Accessed in June 2022]

⁵⁹<https://www.adafruit.com/product/4074> [Accessed in June 2022]

⁶⁰<https://www.qorvo.com/products/p/DWM1000> [Accessed in June 2022]

⁶¹<https://www.u-blox.com/en/product/neo-m8p-series> [Accessed in June 2022]

- Positive power wire
- Negative power wire
- Data transmission
- ESC signal

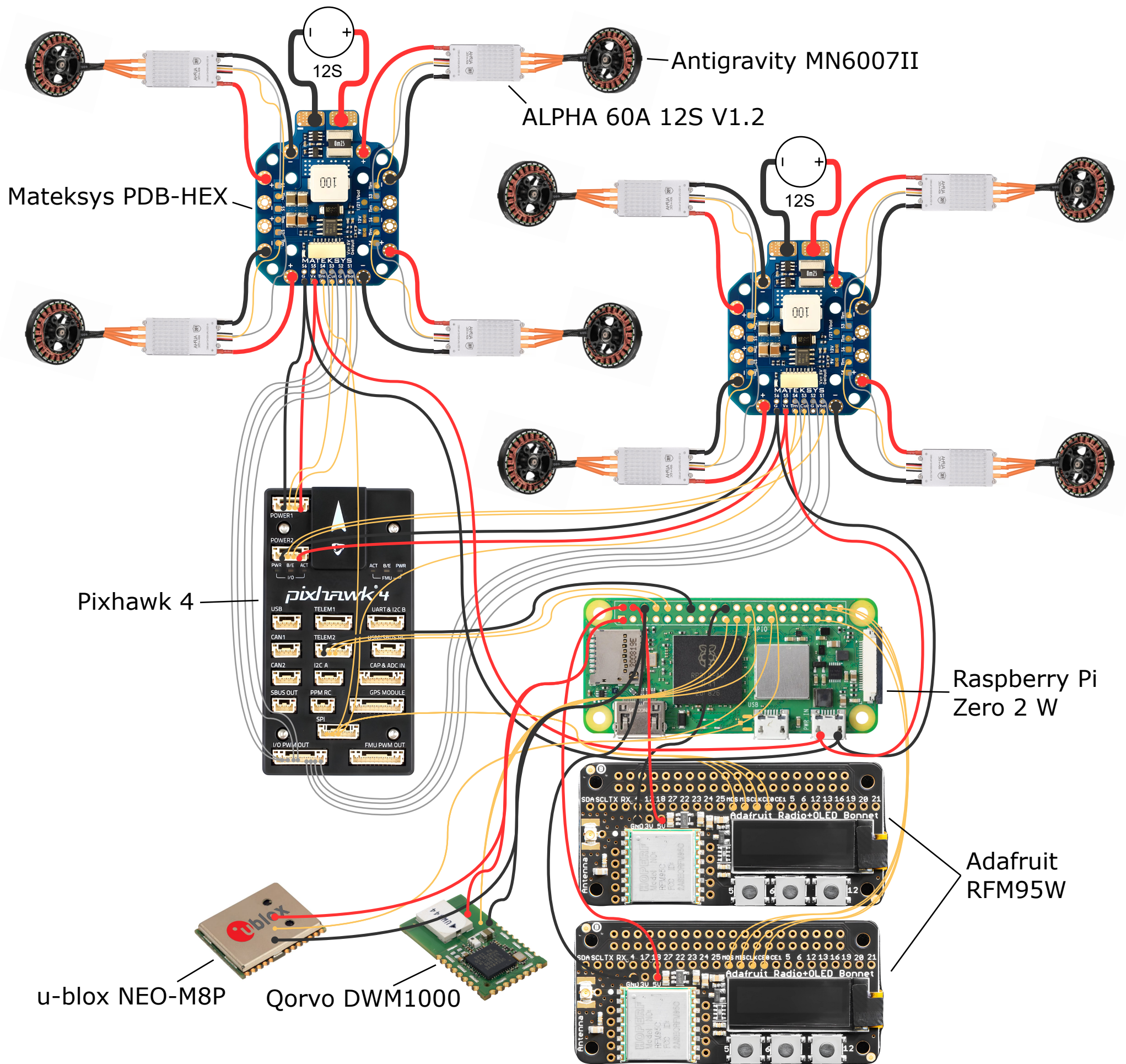


Figure 10.1: The electrical block diagram of a single drone (own work).

10.4. Sensitivity Analysis

This section was written by: *Giacomo*

In this section, a sensitivity analysis is performed for the power subsystem. The goal of this analysis is to define the sensitivity of the chosen design. The main input for the power subsystem and the selection of the batteries comes from the propulsion subsystem, its power and energy usage. In the selected design, the final iteration has a power usage for the power subsystem of 328.108 kW. This input gives a number of battery cells required for the entire swarm equal to 9 300. Figure 10.2 shows the step change in battery cells number for a range in power usage from 290 kW to 350 kW. In addition, the operational point is highlighted in the graph.

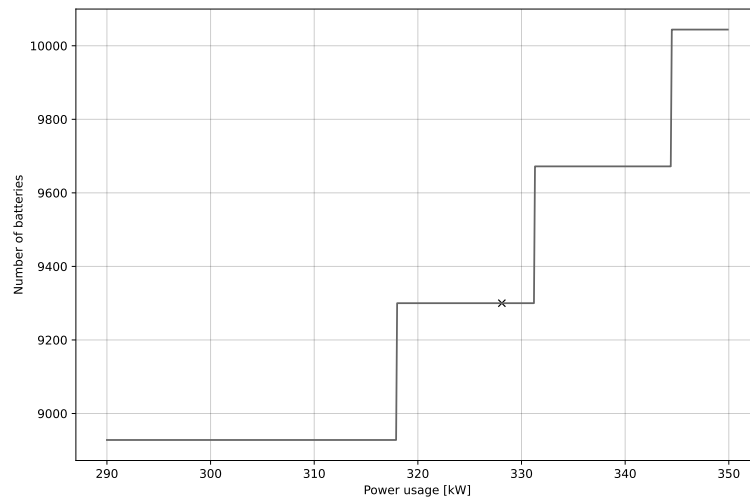


Figure 10.2: Plot of the power usage against the number of battery cells (own work).

As can be seen from Figure 10.2, the number of cells increases with an increase in power usage. However, the number of cells required increases with discrete steps. This is due to the fact that the battery cells are placed in series in each drone, and the number of required strings is rounded up to the next integer. As a consequence, if 4.1 strings are calculated to be required on each drone, 5 will be used leading to an additional 372 battery cells. As seen in Figure 10.2, the operating power of the system does not lie near the step change, and a power of 3 kW is required in order to increase the number of batteries needed in the system. Unless there is a drastic change in the design of the system, it can be expected that the number of batteries will remain the same. Hence, it can be concluded that the design is not sensitive.

10.5. Production Plan

This section was written by: *Aaron*

The electrical power subsystem will be assembled from the discussed off-the-shelf components. The components will be connected by soldering. The battery packs are to be assembled using nickel strips that connect the battery cells. The nickel strips are spot-welded onto the poles of the battery cells. Nickel has high resistance against corrosion, is easy to spot weld, and is for those reasons the standard for assembling battery packs.^{62,63} Care should be taken not to introduce excessive heat into the battery cells while spot welding, as the heat can damage the battery cells, decreasing the properties of the battery pack. The weight and cost of the required nickel strips were deemed to low to be considered in the design at this point. The nickel strips can be bought in bulk and are cheap, on the order of €1 per metre for bulk purchases.⁶⁴ They are relatively thin and hence lightweight compared to the mass of the batteries themselves.

⁶²<https://www.rcrsinnovations.com/product/nickel-strips/> [Accessed in June 2022]

⁶³<https://www.amazon.com/Batteries-0-1x4x100mm-Battery-Welding-Soldering/dp/B07PCN1ZMC?th=1> [Accessed in June 2022]

⁶⁴<https://eu.nkon.nl/nikkel-battijersoldeerstrip-10mm.html> [Accessed in June 2022]

10.6. Reliability

This section was written by: *Aaron*

In order to estimate the reliability of the entire system, the reliability of the subsystems first needs to be estimated. In this section, the reliability of the battery packs will be discussed in Subsection 10.6.1, followed by a brief explanation on the plans for estimation of the reliability of the remaining electric components in Subsection 10.6.2.

10.6.1. Battery packs

The failure rate of lithium-ion batteries is on the order of one in a million to one in ten million batteries that fail [70, 71]. The batteries on DroneCrane are used for 500 cycles before being replaced and that one cycle represents a 30 min mission. The lifetime of the batteries in flight hours is then 250 h. Having 9 300 battery cells and assuming one in a million failing, statistically speaking, 0.0093 battery cells would fail in their lifetime. Hence, the rate at which a single cell on DroneCrane would fail would be $0.0093/250 = 3.72e-5 \text{ h}^{-1}$, corresponding to a probability of $3.72e-5 \cdot 0.5 = 1.86e-5$. Failure of a battery cell would result in the failure of the entire string since those battery cells are connected in series. The battery cells in that string would become overcharged under a short-circuit. To prevent the entire battery pack from failing, a fuse can be placed in the string which blows when a short circuit occurs in the string. The power required for a single drone that is detached from the swarm, i.e. no longer carrying payload, to ascend is 3608 W assuming a safety factor on the power of 1.1. A single string provides $0.8 \cdot 9.8 \cdot 3.6 \cdot 12 = 339 \text{ W}$. Hence, $\lceil 3608/339 \rceil = 11$ strings supplying power is enough to fly a drone detached from the swarm and land it in case of a problem. For a drone not to have sufficient power to fly individually, it would have to lose 15 of its 25 strings. Assuming 15 battery cells fail in unique strings on the same drone within the same mission of 30 min, the probability of a drone ending up not being able to support itself in flight is at most $(1.86e-5)^{15} = 1.1e-71$.

10.6.2. Remaining components

The reliability of the PDBs and the ESCs is hard to estimate since no data could be found on their failure rates. Similar to what was discussed for the control hardware in Subsection 9.6.1, these components will be stress tested to examine their reliability.

11. Structures

This section was written by: *Robin, Thomas*

The design of the structures is again divided between the drone structural design and the LFRS structural design. In this section the processes used to converge to the final design option for both categories are explained.

Section 11.1 discusses the drone structural design giving an overview on the FEM analysis performed on the structure. Consequently, the LFRS structure is analysed in Section 11.2. Finally, the chapter ends with Section 11.3 which gives insights on a virtual reality simulation.

11.1. Drone Structural Design

Up to this point, not much was known about the design of the drone structure apart from the fact that an octagonal shape is used and the weight that it was approximated to have. In order to hone in on an optimised structure, analyses were made on differently shaped structures.

Firstly, it was already decided that the drone structure should be of an octagonal star shape as a result of the trade-off. This means that the structure is primarily loaded in bending as a result of the weight that is carried in the centre of the drone and the propulsion units at the ends of the arms pulling the drone up into the sky. Thus, it is important to find a beam shape that is very resistant against this.

Before the cross-sectional area was considered, an analysis was made comparing a straight beam with an arched structure. The decision was made to create a very simple FEM analysis using CAD software. To ensure the consistency and usability of these FEM analyses, the design weight of the two compared components was kept the same. The cross section was chosen to be of circular shape for both structures as again the consistency is key. Furthermore, the length between the points that are loaded were also set the same at an arbitrarily chosen 1.5 m length. The value of this is not particularly an important matter, as it is the shape that is the deciding factor. The FEM analysis for the straight beam is visualised in Figure 11.1, the analysis for the arched shaped beam is shown in Figure 11.2. The analysis showed that a straight beam could resist more load relative to an arched structure of similar weight, cross section, and size. For the structural design of the drones this meant that the arms in the drone structure would consist out of straight beam sections connected in the centre of the drone.

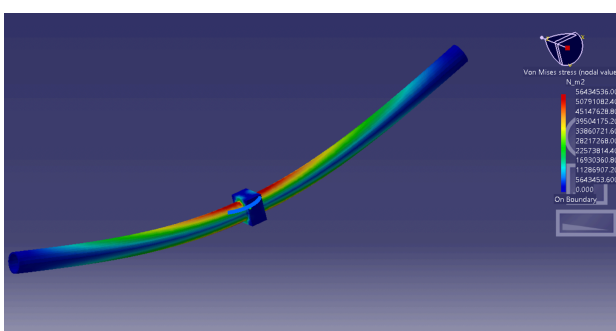


Figure 11.1: FEM analysis for straight drone beam (own work).

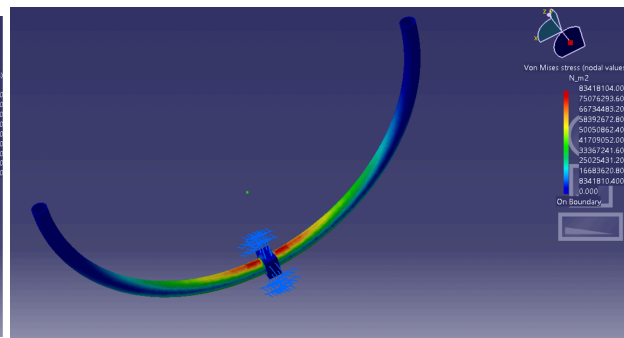


Figure 11.2: FEM analysis for arched shaped drone beam (own work).

The cross section should be optimised against bending in one specific direction, while providing enough resistance against the torsional forces that could be introduced into the beams due to disturbances acting on the propellers of the drone. The theoretically optimal structure against bending in one direction is to have two areas as far away from the neutral axis of this cross section as possible.

This maximises the second moment of inertia of the shape. Physically though, the closest possible cross section to this is an I-beam. This type of beam are known to resist torsion very poorly, so a square cross section was chosen instead [35]. The thicknesses on the top and bottom of the square section are increased to increase the resistance against bending. An example of this cross-section can be seen in Figure 11.3

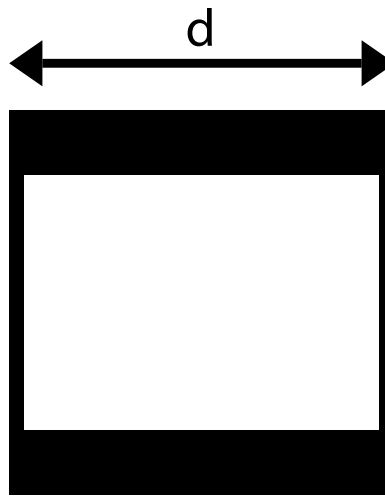


Figure 11.3: *Cross sectional shape of the arms of the drone (own work).*

As more research was done, a new configuration was found. This configuration can be seen in Figure 7.5, this meant that the drone structure had to be adjusted slightly. Instead of an in-plane octagonal star-shape, there are now two plus shapes, that are rotated 45° and have a vertical distance to each other. This did not influence the design decision to create straight beam sections, but it did introduce a need to design a core as well.

The choice of material was made by comparing the properties of many materials. The most important properties for these structures are the density of a material, the tensile yield strength and the Young's modulus. As previously mentioned, the primary loading in the drone structure is bending, which relates to the tensile strength of a material. The best performing materials in this category turned out to be Aluminium-7075, Titanium 6AL-4V and Carbon fibre reinforced composites due to their high yield strength as shown in Table 6.1. The titanium alloy is too expensive to use in the drone structure, so it was excluded from the choices. Carbon fibre composites are hard to recycle, and were thus also excluded due to the sustainability requirements of this design. Unfortunately, after running a few iterations of the software found in Section 7.1, it became apparent that the aluminium alloy did not have sufficient properties for the drone structures. Thus, no options remained. Fortunately, there have been new trends in recent years in the composite industries. As a result of a need for better methods to automate the manufacturing of composite structures, developments have been made in new carbon fibre reinforced thermoplastics, or CFRTP. The main difference between this material and more commonly used carbon fibre composites is the type of plastic used as a matrix to hold the fibres. This difference means that it is much easier to recycle, but more technologically advanced techniques are required to manufacture it. More details about these processes can be read in Section 12.8. Finally, the selected material is a matrix made of PES (Polysulfane) containing carbon fibres. The properties of which can be seen in Table 6.1. To calculate the prices of the structures, the raw material price per kilogram was multiplied with the mass of the structures. Then, a factor of 3 was added to this price for manufacturing costs. The prices of the structures can be found in Table 12.6.

As explained in Section 7.1, software was used in order to converge on the optimal design specifications. The description of the calculations involved in the structures of the design may be found in Section 7.4. From this, the resulting lengths of the beams, the height of the drone and similar properties could be extrapolated.

In order to obtain values for the stress levels within the drone structure, a CAD model of the drone

structure was built. Since building such model takes a significant amount of time and exact dimensions from the software were not fixed yet, the dimensions of the structure were parameterised. This parameterisation of the dimensions of the structure made it possible to start developing the CAD model while the software was still being finalised.

The drone structure was created using two planes that contain a cross shaped beam structure that is connected with an octagonal shaped hollow structure in the centre. The top of the hollow octagonal structure is closed with a octagonal shaped cap that contains the required electronics for the drone. In the centre of the hollow octagonal structure a hollow circular structure is present, within this structure the cables from the electronics are connected to the batteries. The ends of the cross shaped beam structure contains circular pads that are required for the attachment of the motors. The motors were fixed to the pads using a fixed pin connection in the centre of the pad. Furthermore, the battery for the drone was divided into four batteries that are attached within the octagonal hollow core. The batteries were attached in such way that the battery configuration is symmetrical around the centre of the drone structure to minimise inertial effects. At the bottom of the drone an attachment point is created. The drone will be connected to the LFRS using this point. The technical drawing of the drone is shown in Figure A.2.

After the final iteration of the software the finalised dimensions of the drone structure were available for the CAD model. Now the created CAD model was prepared in order to perform a FEM analysis on it. This means that a material and a force need to be applied on the CAD model, and some parts of the structure need to be clamped. As CFRTP is not a default material within 3D-experience, it had to be created using the material definition module. Within the material definition module the characteristics of CFRTP stated in Table 6.1 were applied. A total of 8 forces representing the force created by the propeller are applied on the fixed pin connection on the pad of the beam structure as this will be the place where the forces from the propeller will be introduced into the drone structure. The force applied is equal to 60 N which follows from the 6.1 kg of thrust that the propeller can generate. The clamp will be placed at the attachment point at the bottom of the drone, this is visualised in Figure 11.4. Using the previous described settings, the following stresses within the drone structure were computed. These stresses are shown in Figure 11.7. One can observe that the highest stresses are present in the straight beams near the hollow octagonal centre, a view cut was made in this section to provide a clear visualisation of these stresses and can be seen in Figure 11.5. The lowest stresses within the drone structure are present in the middle of the hollow octagonal centre of the drone, in order to visualise this a view cut was made, this can be seen in Figure 11.6. The displacement of the drone structure is also visualised using a FEM analysis and is shown in Figure 11.8. One can see that the maximum displacement occurs at the position of the attachment of the motor to the drone structure, as expected. The maximum deflection equals 0.32 mm which is acceptable. Note that the visual representation includes a greatly exaggerated displacement to create a clear representation for the loading case.

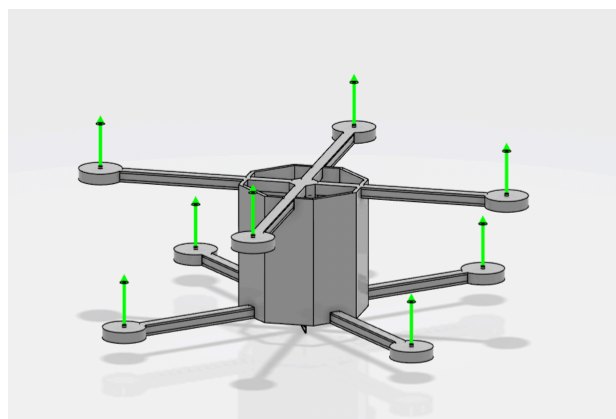


Figure 11.4: Applying forces representing forces that are generated by the propellers on the fixed pin connections of the drone structure as preparation for the FEM analysis (own work).

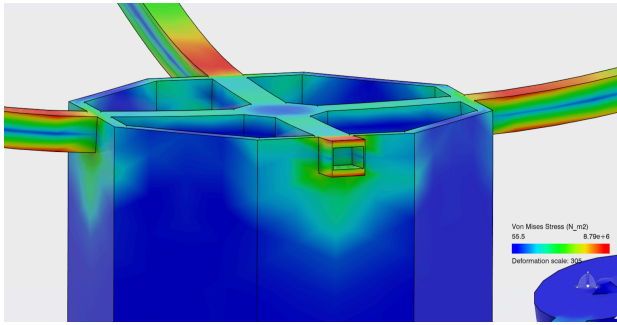


Figure 11.5: A view cut visualising that the highest stresses in the drone structure are present in the straight beam near the hollow octagonal centre of the drone (own work).

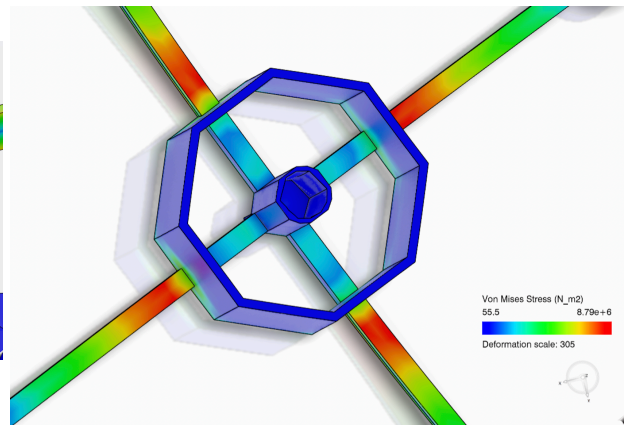


Figure 11.6: A view cut visualising that the lowest stresses in the drone structure are present at the middle of the hollow octagonal centre of the drone (own work).

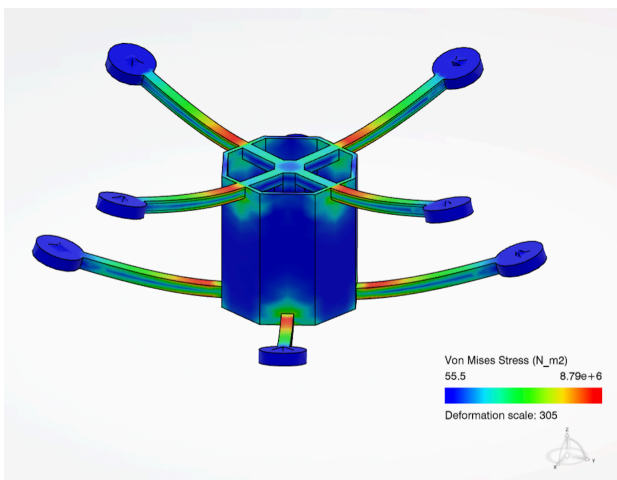


Figure 11.7: FEM analysis showing stresses within drone structure (own work).

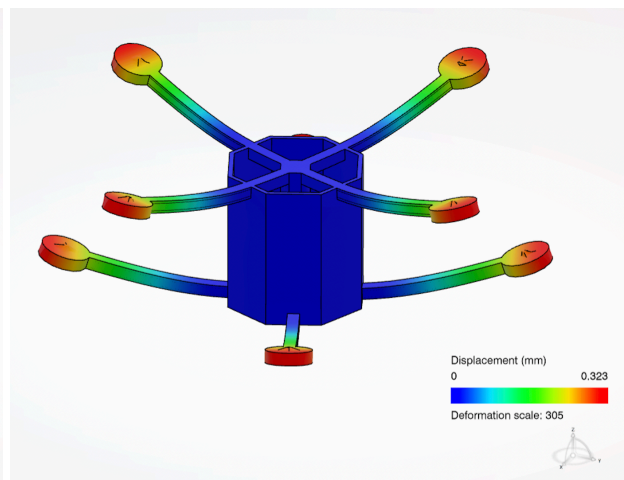


Figure 11.8: FEM analysis showing displacement of drone structure (own work).

11.2. LFRS Structural Design

To be able to finish a design of the LFRS within the scope of this project, it is challenging to create a fully optimised design. The approach of creating three designs, analysing them, and trading off was therefore chosen.

For the selection of the finalised shape of the LFRS the following characteristics were taken into account: modularity, manufacturability and performance. Modularity is taken into account since the flexibility of the DroneCrane system is one of DroneCrane's advantages. The following shapes for the LFRS structure were considered: circular, square and octagonal.

Considering the modularity of the system the octagonal and circular shapes score the best since they consist out repeating structures and are therefore easily scalable with the amount of drones used. For the performance the circular and the octagonal shapes perform the best, the square shaped LFRS performs the worst due to the poor moment of inertia with respect to the loading cases. The performance in this case is evaluated qualitatively with respect to the resulting internal loads within the structure, and the lengths that the longest beam in the structure requires. Finally, considering manufacturing the octagonal and square shaped LFRS score highest since the LFRS only consist out of straight beams that are relatively easy to manufacture in comparison to circular shaped beams that are present within the circular shaped LFRS.

Considering all the previously stated characteristics, the final shape of the LFRS will be octagonal since it scores highest on all characteristics except for performance. While performance is an important consideration, the small difference was weighed against the ease of manufacturing. The octagonal structure was chosen, as the manufacturing of it is significantly easier than that of the circular shape while the circular shape only performs slightly better in performance.

Table 11.1: Overview scores for different characteristics

Shape LFRS	Modularity	Manufacturability	Performance
Octagonal	High	High	High
Square	Medium	High	Low
Circular	High	Low	High

The LFRS structure consists out of a centre octagonal shaped centre to which eight equal shaped cylindrical beams are attached. At the end of each beam a connector will be present that connects the main beam from the centre of the structure to the ends of two other beams from the octagonal centre. Therefore, two sizes of beams, one octagonal centre and 8 connectors will be used in order to construct the complete LFRS structure. On the centre of the LFRS five cameras with a 120° viewing angle will be attached. Three cameras will be oriented to the corners of the LFRS, one camera will be directed towards the drone while the other camera is directed towards the payload. The visualisation of the positioning of the cameras on the LFRS centre is shown in Figure 11.9. The technical drawing of the LFRS is shown in Figure A.1.

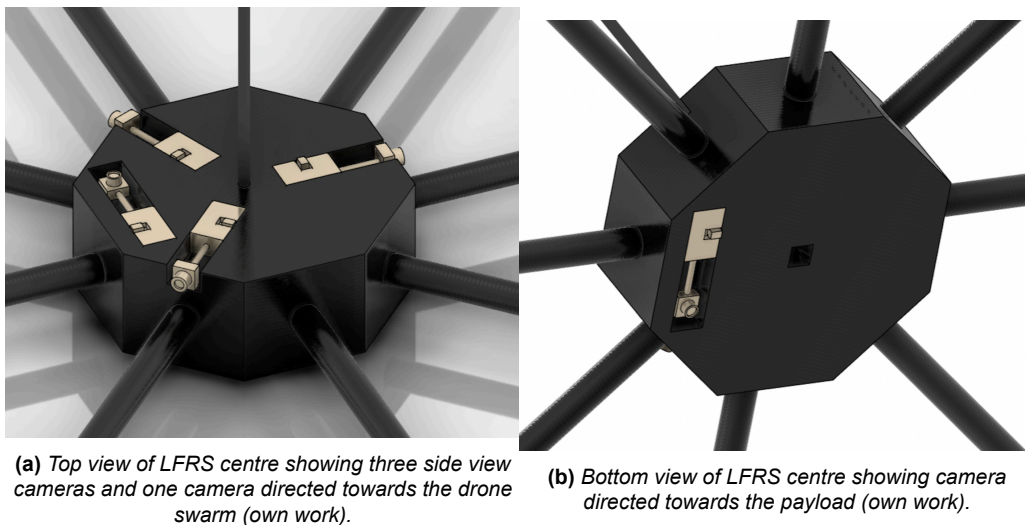


Figure 11.9: Positioning of the cameras on the LFRS centre (own work).

A FEM analysis will also be performed on the LFRS structure. For simplicity and ease of computation the LFRS will be considered as a single part in 3D-experience. In order to prepare the FEM analysis first the material CFRTP will be applied on the LFRS, then the LFRS will be clamped at the octagonal centre and finally the forces will be applied in parallel with the LFRS representing the forces of the payload on the LFRS, this is shown in Figure 11.10 by the green arrows pointing towards the centre of the structure. Each applied force is equal to 1840 N which follows from the weight of a 500 kg payload multiplied with a safety factor of 1.5 which is equally distributed onto the four cables that are attached at the connectors in the corners of the LFRS in a symmetrical manner. Since the LFRS mainly carries lateral forces introduced by the payload that are introduced by the four cables connected to the corners of the LFRS into the LFRS structure, only this loading case has been further investigated into detail using a FEM analysis. This scenario is a non-optimal loading case, but it does show the capability of the LFRS structure. In further considerations for which time was not available, more

optimal loading could be analysed. The primary purpose of this test was to verify that the design would not be sufficiently strong or stiff.

After computation of the FEM model a representation of the structure under load was retained. One can observe that the highest stresses within the structure are present at the cylindrical beam at the octagonal centre which is shown in Figure 11.11 and at the connector in the corner of the LFRS where the load is applied which is shown in Figure 11.12. The lowest stresses in the LFRS structure is present in the connector in the free corner of the LFRS, these stresses are visualised in Figure 11.13. The maximum displacement of the LFRS structure equals 1.3 mm and is located at the connector in the corner of the LFRS where the payload is attached, a visualisation of this deformation is showed in Figure 11.14. Note that the visual representation includes a 925 deformation scale in order to provide a better displacement visualisation for the observer.

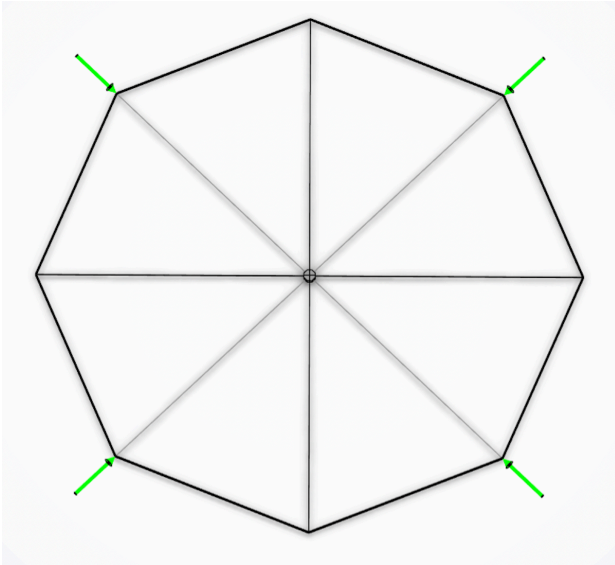


Figure 11.10: Applying the forces representing the pulling forces of the payload on the LFRS for preparation of the FEM Analysis (own work).

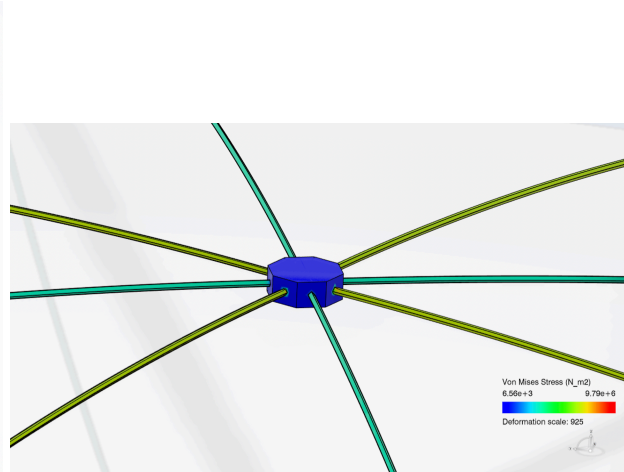


Figure 11.11: FEM analysis showing stresses on octagonal centre of LFRS (own work).

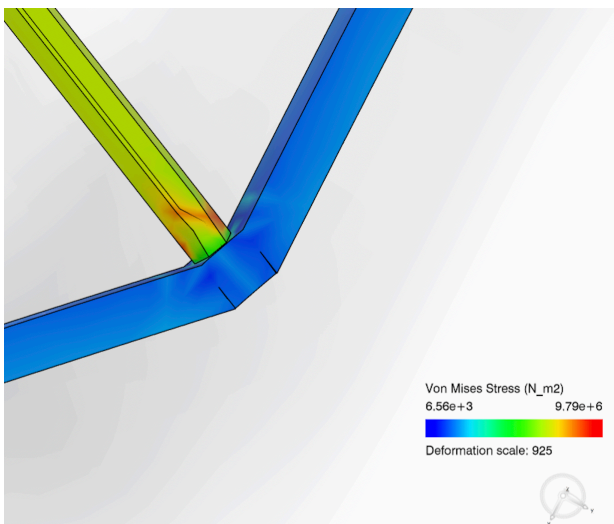


Figure 11.12: FEM analysis showing maximum stresses on the corner of the LFRS where the payload is connected (own work).

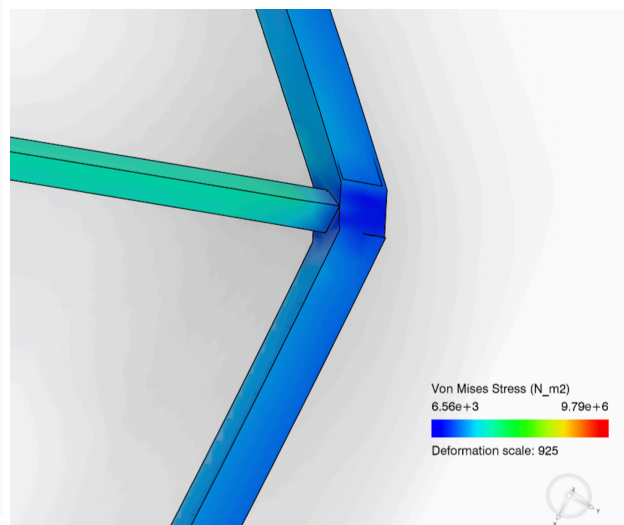


Figure 11.13: FEM analysis showing lowest stresses on the free corner of the LFRS (own work).

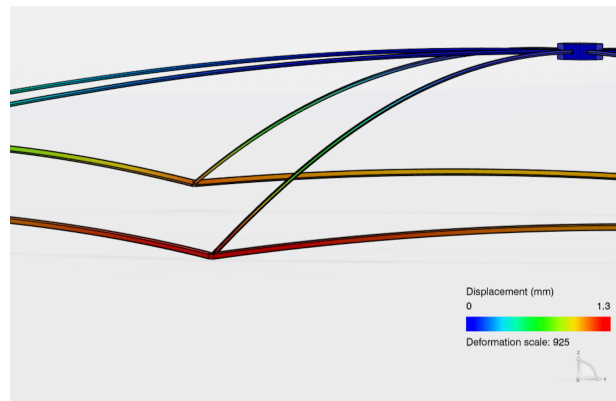


Figure 11.14: FEM analysis showing the maximum deflection present at the connector in the corner of the LFRS where the payload is attached (own work).

11.3. Virtual Reality for Swarm Visualisation

With current day technologies it is possible to view the design within virtual reality. This technology enables developers to let their customers walk around in a world containing a semi-realistic representation of their requested design. Often this representation gives new insights into the design which can lead to early corrections within the design process. Therefore, a virtual representation of the drone swarm connected to the LFRS will also be developed for DroneCrane. In order to make this virtual representation 3D-experience will be used.

First an assembly is constructed that contains 31 drones connected to the LFRS. Each drone will be connected with a beam shaped structure representing a cable to the LFRS, the beam shape structure will be connected at one side to the attachment point at the bottom of the drone and on the other side to the connector at the LFRS. A total of five cables will be used to attach the payload to the LFRS, four cables connected to the connectors in the corners of the LFRS one cable connected to the octagonal centre of the LFRS structure. The number of cables is limited to five to minimise the setup time of the LFRS. A CAD model of the drone swarm connected to the LFRS that is connected to a payload is presented in Figure 11.15.

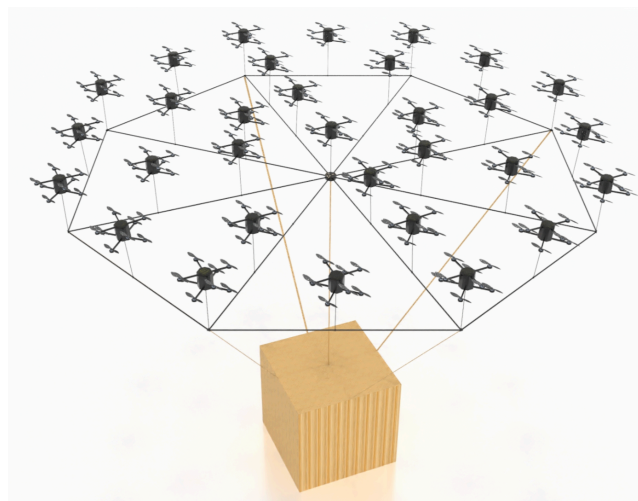


Figure 11.15: CAD model of the drone swarm connected to the LFRS and to the payload which will be used for virtual reality (own work).

12. Detailed Design and Analysis of Properties

Having described both the sizing or selection procedures, as well as the overall design choices for all subsystems, a final assessment of the resulting product must be performed. This assessment will provide not only an answer on whether the design meets the performance requirements, but also how it fares in all other aspects tied to a commercial product.

Section 12.1 will give a brief summary of the specifications of the whole system, subsystem by subsystem. Section 12.2 will analyse the performance of the design and whether it meets certain technical requirements. In Section 12.3 the operational side of things will be discussed, followed by a distribution of budgets in Section 12.4. Section 12.5 and Section 12.6 will contain a RAMS and financial evaluations, respectively. Following that, a requirement compliance analysis will be performed in Section 12.7. Finally, a production plan, detailing the steps to be taken in manufacturing DroneCrane is presented in Section 12.8

12.1. Summary of the Design

This section was written by: *Maxim*

With a converged design and all the subsystems designed to a sufficient level of detail, the design can now be summarised.

Overall Design

The overall system will be comprised of 31 drones, connected to an LFRS. Each drone will weight 24.4 kg, with the total system (without payload) weighing 783 kg, and cost € 2 980, with the total system costing € 97 596.44. In terms of the mass, 94.24% of the swarm mass is recyclable or reusable, which corresponds 94.04% of each individual drone, excluding the LFRS.

Drone Structure

The design of the drone ended up being, as expected, an octocopter. The layout, however, changed from the initial conventional one to a two-layer setup. The diameter of the structure itself is 957.89 mm, which includes the arm and a core, in the centre of the structure. A gap of 300 mm is present between the upper and lower layers of propellers. The material used for the structure is a composite made up of a nylon matrix and carbon fibres. It has a Young's modulus of 137 GPa, with a yield strength of 1.4 GPa and a density of 1800 kg/m^3 . From this it follows that the mass of the core is 0.039 kg and the mass of all the arms is 2.15 kg per drone.

Attachment Structure

The attachment from the drones to the payload has a total mass of 26.05 kg, with the connecting ropes weighing 1.51 kg and the LFRS weighing 24.53 kg. The shape of the LFRS is an octagon, with a diameter of 12.3 m. The material used for the LFRS is the same as for the drone structure. All of the beams in the LFRS have a circular cross section with a small thickness in order to maximise the moment of inertia of these shapes. These sections have a diameter of 13.5 cm and a thickness of 2 mm. The attachment has been designed with a safety factor of 3, as part of a compensation for the non-isometric nature of the materials properties.

Propulsion

The propulsion system consists of a propeller with a 20 inch diameter and a 6.2 inch pitch, and the motor is a T-Motor Antigravity MN6007II KV160. The motor has a peak power of 1120 W and a peak current of 23.7 A. The maximum thrust that the propeller and motor can produce is 60.6 N. At this thrust level, the motor provides a mechanical power of 945.61 W, a torque of 1.37 N m and a rotational

speed of 6304 RPM. The mass of the propeller is 23 g and the mass of the motor 159 g, leading to a total mass for the propulsion per drone of 1.46 kg.

Electrics

The electrics contain many components. First, the batteries used are the Samsung INR21700-50E. Each drone will have 300 batteries, organised into two decoupled battery packs, which are further divided into smaller packs. In total, the batteries will weigh 20.7 kg per drone, will take up a volume of 9.43 dm³ per drone and will provide a total of 5292 Wh of energy per drone. As for the other electrics, multiple sensors, mostly required for control and communication, had to be added, as well as power management electrics. Those relevant to the power system include, per drone, 2 MATEKSYS PDB-HEX power distribution boards and 8 ALPHA 60A 12S V1.2 ESCs.

Control

The control system consists of the swarm controller, present on each drone, namely the Raspberry Pi Zero 2 W; the flight controller on each drone, the Pixhawk 4; u-blox NEO-M8P which will provide RTK GPS sensor information; Adafruit LoRa Radio transceiver used for remote control; Qorvo DWM1000 module for ultra-wide band used for distance measurement between drones and the Caddx Nebula Pro camera system used for camera feeds.

A data protocol has been designed, with specific types of messages sent between the drones for swarm controller communication and coordination. Four drones in the center region of the swarm compute the virtual centre of the swarm at all times, and with this information and the RTK GPS relative location, the drones maintain the swarm formation.

For internal collisions that could occur due to external disturbances, the Internal Collision Avoidance (ICA) system was developed. This system ensures with collision risks that drones mitigate the risk by ensuring that the collision does not occur.

12.2. Performance

This section was written by: *Ojas, Giacomo*

Given the design shown in Section 12.1, the performance of the system can be analysed. This is done to determine whether the requirements on performance are met or not. The time that DroneCrane can hover with a payload of 500 kg and 100 kg is calculated. This is done without taking into account air drag, since vertical acceleration while hovering is 0. In order to calculate it, the thrust per rotor, T_{rotor} , required to lift the payload is calculated with Equation 12.1.

$$T_{rotor} = \frac{m \cdot g}{n_{rotor}} \quad (12.1)$$

The thrust per rotor is then used to find the required mechanical power using the T-Motor NS20x62 propeller and interpolating its specifications. Furthermore, the efficiency is calculated as shown in Equation 7.8 and the required electrical power is found with Equation 7.9. Consequently, the run out time of the battery going from 100% charge to 0% can be calculated by using Equation 12.2.

$$t = \frac{C \cdot 0.8 \cdot V \cdot n_{cell} \cdot n_{string}}{P_{rotor} \cdot (n_{drone} - 1)} \quad (12.2)$$

Where C is the capacity of the battery which is equal to 4.9 Ah, V is the voltage which is calculated with Equation 7.7, n_{cell} is the number of cells in the strings for each drone which is 12 as specified in Section 7.3, n_{string} is the number of strings per drone which is 25, and P_{rotor} is the electrical power needed for each motor. This calculation takes into account a factor of 80% for degradation of batteries and a failure of a drone in the system. Therefore, the time found is the hovering time at end of life of the batteries with a drone failure. For a payload mass of 500 kg, the maximum hovering time at end of life and with a drone failure is 34 min, while for a payload of 100 kg it is 60 min. The requirements on performance for hovering time are thus fulfilled. The same calculation is also performed for normal operation conditions and for end of life without failures.

We can also perform a sample calculation for a mission. This involves an ascent to altitude and 15 minutes of hover, followed by a descent without a payload attached, with both ascent and descent phases occurring at 1.5 m s^{-1} . We can use the same equations shown above, neglecting the thrust decrease due to altitude and the increased power usage due to acceleration and deceleration. For operating a mission with 500 kg payload at end-of-life, with one drone failing, the mission lasts 41 min, going to an altitude of 1170 m. For 100 kg, this is 63.2 min, and an altitude of 2160 m. It is important to note that, although this calculation neglects the decrease in thrust at altitude, the system has been designed to be able to operate at this altitude. This means that in reality, this number is lower due to the changed thrust and power characteristics of the system, yet this number still provides a useful metric to evaluate the performance of the system. It is important to note that this is not an operational ceiling or a parameter with a meaningful physical metric; it simply provides a value to compare with.

The results from the analysis discussed above are summarised in Table 12.1 and Table 12.2 both for 500 kg and 100 kg.

Table 12.1: Performances of DroneCrane with a payload of 500 kg for different operational conditions

Operational conditions	Hovering time [min]	Max mission altitude [m]	Max mission time [min]
Normal	44.9	1800	55.2
End of life	35.9	1260	43.2
End of life with 1 failure	34.4	1170	41.2

Table 12.2: Performances of DroneCrane with a payload of 100 kg for different operational conditions

Operational conditions	Hovering time [min]	Max mission altitude [m]	Max mission time [min]
Normal	77.0	3050	83.0
End of life	61.6	2290	66.1
End of life with 1 failure	60.0	2160	63.2

12.3. Operations and Logistics Description

This section was written by: *Dequan*

Once the design of the product is completed, it is time to understand how customers can deploy and operate DroneCrane. The operations and logistics concept has been divided into four parts: ground operations, flight operations, maintenance, and safety. In Subsection 12.3.5, an operation flow diagram is presented.

12.3.1. Ground Operations

Each drone of DroneCrane will be placed in the foam boxes. Furthermore, the controlling system contains a joystick for manual control and a laptop for monitoring the flight condition, camera, and data. RADIO MASTER TX12⁶⁵ has been chosen as joystick due to the flexibility of its Open TX software. It can be programmed to adapt to our control system. Dell Latitude 5420 Rugged⁶⁶ has been chosen as ground station laptop for its high performance for outdoor use. The LFRS will be broken down into 16 small segments with a maximum size of 5.8 m. All of the above components will be loaded into a 26 foot moving truck that will be driven to the destination.

After the components are delivered to the mission location, DroneCrane needs to be assembled and deployed. The deployment of DroneCrane requires an open and flat ground space of 12 m by 12 m. In case the mission is in a urban environment, measures such as blocking the street can be considered. The set-up of DroneCrane will take 5 operators approximate one hour.

⁶⁵<https://www.radiomasterrc.com/products/tx12-radio-controller> [Accessed in June 2022]

⁶⁶shorturl.at/ovNU7 [Accessed in June 2022]

First, the LFRS can be assembled. The ropes for attaching the payloads will also be connected to the LFRS. This process will take the two operators around 15 minutes. At the same time, the drones can be taken out from the vehicle and placed in their rough position on top of the LFRS, with a rope connecting them. This process will take the two operators around 45 minutes. Operator 5 can start set up the ground station, cameras and establish connections between these hardware. Then, operator 1-4 will spend 5 minutes to do pre-flight check of each drone and boot them up. The set-up timeline is shown in Figure 12.1.

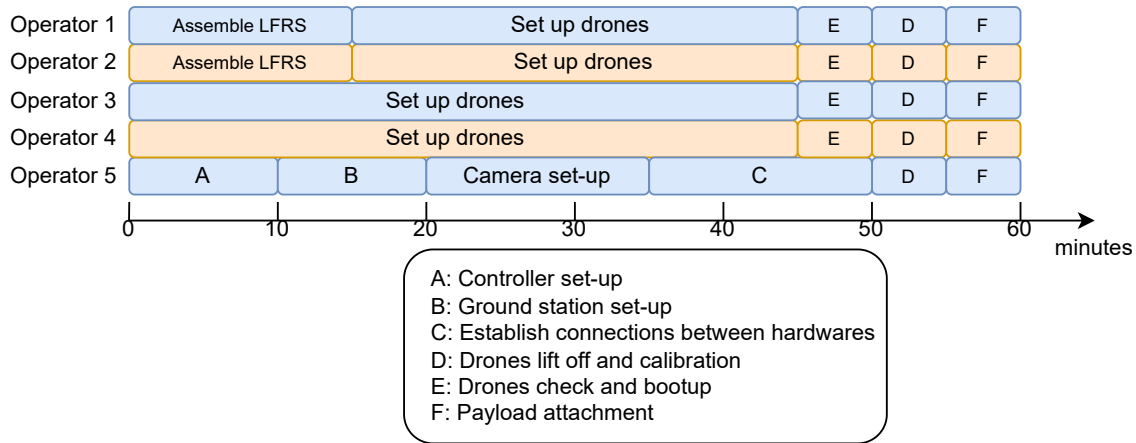


Figure 12.1: Timeline during set-up. (own work)

After all of this is done, DroneCrane will lift off to attach the payloads. The swarm will first lift and hover in an altitude of around 8 metres to form the exact formation and calibrate, controlled by operator 5. And the rope for attaching payload should still be able to touch the ground for attaching the payload. Operator 1,2,3, and 4 will go under DroneCrane to connect the attachment with the payload. Eventually, DroneCrane is ready to lift off. Operator 5 will be controlling the joystick. Operator 1 will get to the delivery destination to give further instructions.

12.3.2. Flight Operations

As previously mentioned in Subsection 12.3.2, a joystick will be used to control the DroneCrane formation. When pushing the joystick forward, the velocity of DroneSwarm can be set to a value between 0 to 2m/s. When turning the joystick left or right, the heading of the drone swarm can yaw with a maximum rate of 5 °/s. To increase or decrease the altitude of the drone swarm, two side buttons on the joystick can increase altitude of the swarm with ascent speed of 1.5 m/s or decrease the altitude with descent speed of 0.5 m/s. The operator 2 can use the camera feed from LFRS for observation. There are 5 cameras equipped in the LFRS: one points at the drones, one points toward the payload, and the other three points toward three different directions horizontally. CADDX NEBULA PRO VISTA KIT - WHITE has been chosen as it has its own transmitter and has a field of view of 122 ° 67.

In the case when the operator wants to keep DroneCrane to stay in a certain position, a lock button in the joystick can be used. Same principle applied to the situation when the joystick fails, DroneCrane will be locked to its last commanded position, until the backup joystick is connected and paired.

During the mission operation, it is crucial to have a safe, stable flight. However, there is possibility that different kinds of failure will occur that affects the operation. As previously mentioned, DroneCrane has been decided to ensure that one drone failure will not lead to the failure of the mission. In case one or even two propellers or motors fail in the swarm, the mission will be resuming due to the redundant drone. In case one drone fails, first the drone will detach from the swarm system. Then the drone will descent with a speed of 0.5 m/s to avoid any hard landing.

⁶⁷<https://droneshop.nl/caddx-nebula-pro-vista-kit> [Accessed in June 2022]

When DroneCrane is approaching the delivering destination, operator 5 moves the payload to its desired payload and direction so that it can be detached or mounted. However, if necessary, operator 1 or workers can give guidance using gesture in the camera.

12.3.3. Maintenance

After each flight, the condition of DroneCrane has to be checked. The process contains checking the conditions of the components such as batteries, propellers, and so on. When the battery capacity of the drones are lower than 80 %, the batteries have to be changed. For the propeller and the drone structure, it necessary to replace them if any fatigue is found on it.

12.3.4. Safety

Safety is always the first factor to be considered. Same as conventional crane, the safety rule number one for DroneCrane is: no human is allowed under the payload. Also, the flight condition have to be limited to a weather without raining and a wind gust speed of lower than 10 m/s. In addition to that, a safety check has to be performed before each new operation as previously mentioned. Finally, before the mission, the flight has to be reported and approved by the local government and air control department.

12.3.5. Summary of Operations

At the end, the operation flow diagram is shown in Figure 12.2.

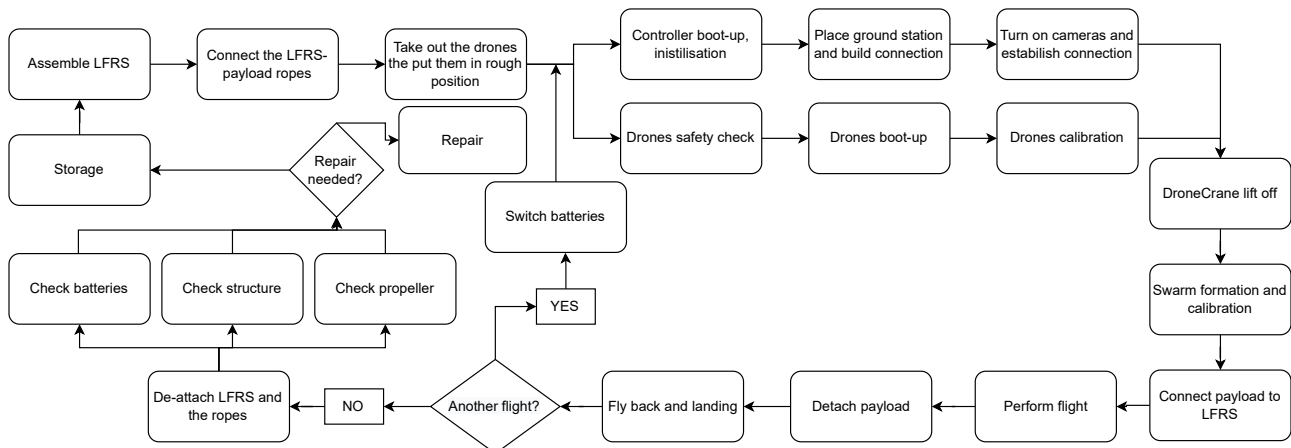


Figure 12.2: Operation flow diagram. (own work)

12.4. Final Design Resource Allocation

This section was written by: *Robin*

In this section, the finalised budgets of DroneCrane are laid out in order to give a complete overview of the specifications in a high level of detail. These budgets cover the mass of each component, the power usage of components and the cost of each component.

12.4.1. Mass Budget

Firstly, the mass budget is discussed. In Table 12.3 the masses of all the components are given, together with the percentage of the total mass that it represents.

Table 12.3: Finalised mass budget

Component	Mass [kg]	% of total mass
Attachment	26.04	3.32%
Drone structure	67.94	8.67%
Electronics	644.80	82.25%
Propulsion	45.14	5.76%
Total	783.92	100%

It is clear from the mass budget, that the electronics pose the largest portion of the mass of DroneCrane. This is caused by the energy that is required to be stored in the batteries, and the limited energy density of these batteries. Section 13.3 This battery mass did exceed the initial estimations by a large amount, and thus the design had to be adjusted and iterated extensively to converge to a working model. This also means that, as technology progresses, the design of DroneCrane could be greatly improved with respect to energy storage and may thus become a much lighter system. Not only would the individual drones become smaller and lighter, the attachment would also decrease in size and fewer drones would be required to lift the same amount. Next, the structures of the drones and the propulsion units provide the largest parts of the system mass after the electronics. This was largely expected. As described in the baseline report written by this group in a previous stage of design[11], it was estimated that the structures group had a relative weight ratio of 60-40 with respect to the propulsion group. This estimation turned out to be very close to the final numbers. Lastly, the mass of the attachment is built up out of the LFRS, and the ropes holding the swarm together. Due to the smart choice of material used for the ropes, the masses of these could be kept exceptionally low. In order to make the LFRS feasible, novel materials had to be used as well. More about this can be read in Subsection 6.3.1

12.4.2. Power Budget

Secondly, the power budget is discussed. This budget describes the total power that is used in a flight by each component. In Table 12.4 the amount of power used by each component is shown, as well as the percentage of power used with respect to the total amount of power used by the swarm.

Table 12.4: Finalised power budget

Component	Power [W]	% of total power
Propulsion	298 090	99.9%
Electronics	310	0.1%
Total	298 400	100%

The power budget is a more limited endeavour in this project. It is clear that the propulsion is the largest part of the energy consumption, which is unsurprising, as keeping a large mass hovering in the air costs a tremendous amount of energy. Though the electronics use energy, the inaccuracies in the current state of design with respect to the propulsion power might be larger than the total use of the electronics. In conclusion nearly all power is used in attempting to lift the total system.

12.5. RAMS

This section was written by: *Giovanni, Tyme, Maxim, Ojas*

As part of the characterisation of the design at the end of this final phase of the design, the RAMS properties of DroneCrane help in informing the reader about its reliability, availability, maintainability, and safety, according to engineering standards. This section illustrates how these four aspects of DroneCrane contribute to the performance of the system, collecting information from the detailed

design process presented earlier in this report. When new material or methods are used, they are described here, otherwise reference to other relevant sections is made.

12.5.1. Reliability of DroneCrane

The reliability analysis of DroneCrane was approached in a quantitative fashion already in each of the chapters concerning the four subsystems identified in Part III. This section expands on each when needed and integrates the numbers to prove that the system meets the reliability requirements expressed in Section 4.2.

The reliability as expressed by the requirement is intended in terms of critical failure rate per operational hour. The unit is defined as the number of mission-critical failures per hour that the system is operational. This excludes from the quantitative analysis the probability that during set-up the operators make mistakes and deviate from instructions. At the same time, the probability that the operator behind the ground controller leads the swarm to fail because of a collision with still obstacles is also extremely hard to predict, and since literature suggests that it may be higher than the requirement set for DroneCrane [72], it is reasonable to consider the requirement only for the system itself, and not accounting for human error during operations.

Having restricted the analysis to technical failures, a mathematical framework for the overall reliability estimates is constructed here. The analysis is simplified by the assumption that all subsystems' reliability rates are independent of each other, in which case the overall failure rate P_{tot} would be the sum of the N individual ones⁶⁸, as in Equation 12.3. The reliability of each subsystem was assessed individually in their own respective chapters above in terms of failure rate of a drone per hour, and is summarised in Table 12.5.

$$P_{tot} = \sum_{n=1}^N P_i \quad (12.3)$$

Table 12.5: Reliability of each subsystem (own work).

Subsystem	Failure rate of a drone per hour [h^{-1}]
Electrics	1.1e-71
Propulsion	3.2e-8

The other subsystems are not included as an estimate for the reliability was not possible to obtain, and will have to be tested to validate them. However, all the subsystems are designed to ensure that a single point failure will not lead to a systems failure, so it can be expected that the probability of failure for the other subsystems not included will not be as critical.

The system is designed such that if one failure of drone occurs, it shall not lead to a system failure. Therefore, an analysis on the probability that two drones in the swarm failing will be performed by considering the different combinations of failure that can occur. Firstly, the probability that the failure of the propulsion system in two different drones is examined, via Equation 12.4.

$$p_{failure} = p_{fail,drone} \cdot n_{drones} \cdot p_{fail,drone} \cdot (n_{drones} - 1) \quad (12.4)$$

From the equation above, it was found that the probability of the propulsion system failing in 2 drones is $9.52 \cdot 10^{-13}$. Next, the probability of the failure of the swarm, via one drone failing due to the electric system and one drone failing due to the propulsion system is calculated. This is done using Equation 12.5.

⁶⁸<https://flexbooks.ck12.org/cbook/ck-12-interactive-middle-school-math-7-for-ccss/section/7.9/related/lesson/probability-of-compound-events-bsc-alg/> [Accessed in June 2022]

$$p_{failure} = p_{fail,propulsion} \cdot n_{drones} \cdot p_{fail,electrics} \cdot (n_{drones} - 1) + p_{fail,electrics} \cdot n_{drones} \cdot p_{fail,propulsion} \cdot (n_{drones} - 1) \quad (12.5)$$

The resulting probability of failure for this mode is $6.54 \cdot 10^{-76}$. Finally, the failure due to electrics system failing in 2 different drones is examined, via Equation 12.4. The probability of this mode of failure is extremely low, in the magnitudes of 10^{-100} , hence it is considered negligible. The different failure modes are then superpose to combine all the different combinations of failure to find the failure rate of the entire swarm via Equation 12.3.

It was found that the probability of the failure rate of the entire swarm is $9.52 \times 10^{-13} \text{ h}^{-1}$, however it is expected to be higher than this if the failure rates of the other subsystems are included as well. In order to meet **REQ-USR-04**, the probability failure rate must be below $1 \times 10^{-5} \text{ h}^{-1}$, and the magnitude of the failure rate calculated remains significantly below the required failure rate, it can be assumed that the failure rate will remain within the margin with the addition of the failure rate of the other subsystems as well.

12.5.2. Availability of DroneCrane

In this section the availability of DroneCrane as a system will be analysed. The availability will be defined as the possibility to start the operation of DroneCrane, when the mission is called for at an unknown time. Firstly the external sources of disturbances that limits the possibility of operation will be identified, then the internal sources that prohibits operations will be identified.

The first external source that disrupts the operation of DroneCrane is the weather, as DroneCrane is designed with certain specification and requirements. If the wind speed at the operational site exceeds 10.2 m s^{-1} , or rain is present, the operation will not be feasible. The probability of the wind speed exceeding this is around 5 % throughout the entire year in the Netherlands.⁶⁹ The larger impeding factor on the operability of DroneCrane is the rain, as it is expected that the volume operations during winter (December - March) will decrease. Next, certain hardware in DroneCrane requires a minimum degree of visibility in order to operate such as the cameras, therefore DroneCrane will not be able to operate at night. Finally, the next limiting external factor is the space available for setting up the system and the airspace available. The diameter of the swarm is 12 m, therefore a ground and air space of 12 x 12 m is required to set up and operate the system. This means that DroneCrane will not be able to operate at all locations, depending on the space available.

Finally, the internal source will be examined. After each operation the batteries will be need to be recharged, hence there will be some downtime where the system will not be able to operate.

12.5.3. Maintainability of DroneCrane

The maintainability of a system is the measure of the ease with which a product can be maintained. This highly depends on the individual subsystems on board of the product. As such, the maintainability analysis will be done subsystem by subsystem.

First, when it comes to the maintainability of the propulsion, the motors should, in theory, last for a very long time, most likely the entire lifetime of the drone. As they are embedded in the frame, they are mostly protected from external damage. Additionally, motors are relatively expensive, thus it would be preferable to make sure that they last for as long as possible. The maintenance that can be performed on them includes adding lubricant to the bearing when needed and ensuring the engines do not overheat. The propellers, on the other hand, are in a much more vulnerable position. They are on the outside of the structure and rotate at a very high speed. Therefore, any collisions will have a much higher chance of causing damage. Thus, the propellers have to be continuously checked after every use and if damage is found, replaced by new ones.

Second, the maintainability of the structures needs to be considered. Overall, maintaining the structures in good condition can be done by keeping them in dry, room temperature conditions. However,

⁶⁹https://www.windfinder.com/windstatistics/hoek_van_holland [Accessed in June 2022]

if the structure starts to fail, either due to fatigue or external damages, it will most likely lead to the total failure of the drone.

Finally, the maintainability of the electrics, in particular the batteries, has to be considered. If not handled correctly, the batteries can lose a large proportion of their capacity, which would lead to a system not operating up to standard. To circumvent this, batteries, similarly to the structures, should be stored in dry conditions at a appropriate temperature and correct voltage.

12.5.4. Safety

Safety is a key consideration in the Aerospace industry, and this becomes even more crucial in a project where the aircraft will be around people, and may operate in urban environments. This has also been reflected in the design of DroneCrane. Safety of the system and the surroundings has been taken into account every step of the way during the design, in order to have a system that will ensure the safety of itself, its payload, the surroundings and the people at all times.

A key condition for safety is that the payload or the drone do not come crashing down, causing damage. This is also reflected in the user requirement **REQ-USR-06**, that a single drone failure should not lead to the payload being dropped. For the design of DroneCrane means that there should be sufficient redundancy, and this is seen at every level of the design. For example, the drones are octocopters, allowing for a two-rotor failure to still leave the drone controllable, allowing it to either continue the mission or safely detach from the swarm and land at a safe location. This theme of redundancy is continued in other aspects as well. The power distribution to the motors, for example, is carried out using two separate boards. These have been wired in such a way that a failure of one of the boards results in the remaining four motors keeping the drone still controllable, such that it can detach from the swarm and land. This is also reflected in the batteries - there are two separate battery packs in the drone, each made from two modules. This allows for a high degree of redundancy in the drone.

However, there is the possibility that a drone fails and detaches from the swarm, leaving one less drone to carry the payload. This has also been designed for, even at end-of-life battery conditions. This allows the mission to be completed even with some failures. If more than one drone fails, there is still enough thrust available to allow the mission to be safely aborted and land, with no damage done.

12.6. Financial Evaluation

This section was written by: *Giacomo, Dequan*

The DroneCrane is a product which needs to be competitive in the market. This means that the cost of production and operation should be lower than the competition explored in Chapter 3. In order to fulfil this, objective requirements on cost were set as displayed in Chapter 4. In this section, a cost breakdown of the components within DroneCrane and of the operations is discussed, as well as an analysis on the return on investment, which this product can achieve.

12.6.1. Cost Analysis

A breakdown of each component used within DroneCrane is displayed in Table 12.6. This table contains the name of the off-the-shelf components selected with their cost per piece, the amount of elements needed and the total cost for the entire swarm. The prices of the components were found on company websites, which means they contain a mark-up that could be reduced if bulk purchases are effectuated. For the batteries, the price per piece was found to be €3.65 for a minimum of 100 pieces bought. Additionally, the propeller and the motor are the components, which required the largest amount of pieces after the batteries, therefore a factor taking into account the discount for bulk purchases of 30% is applied to the total cost. As can be seen from Table 12.6, taking into consideration these discounts, the total cost becomes €97596.44, which is lower than the €100 000 requirement imposed by **REQ-USR-12**. Furthermore, Figure 12.3 shows a clear overview of the cost percentage of the total cost taken by each subsystem. The power and the propulsion subsystem end up being the costliest, accounting for 24% and 52% of the total cost respectively. This was expected as these two subsystems have the highest number of components and are critical to reach the required

performance of DroneCrane.

Table 12.6: Cost of all components per subsystem

Category	Component	Name	Cost per piece [€]	N of pieces	Total cost [€]
Propulsion	Propeller	T-Motor NS20x62 ⁷⁰	57.37	248	9959.43
	Motor	T-Motor Antigravity MN6007II KV160 ⁷¹	124.31	248	21580.22
	PDB	MATEKSYS PDB-HEX ⁷²	22.03	62	1365.86
	ESC	ALPHA 60A 12S V1.2 ⁷³	105.18	248	18259.25
Control	Flight controller	PixHawk 4 ⁷⁴	180.5	31	5595.50
	Swarm controller	Raspberry Pi Zero 2W ⁷⁵	14.34	31	444.54
	Transceiver	LoRa transceiver ⁷⁶	31.08	62	1926.96
	Ultra-wide band	DWM1000 ⁷⁷	18.00	31	558.00
	RTK	NEO-M8P series ⁷⁸	118.58	32	3794.56
Power	Batteries	Samsung INR21700-50E ⁷⁹	2.56	9300	23808.00
Structure	LFRS+cables	-	-	-	2604.84
	Drone frame	-	-	-	5095.28
Other	Joystick	RADIOMASTER TX12 ⁸⁰	99.00	1	99.00
	Laptop	Dell Latitude 5420 Rugged9 ⁸¹	1555.00	1	1555
	Camera	Caddx Nebula Pro Vista Kit ⁸²	190.00	5	950.00
					97596.44

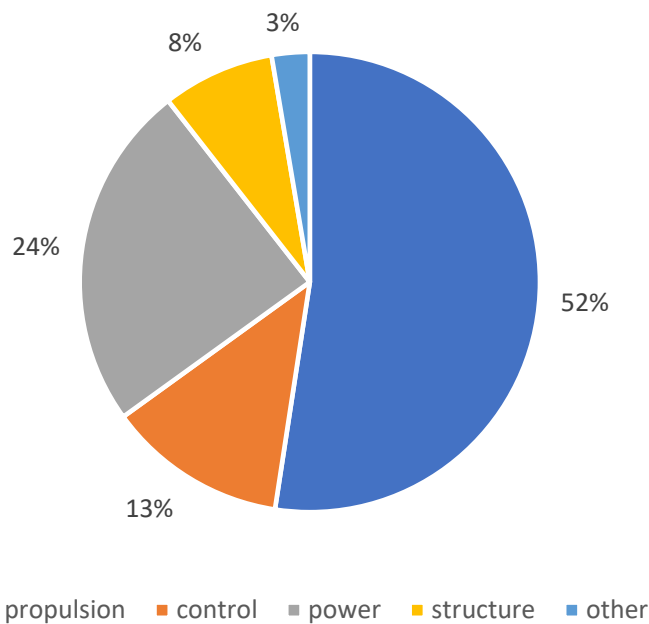


Figure 12.3: Cost breakdown structure of DroneCrane (own work)

⁷⁰<https://store.tmotor.com/goods.php?id=965> [Accessed in June 2022]

⁷¹<https://store.tmotor.com/goods.php?id=1113> [Accessed in June 2022]

⁷²<https://it.aliexpress.com/item/1005001844324949.html?gatewayAdapt=glo2ita> [Accessed in June 2022]

⁷³<https://store.tmotor.com/goods.php?id=582> [Accessed in June 2022]

⁷⁴https://shop.holybro.com/pixhawk-4beta-launch_p1089.html [Accessed in June 2022]

⁷⁵<https://www.raspberrypi.com/products/raspberry-pi-zero-2-w/> [Accessed in June 2022]

⁷⁶<https://www.adafruit.com/product/4075> [Accessed in June 2022]

⁷⁷<https://nl.mouser.com/ProductDetail/Qorvo/DWM1000?qs=TiOZkKH1s2R6b5D6df63Pg%3D%3D> [Accessed in June 2022]

⁷⁸<https://www.digikey.com/en/products/detail/u-blox/NEO-M8P-0/6150644> [Accessed in June 2022]

⁷⁹<https://eu.nkon.nl/samsung-inr21700-50e.html> [Accessed in June 2022]

⁸⁰<https://droneshop.nl/radiomaster-tx12> [Accessed in June 2022]

⁸¹shorturl.at/ovNU7 [Accessed in June 2022]

⁸²<https://droneshop.nl/caddx-nebula-pro-vista-kit> [Accessed in June 2022]

12.6.2. Operational Cost Analysis

For the daily operational costs, the following costs have to be taken into account. First, two operators are needed to operate DroneCrane. The average labour cost for a drone operator in Netherlands is 60 € per hour.⁸³ For two operators to work 8 hours a day, a total labour cost of €960 is needed. Secondly, a transporting cost can be calculated as the components of DroneCrane are transported by a truck. It is assumed that DroneCrane will operate in a range of 100 km around its base, which gives a distance of about 200 km back and forth. It costs €300 per day to rent a 26 foot moving truck. The price for diesel in Netherlands is €2 per litre.⁸⁴ The average fuel consumption of the 26 ft moving truck is 10 MPG which is equivalent to 2.35 liter/km.⁸⁵ This gives a total diesel cost of €941. In addition to that, the cost for the power must be taken into account. The total energy required by DroneCrane is 51.4 kW h. The industry electricity in Netherlands costs €0.105 per kWh.⁸⁶ Thus, given it is charged two times per day, the power cost per day is calculated to be €21.59. Finally, a maintenance cost needs to be taken into consideration. The maintenance cost contains both the battery and drone maintenance. The battery for DroneCrane has a lifetime of 500 discharge cycles. Ideally, the battery is charged two times per day. Therefore, the battery has a life time of 250 working days. Given the price of the battery is €33 945, the maintenance cost for the battery every day is €135.78. For the drone maintenance, the study has shown that common drone has a failure rate of 10^{-3} [73]. Therefore, one drone needs to be replaced every 1000 flight hours. The flight time of DroneCrane per day is estimated to be around 2 hours. Considering 31 drones are in the swarm, the period to replace one drone is 32.26 h, which is equivalent to 16 working days. Given the cost of each drone is about €2639.5. The drone maintenance cost for DroneCrane is €165. A summary of all the operational costs is presented in Table 12.7.

Table 12.7: Operational cost summary.

Cost type	Unit cost	Amounts	Total [€]
Labour Cost	€60/hour	5x8 man hours	2 400.00
26 ft Truck Rental Cost	€300	-	300.00
Diesel Fuel Cost	€2/Litre	470 litres	940.00
Electric Power Cost	€0.105/kWh	205.6 kW h	22.00
Battery Maintenance Cost	€/day	-	135.78
Drone Maintenance Cost	€/day	-	165.00
Total Operational Cost	€/day	-	3962.78

12.6.3. Return on Investment

To determine the return on investment (ROI), the market price, market volume, achievable market share, development cost, and production cost are required. The production cost and operational cost have been analysed in Subsection 12.6.2 and Subsection 12.6.1.

For the market price, it is mainly determined by the competitors' cost and the production cost. DroneCrane wants to be a competitive product in terms of price in the market. Given the price of the mobile crane and helicopter crane from Chapter 3, also taking the relatively shorter life time of DroneCrane, the price of DroneCrane should be at least lower than €500 000. The final market price has been determined to be €200 000 to make a 100% profit from the production cost of €100 000.

For the development cost, in this case it is mainly the labour cost. Given a group of 10 members spent 400 h on this project, and a hourly wage of €100 by the DSE management, a current development cost is estimated to be €400 000. However, there are still steps before DroneCrane goes into market.

⁸³<https://www.eriei.com/salary/job/drone-operator/netherlands> [Accessed in May 2022]

⁸⁴https://nl.globalpetrolprices.com/Netherlands/diesel_prices/ [Accessed in May 2022]

⁸⁵<https://www.uhaul.com/Truck-Rentals/26ft-Moving-Truck/> [Accessed in June 2022]

⁸⁶<https://www.statista.com/statistics/596254/electricity-industry-price-netherlands/> [Accessed in May 2022]

An assumption has been made that this will take 26 more months and 2 prototypes need to be built. Therefore, the total development cost is €1 640 000. This is a rough estimation as many of the cost such as certification or office renting are not taken into consideration.

Furthermore, the aerial market size in 2019 is \$ 2.81 billion from Section 3.1. Europe is one of the biggest market in the world, thus a one third of market share will be assumed, which gives a market size of \$ 937 millions is assumed. Market analyst from Mammoet estimates around 2 % of the payloads are around or below 500 kg. Therefore, the market volume for DroneCrane in Europe is \$18.74 million or €17.8 million. It is also assumed the market share that DroneCrane will take is 10%. Then the market share volume of DroneCrane is estimated to be €1 780 000. Given the price of DroneCrane is €200 000, around 9 DroneCranes can be sold each year.

Therefore, all the relevant information are summarised in Table 12.8:

Table 12.8: *Return on investment relevant information.*

Market price	€200 000
Market volume	€17 800 000
Market share	10%
Development cost	€1 640 000.
Production cost	€95 906
Investment period	5 years

Given a five years of investing period, the return on investment can be calculated by:

$$ROI = \frac{5 \cdot 9 \cdot (200000 - 95906) - 1640000}{5 \cdot 9 \cdot 95906 + 1640000} = 51.1\%$$

12.7. Compliance Matrix

The final analysis that needs to be performed is filling in the compliance matrix. This document's purpose is to showcase whether the design created fully complies with the requirements set out at the start. If any requirements end up not being met, an explanation on why and how this impacts the product is required. Alternatively, if the design is found to not meet key requirements, it may be necessary to modify or redesign it.

Table 12.9: *Compliance matrix of user requirements*

ID	Requirement	Compliance	Proof
REQ-USR-01 🔑	DroneCrane shall have a payload-lifting capacity of 500 kg.	✓	Section 12.2
REQ-USR-02	DroneCrane shall have a minimum altitude ceiling of 1000 m AMSL.	✓	Section 12.2
REQ-USR-03	DroneCrane shall be able to deliver payloads to an altitude of least 200 m AGL.	✓	Section 12.2
REQ-USR-04 🔑	DroneCrane shall have a probability of safety-critical malfunction lower than 1×10^{-5} per system flight hour.	✓	Section 12.5
REQ-USR-05	Failure of one drone of the DroneCrane system shall not lead to dropping of the payload.	✓	Section 12.2

REQ-USR-06	Failure of one drone of the DroneCrane system shall not lead to failure of the other drones.	✓	Section 12.5
REQ-USR-07	The failure of any communication link between drones shall not lead to safety-critical malfunction of the system.	✓	Chapter 9
REQ-USR-08	The loss of GPS signal for the system shall not lead to safety-critical malfunction of the system.	✓	Chapter 9
REQ-USR-09 🔑	DroneCrane shall be fully operated on green energy.	✓	Section 12.1 ⁸⁷
REQ-USR-10 🔑	DroneCrane shall be 80% recyclable or reusable by weight.	✓	Section 12.1
REQ-USR-11 🔑	A single drone of DroneCrane shall not weigh more than 25 kg.	✓	Section 7.6
REQ-USR-12	A single DroneCrane system shall not cost more than €100 000.	✓	Section 7.6
REQ-USR-13	Operation of a DroneCrane system shall not cost more than €5 000 per day.	✓	Subsection 12.6.2
REQ-USR-14	DroneCrane shall be deployable by six operators in an hour.	✓	Section 12.3
REQ-USR-15	DroneCrane shall be operable by two operators.	✓	Section 12.3

As can be seen, all user requirements set out at the start of the design phase have been met. Thus, the system could theoretically be manufactured and put into use. However, in reality, further research and improvement, as well as verification of the system needs to be performed. On top of that, the team had laid out additional technical and operational requirements. The technical requirement compliance matrices are shown below.

Table 12.10: Compliance matrix of requirements deriving from non-technical regulatory mission constraints.

ID	Requirement	Compliance	Proof
REQ-REG-ENV-1	DroneCrane shall comply with environmental regulations as stipulated by the authorities of the Dutch market.	x	
REQ-REG-ENV-2	DroneCrane shall not produce noise greater than 100 dB.	✓	Section 8.3
REQ-REG-AIR-1	DroneCrane shall comply with the Dutch airspace regulations corresponding to its product category.	x	

⁸⁷Electrical energy can be sourced from green sources

Table 12.11: Compliance matrix of requirements generated from operational mission blocks, power, and propulsion.

ID	Requirements	Compliance	Proof
REQ-OPR-WEA-1	DroneCrane shall resist winds up to level 5 on the Beaufort scale [16].	✓	Section 8.3
REQ-OPR-WEA-2	The drone shall have an IP rating of at least 4 for protection against water.	✗	
REQ-OPR-PER-1	DroneCrane shall have a flight time of 30 min with a payload of 500 kg.	✓	Section 7.6
REQ-OPR-PER-2	DroneCrane shall have a flight time of 60 min with a payload of 100 kg.	✓	Section 7.6

Table 12.12: Compliance matrix of requirements generated for the communication system, the swarm, and the structural subsystems.

ID	Requirements	Compliance	Proof
REQ-SCC-STB-1	The swarm configuration shall be able to be stabilised with the control system under all specified conditions.	✓	Chapter 9
REQ-SCC-MAN-1	The swarm configuration shall be able to travel at 1.5 m s^{-1} vertically.	✓	N/A ⁸⁸
REQ-SCC-PER-1	The swarm configuration shall be capable of hovering for 15 min.	✓	Section 12.2
REQ-STR-INT-1	Vibrations induced by the drones on the payload attachment structure shall not match its natural frequency.	✗	

Table 12.13: Compliance matrix of requirements generated for communication.

ID	Requirements	Compliance	Proof
REQ-COM-S&R-1	Any digital wireless communication link of DroneCrane shall be encrypted.	✓	Chapter 9

From the compliance matrix, it can be seen that quite a few requirements weren't met. These will be further explained below.

- **REQ-REG-ENV-1:** The regulations were not looked into during the design, as the goal of the project was already to create a recyclable product, that operates on green energy. Therefore, the team expects to easily comply with this requirement. However, research has not been done further into this matter and thus the requirement cannot be confirmed as met.
- **REQ-REG-AIR-1:** Similarly to the previous requirement, research into this has not been performed yet, mostly due to the fact that getting a design certified by law takes a long amount of time. However, in order to make sure it complies with regulations, further research will have to be performed.
- **REQ-OPR-WEA-2:** This requirement was originally meant for the system to be able to operate in rainy conditions. However, this has since changed and now the swarm can only operate if the weather is within acceptable norms. Thus, the necessary water resistance level has become much lower, and the electronics will mostly be made resistant for humidity and small droplets.

⁸⁸This was the basis for the design, therefore it is implicitly

- **REQ-STR-INT-1**: This requirement is one that actually poses an important obstacle to the design. However, due to time constraints, no vibrational analysis ended up being performed and would be a good recommendation for the future.

Finally, the last set of requirements ties to the operations of the system. Their compliance and proof are shown below.

Table 12.14: *Compliance matrix of transportation requirements*

ID	Requirement	Compliance	Proof
REQ-OPR-TSP-01	The length of any element shall be under 4 m.	✗	
REQ-OPR-TSP-02	The width of any element shall be under 2 m.	Inapplicable	
REQ-OPR-TSP-03	The weight of each LFRS segment shall be under 25 kg.	✓	Section 12.1
REQ-OPR-TSP-04	The frame of the drone shall be retractable.	✗	
REQ-OPR-TSP-05	The landing gear of the drone shall be retractable.	Inapplicable	

Table 12.15: *Compliance matrix of set-up requirements*

ID	Requirement	Compliance	Proof
REQ-OPR-SET-01	The time needed to take out all the drones and connect them shall be lower than 30 min.	✓	Section 12.3
REQ-OPR-SET-02	The time needed to assemble the LFRS shall be under 10 min.	✓	Section 12.3
REQ-OPR-SET-03	The boot time of each drone shall be under 30 s.	✓	Section 12.3
REQ-OPR-SET-04	The boot and set-up time of all controllers shall be under 5 min.	✓	Section 12.3
REQ-OPR-SET-05	The swarm formation shall be completed and position-initialised in under 3 min.	✓	Chapter 9
REQ-OPR-SET-06	The drones shall have labels.	✓	Chapter 9
REQ-OPR-SET-07	The rope connecting device shall be a quick connection.	✗	
REQ-OPR-SET-08	The interference of the propellers with the ground shall be negligible for 4 m below the drones.	✗	

Table 12.16: *Compliance matrix of usage requirements*

ID	Requirement	Compliance	Proof
REQ-OPR-USG-01	DroneCrane shall have a continuous rate of operability of at least 2 hours/day.	✓	Section 12.3
REQ-OPR-USG-02	The range of transmission device in the drone shall be greater than 500 m.	✓	Chapter 9
REQ-OPR-USG-03	The range of transmission device in the controller shall be greater than 500 m.	✓	Chapter 9

Table 12.17: Compliance matrix of end of mission requirements

ID	Requirement	Compliance	Proof
REQ-OPR-END-01	The condition of the drone shall be checkable.	✓	Section 12.5

Table 12.18: Compliance matrix of maintenance requirements

ID	Requirement	Compliance	Proof
REQ-OPR-MTC-01	The battery pack change of each drone shall take less than 1 min.	✓	Section 12.3
REQ-OPR-MTC-02	The charging time for the battery shall be less than 1 h.	✗	

As can be seen, not all operational requirements ended up being met. The ones specified as inapplicable are requirements which were defined at the start of the design, under certain assumptions, but ended up being scrapped due to a different design choice.

As for the requirements deemed unfulfilled, the description of the circumstances are listed below:

- **REQ-OPR-TSP-01**: Due to the design process, it was found that the LFRS needs to be 12.3 m in diameter, meaning that the longest elements will be about half of this. Thus, this requirement is not met. However, this is not catastrophic, as the requirement was mostly meant for ease of operations. Therefore, the system will still function correctly, but it will be harder to set up.
- **REQ-OPR-TSP-04**: Originally, the drone structure was planned to be retractable, to simplify storage and transportation. However, due to the material used, this was later scrapped and deemed unfeasible. This could, however, be analysed in more detail in the future.
- **REQ-OPR-SET-07**: The connection system was not considered during the design, mostly as it is not too complex to design later down the line and also due to the time constrain pushing the team to work on other details. Thus, this is a concept that will have to be created and developed in the future.
- **REQ-OPR-SET-08**: The interference of the system with the ground was not analysed within the scope of the project. On top of that, considering the sheer size of the system it can be assumed that it will, in fact, interfere with the ground at least to some extent. This will have to be further analysed in the future.
- **REQ-OPR-MTC-02**: At the start of the design, the aim was to make the system as fast as possible in terms of setup. Thus, a limited amount of time was given to the charging of the batteries. This time was chosen before any estimations on the number of batteries were performed, and thus after finishing the sizing of the electrics, it was found that the amount of power necessary for the functioning of the system is very high and so is the amount of batteries. Therefore, charging all 9300 batteries within an hour ended up being unrealistic.

12.8. Production Plan

This section was written by: *Robin*

Firstly, the structures are the most intensive part with respect to manufacturing for DroneCrane itself. As the frame is custom designed, it needs to be manufactured by the appropriate parties. As the DroneCrane company is not a manufacturing company, this would have to be done by a third party manufacturer.

The selected material, both for the drone structures and the LFRS, is a carbon fibre reinforced thermoplastic CFRTP. Specifically one that uses a PES (polysulfane) matrix that contains carbon fibres to create a very high performance and light weight material [30]. This material has an ultimate tensile

strength of 1400 MPa, a young's modulus of 137 GPa and an approximate density of 1800 kg/m³. This material was chosen for two primary reasons. The first relates to the use of carbon fibre due to the extremely good properties for creating low weight high performance components. The second reason is the recyclability of composites containing thermoplastics. One of the largest challenges in recycling carbon fibre reinforced materials is the recovery of the separate materials. For composites containing thermoset resins, use is often made of pyrolysis [74]. In this method, the CFRP is heated to temperatures of up to 700 °C in an inert atmosphere. This causes the thermoset material to escape from the matrix, thus making it possible to recover the carbon fibres. It is however, still quite wasteful in use of energy, as well as waste of the thermoset material. When using a thermoplastic matrix, the recovery of material is significantly easier, as the matrix material can be melted down, enabling the recovery of both the fibres and the matrix material.

Carbon fibre reinforced thermoplastics are not easy to manufacture. However, a few promising processes have started to emerge in recent years. One novel method to produce CFRTP components is to 3D print them. It is already possible to use continuous fibres in specialised printing methods, thus giving a large freedom in manufacturing while minimising the waste generated in a process [75]. Other methods include for example hot press moulding, where the material is put in a heated mould, pressed down and left to cool down. A combination of 3D printing and then applying a hot press treatment can result in the high properties mentioned before [76]. Primarily due to the minimal waste, the 3D printing fibre fabrication method was chosen in order to manufacture the drone structures. The complex shape of the drones can quite easily be manufactured with this method, which could then be reinforced by applying hot press treatment after the design has been finished printing. The disadvantage of this method lies in its complexity and manufacturing speed however. A printing process is not fast and it could take hours to complete a single drone. Furthermore, specialised software has to be used to not only optimise the orientation of the fibres with respect to the loading, but also with respect to the printability. These disadvantages are however not large enough to overcome the advantages of waste minimisation and optimisation of the fibre orientations.

While the same material is used for the LFRS, the manufacturing methods are preferably different. It is a relatively large structure in comparison to the drones and has different shaping. The large structure will have to be assembled from many smaller parts to make sure that it is transportable. These smaller components are designed to be modular, thus enabling processes with larger batches. Preferably, the thermoforming process should be used for the manufacturing of the components of the LFRS [77]. The components consist out of cylindrical components. These components could be made with the thermoforming process, where two small plates with constant thickness may be formed around a rod while being heated to make the material ductile. Due to the nature of thermoplastics, the unattached ends can practically be welded together with sufficient heat, creating a process with little waste and good properties. These rods can then be assembled into the smaller sections out of which the LFRS consists with strong adhesives.

After the structures have been assembled, the electronics can be added onto the frame. All of the selected electronics are components that can be bought off the shelf, so no manufacturing is required on the side of the DroneCrane company. In assembly, the electronics are bolted on with light weight bolts to make sure that the components are easily removable and replaceable.

Finally, the propulsion systems can be assembled onto the frame of the drones. The electric motors and the propellers are bought as off-the-shelf components and thus do not require manufacturing on the side of the DroneCrane company. In assembly, the electronic motors are again attached to the frame by bolts to make sure they are easy to replace and remove for repairs.

IV

Outlook of the Future

13. Future Endeavours

With the current phase of the design ending, the working team looks ahead to the work needed to bring DroneCrane to market. The detail design presented in previous chapters would certainly benefit from a deeper level of engineering optimisation targeted at reducing its energy consumption, operational efficiency, and controllability. To bring DroneCrane to market the team has to also account for manufacturing procedures, testing, certification, and delivery to the potential customers. Proposing a plan that outlines the steps that need to be taken and the respective workload projections can guarantee to DroneCrane a future and solid way forward. Additionally, in collaboration with the intended users, the customer requirements may be revisited and the design adapted accordingly. This chapter presents the outlook on the future of DroneCrane by illustrating the Project Design and Development Logic in Section 13.1, followed by the Gantt chart for its application Section 13.2.

13.1. Project Design & Development Logic

This section was written by: *Giovanni*

Looking ahead to the future development steps that DroneCrane should undertake, the working group recognise the importance of learning from the experience accumulated in the recent weeks to address the specific needs of DroneCrane and manage the challenges that arise from a drone-swarm design from which some valuable and applicable insight has already been gained. The reader can find a graphical representation of the D&D Logic in Figure 13.1.

With the current state of the design, it is advisable to continue on with design optimisation work so to target the weak points of the design outlined in Chapter 12. This is naturally expected to be an iterative process, and with more time being dedicated to the development process it could be possible to both find off-the-shelf components that outperform the current selection, or develop some parts internally. For instance, the motor-propeller assembly could gain some points in efficiency if time allows for numerical simulations to be conducted on the design. The blocks concerned with design in the leftmost column of Figure 13.1 include the extra efforts and computational time that could improve the design. For sure, the additional time that comes with a longer design process is not intended as a wait for research centres and industry to advance technology.

Once the design has reached a complete level of definition, the team should consider both validating DroneCrane while formally ensuring it can have a future: the search for investors or direct customers should begin. The validation process at this stage shall be limited to subsystem by subsystem, possibly with the development of ad hoc testing frameworks depending on departmental needs, as specified in Figure 13.1 in the blocks with a grey-to-black background. If validation fails, the design must be revisited; otherwise, manufacturing of the whole system may begin, followed by its validation and stress-testing, concluding the "circle" initiated with the customer search. This brings DroneCrane to market. Specific timelines and expected workloads for future developments are presented in Section 13.2.

13.2. Gantt Chart

This section was written by: *Giovanni*

Going through the work packages outlined in Section 13.1 requires time which is allocated with the Gantt chart in Figure 13.2, where past experience has been taken into account to give what is an appreciable amount of work hours to design optimisation (which includes verification). The subsystem validation steps are not expected to take up as much time as the whole system validation because the single drone system is not a complex system per se in the aerospace field, but when it comes together as a swarm the most challenges may arise.

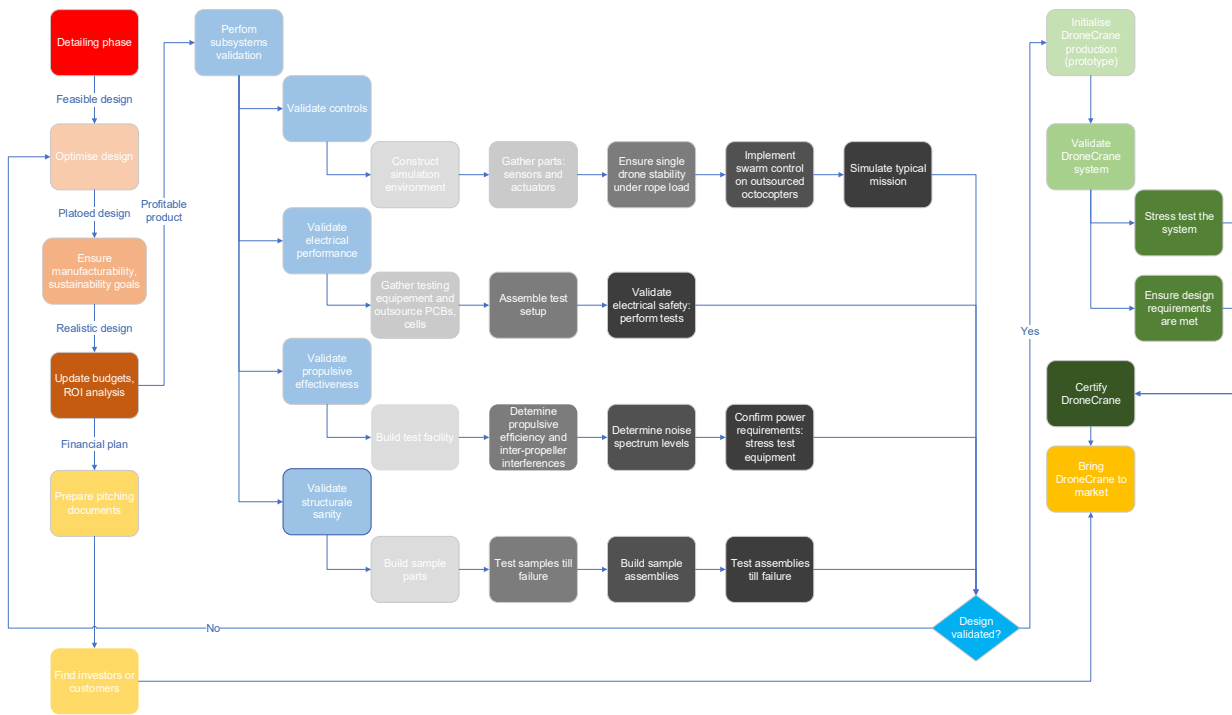


Figure 13.1: Design & Development Logic workflow for DroneCrane's future development, colour coded so to highlight the grouping of the work packages that touch upon closely related tasks (own work).

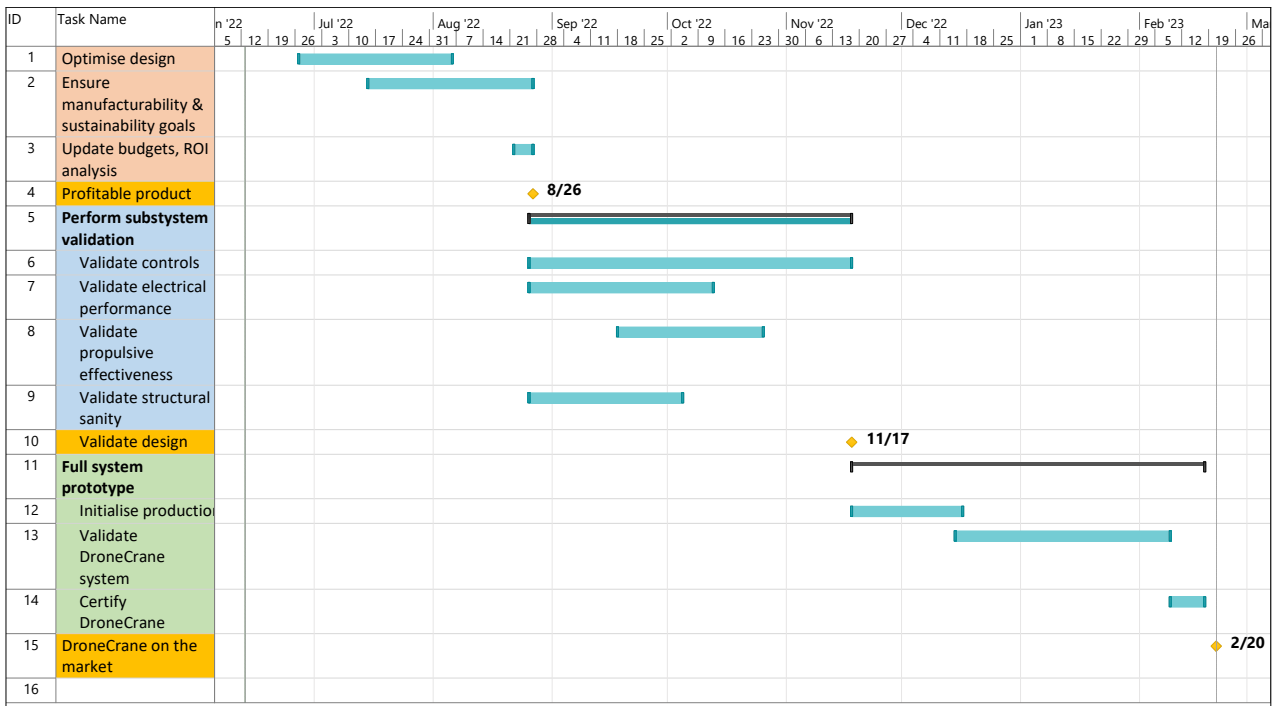


Figure 13.2: Gantt chart for the future of DroneCrane (own work).

13.3. Recommendations

This section was written by: *Robin*

In this section, recommendations for the future are given. Inclusions might cover points of improvement, tasks that would have been too time intensive to perform in the time span of this DSE or even ideas that might become more valuable in the future. Each department has searched for methods to improve the current design specifications, those that cannot be included in the current stage of design anymore have been included in this section.

13.3.1. Propulsion Recommendations

While the propulsion units are planned to be bought for the design of DroneCrane, it would pose an interesting endeavour to optimise an in-house designed propeller. The aim of this would be to increase the performance for DroneCrane specifically. Cost may be reduced, but could also be increased depending on the complexity and scale of manufacturing. Furthermore, it would also be possible to examine the possibility to create custom electric motors for DroneCrane. Paired with the propellers, significant performance could be gained in designing motors specifically for DroneCrane. The cost of development would again have to be weighed against the benefits of a possibly improved performance. Lastly, an in depth analysis covering the aerodynamics of the drones as individuals, and the drone swarm as a whole could be done. The aim would not only be to gain insight into the aerodynamic properties of DroneCrane, but it would also make it possible to create a noise analysis.

13.3.2. Electronics Recommendations

The electronics in DroneCrane are plentiful, and many intricate components have to interface. One of the improvements that could be made if more time was available, is an integrated circuit board that could combine some of the functionalities now required to be performed by multiple components. Another recommendation is to test the proposed configuration of battery pack by building a small prototype. The discharging and charging properties can be analysed and compared to the expected properties, and thermal effects can be examined. This could lead to a validation that is currently lacking without any experimental evidence. Lastly, the success of DroneCrane is quite reliant on the performance of the batteries. The energy density is especially important, as the batteries are currently over 80% of the mass of DroneCrane as can be seen in table Table 12.3. As technology improves in this area, the DroneCrane can potentially become smaller, lighter and more energy efficient. Due to the incredibly large portion of battery mass in the total system mass. For example, an improvement of only one percent with respect to the energy density could improve the direct weight of over 80% of the swarm. The snowball effect then causes the remainder of the swarm to become lighter and smaller as well, as a more indirect consequence. Thus small improvements in only this area can already have a large impact on DroneCrane. Thus it is important to check the trends in energy storage throughout all of the remainder of the design and especially for possible future designs.

13.3.3. Controls Recommendations

The calculations in the controls of a swarm of drones is quite complicated. As the drones in the current design have both an individual flight controller and swarm controller, an inquiry could be made about combining these two boards in order to optimise the interface between them. This could improve the computational performance of the swarm and reduce energy consumption. In a last minute controls simulation, the results showed a very small margin until the saturation of the design of the motors, which causes a need for a further analysis of the amount of power required for proper controls in all flight conditions. This may require redoing some calculations in propulsion, as well. This would ensure that DroneCrane can perform properly in all required conditions.

13.3.4. Structures Recommendations

The structural design of DroneCrane currently uses CFRTP, a composite with directionally dependant performance. Due to the time limits, no optimisation has been made with respect to this complex part of composite design. It is very beneficial for the future of the design to further analyse the structure from the point of view of this directional performance. The inquiries into novel materials with high performance have provoked further interest. Due to the novelty of the materials and their manufac-

turing methods, it could prove interesting to create an investigation into the performance of CFRTP's. The properties in this report may have been an underestimate of the possibilities, compared to other carbon fibre reinforced materials. So further research is required in order to validate this data. Furthermore, it is recommended to perform some experimental data on these novel materials to find out more about the behaviour, both uni-directionally as well as manufactured in different layouts such as a quasi-isotropic one. A last important consideration is the transportability of the LFRS. Though conceptually the structure should be disassemblable, in its current state there is still little research done on this. It is required to make this work in order to be able to properly transport the LFRS, but not enough time was available to design this element. The connection points between the LFRS, cables and drones still have to be designed in detail, especially with respect to a release mechanism that can enable drones to disconnect from the swarm at command. A significant amount of work is still necessary in order to create a well functioning design with respect to these connections, so it has not been performed in the past ten weeks. One more consideration, is the influence of vibrations of the structure of DroneCrane. These could potentially destroy the structure, and should therefore be analysed. It is estimated that this will take a serious amount of time to do properly, so it has not yet been performed in this project. Lastly, the same is true for the design of the legs of the drones. While the design does not have to be intensively analysed due to the simplistic purpose, there can still be some influences on the swarm, causing another analysis to be required before the swarm could be manufactured.

13.3.5. Operations Recommendations

The operations of DroneCrane could still be improved upon. Some research into optimising the procedures could be done to reduce the amount of time that will have to be spent on setup time. Especially the complexity of the operations may be reduced. Furthermore, more safety procedures should be analysed. Currently, the payload will have to be attached after the swarm becomes airborne, but this would preferably be done differently due to safety reasons. On top of this, the addition of better visualisation in flight would be preferable. One of the ways to do this could be to use First-Person-View, or FPV technology. Time did not allow for this, but the inclusion does not need to be expensive, while making operations safer and easier. This is also related to the controllability. If the visualisation of the current position of the swarm is improved, it is also easier to control. Lastly, the controls could be made more sophisticated than the setup used in the current design, which is simplistic in the current design due to time constraints.

14. Conclusion

This chapter was written by: *Maxim*

The design process for DroneCrane was a long and arduous journey. From the early preliminary design, in which the outline of what DroneCrane would become was drawn, through the trade-off of the midterm phase, where all possible solutions to the design problem were analysed, evaluated and finally decided upon, to the detailed design of each subsystem, the team devoted itself to the creation of the best system it could come up with.

The design was concluded with this report, laying out the steps taken during the detailed phase, from a summary of the preliminary and midterm phases, through an explanation of the iterative design approach, onto a detailed description and analysis of the subsystems. The last chapter of the report outlines the future challenges to be undertaken. While the design is, in theory, completed, many steps still need to be performed before the system can take its maiden flight.

Overall, the group is satisfied with what it has managed to achieve during the ten weeks of designing. The team is confident that the proposed design is feasible and can be implemented as a real product. If the opportunity presents itself, the team will attempt to further improve upon the design, according to the recommendations. Eventually, the hope is to manufacture a prototype and present it as a validation of the entire design exercise.

Bibliography

- [1] F. B. Insights. "Cranes market size, share & trends [2028] | covid-19 impact." (Jan. 2022). (accessed Apr. 26, 2022).
- [2] K. Nonami and Autonomous Control Systems Laboratory Ltd. WBG Marive West 32F, 2-6-1 Nakase, Mihama-ku, Chiba-city, Chiba 261-7132, Japan, "Research and development of drone and roadmap to evolution," *Journal of Robotics and Mechatronics*, vol. 30, no. 3, pp. 322–336, Jun. 20, 2018, ISSN: 1883-8049, 0915-3942. DOI: [10.20965/jrm.2018.p0322](https://doi.org/10.20965/jrm.2018.p0322). (visited on 05/16/2022).
- [3] S. Shetty, S. S, and D. M.A., *IRJET-V5I961*. Jun. 3, 2018.
- [4] U. R. Mogili and B. B. V. L. Deepak, "Review on application of drone systems in precision agriculture," *Procedia Computer Science*, International Conference on Robotics and Smart Manufacturing (RoSMA2018), vol. 133, pp. 502–509, Jan. 1, 2018, ISSN: 1877-0509. DOI: [10.1016/j.procs.2018.07.063](https://doi.org/10.1016/j.procs.2018.07.063). (visited on 05/16/2022).
- [5] J. Liu, Z. Guan, J. Shang, and X. Xie, "Application of drone in solving last mile parcel delivery," *Journal of Systems Science and Information*, vol. 6, no. 4, pp. 302–319, Aug. 1, 2018, Publisher: De Gruyter, ISSN: 2512-6660. DOI: [10.21078/JSSI-2018-302-18](https://doi.org/10.21078/JSSI-2018-302-18). (visited on 05/16/2022).
- [6] Z. Xiaoning, "Analysis of military application of UAV swarm technology," in *2020 3rd International Conference on Unmanned Systems (ICUS)*, 2020, pp. 1200–1204. DOI: [10.1109/ICUS50048.2020.9274974](https://doi.org/10.1109/ICUS50048.2020.9274974).
- [7] J. O. Choi and D. Kim, *A New UAV-based Module Lifting and Transporting Method: Advantages and Challenges*. May 24, 2019. DOI: [10.22260/ISARC2019/0086](https://doi.org/10.22260/ISARC2019/0086).
- [8] M. Abdelkader, S. GÃ¼ler, H. Jaleel, and J. S. Shamma, "Aerial swarms: Recent applications and challenges," *Current Robotics Reports*, vol. 2, no. 3, pp. 309–320, Sep. 1, 2021, ISSN: 2662-4087. DOI: [10.1007/s43154-021-00063-4](https://doi.org/10.1007/s43154-021-00063-4). (visited on 05/11/2022).
- [9] Group 19: DroneCrane, *Dronecrane midterm report (unpublished)*, May 2022.
- [10] B. J. Olivieri de Souza and M. Endler, "Coordinating movement within swarms of UAVs through mobile networks," in *2015 IEEE International Conference on Pervasive Computing and Communication Workshops (PerCom Workshops)*, St. Louis, MO: IEEE, Mar. 2015, pp. 154–159, ISBN: 978-1-4799-8425-1. DOI: [10.1109/PERCOMW.2015.7134011](https://doi.org/10.1109/PERCOMW.2015.7134011). (visited on 05/10/2022).
- [11] Group 19: DroneCrane, *Dronecrane baseline report (unpublished)*, May 2022.
- [12] Smeur, E., *Project Guide Design Synthesis Exercise (unpublished)*, Apr. 2022.
- [13] Group 19: DroneCrane, *Dronecrane project plan report (unpublished)*, Apr. 2022.
- [14] TU Delft, *Risk Management and Concurrent Engineering*, Feb. 2022.
- [15] F. B. Insights. "Air crane helicopter market size, share & trends | forecat [2027]." (Sep. 2020).
- [16] *Can Drones Fly In Strong Winds? (Drone Table Comparison)*, en-us, Running Time: 168 Section: Tutorial, Feb. 2022. (visited on 05/03/2022).
- [17] K. D. Goepel, "Implementation of an online software tool for the analytic hierarchy process (AHP-OS)," *International Journal of the Analytic Hierarchy Process*, vol. 10, no. 3, Dec. 6, 2018, ISSN: 1936-6744. DOI: [10.13033/ijahp.v10i3.590](https://doi.org/10.13033/ijahp.v10i3.590). (visited on 05/10/2022).
- [18] "A general discussion of li ion battery safety," *Electrochemical Society Interface*, Jan. 2012. DOI: [10.1149/2.f03122if](https://doi.org/10.1149/2.f03122if).
- [19] O. US EPA. "Used lithium-ion batteries." (May 16, 2019), (visited on 06/15/2022).
- [20] P. Intelligence. "Lithium-ion battery market set to grow at 15.3% CAGR through 2030, says p&s intelligence." (), (visited on 06/15/2022).

- [21] G. Harper *et al.*, “Recycling lithium-ion batteries from electric vehicles,” *Nature*, vol. 575, no. 7781, pp. 75–86, Nov. 2019, Number: 7781 Publisher: Nature Publishing Group, ISSN: 1476-4687. DOI: [10.1038/s41586-019-1682-5](https://doi.org/10.1038/s41586-019-1682-5). (visited on 06/15/2022).
- [22] J. Wilkerson. “Recycled lithium-ion batteries can perform better than new ones,” *Scientific American*. (), (visited on 06/15/2022).
- [23] L. Ahmadi, S. B. Young, M. Fowler, R. A. Fraser, and M. A. Achachlouei, “A cascaded life cycle: Reuse of electric vehicle lithium-ion battery packs in energy storage systems,” *The International Journal of Life Cycle Assessment*, vol. 22, no. 1, pp. 111–124, Jan. 1, 2017, ISSN: 1614-7502. DOI: [10.1007/s11367-015-0959-7](https://doi.org/10.1007/s11367-015-0959-7). (visited on 06/15/2022).
- [24] M. Pagliaro and F. Meneguzzo, “Lithium battery reusing and recycling: A circular economy insight,” *Heliyon*, vol. 5, no. 6, e01866, Jun. 1, 2019, ISSN: 2405-8440. DOI: [10.1016/j.heliyon.2019.e01866](https://doi.org/10.1016/j.heliyon.2019.e01866). (visited on 06/15/2022).
- [25] X. Ma *et al.*, “Recycled cathode materials enabled superior performance for lithium-ion batteries,” *Joule*, vol. 5, no. 11, pp. 2955–2970, Nov. 17, 2021, ISSN: 2542-4351. DOI: [10.1016/j.joule.2021.09.005](https://doi.org/10.1016/j.joule.2021.09.005). (visited on 06/15/2022).
- [26] N. J. coderman. “What are drones made of? - materials and engineering resources - matmatch,” *Materials and Engineering Resources - Matmatch - Get the latest in materials science and engineering news, educational content and material use cases*. (Oct. 23, 2019), (visited on 05/12/2022).
- [27] T. Hall. “What are consumer drones made of?” *Let Us Drone*. (Sep. 15, 2019), (visited on 05/12/2022).
- [28] “Aluminum alloys for aerospace,” *Aerospace Manufacturing and Design*. (), (visited on 05/16/2022).
- [29] I. Inagaki, Y. Shirai, T. Takechi, and N. Ariyasu, “Application and features of titanium for the aerospace industry,” no. 106, p. 6, 2014.
- [30] S.-S. Yao, F.-L. Jin, K. Y. Rhee, D. Hui, and S.-J. Park, “Recent advances in carbon-fiber-reinforced thermoplastic composites: A review,” *Composites Part B: Engineering*, vol. 142, pp. 241–250, 2018, ISSN: 1359-8368. DOI: <https://doi.org/10.1016/j.compositesb.2017.12.007>.
- [31] C. Dahal, H. B. Dura, and L. Poudel, “Design and analysis of propeller for high-altitude search and rescue unmanned aerial vehicle,” *International Journal of Aerospace Engineering*, vol. 2021, e6629489, Jan. 23, 2021, Publisher: Hindawi, ISSN: 1687-5966. DOI: [10.1155/2021/6629489](https://doi.org/10.1155/2021/6629489). (visited on 05/23/2022).
- [32] I. Penkov and D. Aleksandrov, “Analysis and study of the influence of the geometrical parameters of mini unmanned quad-rotor helicopters to optimise energy saving,” vol. 14, pp. 4730–4746, Dec. 2017. DOI: [10.15282/ijame.14.4.2017.11.0372](https://doi.org/10.15282/ijame.14.4.2017.11.0372).
- [33] H. Zhu, H. Nie, L. Zhang, X. Wei, and M. Zhang, “Design and assessment of octocopter drones with improved aerodynamic efficiency and performance,” *Aerospace Science and Technology*, vol. 106, p. 106206, Nov. 2020, ISSN: 12709638. DOI: [10.1016/j.ast.2020.106206](https://doi.org/10.1016/j.ast.2020.106206). (visited on 06/14/2022).
- [34] MIT Lab, *DC Motor / Propeller Matching*, Mar. 2005.
- [35] K. S. V. Sekar, “Mechanics of materials,” in *9th AIAA/SAE/ASME Mechanics of materials*, ser. ISBN 978-981-06-9436-4. Pearson Education South Asia Pte Ltd, Jan. 2014. DOI: [10.2514/6.2017-4955](https://doi.org/10.2514/6.2017-4955).
- [36] B. Schäffer, R. Pieren, K. Heutschi, J. M. Wunderli, and S. Becker, “Drone noise emission characteristics and noise effects on humans—a systematic review,” *International Journal of Environmental Research and Public Health*, vol. 18, no. 11, p. 5940, Jun. 1, 2021, ISSN: 1660-4601. DOI: [10.3390/ijerph18115940](https://doi.org/10.3390/ijerph18115940). (visited on 06/16/2022).

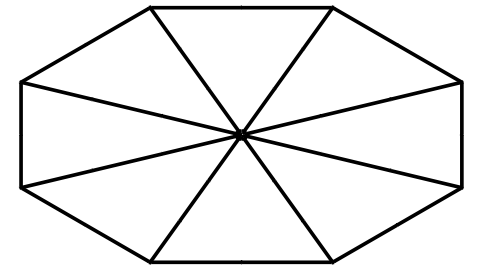
- [37] L. Ding and Y. Li, "Optimal attitude tracking control for an unmanned aerial quadrotor under lumped disturbances," *International Journal of Micro Air Vehicles*, vol. 12, p. 175 682 932 092 356, Jan. 1, 2020. DOI: [10.1177/1756829320923563](https://doi.org/10.1177/1756829320923563).
- [38] I. Toerist, "Handbook of reliability prediction procedures for mechanical equipment NSWC 11," (visited on 06/14/2022).
- [39] D. Shi, B. Yang, and Q. Quan, "Reliability analysis of multicopter configurations based on controllability theory," en, in *2016 35th Chinese Control Conference (CCC)*, Chengdu: IEEE, Jul. 2016, pp. 6740–6745, ISBN: 978-988-15639-1-0. DOI: [10.1109/ChiCC.2016.7554418](https://doi.org/10.1109/ChiCC.2016.7554418).
- [40] L. Meier, P. Tanskanen, F. Fraundorfer, and M. Pollefeys, "PIXHAWK: A system for autonomous flight using onboard computer vision," en, in *2011 IEEE International Conference on Robotics and Automation*, Shanghai, China: IEEE, May 2011, pp. 2992–2997, ISBN: 978-1-61284-386-5. DOI: [10.1109/ICRA.2011.5980229](https://doi.org/10.1109/ICRA.2011.5980229). (visited on 06/14/2022).
- [41] T. Paul and T. Ogunfunmi, "Wireless lan comes of age: Understanding the ieee 802.11 n amendment," *IEEE Circuits and systems magazine*, vol. 8, no. 1, pp. 28–54, 2008.
- [42] A. Guillen-Perez, R. Sanchez-Iborra, J. Sanchez-Aarnoutse, M.-D. Cano, and J. Garcia-Haro, "Wifi networks on drones," Nov. 2016, pp. 183–190. DOI: [10.1109/ITU-WT.2016.7805730](https://doi.org/10.1109/ITU-WT.2016.7805730).
- [43] Q. Quan, *Introduction to Multicopter Design and Control*, en. Singapore: Springer Singapore, 2017, ISBN: 978-981-10-3382-7. DOI: [10.1007/978-981-10-3382-7](https://doi.org/10.1007/978-981-10-3382-7). (visited on 06/01/2022).
- [44] O. Oscarson, *Design, Modeling and Control of an Octocopter*, eng. 2015. (visited on 05/30/2022).
- [45] R. Niemiec and F. Gandhi, "Multirotor Controls, Trim, and Autonomous Flight Dynamics of Plus- and Cross-Quadcopters," *Journal of Aircraft*, vol. 54, pp. 1–11, May 2017. DOI: [10.2514/1.C034165](https://doi.org/10.2514/1.C034165).
- [46] R. Niemiec, F. Gandhi, and R. Singh, "Control and Performance of a Reconfigurable Multicopter," *Journal of Aircraft*, vol. 55, no. 5, pp. 1855–1866, Sep. 2018, Publisher: American Institute of Aeronautics and Astronautics. DOI: [10.2514/1.C034731](https://doi.org/10.2514/1.C034731). (visited on 05/31/2022).
- [47] P. Wang, Z. Man, Z. Cao, J. Zheng, and Y. Zhao, "Dynamics modelling and linear control of quadcopter," in *2016 International Conference on Advanced Mechatronic Systems (ICAMechS)*, ISSN: 2325-0690, Nov. 2016, pp. 498–503. DOI: [10.1109/ICAMechS.2016.7813499](https://doi.org/10.1109/ICAMechS.2016.7813499).
- [48] T. Luukkonen, "Modelling and control of quadcopter," en, p. 26,
- [49] T. Tengis and A. Batmunkh, "State feedback control simulation of quadcopter model," in *2016 11th International Forum on Strategic Technology (IFOST)*, Jun. 2016, pp. 553–557. DOI: [10.1109/IFOST.2016.7884178](https://doi.org/10.1109/IFOST.2016.7884178).
- [50] F. Kendoul, Z. Yu, and K. Nonami, "Guidance and nonlinear control system for autonomous flight of minirotorcraft unmanned aerial vehicles," en, *Journal of Field Robotics*, vol. 27, no. 3, pp. 311–334, 2010, _eprint: <https://onlinelibrary.wiley.com/doi/pdf/10.1002/rob.20327>, ISSN: 1556-4967. DOI: [10.1002/rob.20327](https://doi.org/10.1002/rob.20327). (visited on 06/10/2022).
- [51] J. Anderson, *Fundamentals of Aerodynamics*, en, 6th ed. McGraw Hill, Mar. 2016, ISBN: 978-1-259-12991-9. (visited on 06/19/2022).
- [52] M. W. Oppenheimer, D. B. Doman, and M. A. Bolender, "Control Allocation for Over-actuated Systems," in *2006 14th Mediterranean Conference on Control and Automation*, Jun. 2006, pp. 1–6. DOI: [10.1109/MED.2006.328750](https://doi.org/10.1109/MED.2006.328750).
- [53] C. D. Pose, J. I. Giribet, and A. S. Ghersin, "Hexacopter fault tolerant actuator allocation analysis for optimal thrust," in *2017 International Conference on Unmanned Aircraft Systems (ICUAS)*, Jun. 2017, pp. 663–671. DOI: [10.1109/ICUAS.2017.7991321](https://doi.org/10.1109/ICUAS.2017.7991321).
- [54] E. J. J. Smeur, D. C. Höppener, and C. de Wagter, "Prioritized Control Allocation for Quadrotors Subject to Saturation," en, *International Micro Air Vehicle Conference and Flight Competition 2017*, 2017. (visited on 06/10/2022).
- [55] *Control Theory: Multivariable and Nonlinear Methods*, en, Dec. 2010. (visited on 06/15/2022).

- [56] J. Moreno-Valenzuela, R. Pérez-Alcocer, M. Guerrero-Medina, and A. Dzul, "Nonlinear PID-Type Controller for Quadrotor Trajectory Tracking," *IEEE/ASME Transactions on Mechatronics*, vol. 23, no. 5, pp. 2436–2447, Oct. 2018, Conference Name: IEEE/ASME Transactions on Mechatronics, ISSN: 1941-014X. DOI: [10.1109/TMECH.2018.2855161](https://doi.org/10.1109/TMECH.2018.2855161).
- [57] E. J. J. Smeur, G. C. H. E. de Croon, and Q. P. Chu, "Cascaded incremental nonlinear dynamic inversion for MAV disturbance rejection," en, *Control Engineering Practice*, vol. 73, 2018, ISSN: 0967-0661. DOI: [10.1016/j.conengprac.2018.01.003](https://doi.org/10.1016/j.conengprac.2018.01.003). (visited on 06/14/2022).
- [58] K. Bergman and J. Ekström, *Modeling, Estimation and Attitude Control of an Octorotor Using PID and L1 Adaptive Control Techniques*, eng. 2014. (visited on 06/16/2022).
- [59] C. Chéron, A. Dennis, V. Semerjyan, and Y. Chen, "A multifunctional HIL testbed for multirotor VTOL UAV actuator," in *Proceedings of 2010 IEEE/ASME International Conference on Mechatronic and Embedded Systems and Applications*, Jul. 2010, pp. 44–48. DOI: [10.1109/MESA.2010.5552032](https://doi.org/10.1109/MESA.2010.5552032).
- [60] A. Marks, J. F. Whidborne, and I. Yamamoto, "Control allocation for fault tolerant control of a VTOL octorotor," in *Proceedings of 2012 UKACC International Conference on Control*, Sep. 2012, pp. 357–362. DOI: [10.1109/CONTROL.2012.6334656](https://doi.org/10.1109/CONTROL.2012.6334656).
- [61] A. Walter, M. McKay, R. j. Niemiec, and F. Gandhi, "Trim Analysis of a Classical Octocopter After Single-Rotor Failure," in *2018 AIAA/IEEE Electric Aircraft Technologies Symposium*, ser. AIAA Propulsion and Energy Forum, American Institute of Aeronautics and Astronautics, Jul. 2018. DOI: [10.2514/6.2018-5035](https://doi.org/10.2514/6.2018-5035). (visited on 06/20/2022).
- [62] H. Mammadov and C. Hajiyev, "Reconfigurable Fault Tolerant Flight Control for UAV with Pseudo-Inverse Technique," en, *IFAC-PapersOnLine*, 18th IFAC Conference on Technology, Culture and International Stability TECIS 2018, vol. 51, no. 30, pp. 83–88, Jan. 2018, ISSN: 2405-8963. DOI: [10.1016/j.ifacol.2018.11.253](https://doi.org/10.1016/j.ifacol.2018.11.253). (visited on 06/20/2022).
- [63] S. Kumar, S. Dalal, and V. Dixit, "THE OSI MODEL: OVERVIEW ON THE SEVEN LAYERS OF COMPUTER NETWORKS," vol. 2, no. 3, p. 7, 2014.
- [64] N. Khan, N. Zaman, S. Brohi, and A. Nayyar, "Emerging use of uav's: Secure communication protocol issues and challenges," in Jan. 2020, pp. 37–55, ISBN: 9780128199725. DOI: [10.1016/B978-0-12-819972-5.00003-3](https://doi.org/10.1016/B978-0-12-819972-5.00003-3).
- [65] X. Q. Longfei Dong Yangzhou Chen, "Formation control strategy for nonholonomic intelligent vehicles based on virtual structure and consensus approach," *Procedia Engineering*, vol. 137, pp. 415–424, Jan. 1, 2016, Publisher: No longer published by Elsevier, ISSN: 1877-7058. DOI: [10.1016/j.proeng.2016.01.276](https://doi.org/10.1016/j.proeng.2016.01.276). (visited on 06/16/2022).
- [66] N. H. M. Li and H. H. T. Liu, "Formation UAV flight control using virtual structure and motion synchronization," in *2008 American Control Conference*, ISSN: 2378-5861, Jun. 2008, pp. 1782–1787. DOI: [10.1109/ACC.2008.4586750](https://doi.org/10.1109/ACC.2008.4586750).
- [67] A. Fotouhi, M. Ding, and M. Hassan, "Understanding autonomous drone maneuverability for internet of things applications," in *2017 IEEE 18th International Symposium on A World of Wireless, Mobile and Multimedia Networks (WoWMoM)*, Macau, China: IEEE, Jun. 2017, pp. 1–6, ISBN: 978-1-5386-2723-5. DOI: [10.1109/WoWMoM.2017.7974336](https://doi.org/10.1109/WoWMoM.2017.7974336). (visited on 06/20/2022).
- [68] E. Nelson, "Estimating software reliability from test data," *Microelectronics Reliability*, vol. 17, no. 1, pp. 67–73, Jan. 1, 1978, ISSN: 0026-2714. DOI: [10.1016/0026-2714\(78\)91139-3](https://doi.org/10.1016/0026-2714(78)91139-3). (visited on 06/19/2022).
- [69] E. Lavrischeva, S. Zelenov, and N. Pakulin, "Methods for assessing the reliability of software and hardware systems," *Proceedings of the Institute for System Programming of the RAS*, vol. 31, no. 5, pp. 95–108, 2019, ISSN: 20798156, 22206426. DOI: [10.15514/ISPRAS-2019-31\(5\)-7](https://doi.org/10.15514/ISPRAS-2019-31(5)-7). (visited on 06/19/2022).
- [70] D. H. Doughty, "Battery safety and abuse tolerance," in *Handbook of Battery Materials*. John Wiley & Sons, Ltd, 2011, pp. 905–938, ISBN: 978-3-527-63718-8. DOI: <https://doi.org/10.1002/9783527637188.ch27>.

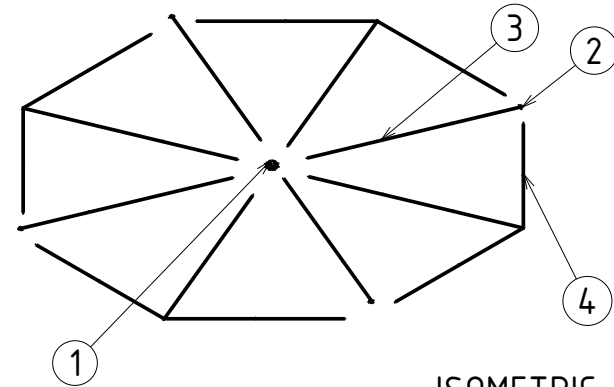
- [71] V. Challa, "Top causes of lithium ion field failures," en, p. 42,
- [72] A. Zikriyoev, "Human errors is continuous risky in construction industry: Is it because of negligence or lack of knowledge?" *Academia Open*, vol. 1, Aug. 2019. DOI: [10.21070/acopen.v1i1.7](https://doi.org/10.21070/acopen.v1i1.7).
- [73] E. Petritoli, F. Leccese, and L. Ciani, "Reliability and maintenance analysis of unmanned aerial vehicles," *Sensors (Basel, Switzerland)*, vol. 18, no. 9, p. 3171, Sep. 19, 2018, ISSN: 1424-8220. DOI: [10.3390/s18093171](https://doi.org/10.3390/s18093171). (visited on 05/25/2022).
- [74] S. Pimenta and S. T. Pinho, "Recycling carbon fibre reinforced polymers for structural applications: Technology review and market outlook," *Waste Management*, vol. 31, no. 2, pp. 378–392, 2011, Environmental Implications of Alternative Materials in Construction and Treatment of Waste, ISSN: 0956-053X. DOI: <https://doi.org/10.1016/j.wasman.2010.09.019>.
- [75] e. a. Frank Van Der Klift, "3d printing of continuous carbon fibre reinforced thermo-plastic (cfrtp) tensile test specimens," *Open journal of composite materials*, vol. 6, no. 1, pp. 18–27, 2016. DOI: [10.4236/ojcm.2016.61003](https://doi.org/10.4236/ojcm.2016.61003).
- [76] M. Yamawaki and Y. Kouno, "Fabrication and mechanical characterization of continuous carbon fiber-reinforced thermoplastic using a preform by three-dimensional printing and via hot-press molding," *Advanced Composite Materials*, vol. 27, no. 2, pp. 209–219, 2017. DOI: <https://doi.org/10.1080/09243046.2017.1368840>.
- [77] e. a. R McCool, "Thermoforming carbon fibre-reinforced thermoplastic composites," *Sage Journals*, vol. 226, no. 2, pp. 91–102, 2012. DOI: <https://doi.org/10.1177/1464420712437318>.

A. Technical Drawings

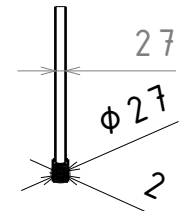
Item No.	Quantity	Title	Description	Material
1	1	DC19_Attachment_Core	Octagonal center of LFRS structure and connection point for camera's	CFRTP
2	8	DC19_Attachment_Connector	Connects the circular hollow beams together	CFRTP
3	8	DC19_Attachment_BeamInner	Circular beam that is connect to the octagonal centre of the LFRS structure.	CFRTP
4	8	DC19_Attachment_BeamCorner	Circular beam that connects the outer edges of the LFRS structure.	CFRTP



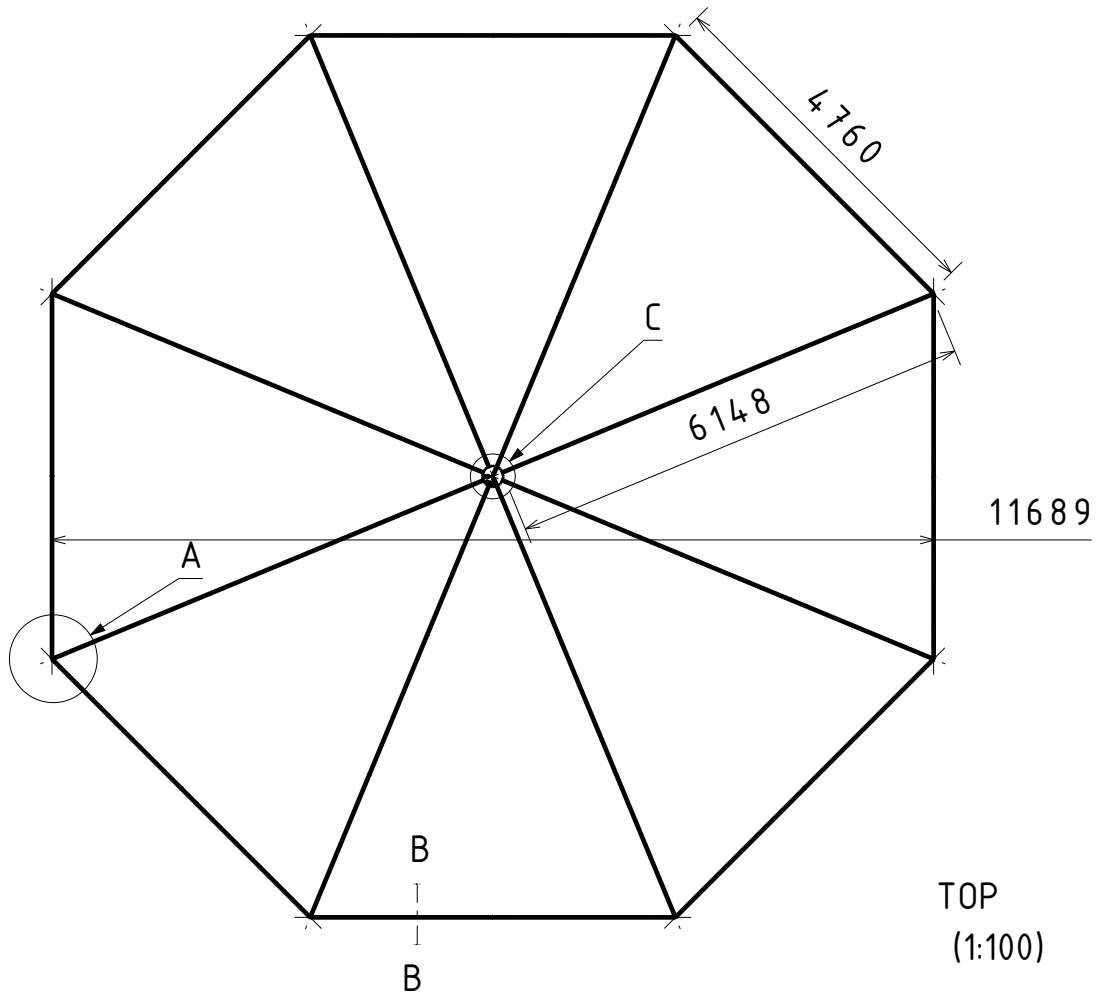
ISOMETRIC
(1:200)



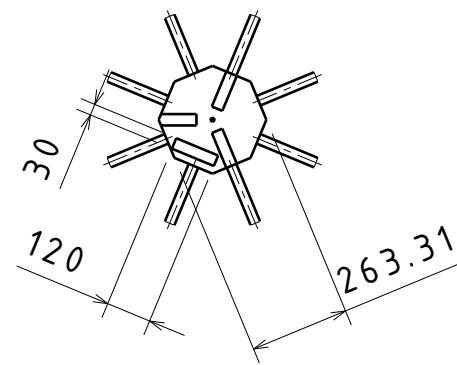
ISOMETRIC
(1:200)



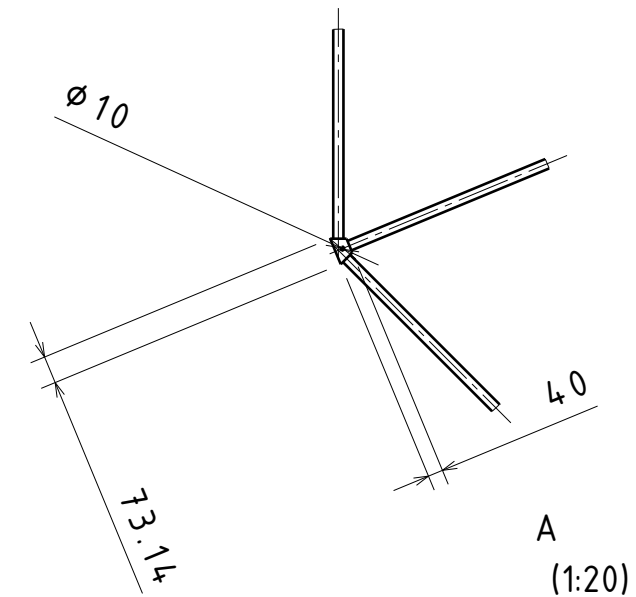
B-B
(1:20)



TOP
(1:100)



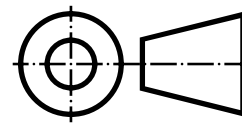
C
(1:20)



A
(1:20)



FRONT
(1:70)



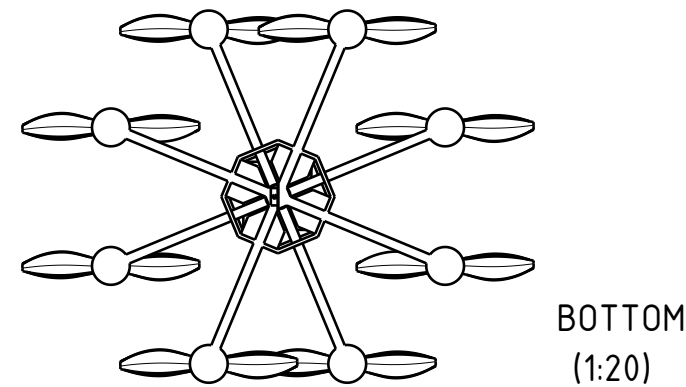
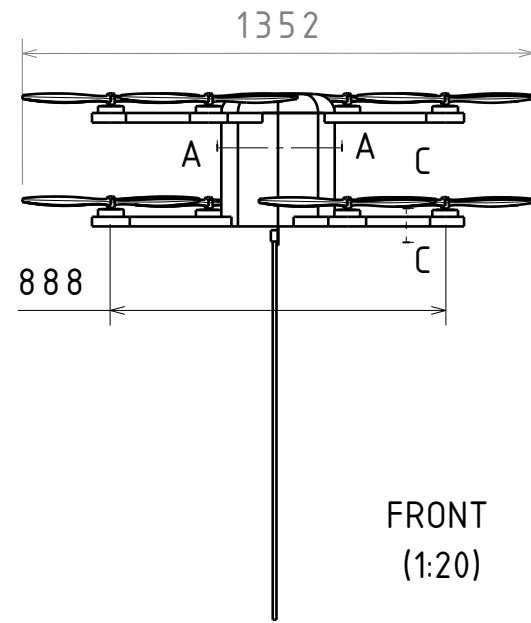
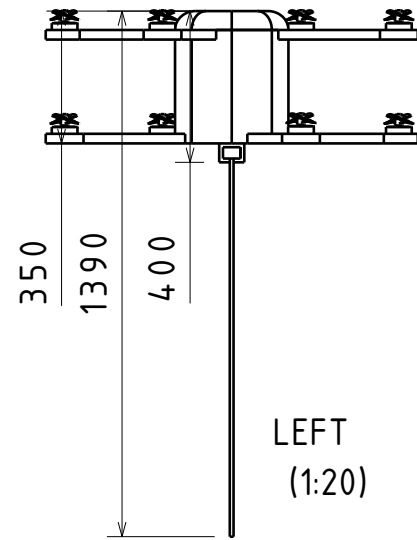
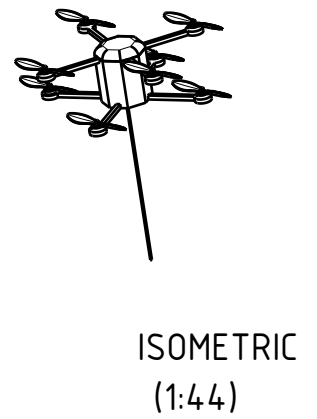
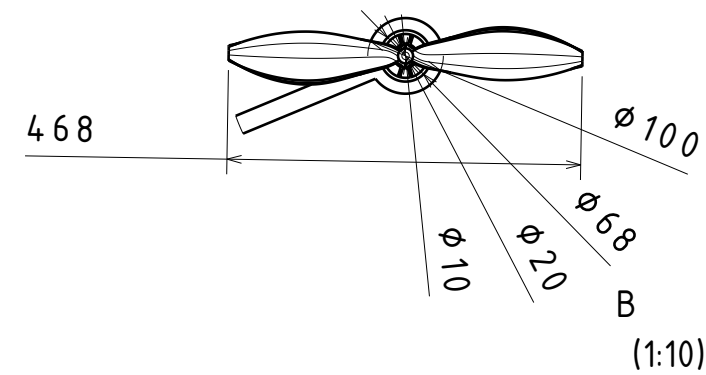
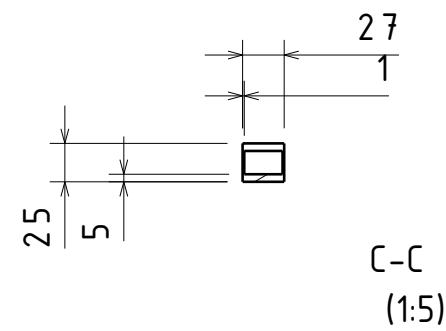
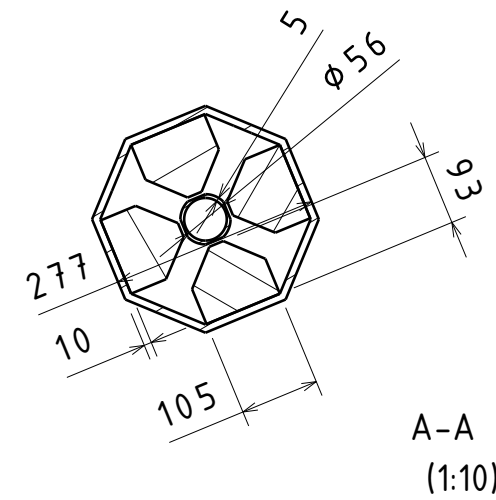
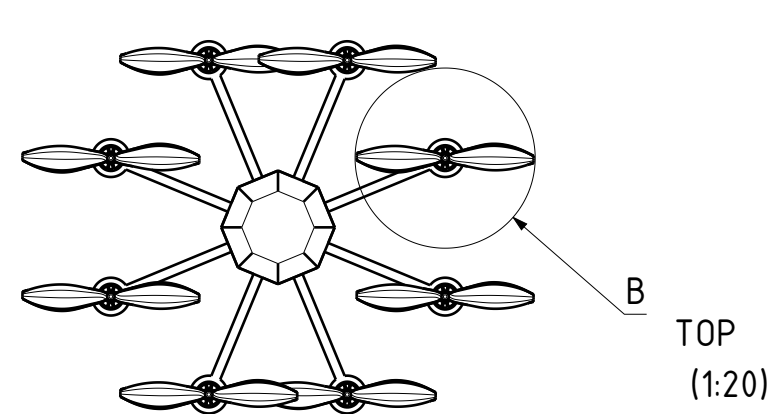
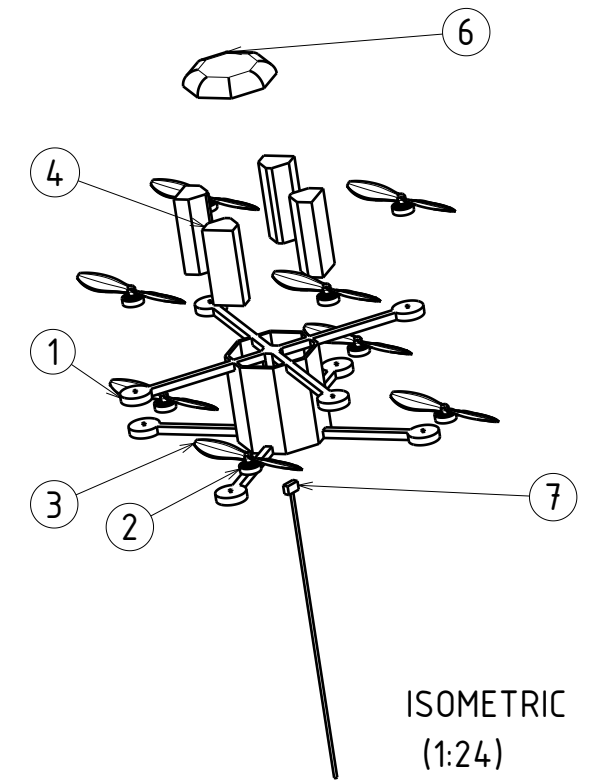
TU Delft

DRAWN BY Thomas Groothoff	DATE 20-6-2022
CHECKED BY XXX	DATE xxx
DESIGNED BY XXX	DATE xxx

Description		LFRS		
SIZE	Title	REV		
A3	DC19_Attachment_Assembly_LFRS	X		
SCALE	1:10	WEIGHT(kg)	XXX	SHEET 1/1

Figure A.1: Technical drawing of the LFRS

Item No.	Quantity	Title	Description	Material
1	1	DC19_Structures_Core	Core structure of the drone	CFRTP
2	8	DC19_Propulsion_Motor	Anitgravity motor from tmotors	-
3	8	DC19_Propulsion_Propeller	Propeller	-
4	4	DC19_Electrics_battery	-	-
5	1	DC19_Electronics_ComputerSensors	Electronics of the drone	-
6	1	DC19_Structures_ElectronicCompartment	Top cap for the drone that contains place for the electronics of the drone	CFRTP
7	1	DC19_Attachment_Cable	Cable with connector that connects the drone to the LFRS	-



		Description			
		DRONE			
DRAWN BY Thomas Groothoff	DATE 20-6-2022	SIZE A3	Title DC19_Drone_Complete	REV X	
CHECKED BY XXX	DATE xxx	SCALE 1:20	WEIGHT(kg) xxx	SHEET 1/1	
DESIGNED BY XXX	DATE xxx				

Figure A.2: Technical drawing of the drone